Computer-Aided Engineering Concept in the Design and Analysis Of An Off-Road Motorcycle Suspension and Frame

Tomasz Jacek Judek

A Thesis

in the

Faculty of Engineering and Computer Science

Presented in Partial Fulfillment of the Requirements
for the
Degree of Master of Engineering
at
Concordia University
Montreal, Quebec, Canada

August 1983

DEDICATION

Dedicated to my parents

ABSTRACT

COMPUTER-AIDED ENGINEERING CONCEPT IN THE DESIGN AND ANALYSIS OF AN OFF-ROAD MOTORCYCLE SUSPENSION AND FRAME

T.J. Judek
Concordia University, 1983

This thesis illustrates the concept of Computer-Aided Engineering (CAE) applied to the design and analysis of an off-road motorcycle. The study is divided into four stages:

The first stage consists of mathematically modelling the motorcycle suspension of the front fork and evaluating the suspensions' performance for sinusoidal and transient inputs. Laboratory testing is carried out and compared with the theoretical results. An optimal design of the suspension is then carried out.

In the second stage, the equations of motion are derived using Lagrange's method. For sinusoidal inputs of varying frequencies, the transmissibility curves of generalized coordinates are obtained for the average case. The transmissibility plots show the resonance of bounce and pitching vibrations to occur at 2 Hz and 4 Hz respectively.

In the third stage, a parametric study is carried out with variation of stiffness and damping of the tires and the shock absorbers, and the mass of the rider. A study on the effect of variation of the geometrical configuration of the motorcycle is also carried out and it is observed that these geometric parameters have considerable influence on the absolute displacements of the motorcycle.

In addition, an interactive computer software with dynamic graphics is developed on a VAX 11/780-NORPAK Graphics system to display the dynamic motion of the motorcycle suspension.

In the fourth stage, a Finite Element Analysis (FEA) of the motorcycle frame is carried out. Theoretical aspects and various steps required in FEA are discussed with an example of typical input data sequence for the motorcycle frame. Using Finite Element Technique in conjunction with modal analysis, the natural frequencies and mode shapes of an off-road motorcycle frame are obtained and presented. Procedure for developing graphics for mode animation of the motorcycle frame is also explained.

ACKNOWLEDGEMENTS

The author would like to express his gratitude and deep appreciation to his thesis supervisor, Dr. S. Sankar, for initiating this project and providing continued discussion during the course of the project.

The author also gratefully acknowledges the financial assistance provided through an NSERC-PRAI grant, P-8007, the helpful discussions with Mr. G. Burgess and for the materials supplied by Bombardier Ltd.

Finally, the author wishes to thank Mrs. Bharati Keshavan for typing this thesis and the Computer Research and Interactive Graphics Laboratory at Concordia University for the use of its facility.

TABLE OF CONTENTS

CHAPTER 3

DYNAMIC RESPONSE OF THE SUSPENSION SYSTEM UNDER PARAMETRIC VARIATION

CHAPTER 4

INTERACTIVE AND DYNAMIC GRAPHICS IN THE DYNAMIC ANALYSIS

CHAPTER 5

CHAPTER 6

APPENDICES

LIST OF FIGURES

LIST OF TABLES

NOMENCLATURE

A	piston area
[B]	stress matrix
[C]	total structure damping matrix
[c]	element damping matrix
C_1, C_4	tire damping
C_2, C_3	shock absorber damping
[D]	elasticity matrix
DF	relative displacement of front fork
DR	relative displacement of rear shock
f	road input excitational frequency
F	piston force
H_1	geometrical length
J	mass moment of inertia
[K]	total structure stiffness matrix
[k]	element stiffness matrix
K_1, K_4	tire stiffness
K_2, K_3	stifness of the shock absorber
L	wheel base length
L_2, L_3, L_4, L_5, L_6	geometrical length
[M]	total structure mass matrix
[m]	element mass matrix
M_2, M_4	mass of the wheels
M_3	mass of the motorcycle frame including the rider
[N]	assumed displacement matrix
T	turbulent flow coefficient

TR	transmissibility
XL	road wavelength
X_0	road input amplitude
X_1, X_2, X_3, X_4	generalized coordinates
α_1, α_6, ϕ	angles of shock absorbers
θ_3	generalized coordinate
$\{\delta\}$	displacement vector
ω_i	circular natural frequency

CHAPTER 1

INTRODUCTION

1.1 Computer-Aided Engineering

Most products today are designed from experience. The designer often uses creative thinking and performs a synthesis. Thus, the design is carried out without considering any detailed analysis. Usually prototypes are built and tested for performance. Any failures are identified and the build-and-test cycle is repeated until design specifications are met. Traditional product development, design and manufacturing methods cannot cope with demands for improved engineering productivity and is often time consuming and cost-ineffective.

To overcome these deficiences, at present several industries are introducing the new and emerging technology of Computer-Aided Design (CAD) and Computer-Aided Manufacturing (CAM). The philosophy of implementing such new technologies differ widely from industry to industry, however, the following description outlines some of the sequence in which such an implementation is currently attempted.

In any design, drawings have historically been the means to communicate the product geometry. The generation of drawings was done normally and any design changes required many hours of drawing corrections. This necessitated the development of Computer-Aided Drafting [6,10]*. Using computer-aided drafting, the drafting person can create complicated two-and three-dimensional drawings with increased speed and

* Numbers within square brackets [ ] indicate references.

accuracy. Changes made during any stage of the design are immediately accessible through graphics terminals to others involved in the project. Computer-assisted drafting increases productivity by freeing the user from performing the time-consuming, repetitive task such as drawing the same shape many times. Moreover, the drawing is stored in computer memory and can easily be changed and replotted in a few minutes to accommodate engineering modifications.

The computer-aided drafting systems, however, are widely used for the production of 2D drawings and not for design tasks such as geometric modeling, finite element analysis or kinematics. Until recently, large maxi frame computers were required to perform structural analysis, kinematic design and geometric modeling. With the introduction of so called super mini computers which have 32-bit word length, large memory size and operate at high speeds, the computer-aided design [7] process became a reality. There are various turn key CAD/CAM packages available on the market. The most common CAD/CAM stations used in industry are CALMA [30], APPLICON [31], COMPUTER VISION [32], LOCKHEED-CADAM [33], PERKIN-ELMER [34], AUTO-TROI [35], and NES [36]. All of these systems have the capabilities of design and limited analysis. The turn key systems have their own mesh generation and therefore the analysis is limited to only a specific finite element program. In addition the analysis is not suitable for very specialized products. These stations have extensive capabilities of data base creation and drafting. Some of these stations have limited capabilities in tool design and NC programming and some are interconnected with part inspection.

The computer-aided manufacturing [7] adds machining instructions while displaying an animated representation of the machining process on the screen. After refining and verifying the data, the system automatically generates computerized numerical control (CNC) machine tool commands. Finally, the proven CNC commands are written onto a magnetic tape cartridge for controlling the machine tools.

At present, there are systems which integrate the CAD and CAM into a system called CAD/CAM. For example, Lockheed Integrated Programs for Aerospace-Vehicle Design (IPAD) incorporated that capability.

As the use of mini computers in engineering practice continues to grow, the concept is being developed to integrate the product development and manufacturing into a computer automated system. This can be achieved through the integration of geometric modeling, design, analysis and testing, manufacturing drawings and tapes for NC machines. This process of integration is called Computer-Aided Engineering (CAE) [1,2].

In comparison to the CAD/CAM process which relies heavily on the testing of prototypes, the need for extensive prototype testing can be reduced by a CAE process. CAD/CAM presently addresses only the physical description of the product. The CAE method includes the analysis of functional characteristics such as vibration, noise and service life. In the CAE process, the computer simulation is used to determine precise loads for many alternative designs. The most important part of CAE is the systems model. The entire machine structure is represented mathematically in the computer. The model is created by combining various components and is analysed by computer programs.

In addition the mathematical model is checked with experiments and refined if necessary for conformity.

1.2 Problem Formulation

The objective of this thesis is to develop and apply the concept of computer-aided engineering and interactive graphics in the design, analysis and testing of an off-road motorcycle suspension and frame. The source of vibration due to rough terrain is of paramount importance in the design of off-road motorcycles used in the trail riding and motorcross.

The main design requirements are to minimize the severity of shock and vibration to the rider while maintaining the vehicle control.

In Canada, Bombardier Ltd. is the only manufacturer of off-road motorcycles under the trade name "CAN-AM". Various discussions with the manufacturer have revealed serious vibration problems. The biggest problem is with respect to the suspension. Due to large inputs from an off-road terrain, the motorcycle vibration exceeds the acceptable levels and the vehicle becomes uncontrollable. In addition, the manufacturer has experienced breakage of various members in the frame. Very broad and extensive analysis of the entire suspension and frame is required to find solution for such problems.

1.3 Literature Survey

The CAE approach to mechanical product development emphasizes the use of testing, simulation, modeling, analysis, and graphics as an integrated set of total systems design. A detailed description of this concept can be found in [1]. In this reference, an overview of CAE

is presented with emphasis on dynamic testing, finite element analysis, graphics software and systems modeling. The CAE concept is illustrated through various examples in vehicles, piping and rotating machinery.

Details of integration and implementation of CAE and related manufacturing capabilities into mechanical product development process can be found in [2]. In that paper, the comparison of design by manual, CAD/CAM and CAE methods is presented. The integration process is then illustrated through the example of robot and front end loader designs.

An important element of computer-aided engineering: geometric modeling is described in [3]. That paper illustrates the use of solid modeling, advanced graphics and system geometric models used in three dimensional space layouts, interference considerations, serviceability

Geometric modeling survey is given in the paper by A. Baer, C. Eastman and M. Hension [4]. Issues and alternatives in geometric modeling are discussed with emphasis on solid modeling. The data storage, handling, languages, conceptual design, logic structure are reviewed. Geometric models from building blocks are discussed in the paper by J. Krouse [5]. Wire frame modeling, surface modeling and solid modeling is illustrated.

The concept of automated drafting is described by J.K. Krouse [6]. The hardware, software and the usage of automated drafting is explained. The concept of computer-aided design is also explained by J.K. Krouse [7]. In this paper the emphasis is on structural analysis using finite element programs and modal analysis testing software.

Paper by T. Cokonis [8] describes the use of mini-computers that tackle CAD/CAM. The emphasis is on the system integration between computer-aided design, manufacturing and testing as a means of improving productivty. Publication by R. Fulton [9] gives the overview of integrated programs for aerospace and vehicle design. Very detailed methodology of CAD/CAM is illustrated followed by the application of that methodology to space shuttle.

The modular construction of CAD drawings is presented by T. Winkler [10]. The article discusses the application of 2D automatic drawing modules. Both the modular structure of drawings and the method of coding modules are discussed.

The models proposed in the past for the study of ride dynamics of vehicles relied mainly on simplified linear dynamic models, operating on a road profile simulated by a sinusoidal input. Recent studies, however, have based the analysis on complex multi-degree-of-freedom linear and nonlinear models subjected to road inputs of a random nature approaching 'real world' conditions. System modeling techniques to improve the ride and vibration isolation characteristics are presented in the paper by R. Shryock, J. Klahs, D. Dieterich [11]. The paper presents a computerized design analysis approach for 'optimizing' the vehicle structural dynamics to achieve improved ride quality.

The motorcycle modeling and simulation can be categorized into two areas of handling and ride. Handling involves stability, cornering ability, acceleration and braking and response to steering inputs. Ride involves comfort of the rider. Lateral, leaning and yawing motions are considered as handling responses while vertical and pitching motions are considered as ride responses.

S. Sharp [12] has developed a mathematical model for the stability and control of motorcycles and shown the use of such a model in establishing the stability characteristics and how these characteristics depend on various parameter values. The main conclusion from his work is that the fixed control characteristics of the motorcycle are unimportant, and the steady state response to steering torque is of secondary importance.

As a continuation of this study, S. Sharp [13] extended his mathematical model to include the effects of torsional flexibility between the rear wheel and the frame. The paper concludes that the torsional flexibility in the rear forks of a motorcycle will reduce the damping of weaving at high speeds, while affecting the capsize and wobble modes very little. G.E. Roe, M. Pickering and A. Zinober [14] have investigated the oscillations of a flexible castor and the effect of front fork flexibility on the stability of motorcycles. The equations of motions for small deflections were derived and solved numerically for many parameter variations. From the results, it was concluded that the lateral stiffness of the front fork affects the stability of the motorcycles.

D. Weit and W. Zellner [15] have considered the lateral-directional motorcycle dynamics and rider control behaviour. The analytical development included equations of motion for the vehicle and a multiple loop feedback model for the control response of the rider and motorcycle systems. The effects of changing fork geometry and operating conditions were discussed. The analytical procedure developed can be used to determine the adjustment of the design parameters of a given

motorcycle configuration to achieve desired handling properties and system performance.

Motorcycle ride dynamcis is discussed by S.H. Black and D.L. Taylor [16]. The investigation is based on a four-degree-of-freedom computer simulation (bounce, pitch and movement of each wheel). The simulation is nonlinear in terms of geometry and suspension components. The paper concludes that the response is very nonlinear due to wheel lift-off and limited suspension travel.

Computer-aided analysis and experimental verification of a motorcycle suspension has been carried out in detail by M. van Vliet and S. Sankar [19]. A mathematical model describing the flow characteristics in a front fork and rear shock absorber was developed for compression and extension. The model considered laminar and turbulent flow. For sinusoidal inputs the model was simulated and then checked with experiments for comparisons.

Vehicle modeling techniques applied to structures using finite element methods are outlined in several papers. The system modeling procedure, substructuring and the analysis method is presented by J.K. Horvath [20]. This paper illustrates that the vehicle system models can be formulated with all empirically (test) modeled subsystems with all analytically (finite element) modeled subsystems or with combinations of each.

Paper by M. Kamal and J. Wolf [21] shows the use of finite element method (FEM) in automotive structural analysis. The state-of-the-art in FEM for vibration and impact dynamics has been surveyed. Early

finite element vehicle models are discussed followed by detailed models using beams, plates and shell elements. Substructuring technique is explained for a typical automobile. In addition the steps in dynamic analysis are discussed followed by graphical representation of the results.

A recent book by M. Kamal and J. Wolf [22] is totally dedicated to the modern automotive structural analysis. This book describes the structural analysis using FEM and presents the examples of their application. It discusses in detail structural design criteria and finite element modeling of automotive structures.

The paper by K.H. Wadleigh [23] shows the minimum complexity models of complete body chassis structures. Calculations of deflections, loads and stresses resulting from load applications are presented and are compared with the test results.

The paper by Y. Luk and L.D. Mitchell illustrates the use of interactive graphics in the analysis of undamped beam system [24]. The graphics software developed allows the beam animation in time and space. J. Fowler and K. Newman [25] describes the use of graphics in the simulation of the victim response to crash loading. The paper illustrates that the computer graphics simulation gives exact repeatability. The results of any feature of interest can be immediately examined, whereas in physical tests only a limited number of parameters can be measured. The main disadvantage is that to adequately represent a crash victim requires a complex model with many degrees of freedom and access to a large computer. The Calspan/PST program described has the capabilities of fully 3-dimensional graphical simu-

lation of any victim-vehicle impact situation. Program output is both by print out of simulation parameters and by post processor plotting of dummy kinematics at specified times and of selected parameters in graphical form.

A. Hathaway [26] explains how the animation is achieved using Honeywel] 66/DPS to the Adage 340. The software developed has the capability of animating three different types of dynamic analyses in three dimensions: frequencies, and mode shapes, transient response using modal superposition, and nonlinear transient response using modal superposition, and nonlinear transient response using time step integration. The animation of each of these analyses has revealed complex coupled motions in 3-dimensions and desirable locations for stiffness modifications to improve the performance of a structure.

1.4 Detailed Outline of the Thesis

Overall CAE concept as applied to motorcycle is presented at first in Chapter 2 where four stages of CAE are discussed. The first stage concerns with mathematical modeling and testing of shock absorbers. In the second stage, the equations of motion for the motorcycle are formulated for a lumped mass analysis. The third stage discusses dynamic and interactive graphics concepts as applied to the suspension system. The fourth stage outlines the finite element analysis of the motorcycle frame and the concept of animated mode shape generation. The chapter concludes with typical results of the motorcycle suspension response presented through transmissibility types plots.

Chapter 3 presents the detailed parametric study for variation of stiffness and damping of the tires and the shock absorbers and the mass

of the rider. In addition, the effect of geometrical variation of the suspension on the displacement and acceleration response of the motorcycle is presented. Furthermore, three types of damping for the front fork and rear shock absorber are considered and studied for their influence on the suspension response. In the first case, the damping is considered linear with symmetrical characteristic for compression and extension strokes. In the second case, the damping is linear but has non-symmetrical characteristic for compression and extension. In the third case, the damping is non-linear and has non-symmetrical characterisitc for compression and extension.

Chapter 4 illustrates the application of the interactive and dynamic graphics in the design and analysis of the motorcycle suspension and frame. VAX-11/780 computer system configuration and NORPAK graphics hardware is explained. The methodology of developing dynamic graphics software is introduced initialy on simple systems followed by dynamic graphics of the entire motorcycle suspension. In addition, the capabilities of the interactive computer programs are discussed through detailed explanation of a user friendly menu.

Chapter 5 illustrates the application of finite element method in the analysis of the motorcycle frame. Theoretical aspects and various steps required in FEA are discussed with a typical input data sequence for the motorcycle frame. Graphical representation of the mode shapes calculated and the natural frequencies estimated from the ANSYS-FEA package are also illustrated. Procedure for developing graphics for mode animation is discussed in detail.

CHAPTER 2

LUMPED MASS ANALYSIS OF THE MOTORCYCLE SUSPENSION SYSTEM

2.1 CAE Concept in the Design and Analysis of an Off-Road Motorcycle

This thesis illustrates the concept of Computer-Aided Engineering (CAE) applied to the design and analysis of an off-road motorcycle. The purpose of the thesis is to develop a comprehensive computer software package that includes most of the steps invovled in CAE with interactive and dynamic graphics support.

The general concept of CAE as applied to the motorcycle is illustrated in Fig. 2.1. The study is divided into four main stages.

The first stage consists of mathematically modelling the motorcycle suspension system and evaluating the suspension's performance for sinusoidal, transient and random inputs. Laboratory testings were carried out and compared with theoretical results to verify and improve the mathematical model. An optimal design of the suspension is then carried out by adopting numerical optimization method. A detailed description of this stage is presented in Ref. [19] and a brief summary is presented in Appendix A.

In the second stage the equations of motion were derived using Lagrange's method. For sinusoidal inputs of varying frequenices, the equations were solved in time domain by using variable order Adams' Predictor Corrector method. A parametric study was carried out to evaluate the relative influence of both geometric and physical parameters on the suspension behavior.

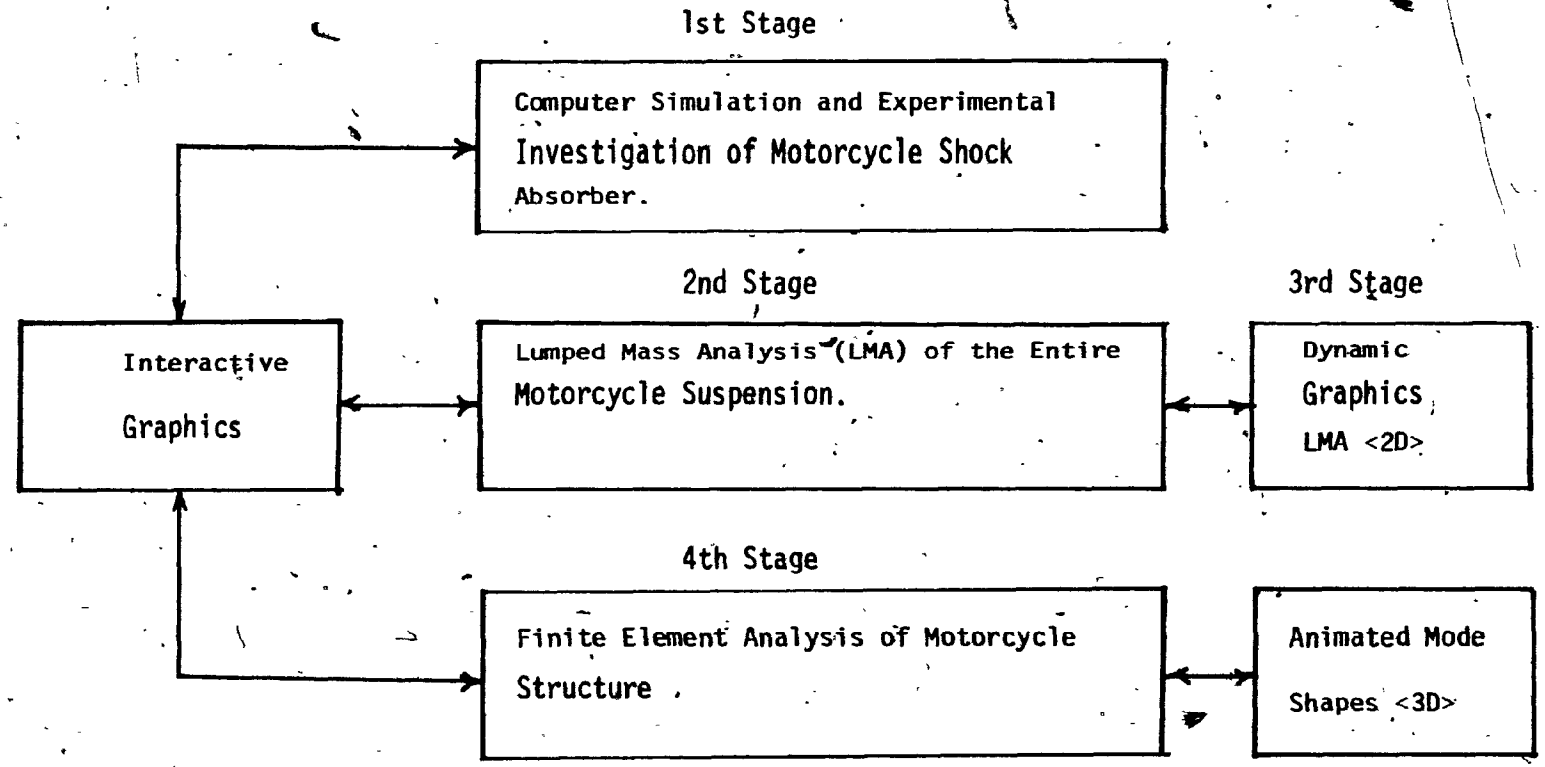

Figure 2.1: CAE Steps in Motorcycle Suspension System

In the third stage, a dynamic graphics software was developed on a VAX-11/780 NORPAK graphics system to investigate visually the response of the system for variation in parameters. The major feature of this is that one can interactively change the parameters and see its effect by using the dynamic graphics approach which provides an additional dimension in interpreting the solution.

The fourth stage involves the finite element analysis (FEA) of the frame using ANSYS [37] software package. For this purpose, the motorcycle frame was discretized with beam elements and the weights of the driver, gas tank, engine, etc., were lumped at the appropriate nodes. Using the ANSYS-FEA software, the natural frequencies and mode shapes were calculated.

In addition, the technique and methodology for animated mode shapes and responses are also illustrated. The animation is a great tool for the designer for solving the problems of complex interaction between the components.

2.2 Mathematical Model of the Suspension System

The first step in the establishment of the CAE concept is to develop a comprehensive mathematical model of the suspension system that takes into account the front fork assembly, the rear shock absorber mounted on the swing arm, the frame, the front and rear wheels and tires, the various physical geometry and inertia of the vehicle and the mass of the rider.

Through this mathematical model, it is possible to study the dynamic response of the vehicle in terms of displacements or velocities

or accelerations at the C.G.of the vehicle and at the wheels for any type of off-road terrain inputs. The maximum acceleration level and the displacement at the C.G. which are of paramount importance for reducing the rider fatigue and for vehicle control can also be investigated through the variation of system parameters or by changing the geometrical configuration of the vehicle.

In the process of developing the mathematical model, the following assumptions are made:

1. Spring elements are considered to be ideal with no inertia or friction.

2. Spring elements are also assumed to be linear.

3. Tires are modeled to be linear spring with viscous damper operating in parallel.

4. The tires are assumed to be in contact with the road at a single point.

5. Wheels are assumed to be always in contact with the road.

6. The motorcycle frame is assumed to be rigid.

7. Front fork and rear shock absorber are considered to have negligible flexural displacement.

8. The vehicle model is considered to be in-plane with motions limited to pitch, vertical and transverse translations.

9. All displacements are assumed to be small.

A schematic model of the suspension system for lumped mass analysis is shown in Fig. 2.2. From this model and using the Lagrange's energy method, the equations of motion of the suspension system are derived as:

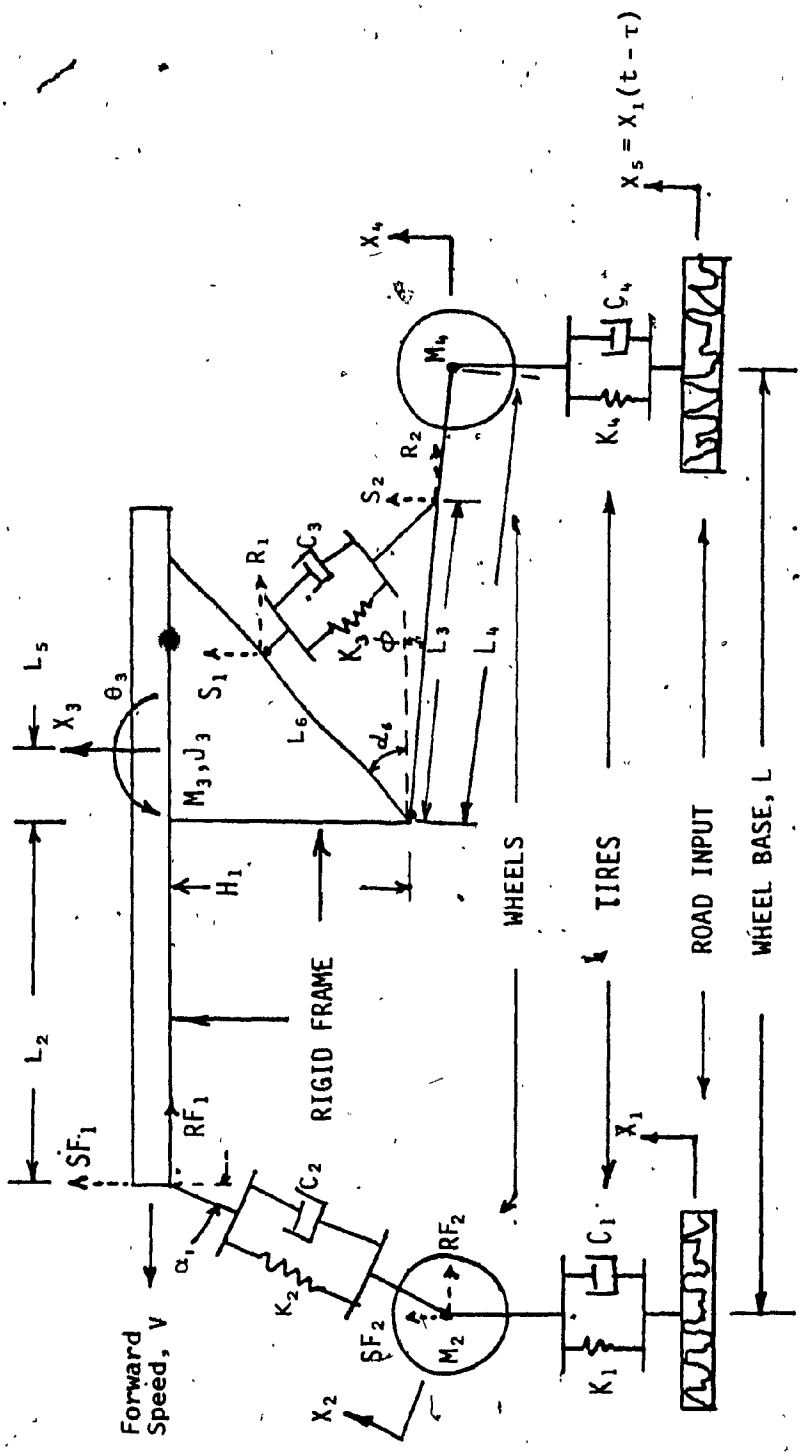

Figure 2.2: Lumped Mass Model of the Motorcycle

$$M_2\ddot{X}_2 + K_1A_1 + K_2A_2 + C_1A_3 + C_2A_4 = 0 \qquad (2.1)$$

$$M_3\ddot{X}_3 + K_2B_1 + K_3B_2 + C_2B_3 + C_3B_4 = 0 \qquad (2.2)$$

$$J_4\ddot{\theta}_3 + K_1D_1 + K_2D_2 + K_3D_3 + C_2D_4 + C_3D_5 = 0 \qquad (2.3)$$

$$M_4\ddot{X}_4 + K_2E_1 + K_3E_2 + K_4E_3 + C_2E_4 + C_3E_5 + C_4E_6 = 0 \qquad (2.4)$$

where

$$A_1 = [X_2\cos(\alpha_1 - \theta_3) - X_1]\cos(\alpha_1 - \theta_3)$$

$$A_2 = -[SF1 - SF2]\cos(\alpha_1 - \theta_3) - [RF1 - RF2]\sin(\alpha_1 - \theta_3)$$

$$A_3 = [\dot{X}_2\cos(\alpha_1 - \theta_3) - \dot{X}_1]\cos(\alpha_1 - \theta_3)$$

$$A_4 = -[\dot{SF1} - \dot{SF2}]\cos(\alpha_1 - \theta_3) - [\dot{RF1} - \dot{RF2}]\sin(\alpha_1 - \theta_3)$$

$$B_1 = [SF1 - SF2] - [RF1 - RF2]\tan\alpha$$

$$B_2 = [S1 - S2]\,L_3/L_4 - [R1 - R2]\,L_3/L_4\tan\alpha$$

$$B_3 = [\dot{SF1} - \dot{SF2}] - [\dot{RF1} - \dot{RF2}]\sec^2\alpha\sin\alpha\cos\alpha$$

$$B_4 = [\dot{S1} - \dot{S2}]\,L_3/L_4\sec^2\alpha\cos^2\alpha - [\dot{R1} - \dot{R2}]\,L_3/L_4\sec^2\sin\alpha\cos\alpha$$

$$D_1 = [X_2\cos(\alpha_1 - \theta_3) - X_1]X_2\sin(\alpha_1 - \theta_3)$$

$$D_2 = [SF1 - SF2][-L_2\cos\theta_3 - X_2\sin(\alpha_1 - \theta_3)] +$$

$$[RF1 - RF2][(L_2 - L_5)\sin\theta_3 - H_1\cos\theta_3 + X_2\cos(\alpha_1 - \theta_3)] +$$

$$L_7\tan\alpha\cos(\theta_3 + \alpha_5)$$

$$D_3 = [S1 - S2][L_9\cos(\alpha_4 - \theta_3) + L_7\cos(\theta_3 + \alpha_5) -$$

$$L_3L_7/L_4\cos(\theta_3 + \alpha_5)] + [R1 - R2][L_9\sin(\alpha_4 - \theta_3) -$$

$$L_7\sin(\theta_3 + \alpha_5) + L_3L_7/L_4\tan\alpha\cos(\theta_3 + \alpha_5)$$

$$D_4 = [\dot{SF1} - \dot{SF2}]\,[-L_2\cos\theta_3 - X_2\sin(\alpha_1 - \theta_3)] +$$

$$[\dot{RF1} - \dot{RF2}]\,[(L_2 - L_5)\sin\theta_3 - H_1\cos\theta_3 + X_2\cos(\alpha_1 - \theta_3) +$$

$$L_7\cos(\theta_3 + \alpha_5)\sec^2\alpha\sin\alpha$$

$$D_5 = [\dot{S1} - \dot{S2}]\,[L_9\cos(\alpha_4 - \theta_5) + L_7\cos(\theta_3 + \alpha_5) -$$

$$L_3L_7/L_4\cos(\theta_3 + \alpha_5)\sec^2\alpha\cos^2\alpha] + [\dot{R1} - \dot{R2}][L_9\sin(\alpha_4 - \theta_3) -$$

$$L_7\sin(\theta_3 + \alpha_5) + L_3L_7/L_4\cos(\theta_3 + \alpha_5)\sec^2\alpha\cos\alpha\sin\alpha]$$

$$E_1 = [RF1 - RF2]\tan\alpha$$

$$E_2 = [S1 - S2]\,L_3/L_4 + [R1 - R2]\,L_3/L_4\tan\alpha$$

$$E_3 = X_4 - X_5$$

$$E_4 = [\dot{RF1} + \dot{RF2}]\sec^2\alpha\sin\alpha\cos\alpha$$

$$E_5 = -[\dot{S1} - \dot{S2}]\,L_3/L_4\sec^2\alpha\cos^2\alpha + [\dot{R1} - \dot{R2}]\,L_3/L_4\sec^2\alpha\sin\alpha\cos\alpha$$

$$E_6 = \dot{X}_4 - \dot{X}_5$$

SF1, SF2, RF1, RF2 are the displacements as illustrated in Fig. 2.2.
S1, S2, R1, R2

For a detailed derivation of these equations refer to Appendix B. A complete list of the equations and their derivations for the case of large displacements are presented in Appendix C.

2.3 Road Input

The mathematical model developed in Section 2.2 is capable of taking into account any types of road input, namely, sinusoidal, transient and random. If X(t) is the road input, then for the model

$$X_1 = X(t) \qquad X_5 = X(t - \tau)$$

where τ is the time required for the rear wheel to travel a distance of motorcycle wheel base.

2.4 Results and Discussion of Lumped Mass Model: Analysis

In this thesis, a sinusoidal signal with constant amplitude is considered as the road input.

$$X_1 = X_0 \sin \omega t \qquad X_5 = X_0 \sin \omega(t-\tau)$$

In the variation of ω, it is assumed that both V and XL are simultaneously changed so that the ratio satisfies the equation $\omega = \frac{2\pi V}{XL}$ and the value of τ has a L constrained variation according to the equation $\tau = \frac{L}{V}$

X_0 is considered to be 2.54 cm (1 in.). This value was chosen arbitrarily to reflect the assumption of small displacements. All the relevant parameters for this analysis are given in Table 2.1.

The system equations were solved as an initial value problem under harmonic excitation. When steady-state is reached, the desired amplitude ratio (eg: X_3/X_1) is stored and the initial value routine restarted at an increased excitation frequency. In this manner, a frequency sweep is performed and the quantities of interest are obtained. The equations were solved in time domain by using variable order Adam's Predictor Corrector method. The peak to peak amplitude ratios of X_2/X_1, X_3/X_1, X_4/X_1 and θ_3 wheel base/X_1 were obtained for fixed amplitude of 2.54 cm (1 in.) with variation of frequency. The transmissibility plots of the generalized coordinates, are shown in Fig. 2.3 to 2.6.

The transmissibility plot for X_2 shows a typical isolation characteristic with the peak transmissibility occurring around ω = 2Hz, and having good vibration isolation for higher frequencies.

TABLE 2.1

Input Parameters

PARAMETERS						UNITS
K_1		K_2	K_3	K_4		Stiffness
122 583		7005	43 780	122 583		N/m
700		40	250	700		lb/in
C_1		C_2	C_3	C_4		Damping
3502		1401	1401	3502		N.sec/m
20		8	8	20		lb.sec/in
M_1			M_4	M_3		Masses
7			17.5	140		kg
0.04			0.1	0.8		lb.sec^2/in
J_3						Inertia
13.6						kg.m^2
120						in.lb.sec^2
L_2	L_3	L_4	L_5	L_6	H_1	Length
63.5	29	56,9	12.7	29	34.3	cm
25	11.4	22.4	5	11.4	13.5	in
α_6			ϕ		α_1	Angle
1.4			0.2		0.47	rad

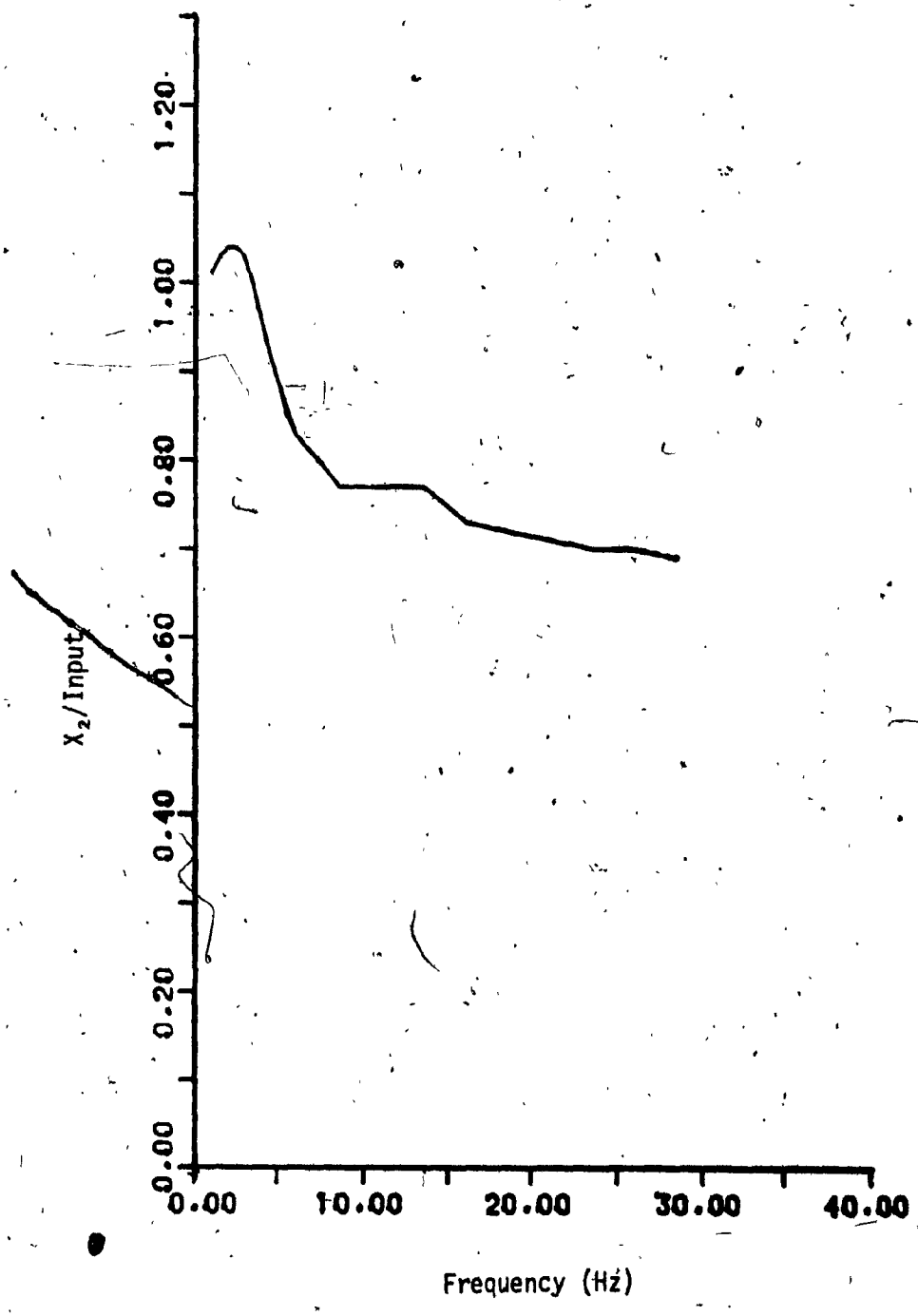

Figure 2.3 : X_2 Transmissibility for Average Case

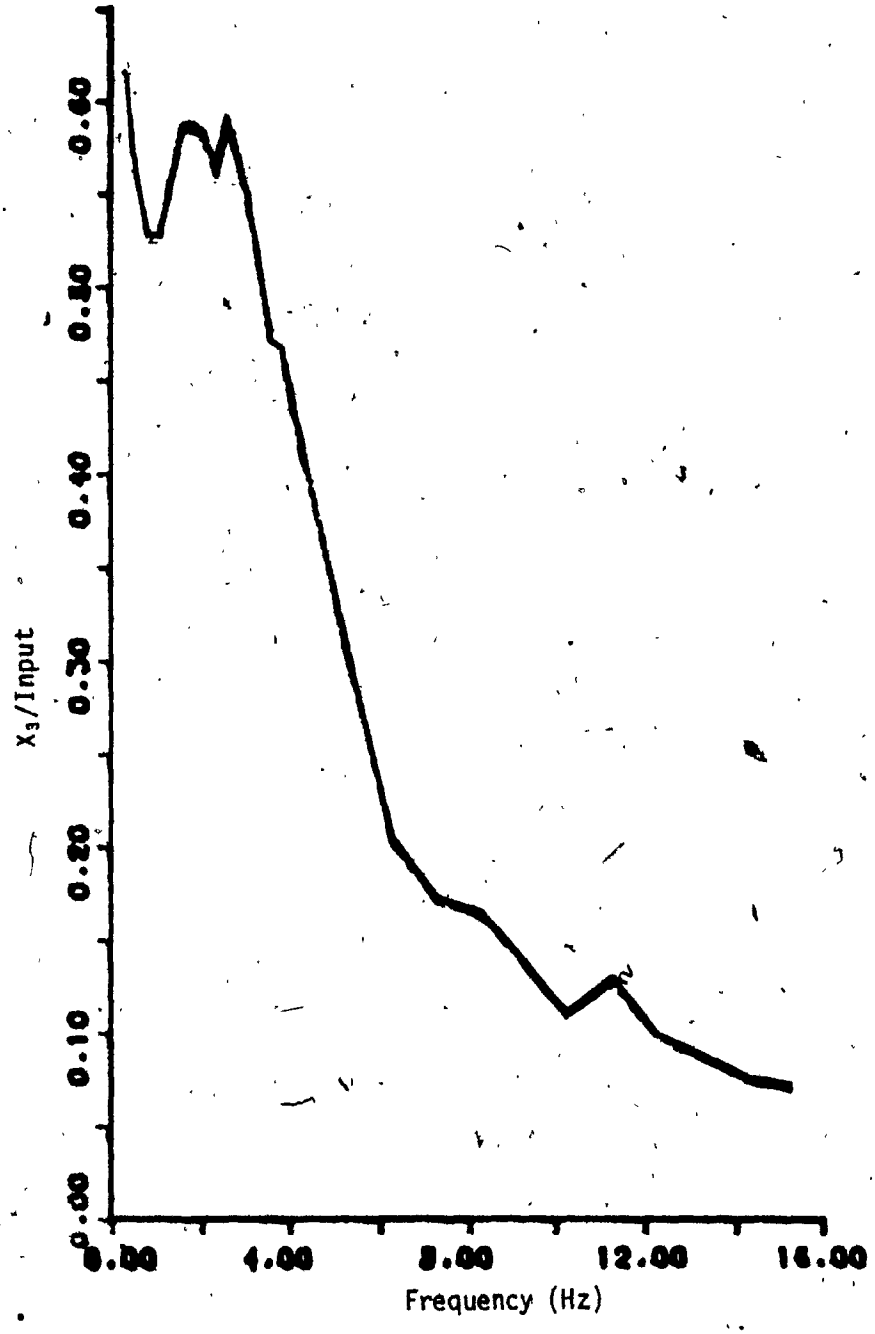

Figure 2.4 : X_3 Transmissibility for Average Case

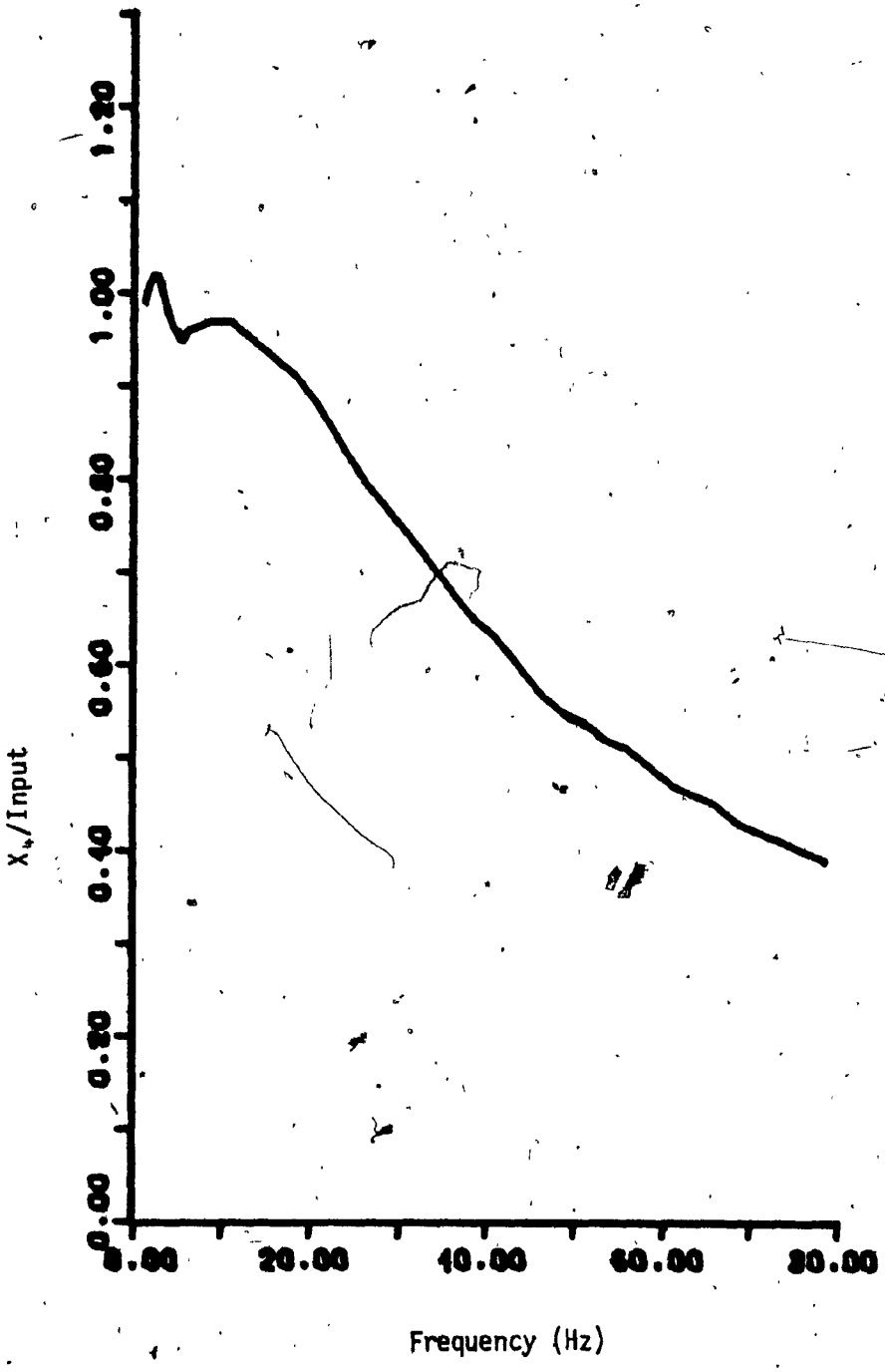

Figure 2.5 : X_4 Transmissibility for Average Case

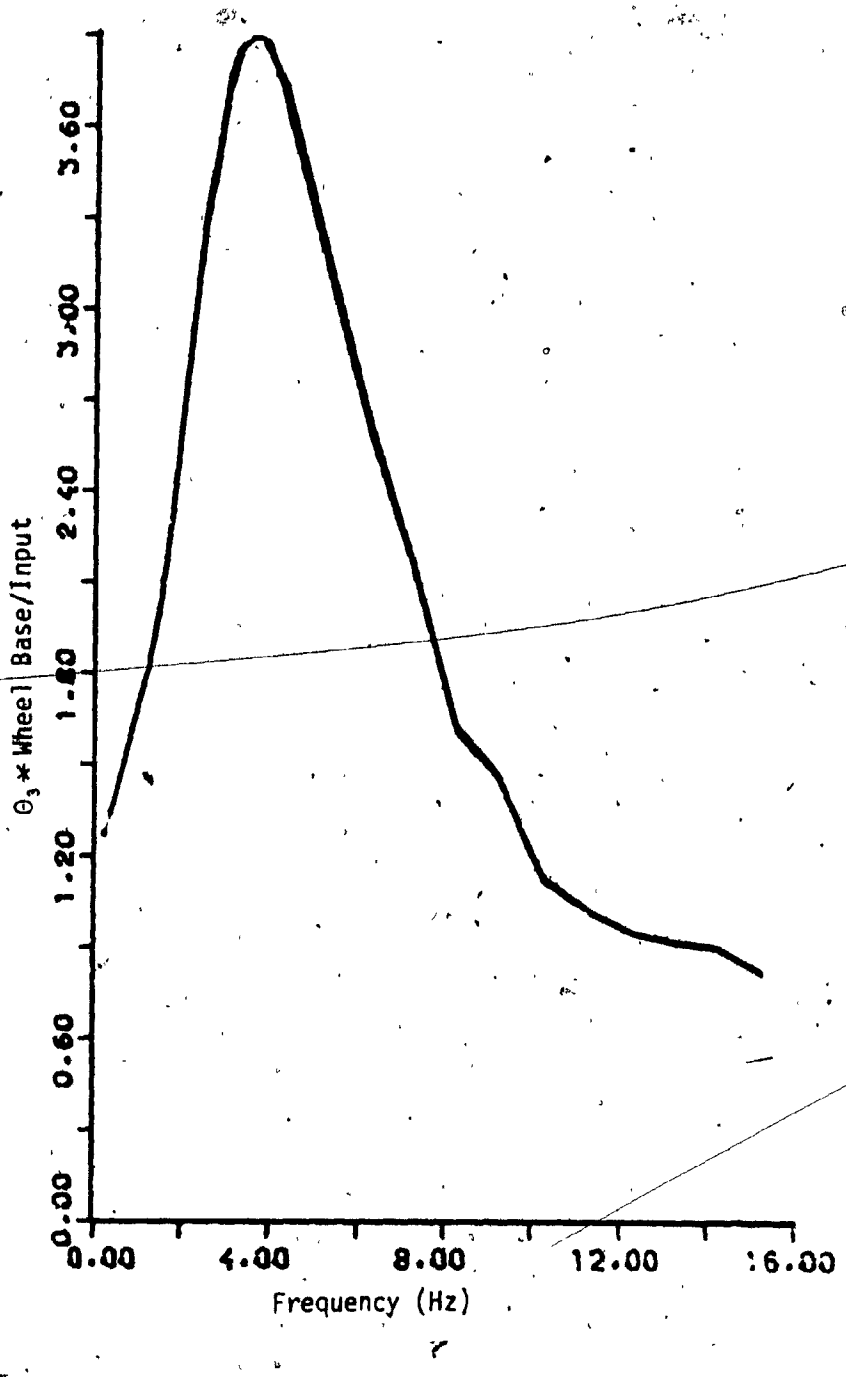

Figure 2.6 : θ_3 Transmissibility for Average Case

In Fig. 2.4, the transmissibility plot for X_3 shows an oscillatory behaviour at low frequencies below resonance and this may be attributed to the non-linear behaviour of the vehicle and due to the coupled bounce-pitching vibration.

The transmissibility plot of X_4 shows a very similar behaviour like X_2 with a secondary peak occurring in the high-frequency region just beyond the resonance.

The transmissibility plot of θ_3 shows a very high peak at the pitching resonance frequency, ω = 4Hz and with good vibration isolation at higher frequencies.

In order to gain the confidence in the mathematical model and analysis, a simplified model of rigid bar supported by two springs was investigated. The pitch and bounce natural frequencies of the simplified model agreed with the frequencies corresponding to the transmissibility peaks as shown in Fig. 2.4 and 2.6.

To gain further confidence in the mathematical model of the motorcycle, a laboratory testing should be carried out as recommended in Chapter 6 under the heading 'Future Work'.

CHAPTER 3

DYNAMIC RESPONSE OF THE SUSPENSION SYSTEM UNDER PARAMETRIC VARIATION

3.1 General

Dynamic response of the suspension system for a sinusoidal input is presented in Chapter 2 for an average set of parameter values. The transmissibility (TR) plots are presented for the generalized coordinates X_2, X_3, X_4, θ_3 and for the bounce acceleration $\ddot{X}_3$.

In order to study the influence of variation of system parameters on the dynamic response of the system, a detailed analysis is carried out. The parameters under consideration are: front and rear tire characteristics, mass and moment of inertia of the motorcycle, mass of the rider and various geometric lengths and angles of the suspension linkage.

3.2 Influence of Tire Characteristics

3.2.1 Tire Damping Variation (C_1, C_4)

As illustrated in Fig. 3.1, the tire damping has very little effect on X_3 transmissibility, however, at resonance the peak TR increases marginally with increasing damping.

Figure 3.2 shows the plot of θ_3 transmissibility. By increasing the front and rear tire damping, the θ_3-TR decreases at resonance with very little variation above the resonance. Figures 3.3 and 3.4 show the TR plot for X_2 and X_4 coordinates. In both cases, increasing the tire damping, decreases the response at resonance and increases the

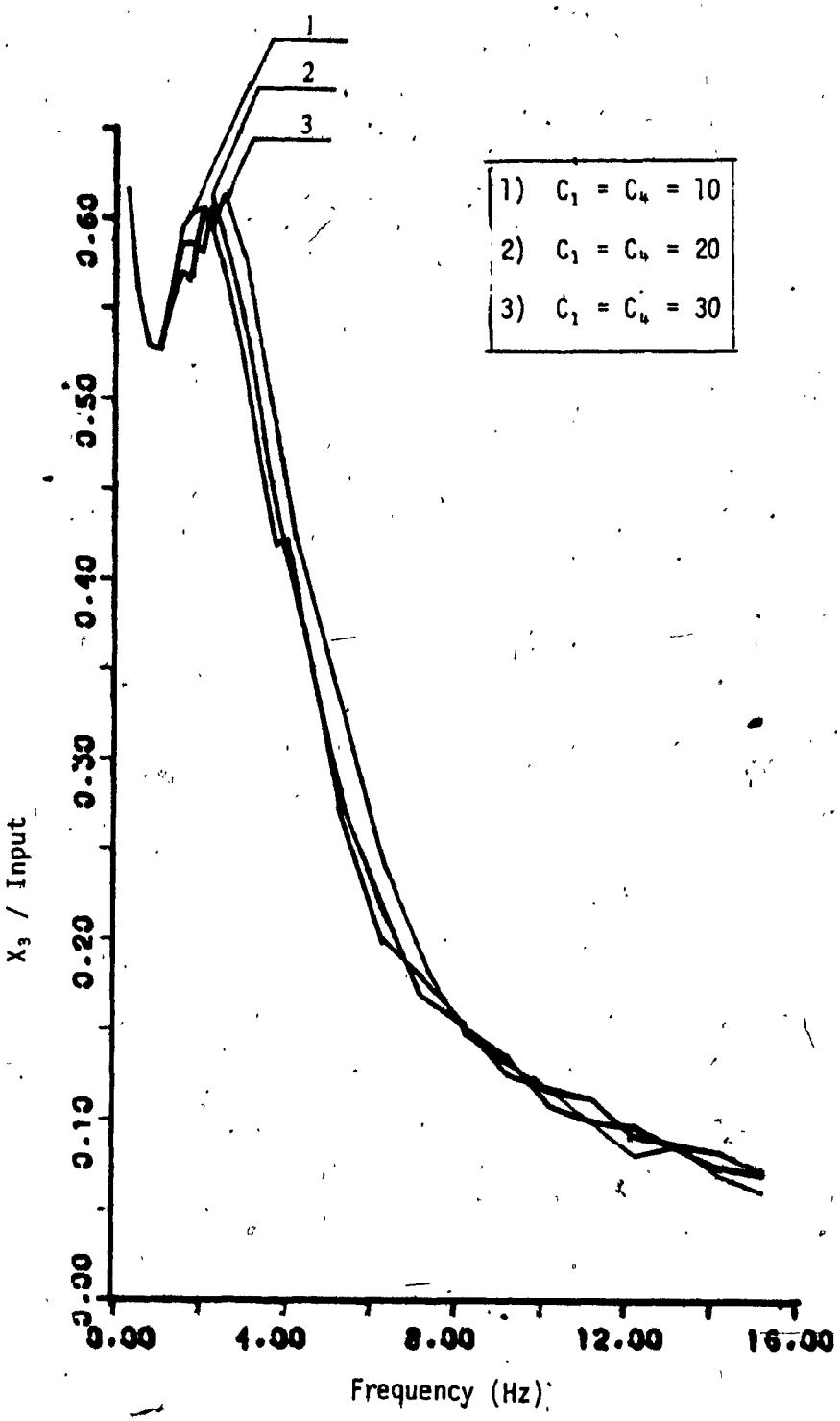

Figure 3,1 : Effect of X_3 Vs f for Variation in C_1 and C_4: Input Amplitude of 1.25 cm (0.5in)

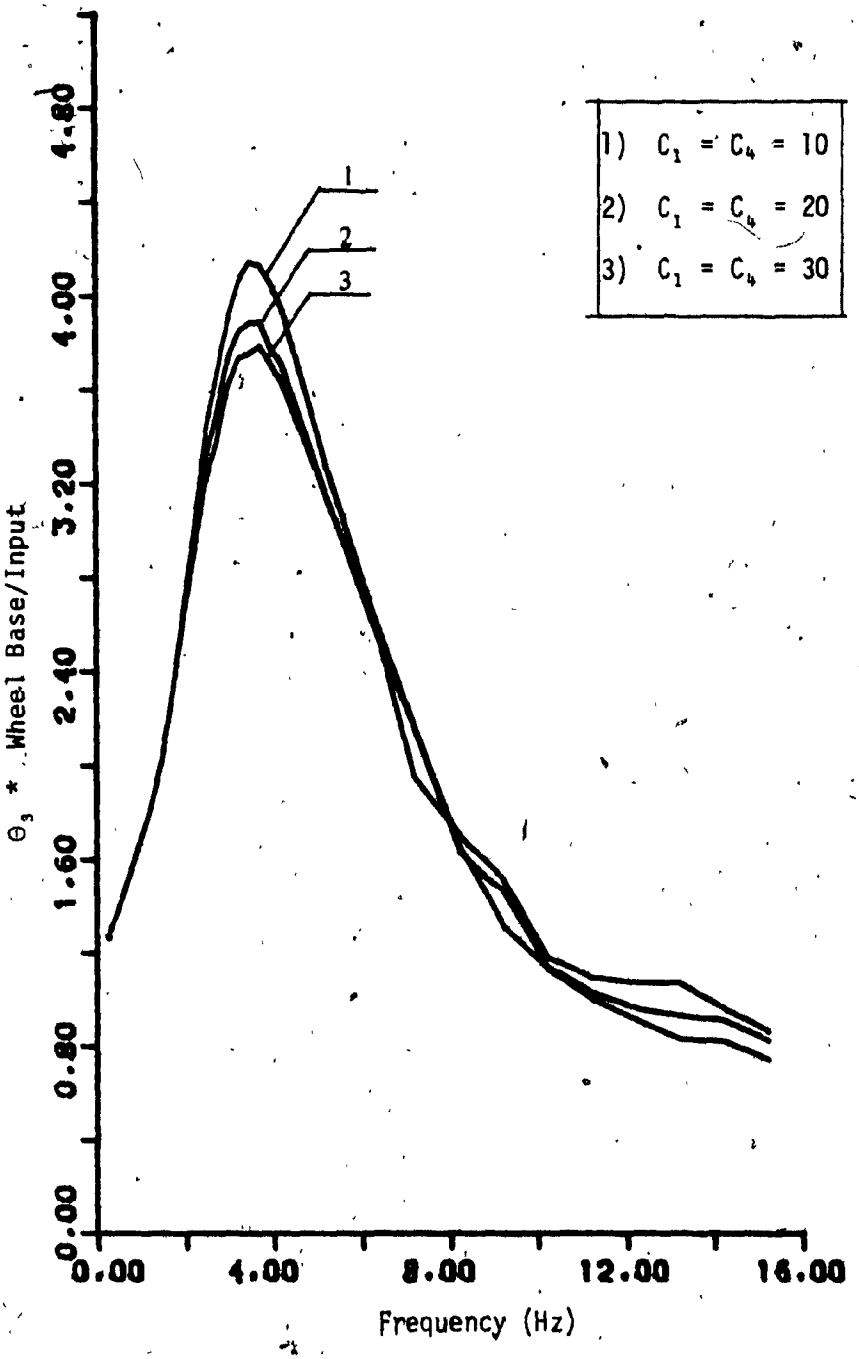

Figure 3,2: Effect of Θ_3 Vs f for Variation in C_1 and C_4: Input Amplitude of 1.25 cm (0.5 in)

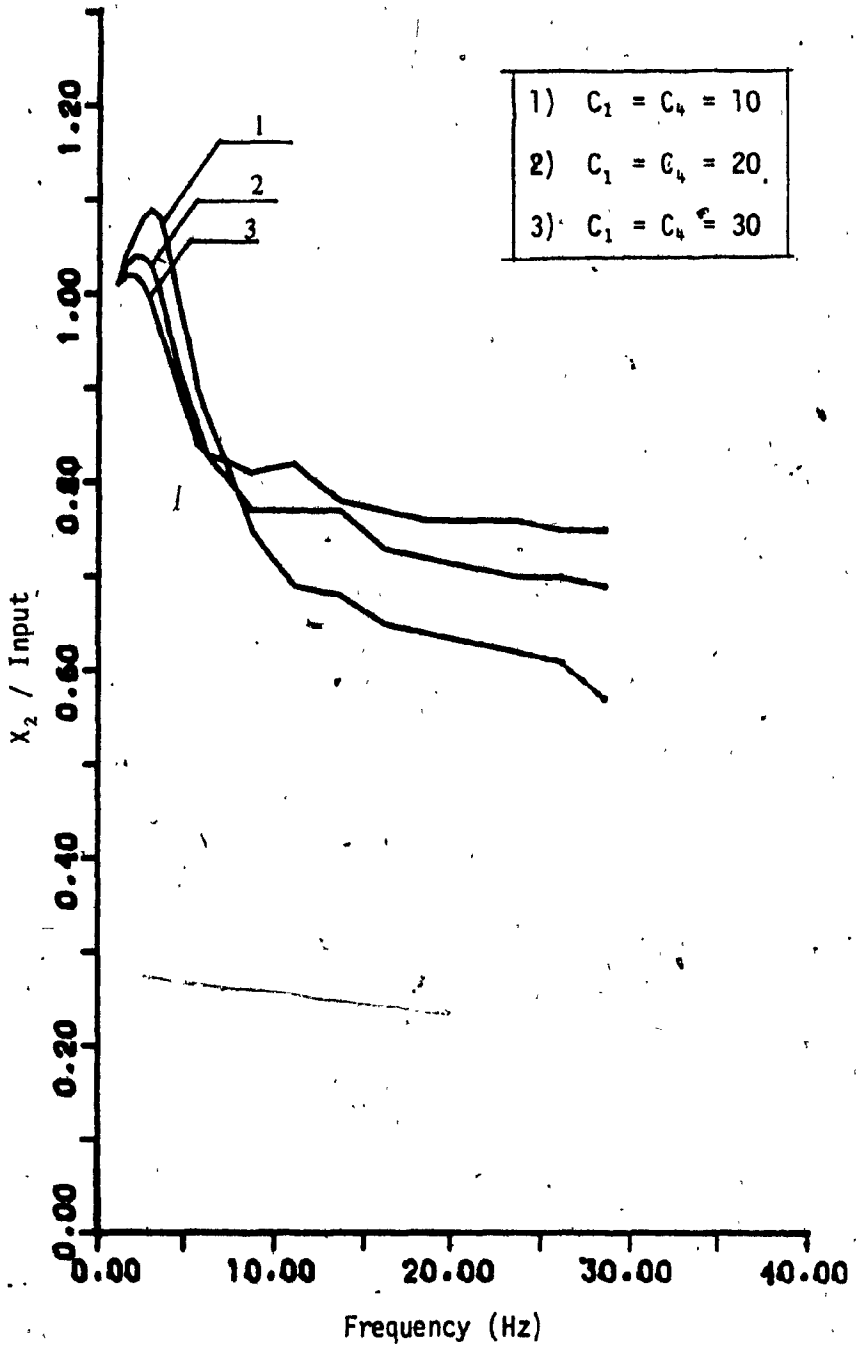

Figure 3.3 : Effect of X_2 vs f for Variation in C_1, C_4: Input Amplitude of 1.25 cm (0.5 in).

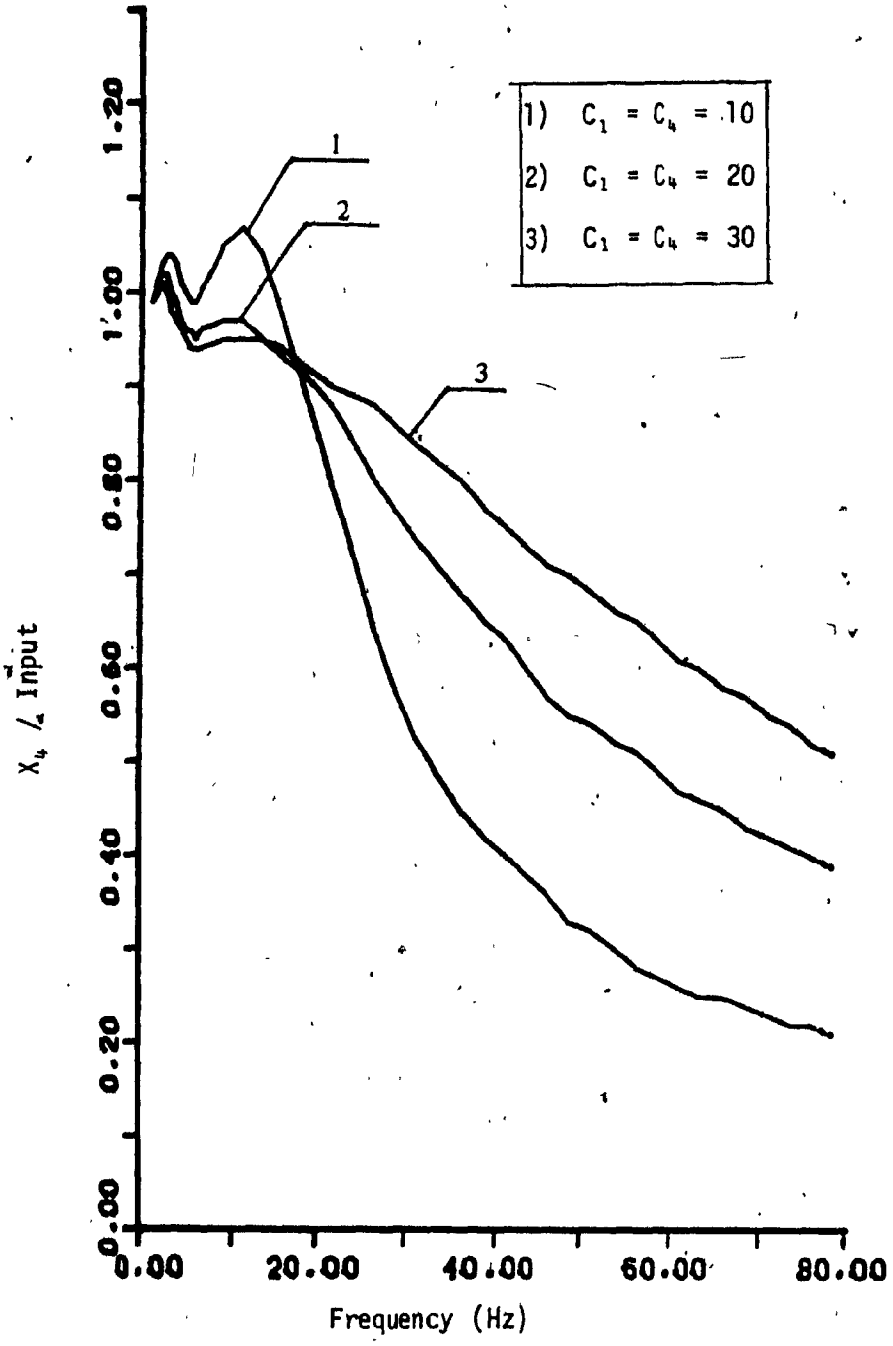

Figure 3.4: Effect of X_4 Vs f for Variation in C_1 and C_4: Input Amplitude of 1.25 cm (0.5 in).

transmissibility value beyond the resonance. The acceleration transmissibility of $\ddot{X}_3$ shown in Fig. 3.5 indicates that the peak transmissibility decreases with increasing tire damping.

3.2.2 Tire Stiffness Variation (K_1, K_4)

There is very little effect on the X_3 transmissibility due to the tire stiffness variation. At resonance the increase of stiffness causes slight drop in X_3 response as shown in Fig. 3.6.

There is not very much effect on θ_3 transmissibility either. However at resonance, the increase of tire stiffness causes the increases of θ_3 response as shown in Fig. 3.7.

The variation of K_1 and K_4 stiffness has no influence on X_2 and X_4 response.

The $\ddot{X}_3$ transmissibility shown in Fig. 3.8 illustrates a decreasing peak transmissibility with decreasing tire stiffness.

3.3 Influence of Front Fork and Rear Shock Absorber Variation

3.3.1 Front Fork Damping Variation (C_2)

Increasing the front fork damping, decreases the X_3 transmissibility at resonance and increases away from the resonance (Fig. 3.9). Case 3 in that figure represents an overdamped system.

By increasing the damping of the front fork, the peak θ_3 transmissibility is the highest for the medium damping and lowest for highest damping (Fig. 3.10)

Increasing the front fork damping, the X_2 transmissibility increases at resonance and decreases away from the resonance (Fig. 3.11). C_2 variation does not have any effect on X_4.

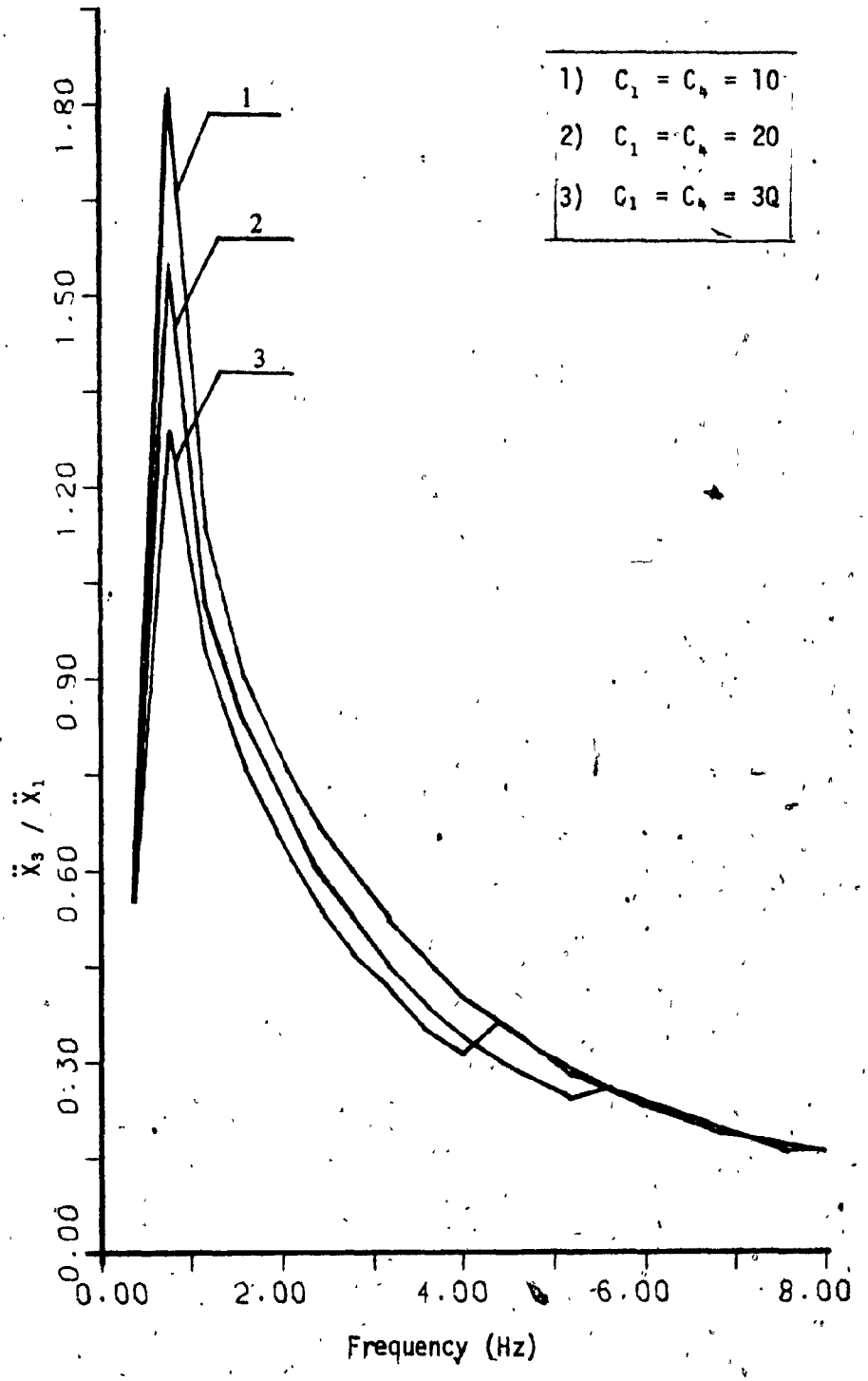

Figure 3.5: Effect of $\ddot{X}_3$ Vs f for Variation in C_1 and C_4: Input Amplitude of 1.25 cm (0.5 in).

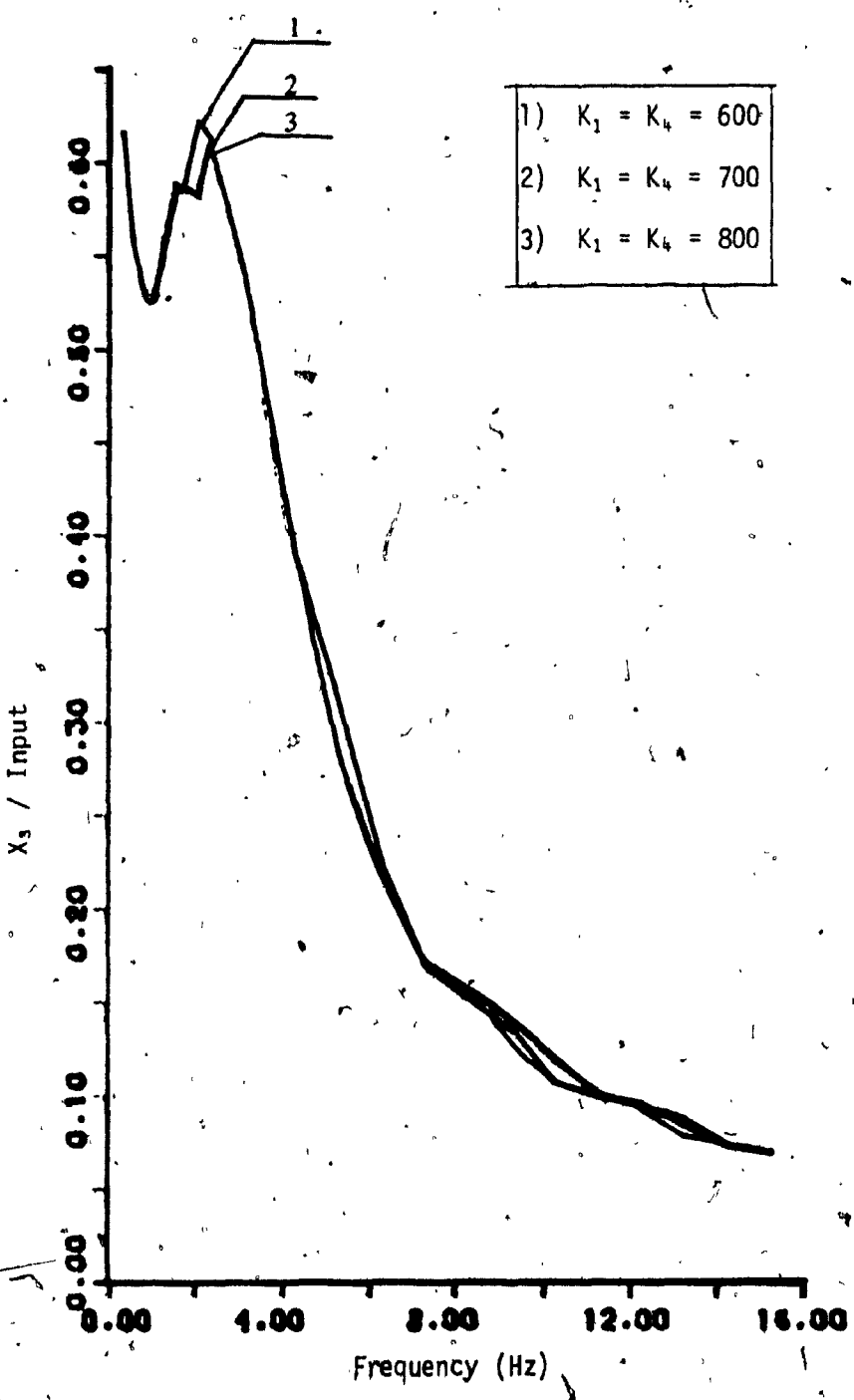

Figure 3,6: Effect of X_3 Vs f for Variation in K_1 and K_4 : Input Amplitude of 1.25 cm (0.5 in).

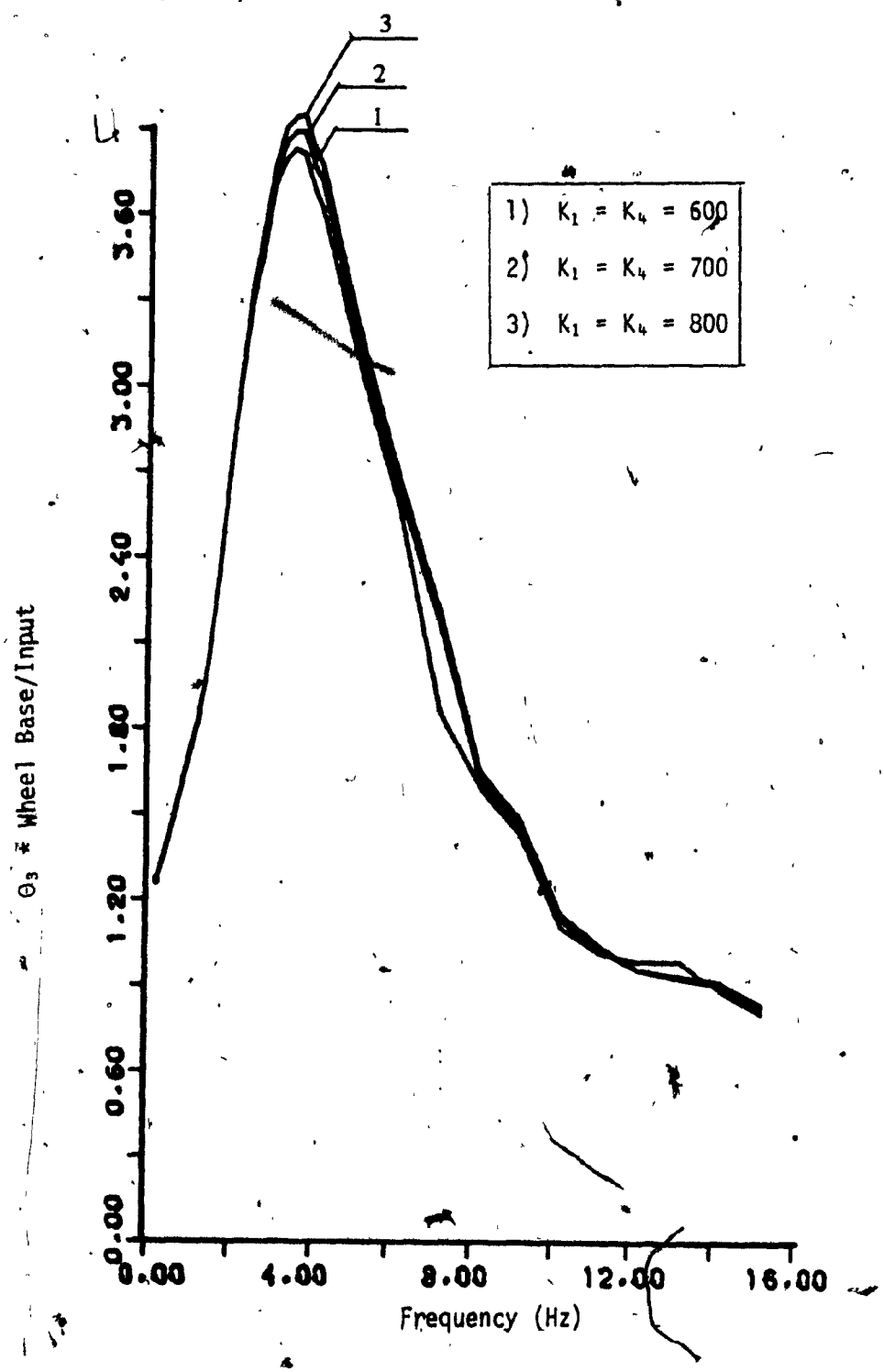

Figure 3.7: Effect of θ_3 Vs f for Variation in K_1 and K_4 : Input Amplitude of 1.25 cm (0.5 in).

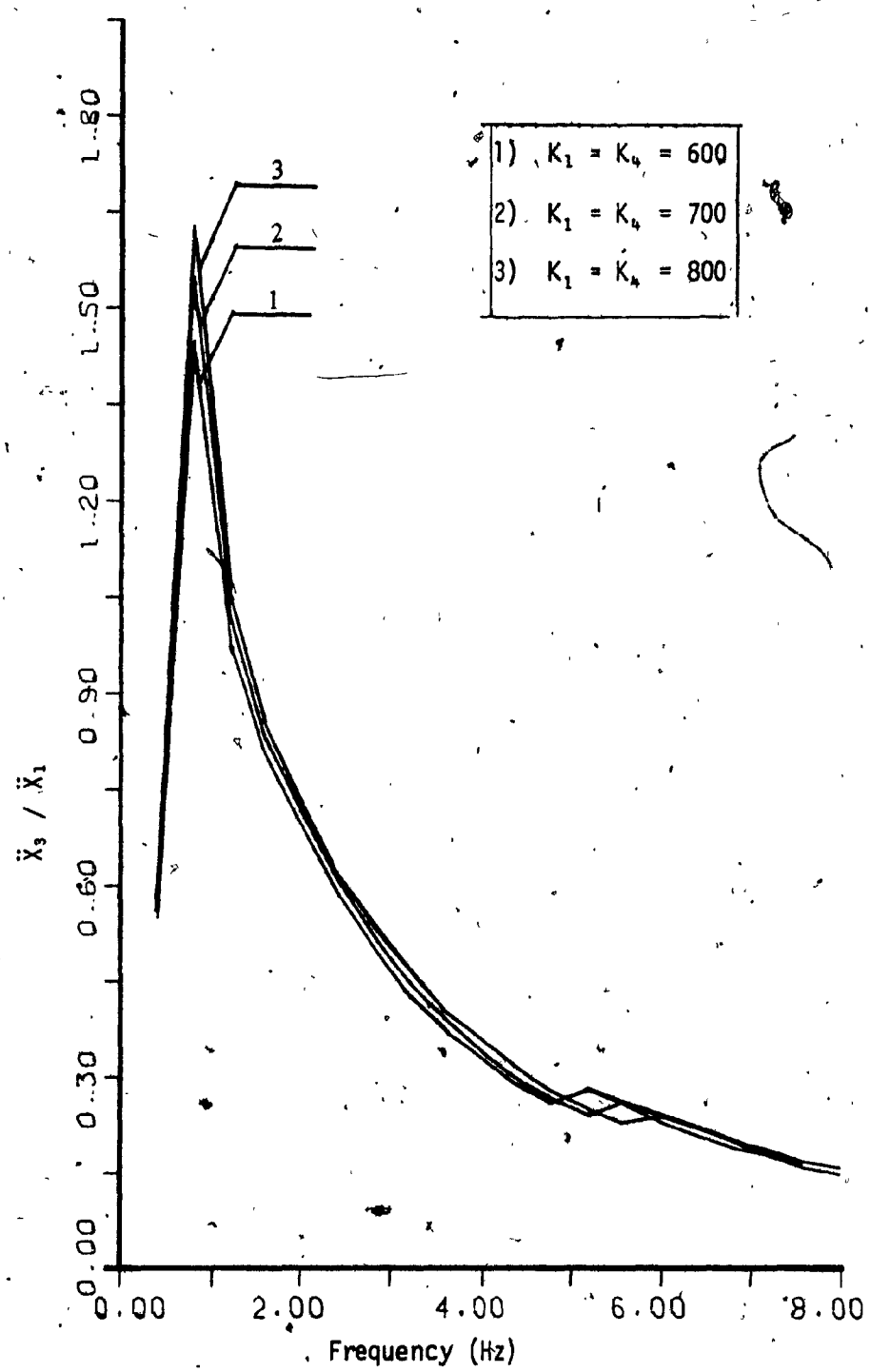

Figure 3,8: Effect of $\ddot{X}_3$ Vs f for Variation in K_1 and K_4 Input Amplitude of 1.25 cm (0.5 in).

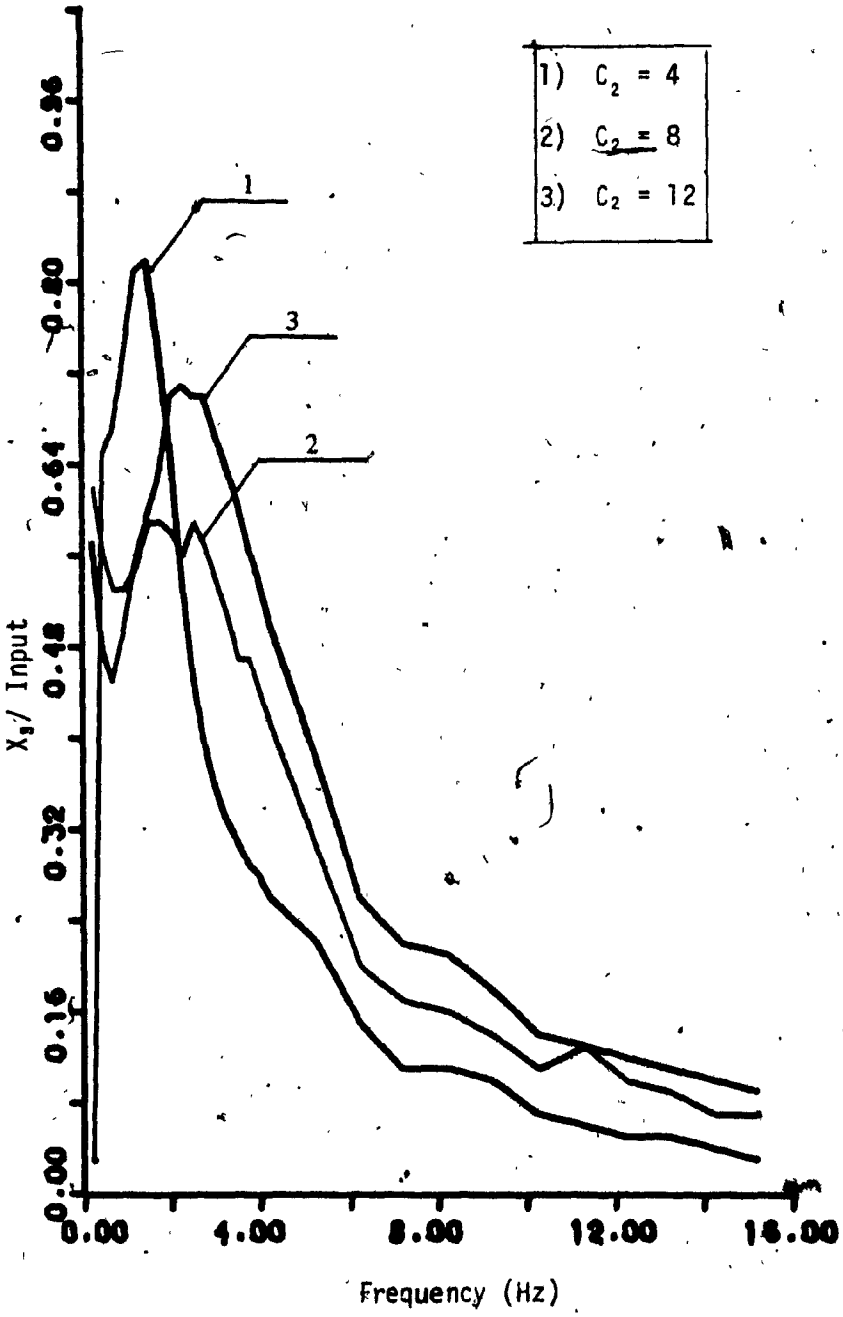

Figure 3.9: Effect of X_3 Vs f for Variation in C_2 : Input Amplitude of 1.25 cm (0.5 in).

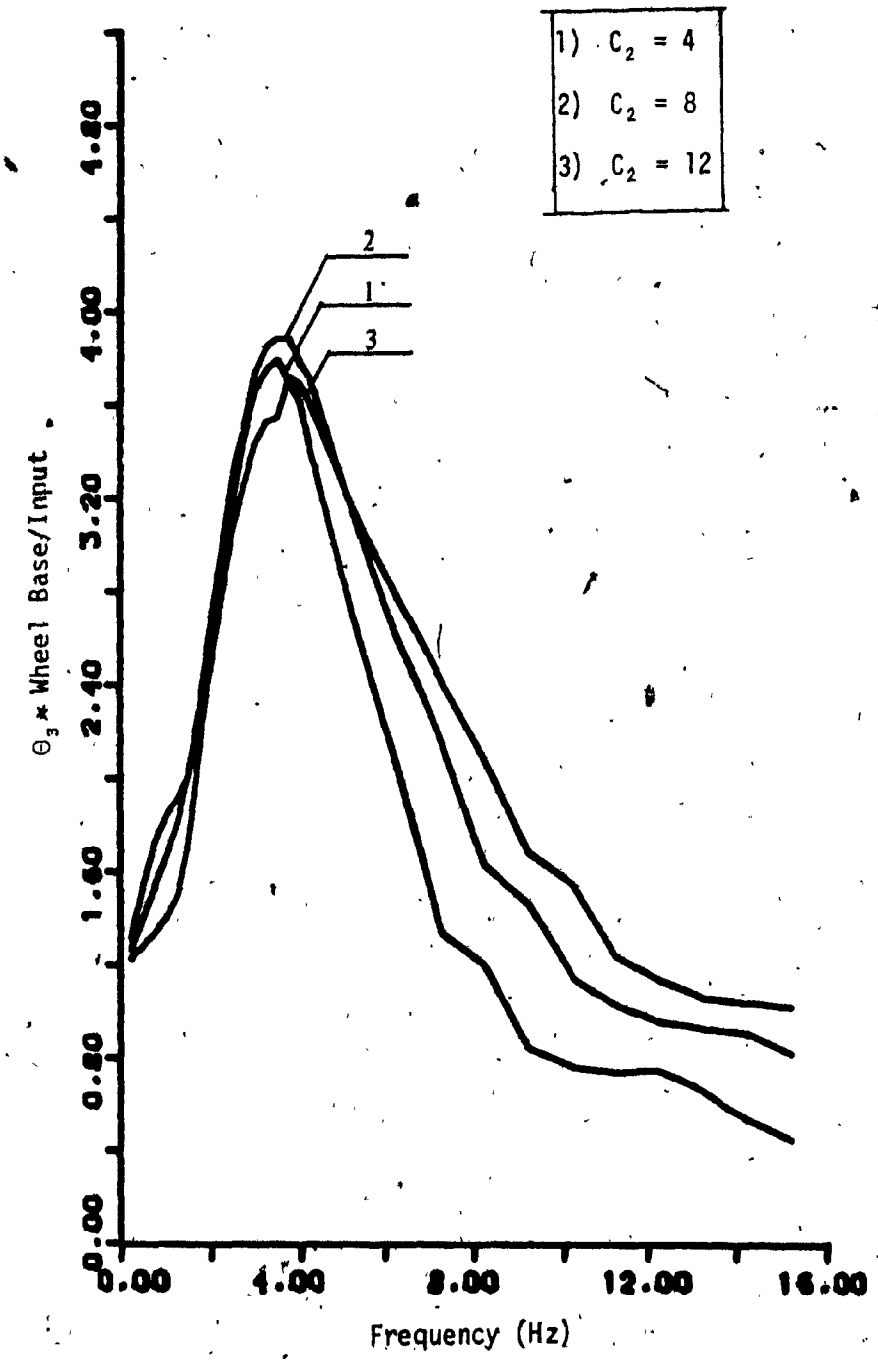

Figure 3,10: Effect of θ_3 Vs f for Variation in C_2: Input Amplitude of 1.25 cm (0.5 in).

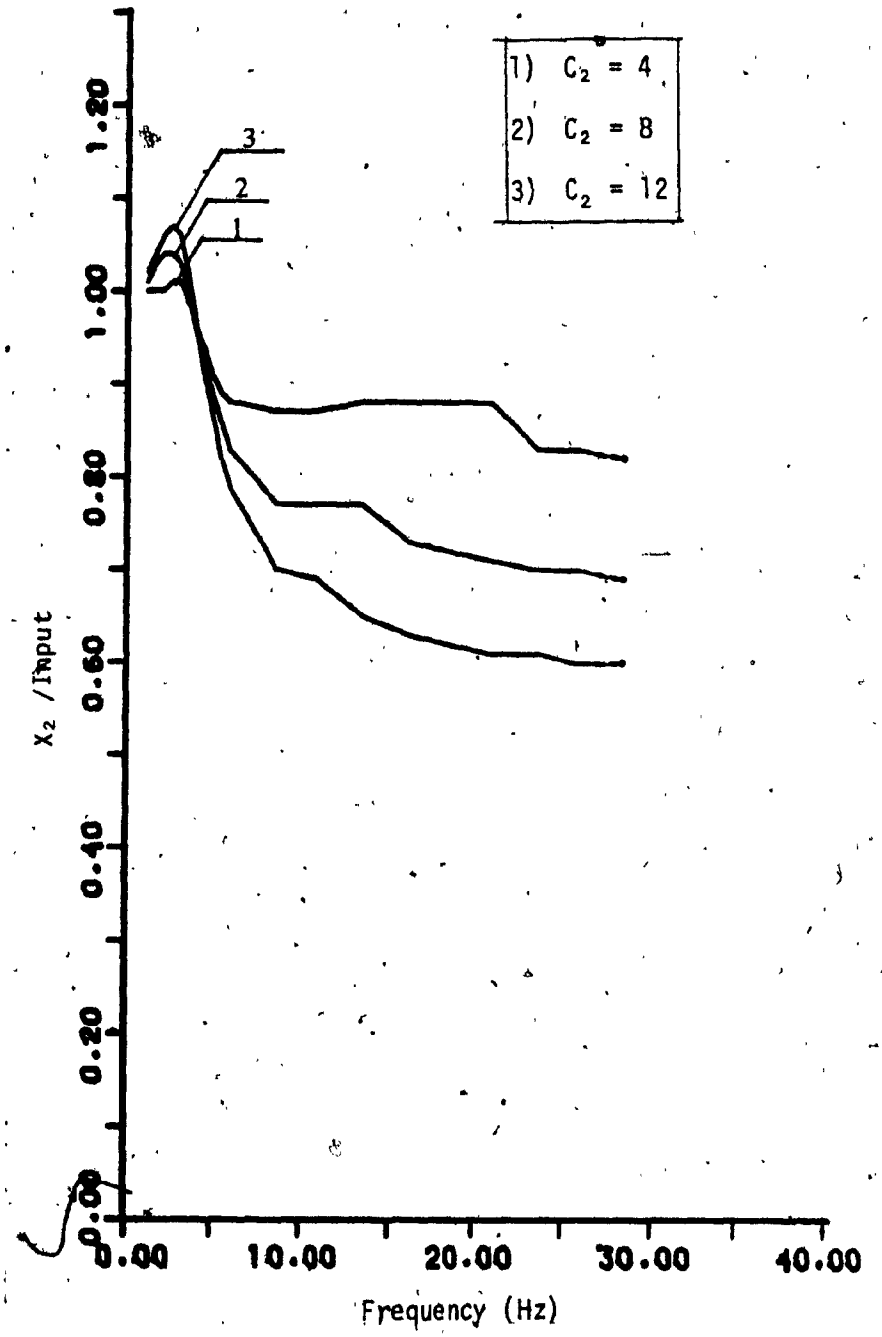

Figure 3.11; Effect of X_2 Vs f for Variation in C_2: Input Amplitude of 1.25 cm (0.5 in).

Figure 3.12 shows the $\ddot{X}_3$ transmissibility plots for variation in C_2. The results show considerable variation with peak transmissibility values decreasing with increase of C_2.

3.3.2 Front Fork Stiffness Variation (K_2)

Increasing the front fork stiffness decreases both the X_3 and θ_3 transmissibilities at resonance (Fig. 3.13 and 3.14). K_2 variation does not affect X_2, X_4 and $\ddot{X}_3$ responses.

3.3.3 Rear Shock Absorber Damping Variation (C_3)

Increasing the rear shock absorber damping decreases the X_3 transmissibility at resonance and increases away from the resonance (Fig. 3.15). Case 3 in that figure illustrates a overdamped system. By increasing the rear shock absorber damping, the θ_3 transmissibility decreases (Fig. 3.16). C_3 variation does not affect X_2 response. Increasing the rear shock absorber damping causes the X_4 transmissibility (Fig. 3.17) to be about the same at resonance and decreases away from the resonance. The $\ddot{X}_3$ transmissibility shown in Fig. 3.18 illustrates a decreasing peak transmissibility with decreasing C_3.

3.3.4 Rear Shock Stiffness Variation (K_3)

Increasing the rear shock stiffness increases both the X_3 and θ_3 transmissibilities at resonance (Fig. 3.19 and 3.20). Variation of K_3 does not affect X_2 and X_4 and $\ddot{X}_3$ responses.

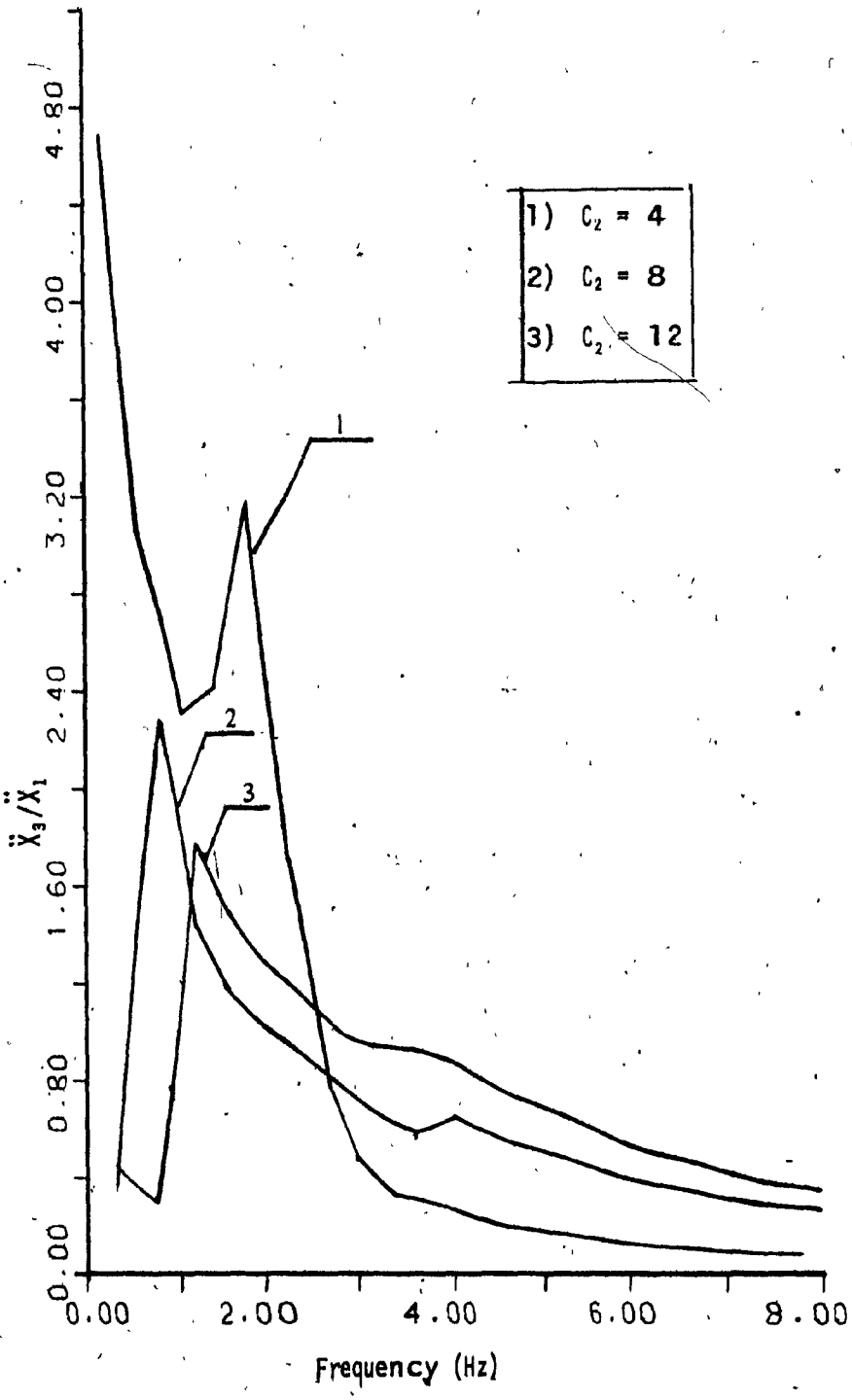

Figure 3.12: Effect of $\ddot{X}_3$ Vs f for Variation in C_2: Input Amplitude of 1.25 cm (0.5 in).

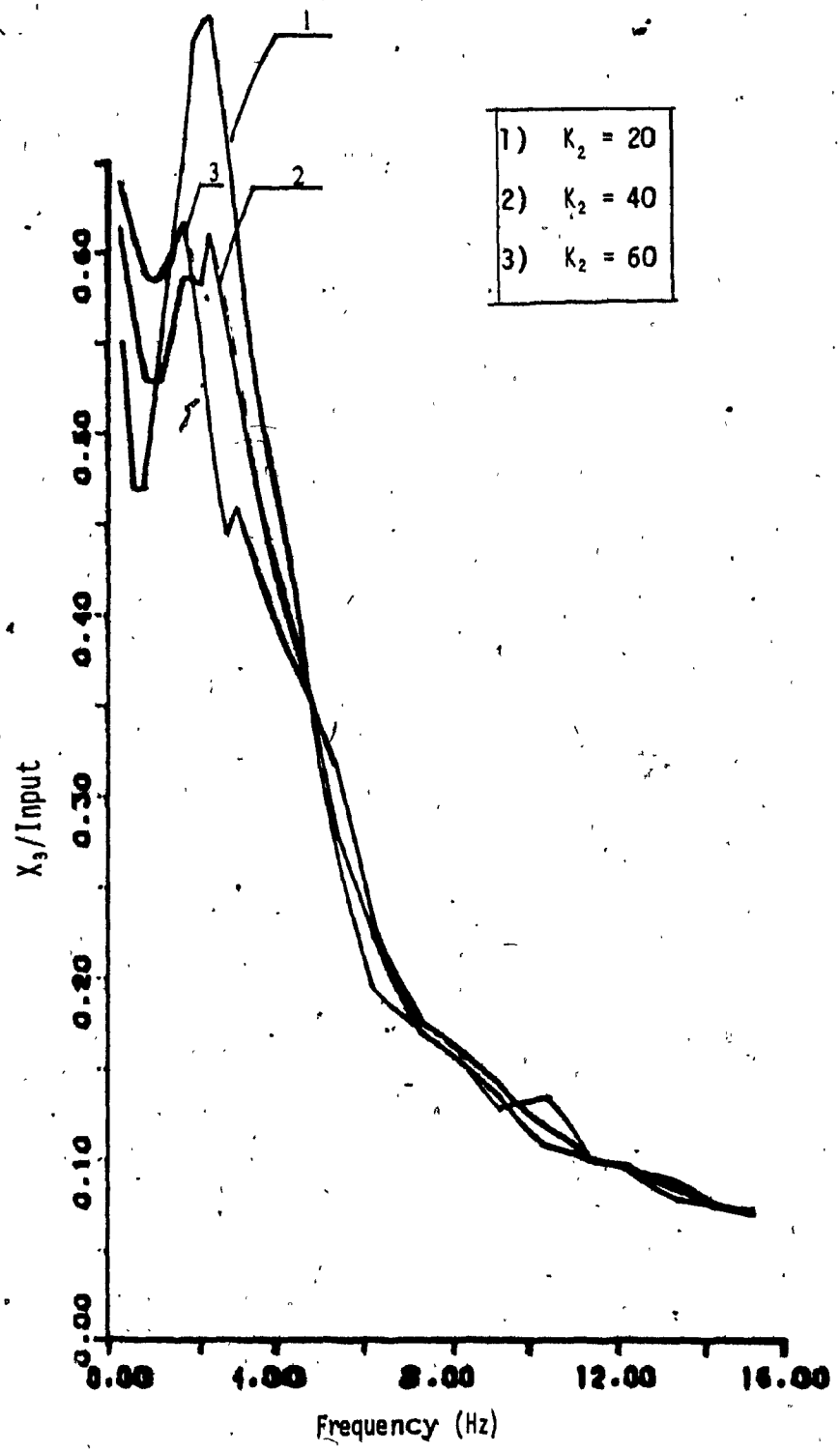

Figure 3.13: Effect of X_3 Vs f for Variation in K_2: Input Amplitude of 1.25 cm (0.5 in).

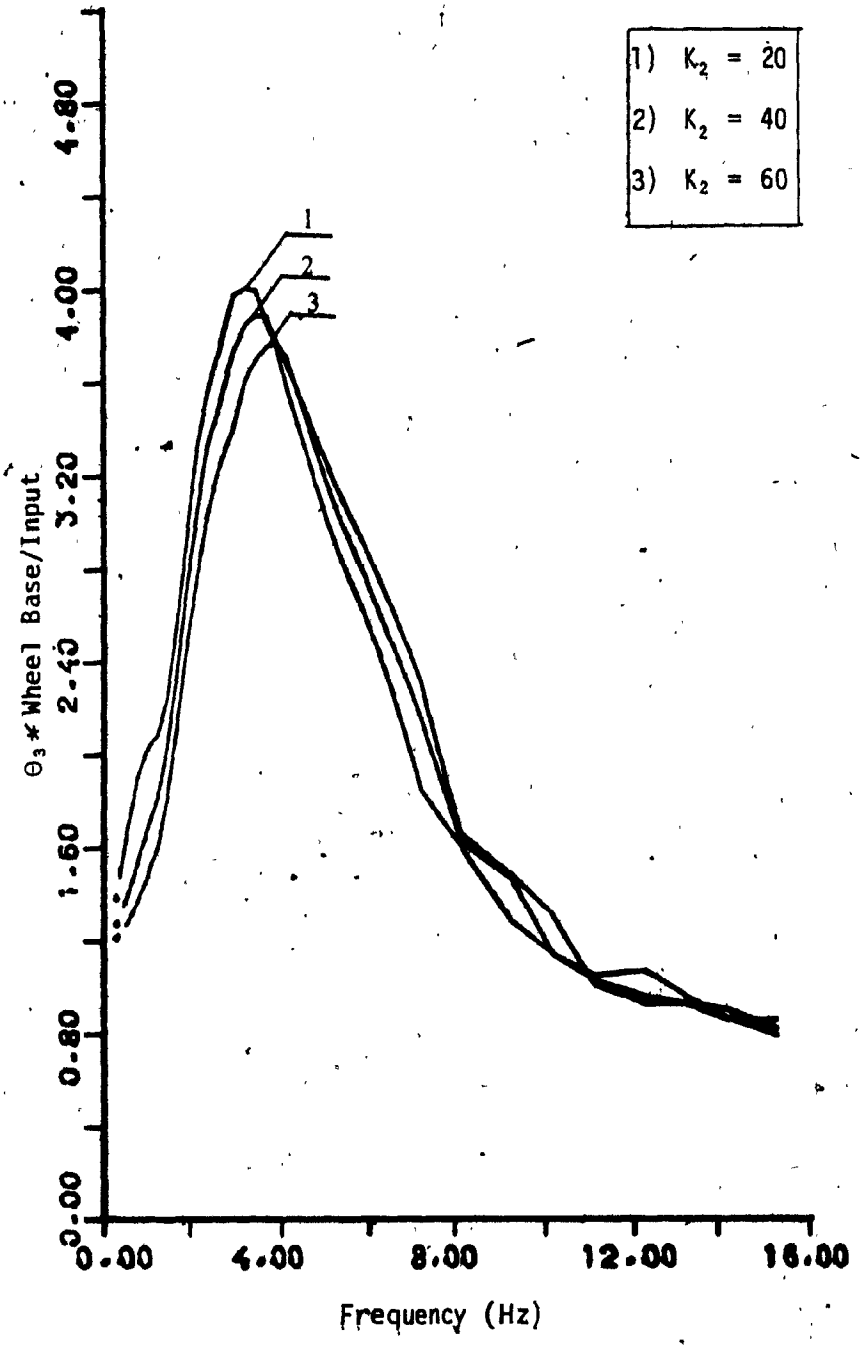

Figure 3.14: Effect of θ_3 Vs f for Variation in K_2: Input Amplitude of 1.25 cm (0.5 in).

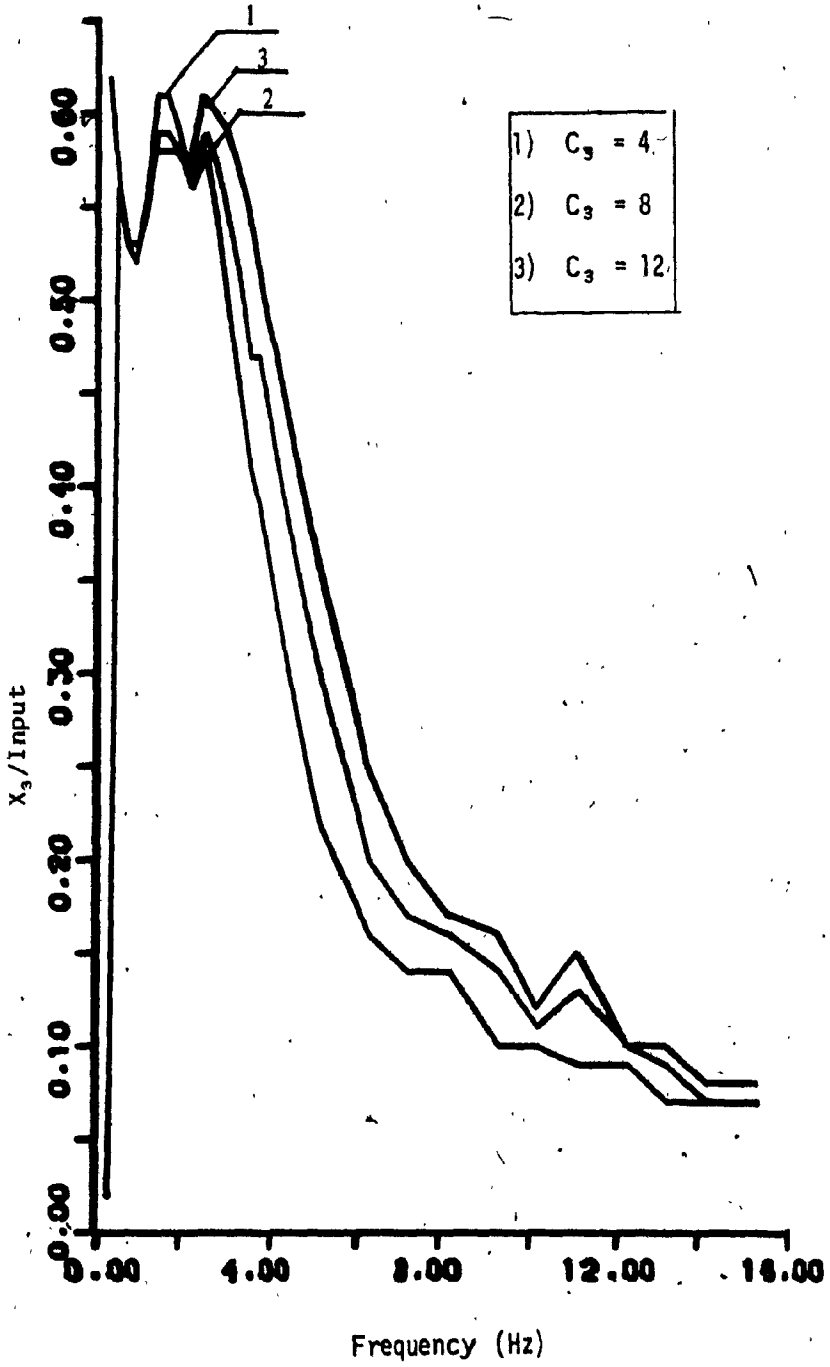

Figure 3.15: Effect of X_3 Vs f for Variation in C_3: Input Amplitude of 1.25 cm (0.5 in).

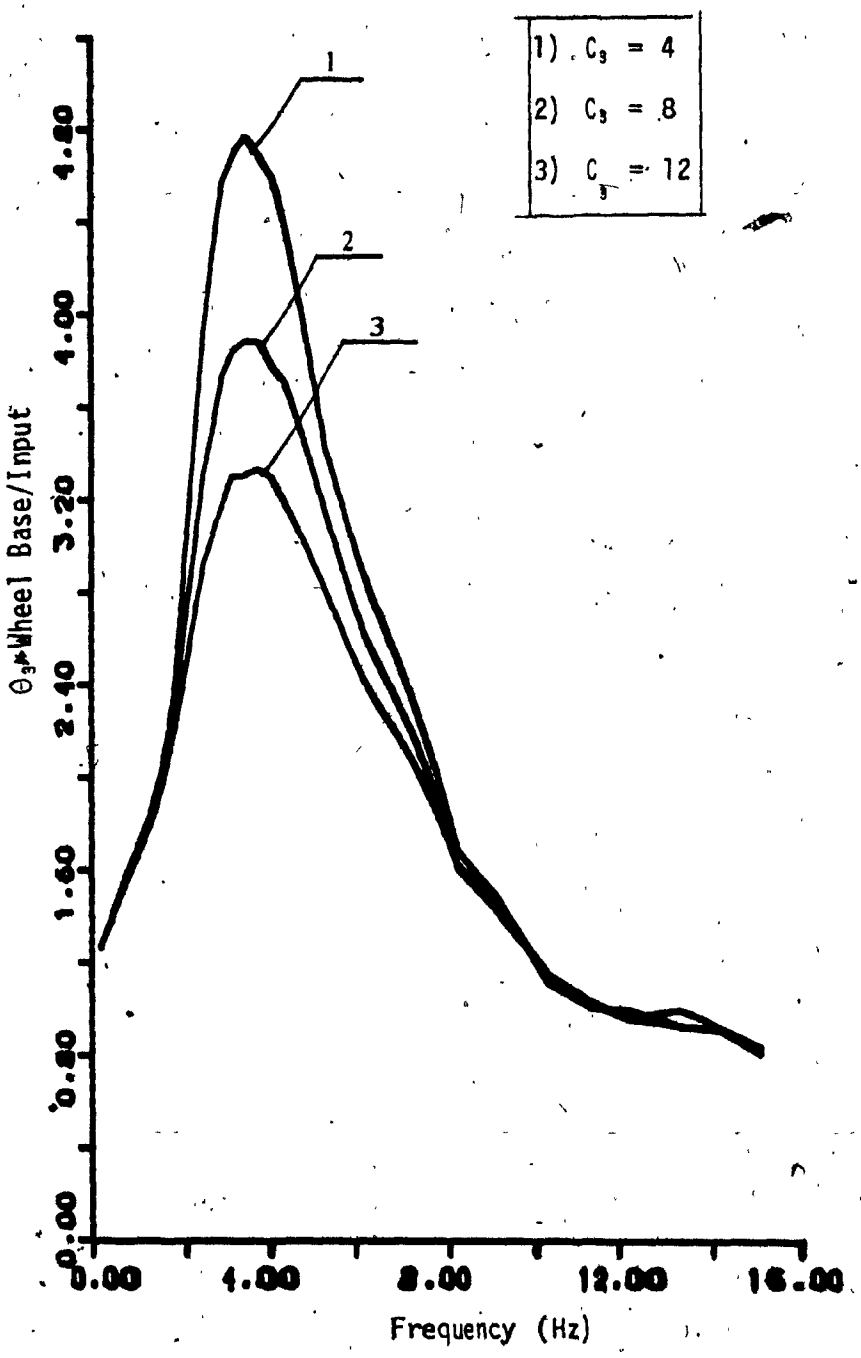

Figure 3.16: Effect of θ_3 Vs f for Variation in C_3: Input Amplitude of 1.25 cm (0.5 in).

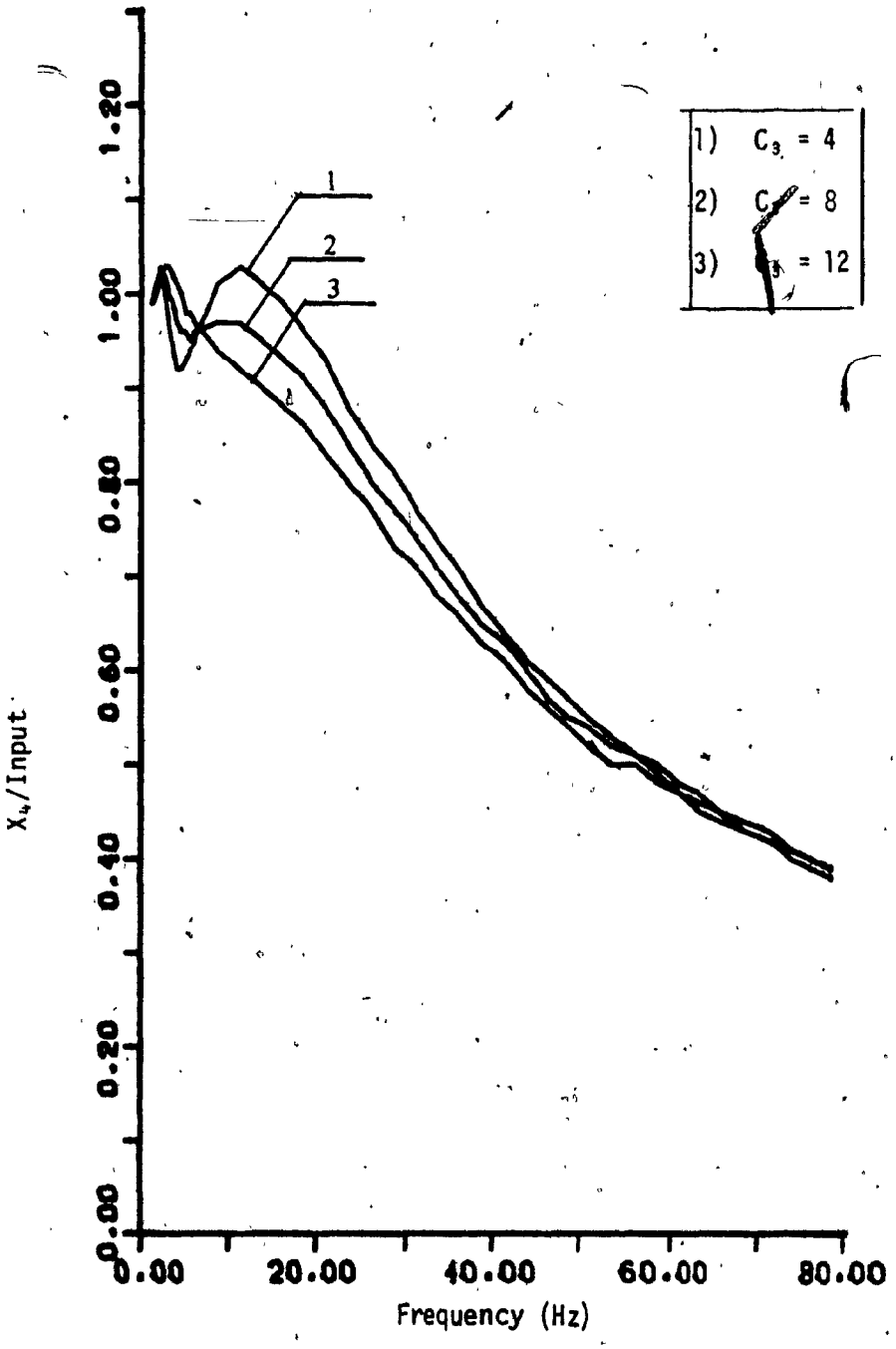

Figure 3.17: Effect of X_4 Vs f for Variation in C_3: Input Amplitude of 1.25 cm (0.5 in).

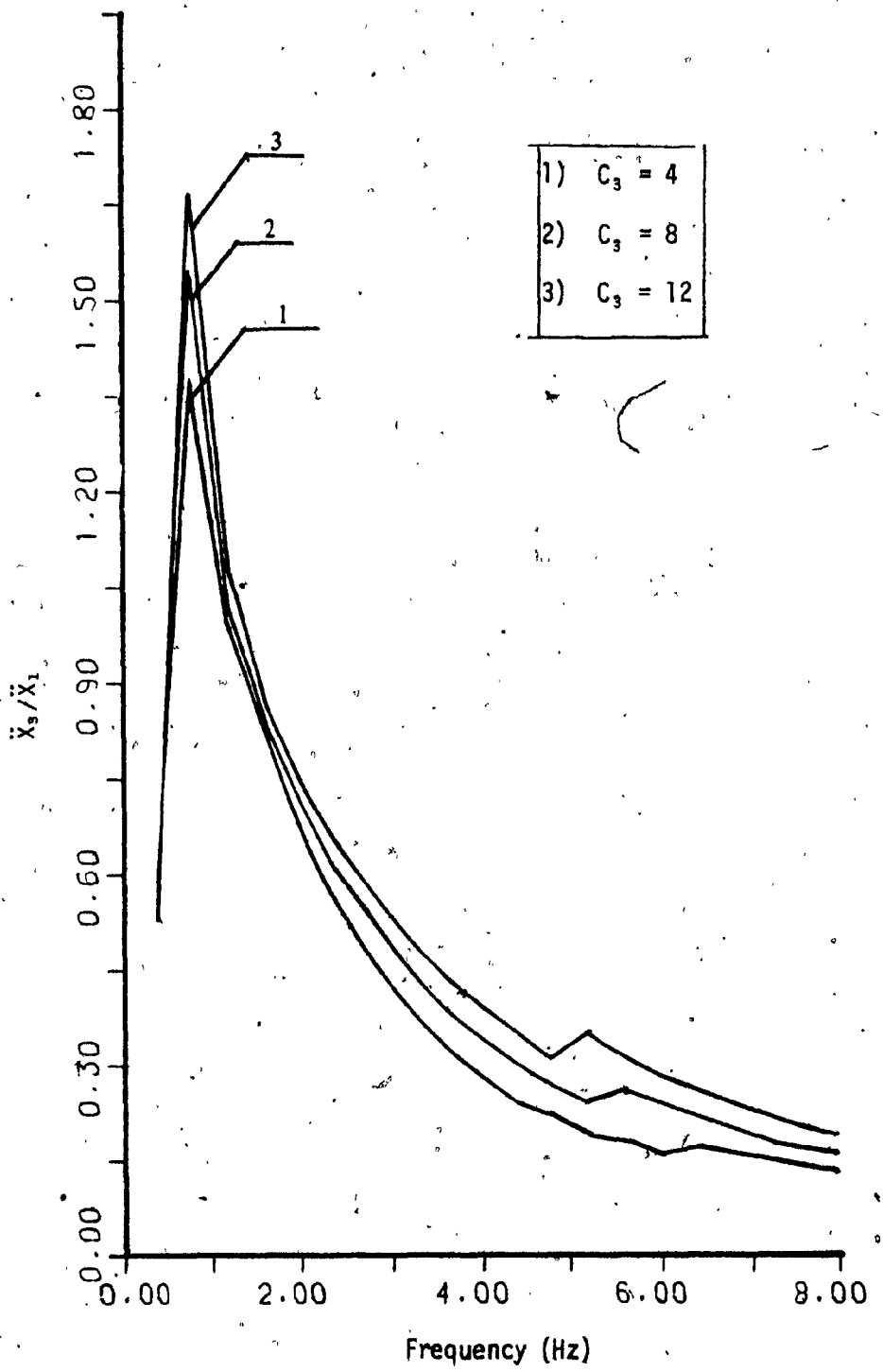

Figure 3.18: Effect of $\ddot{X}_3$ Vs f for Variation in C_3: Input Amplitude of 1.25 cm (0.5 in).

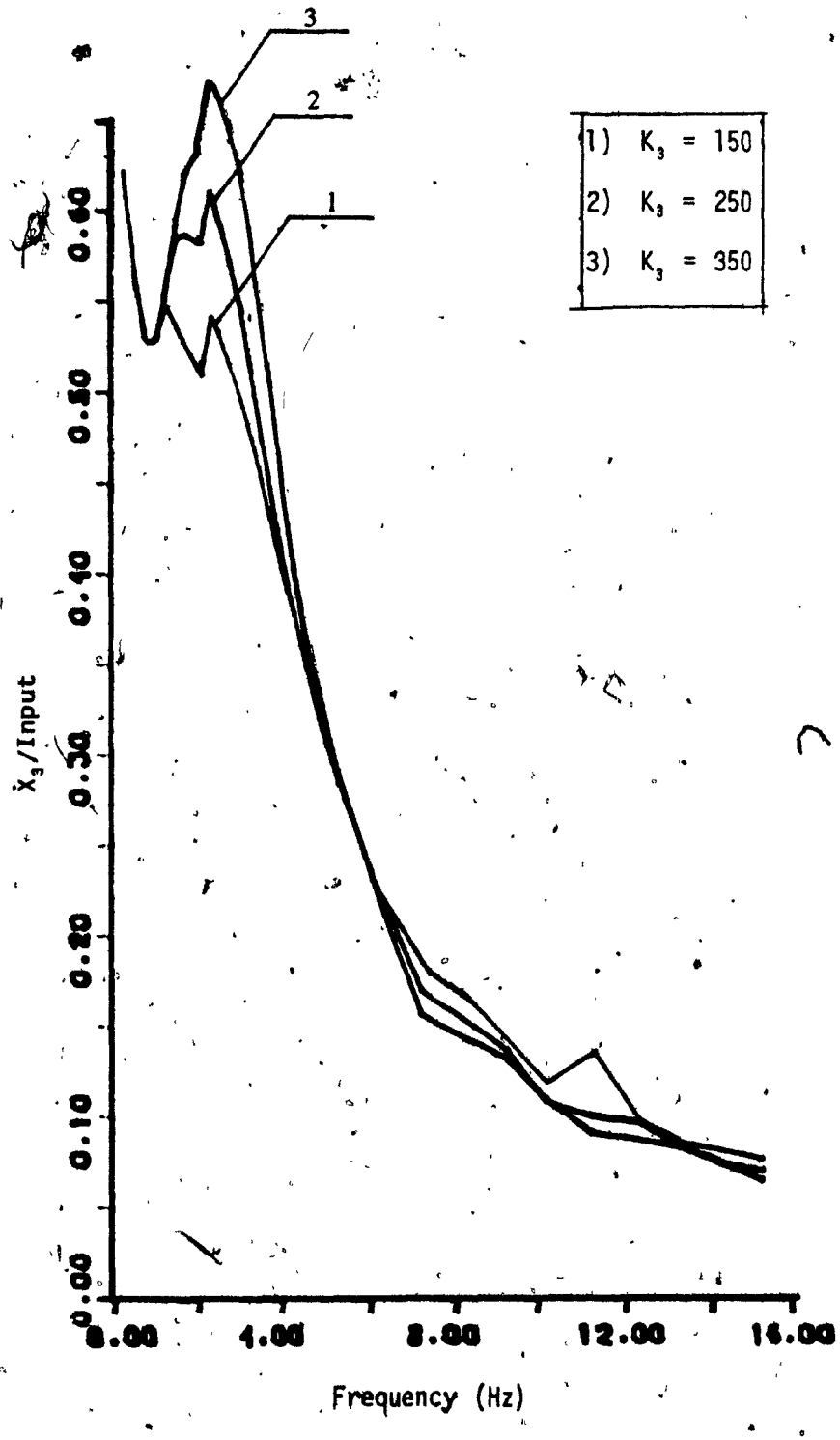

Figure 3.19: Effect of X_3 Vs f for Variation in K_3: Input Amplitude of 1.25 cm (0.5 in).

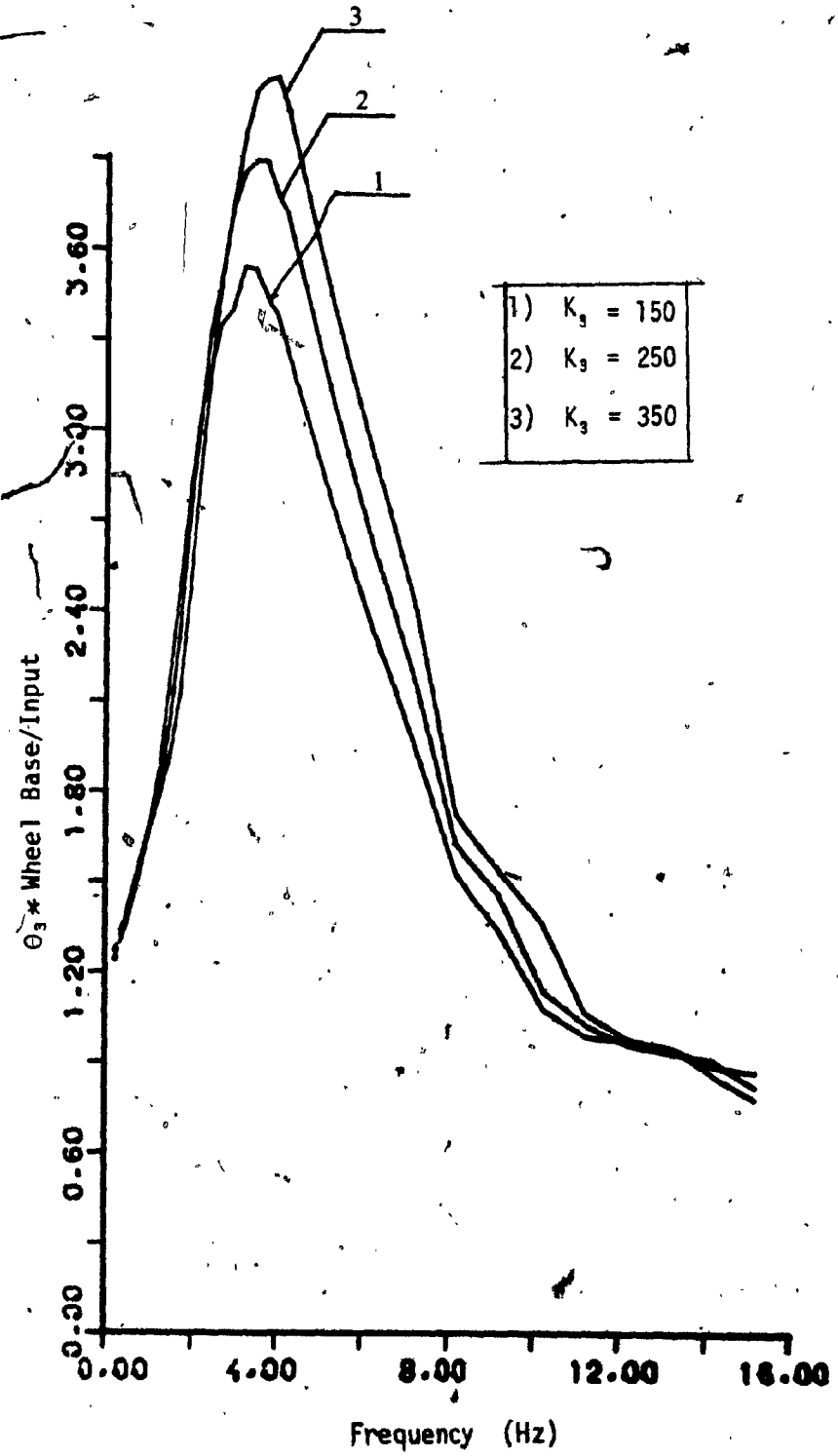

Figure 3.20: Effect of θ_3 Vs f for Variation in K_s: Input Amplitude of 1.25 cm (0.5 in).

3.4 Mass Variation

3.4.1 Front and Rear Wheel Mass Variation (M_2, M_4)

Variation of M_2 and M_4 has very little influence on X_3 transmissibilities (Fig. 3.21 and 3.22) and Θ_3 transmissibilities (Fig. 3.23 and 3.24). X_2 is not affected at all by variation in M_2 or M_4. Only X_4 shows the significant effect. Increasing the rear wheel mass gives the X_4 transmissibility about the same at resonance and decreases away from the resonance (Fig. 3.25). The results of M_2 and M_4 variation on $\ddot{X}_3$ transmissibility shown in Fig. 3.26 and 3.27 illustrates their insignificant influence.

3.4.2 Motorcycle Mass Variation (M_3, J_3)

Increasing the mass of the bike and the rider decreases the X_3 transmissibility away from the resonance (Fig. 3.28).

At resonance, by increasing the mass, the peak X_3 transmissibility initially decreases and then increases. It can also be seen that the natural frequency of the bounce oscillation is lowered as M_3 is increased. Increasing the rotational inertia of the motorcycle frame increases the X_3 transmissibility at resonance (Fig. 3.29). Increasing M_3 causes increase in Θ_3 response at resonance (Fig. 3.30). Increasing J_3 causes increase in Θ_3 response at resonance and [illegible] pitching resonant frequency is lowered (Fig. 3.31). Response of [illegible] and X_4 is not affected by variation of M_3 and J_3.

In Fig. 3.32, the $\ddot{X}_3$ transmissibility shows that the peak value decreases initially and then increases as the value of M_3 increases. However at high frequencies, increasing value of M_3 decreases the transmissibility.

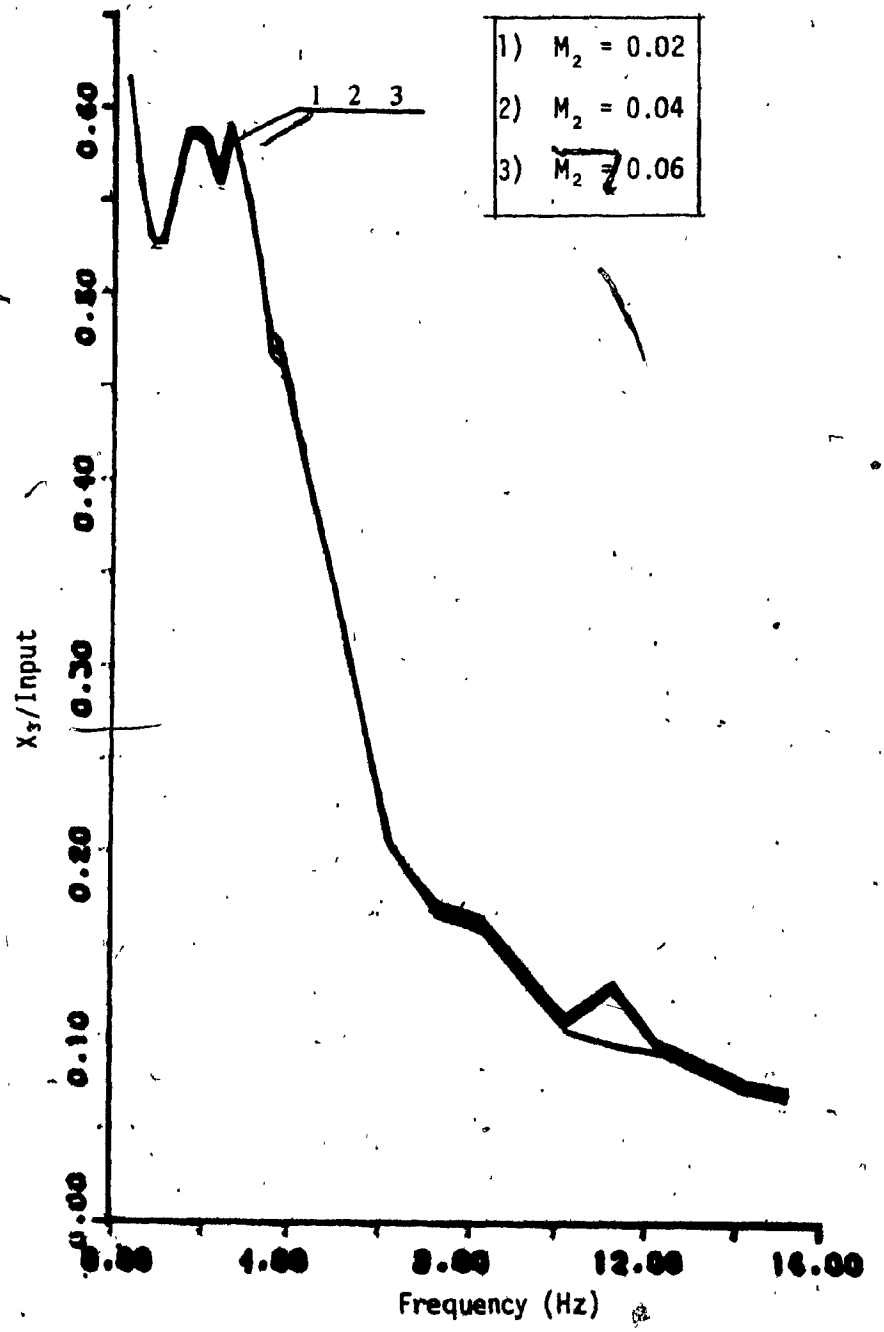

Figure 3.21: Effect of θ_3 Vs f for Variation in M_2: Input Amplitude of 1.25 cm (0.5 in).

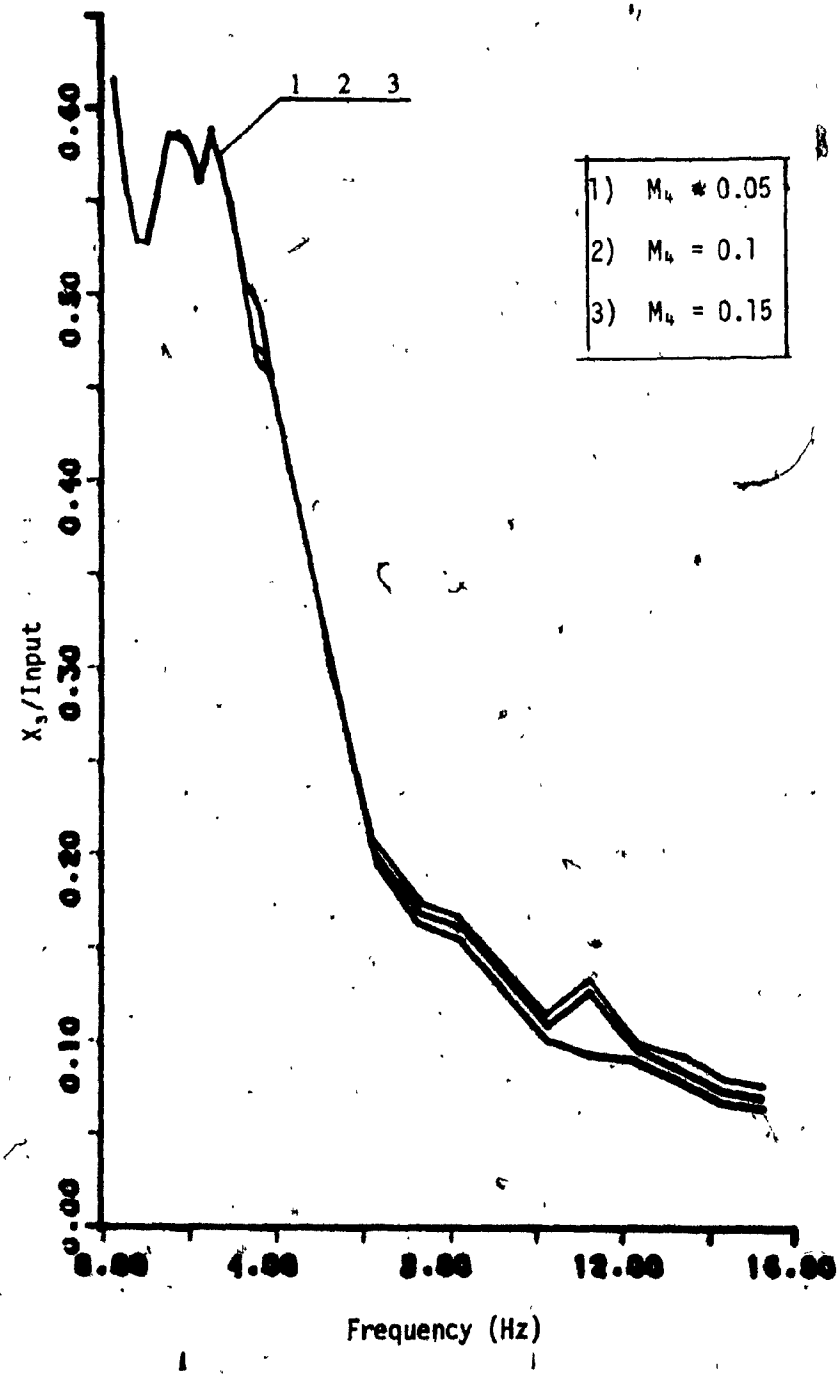

Figure 3.22: Effect of θ_3 Vs f for Variation in M_4 : Input Amplitude of 1.25 cm (0.5 in).

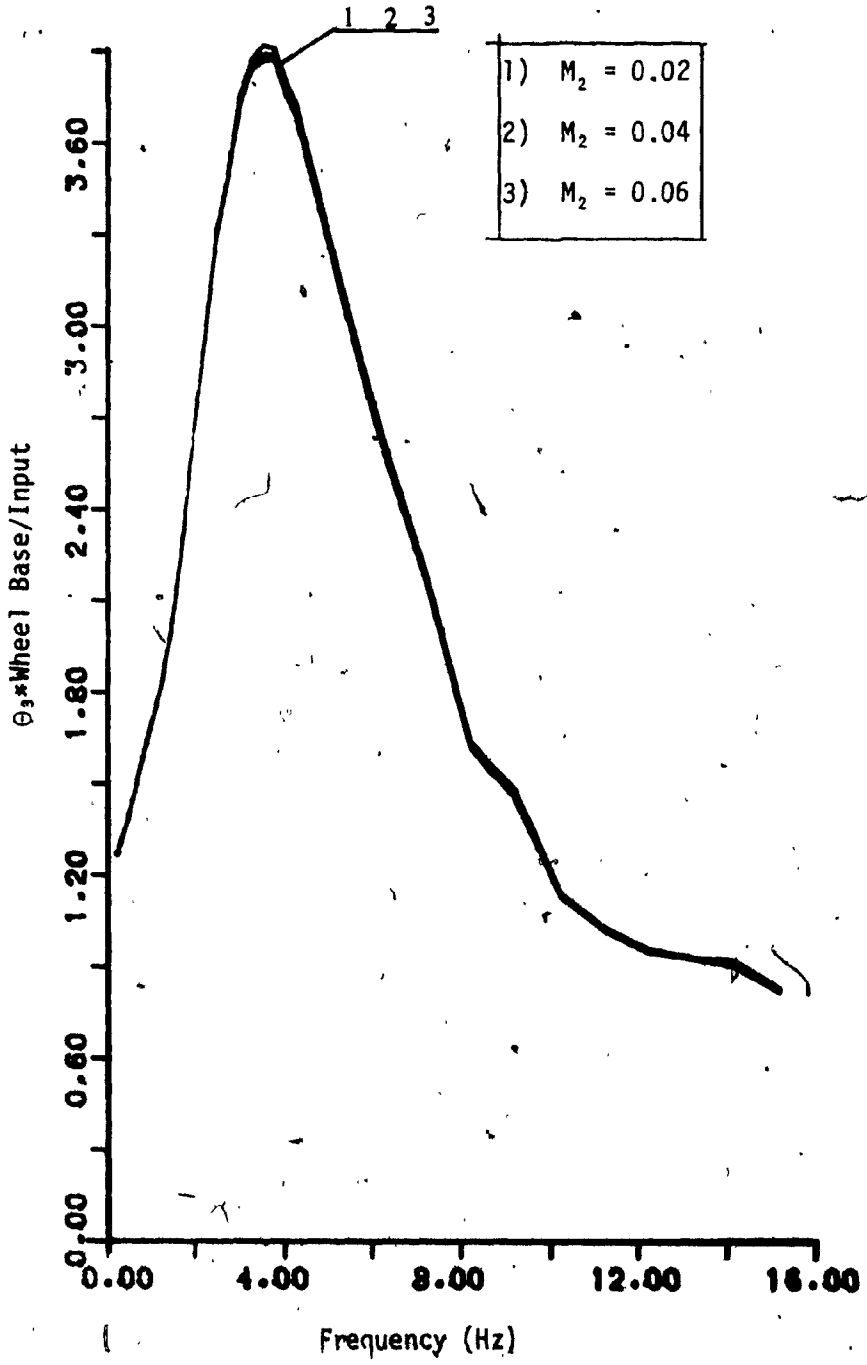

Figure 3.23: Effect of θ_3 Vs f for Variation in M_2 : Input Amplitude of 1.25 cm (0.5 in).

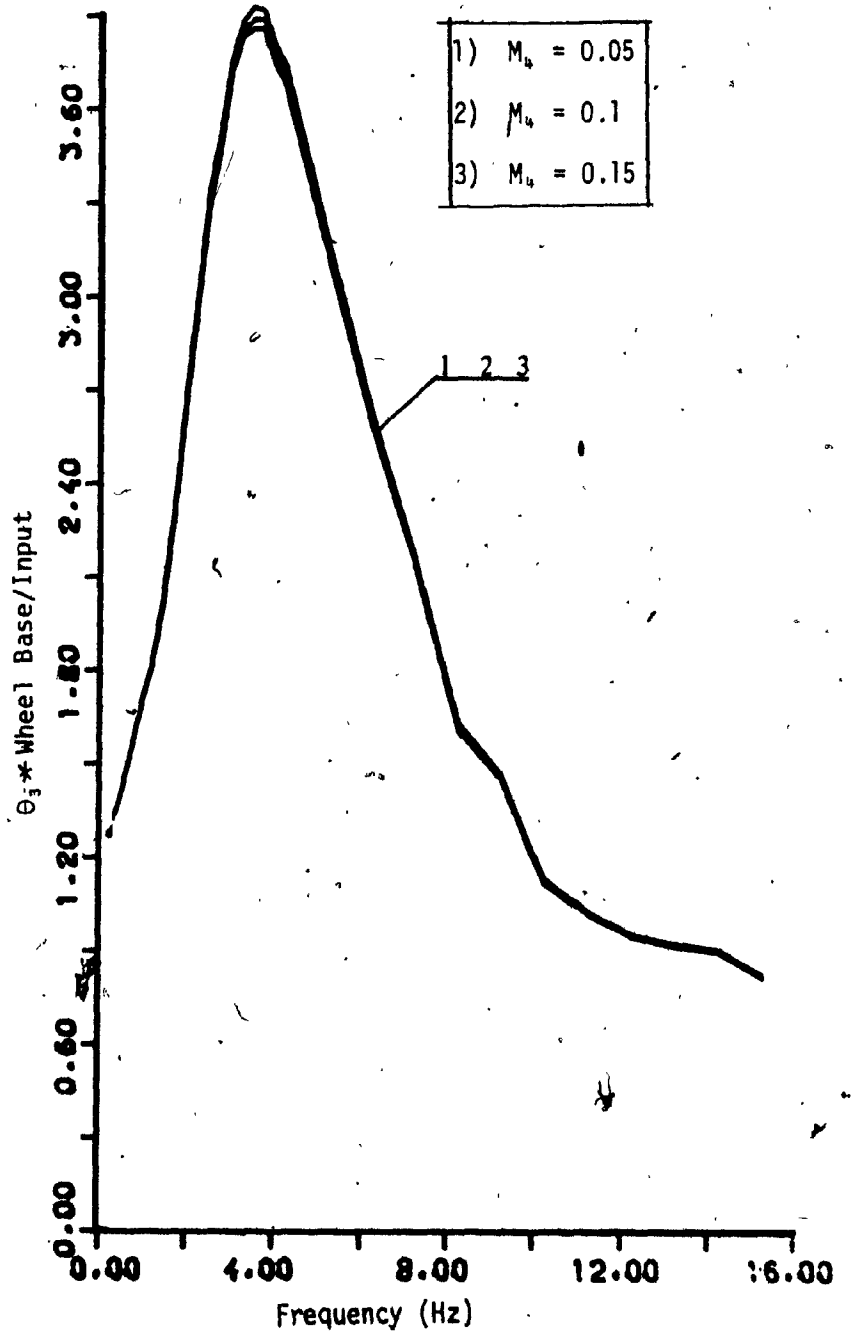

Figure 3.24: Effect of Θ_3 Vs f for Variation in M_4: Input Amplitude of 1.25 cm (0.5 in).

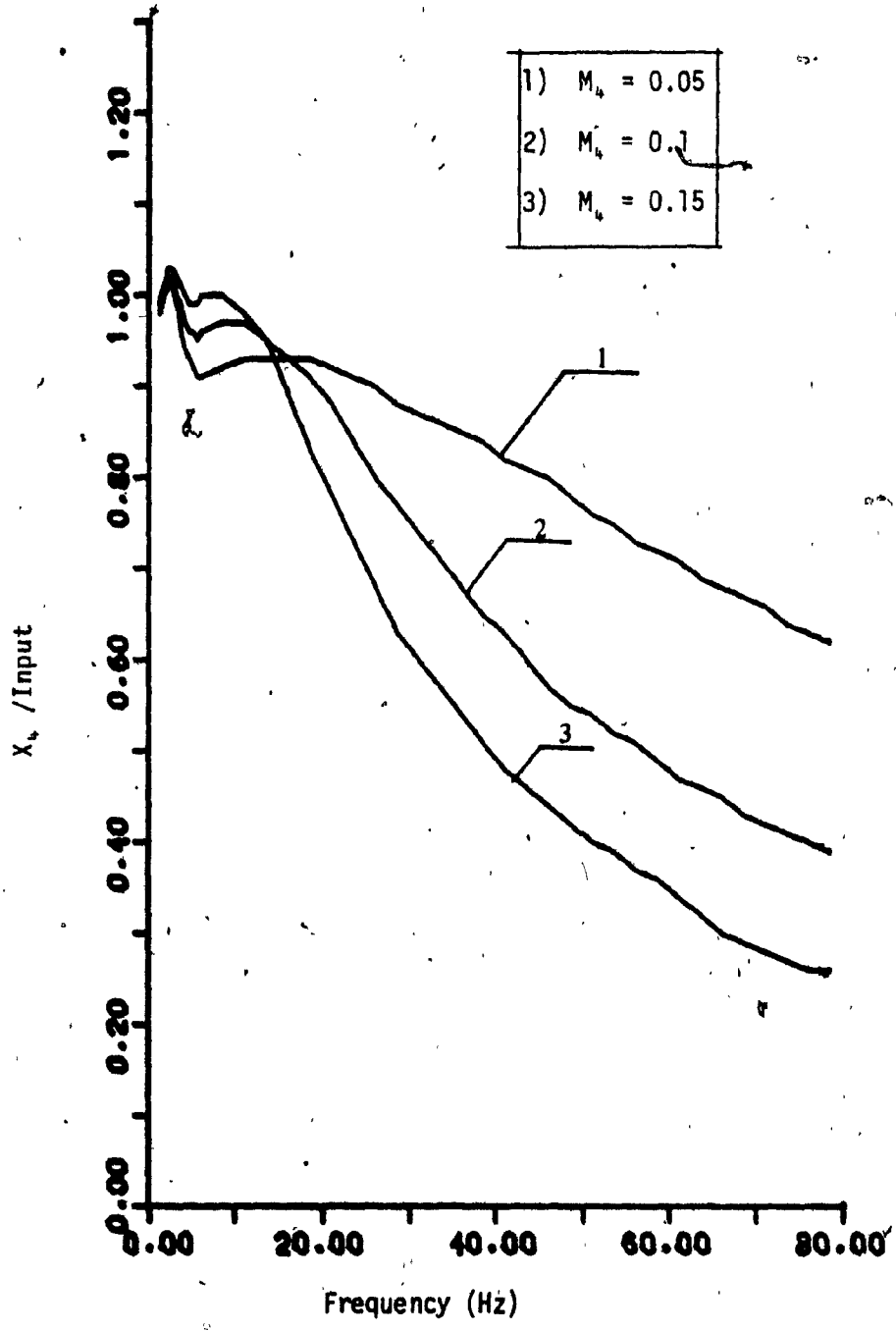

Figure 3.25: Effect of X_4 Vs f for Variation in M_4 : Input Amplitude of 1.25 cm (0.5 in).

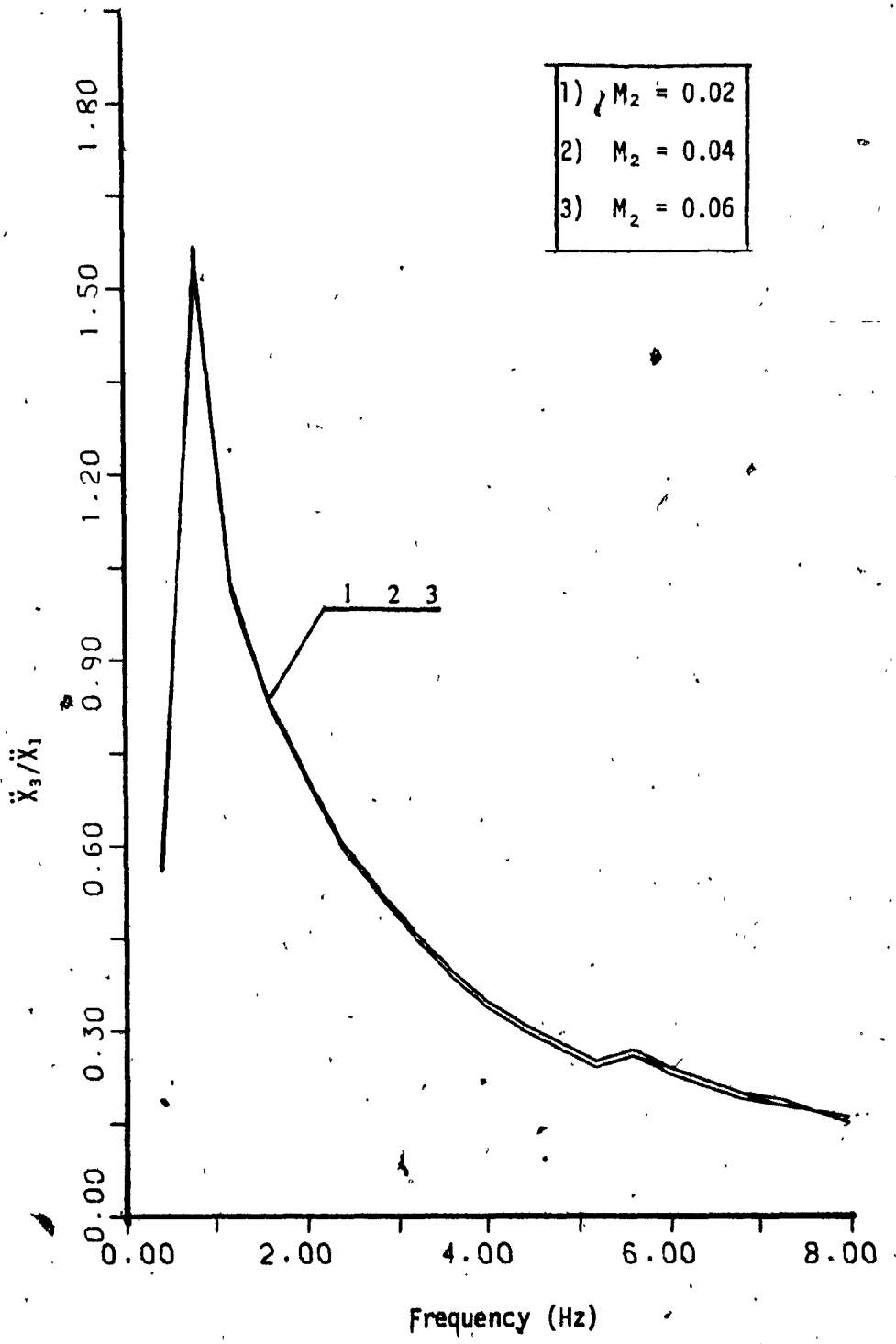

Figure 3.26: Effect of $\ddot{X}_3$ Vs f for Variation in M_2: Input Amplitude of 1.25 cm (0.5 in).

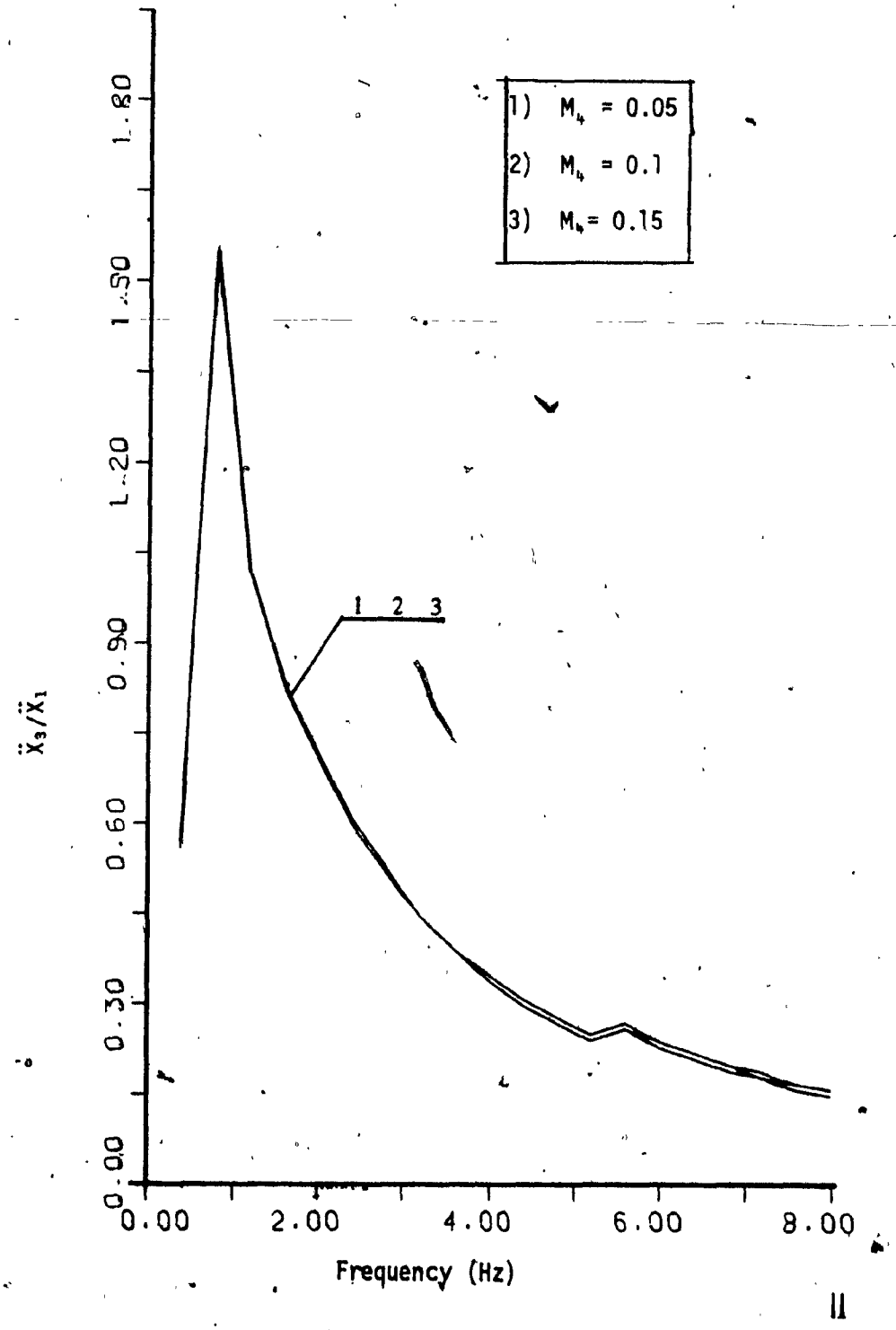

Figure 3.27: Effect of $\ddot{X}_3$ Vs f for Variation in M_4 : Input Amplitude of 1.25 cm (0.5 in).

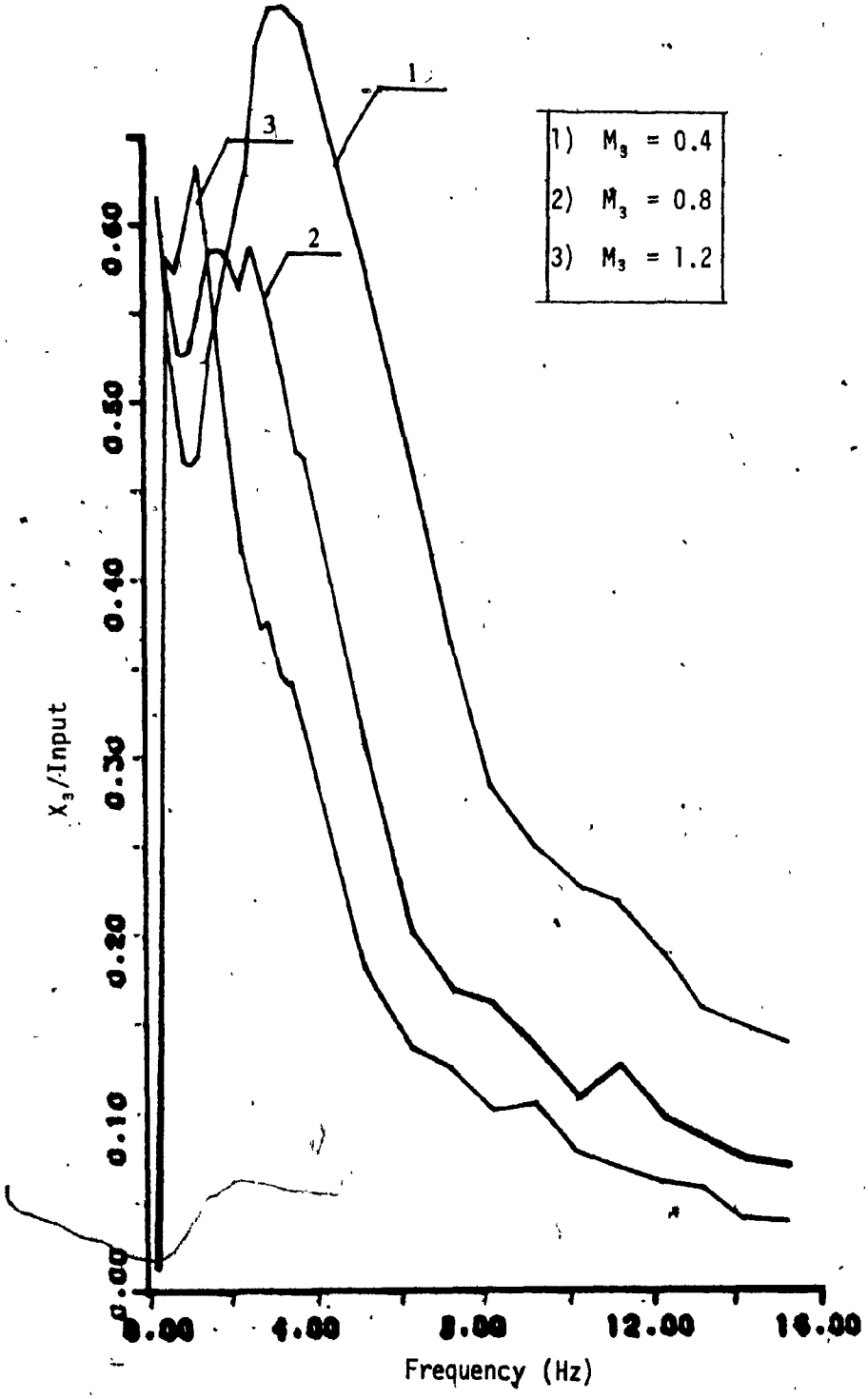

Figure 3.28: Effect of X_3 Vs f for Variation in M_3 : Input Amplitude of 1.25 cm (0.5 in).

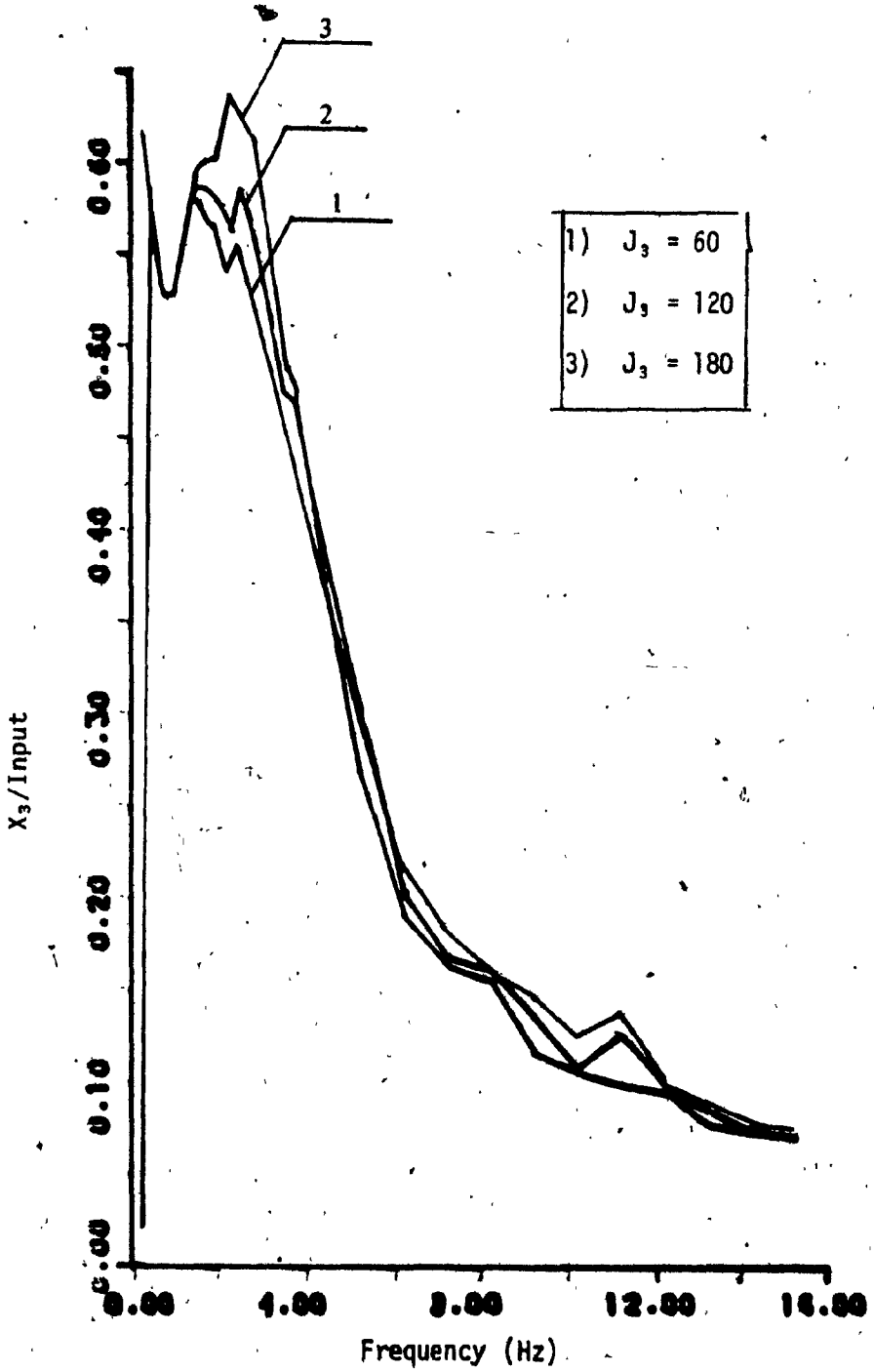

Figure 3.29: Effect of X_3 Vs f for Variation in J_3: Input Amplitude of 1.25 cm (0.5 in).

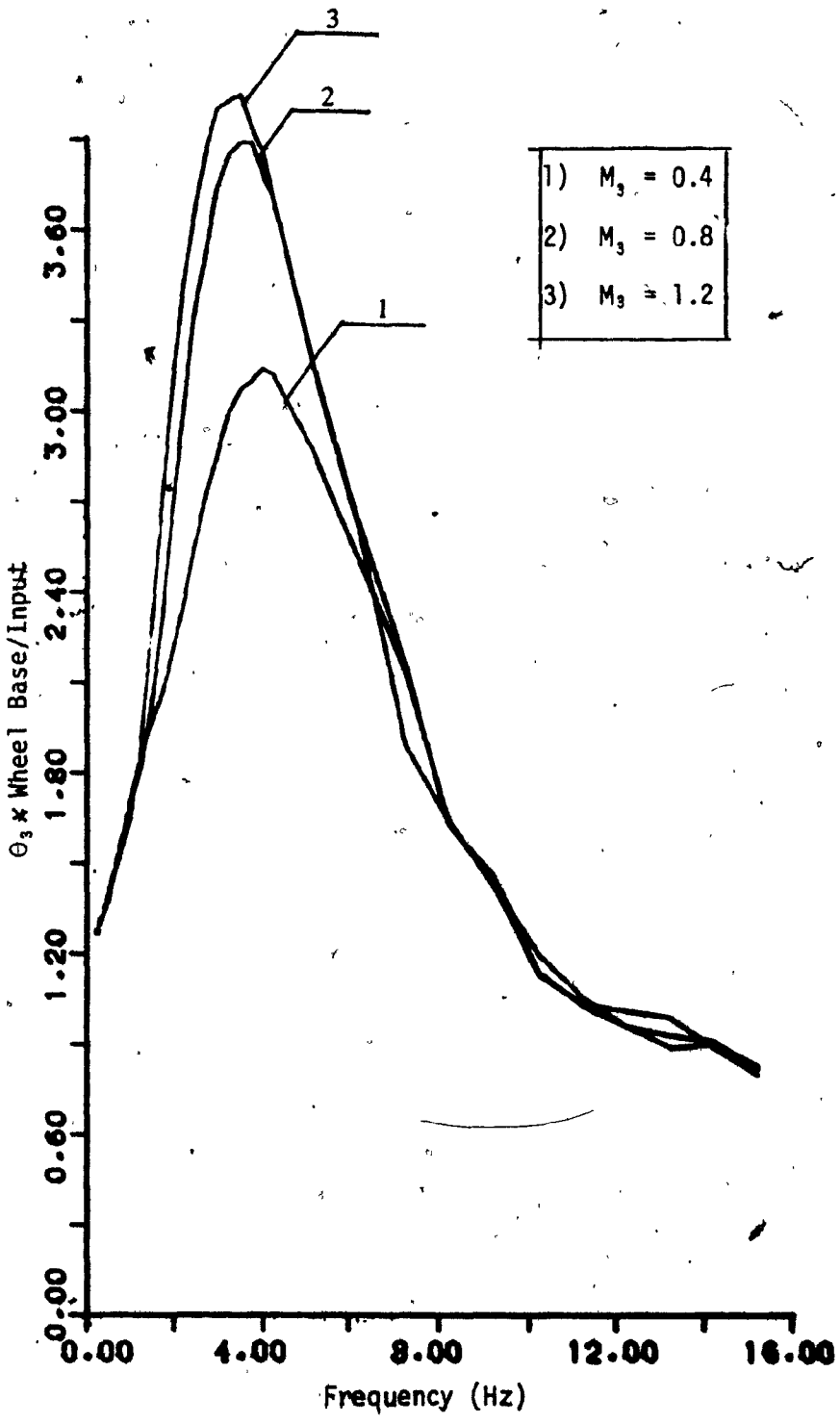

Figure 3.30 : Effect of Θ_3 Vs f for Variation in M_3: Input Amplitude of 1.25 cm (0.5 in).

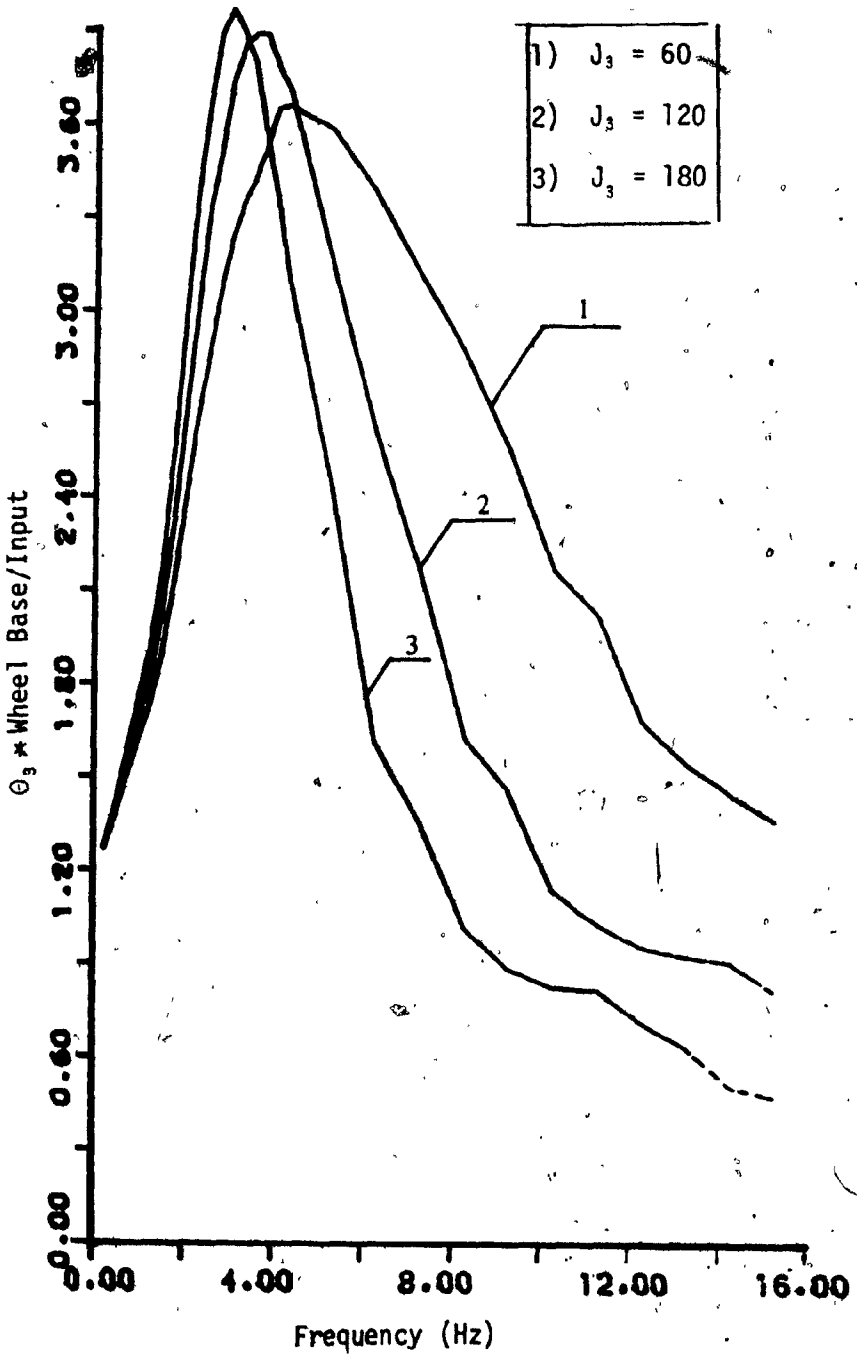

Figure 3.31: Effect of Θ_3 Vs f for Variation in J_3: Input Amplitude of 1.25 cm (0.5 in).

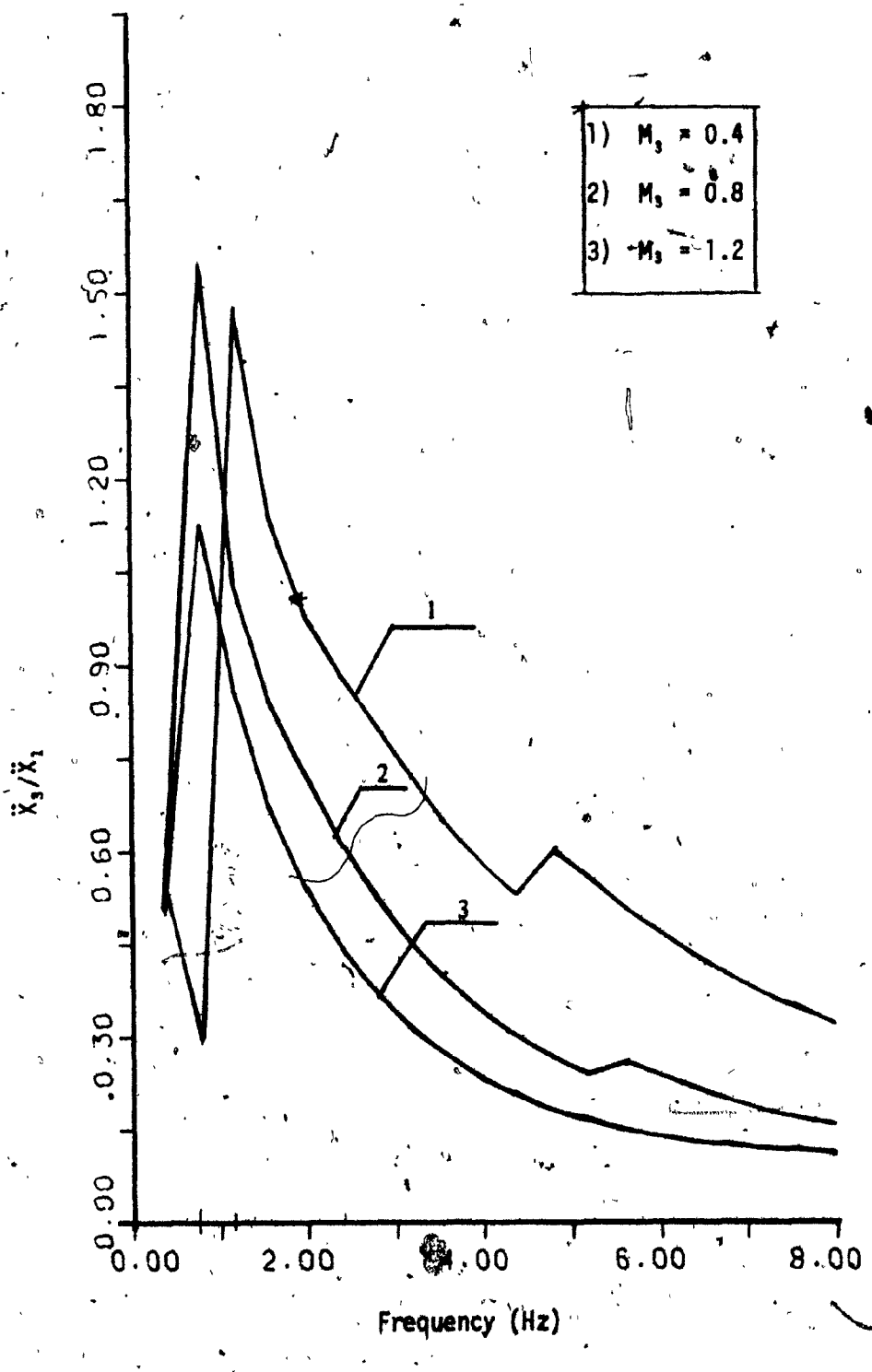

Figure 3.32: Effect of $\ddot{X}_3$ Vs f for Variation in M_3: Input Amplitude of 1.25 cm (0.5 in).

3.5 Road Amplitude Variation (X_0)

Variation of road amplitude has no effect on X_3, θ_3 , X_2, X_4, $\ddot{X}_3$ transmissibilities. The results are shown in Figs. 3.33 and 3.34

3.6 Geometric Variations (L_3, ϕ, L_6, α_6)

Increase in L_3, initially causes a decrease in X_3 transmissibilities at resonance, however, for larger values of L_3 (i.e. $L_3 = 20$), the X_3-TR starts to increase (Fig. 3.35). As it can be seen from Fig. 3.36, an increase in L_3 causes increase in θ_3 transmissibility. X_2 is not affected by the variation in L_3. X_4 transmissibility decreases with increase of L_3 (Fig. 3.37). Figure 3.38 illustrates that $\ddot{X}_3$-TR at resonance decreases with increase of L_3.

Increasing ϕ initially decreases X_3-TR at resonance (Fig. 3.39). For large ϕ values, however, the X_3-TR at resonance starts increasing. Increasing ϕ decreases θ_3-TR (Fig. 3.40). X_2 and X_4 are not affected by any change of ϕ. Figure 3.41 shows that $\ddot{X}_3$-TR decreases as ϕ value is increased. Increase in L_6 increases X_3-TR (Fig. 3.42) and θ_3-TR (Fig. 3.43). X_2 and X_4 are not affected by change of L_6. $\ddot{X}_3$-TR decreases slightly with increase in L_6 value (Fig. 3.44).

Increasing α_6 decreases X_3-TR at resonance at first and then increases as α_6 is further increased (Fig. 3.45). In the case of θ_3-TR, increasing α_6 increases the transmissibility value at resonance. However, for large value of α_6, peak θ_3-TR decreases (Fig. 3.46).

X_2 and X_4 are not affected by α_6 variation. As it can be seen from Fig. 3.47., $\ddot{X}_3$-TR at resonance decreases initially with α_6 increase and then increases for large value of α_6.

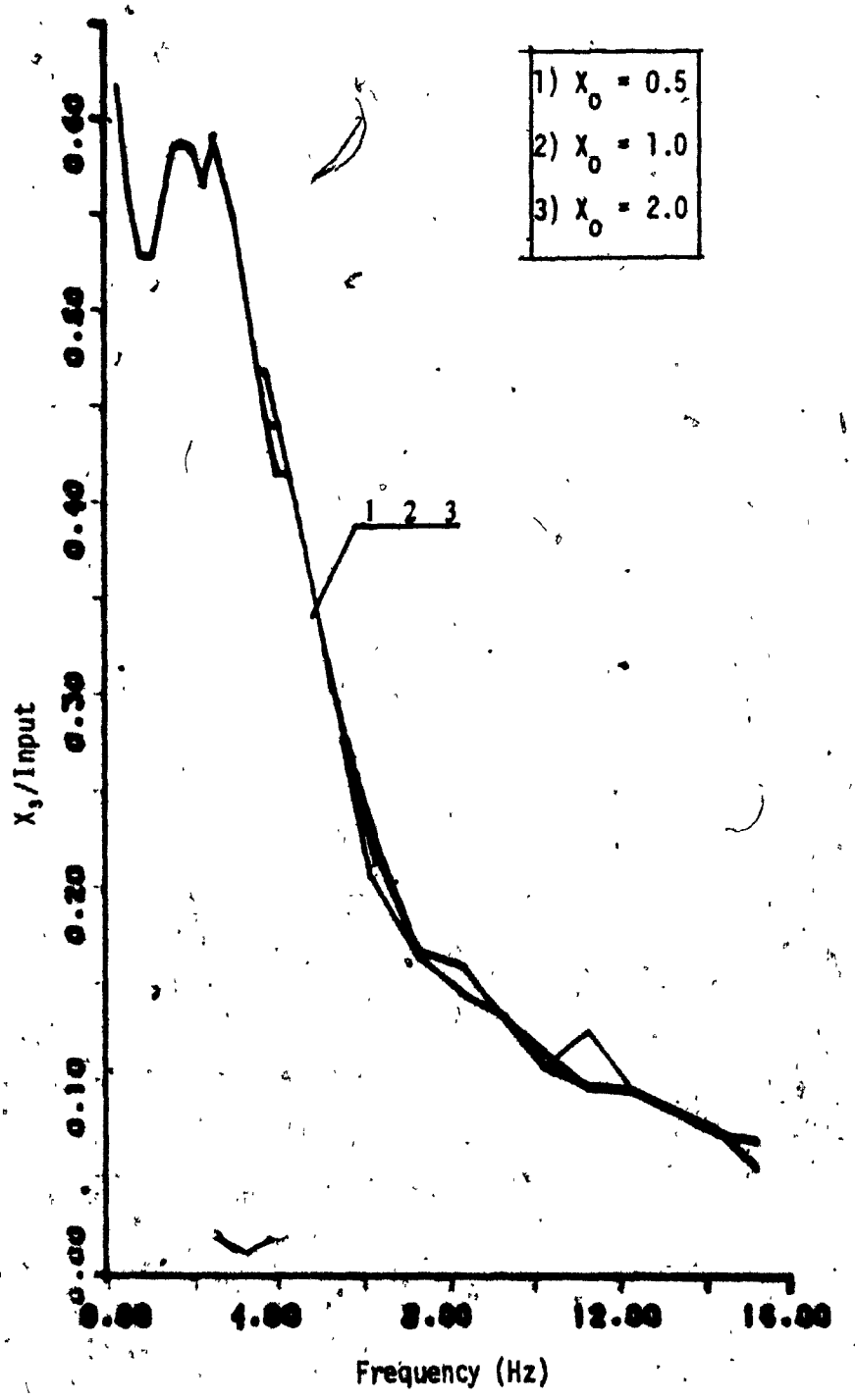

Figure 3.33: Effect of X_3 Vs f for Variation in X_0.

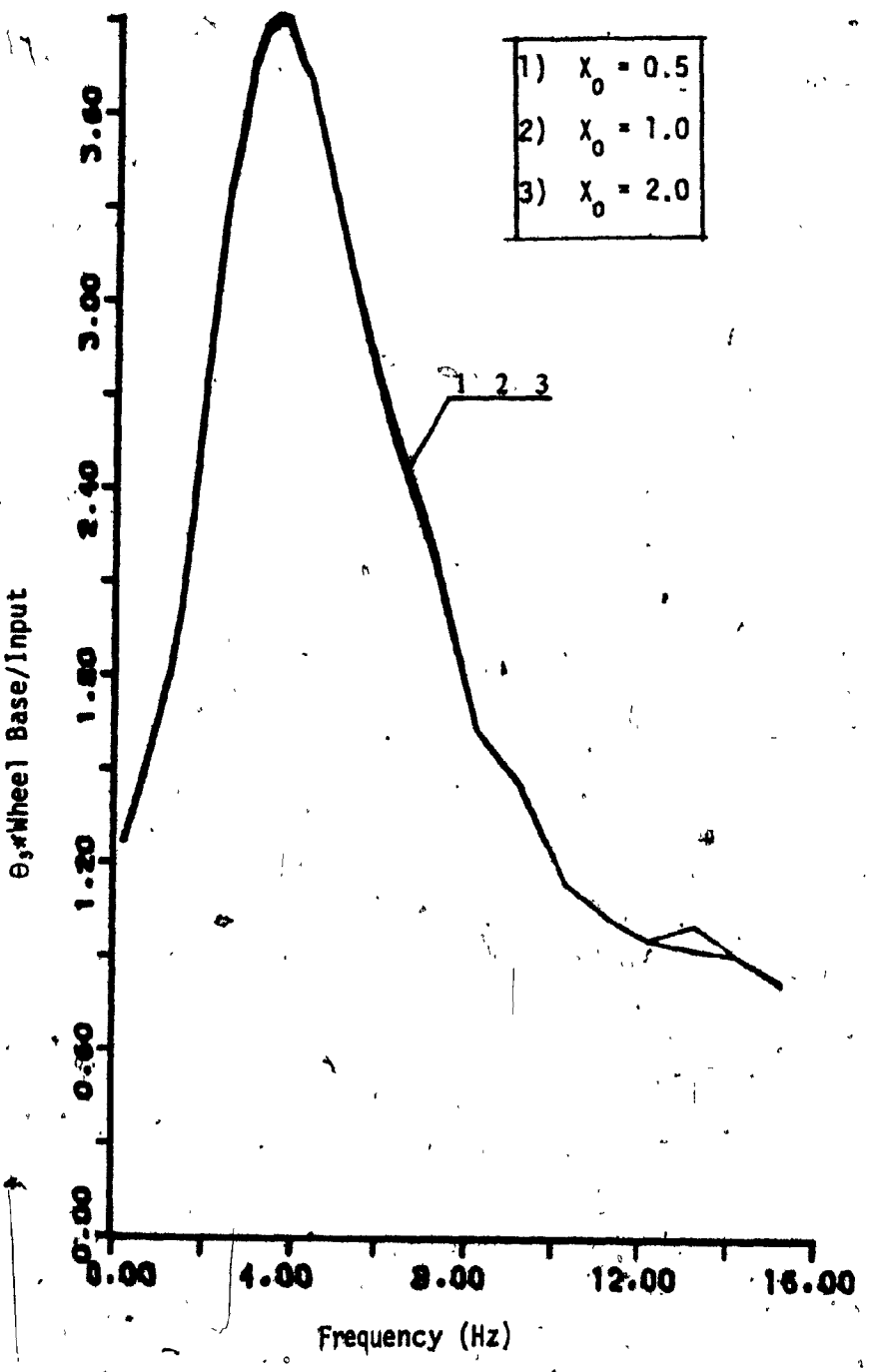

Figure 3.34: Effect of θ_3 Vs f for Variation in X_0

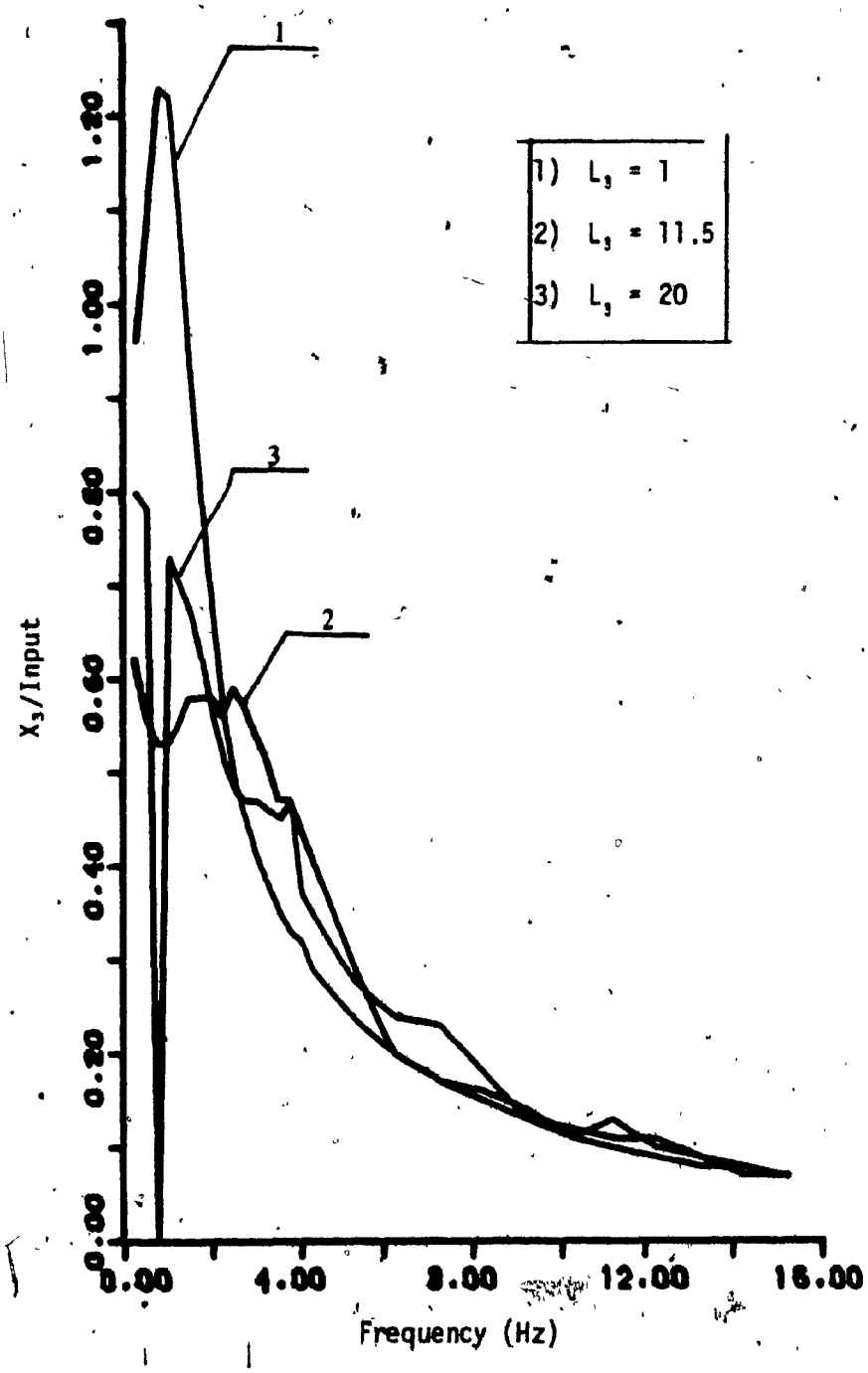

Figure 3.35 : Effect of X_3 Vs f for Variation in L_3: Input Amplitude of 1.25 cm (0.5 in).

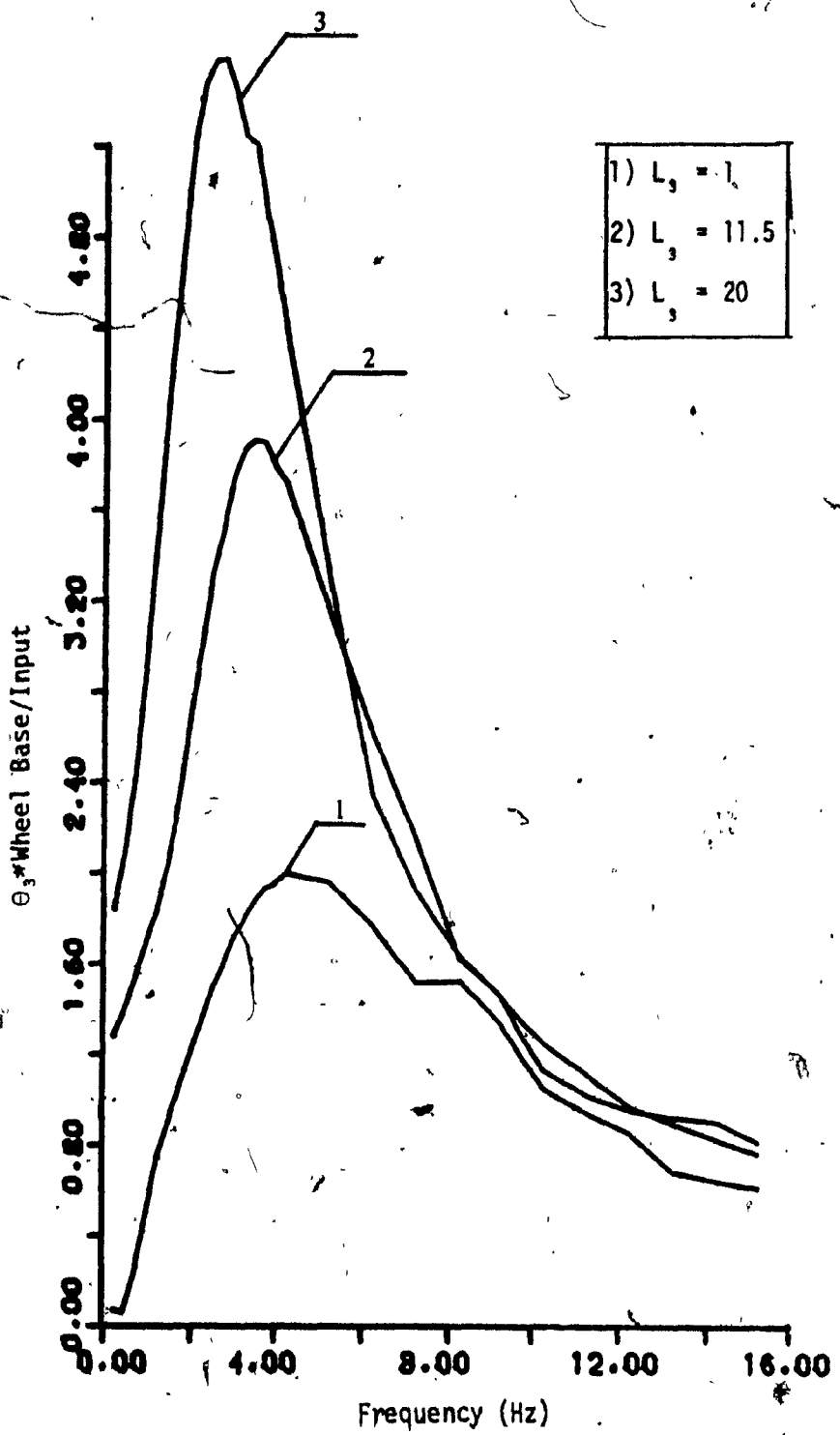

Figure 3.36 : Effect of θ_3 Vs f for Variation in L_3: Input Amplitude of 1.25 cm (0.5 in).

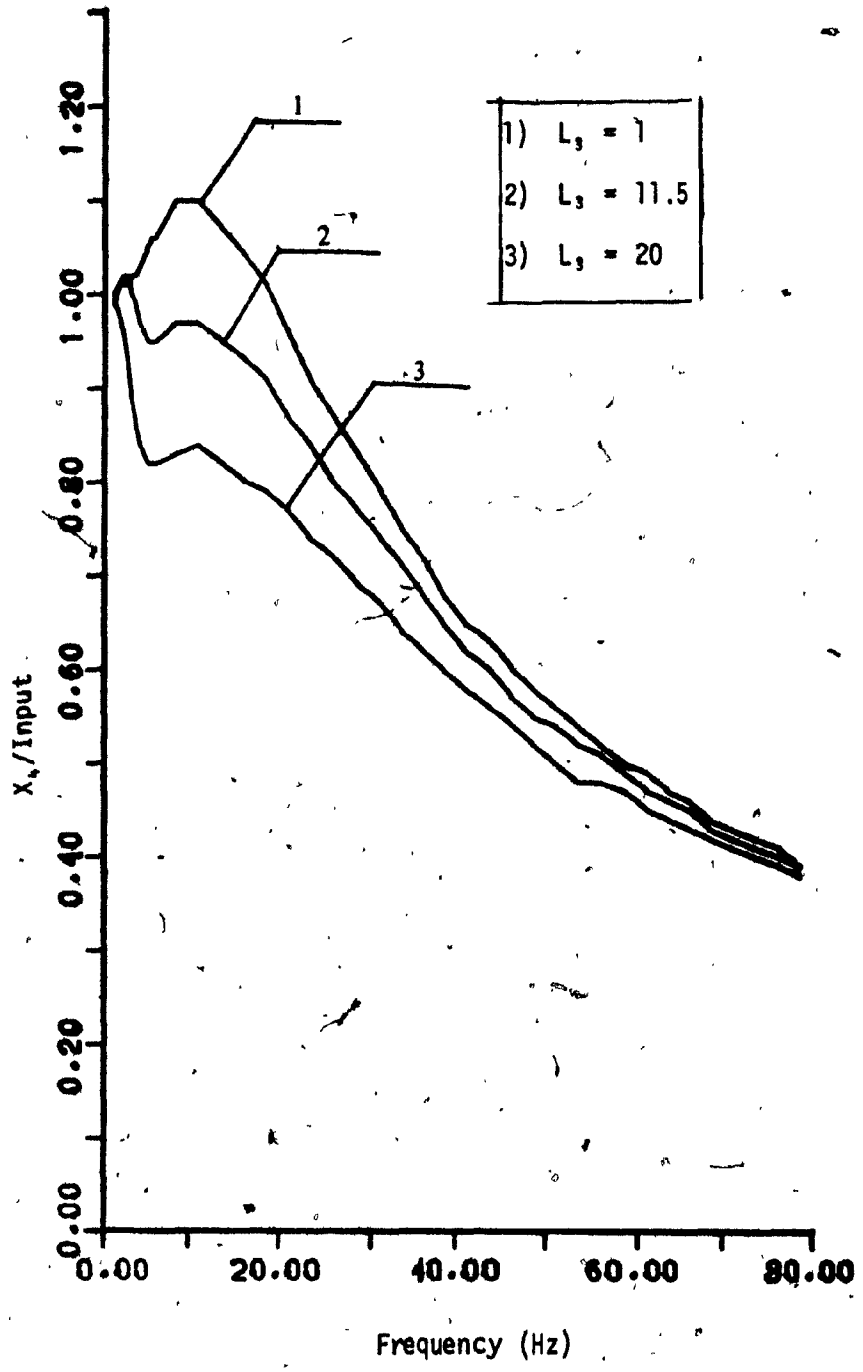

Figure 3.37: Effect of X_s Vs f for Variation in L_s: Input Amplitude of 1.25 cm (0.5 in).

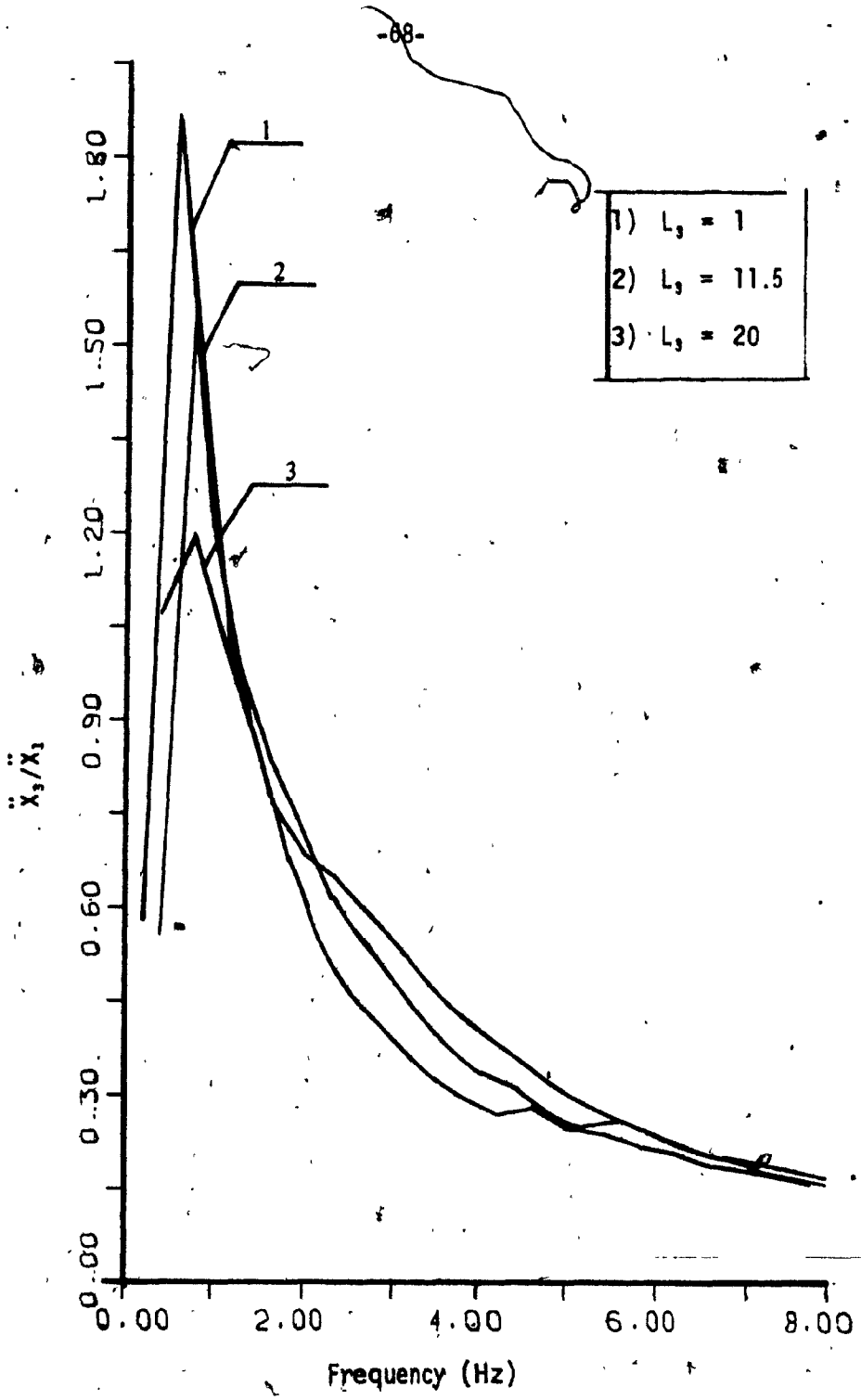

Figure 3.38: Effect of $\ddot{X}_3$ Vs f for Variation in L_3: Input Amplitude of 1.25 cm (0.5 in).

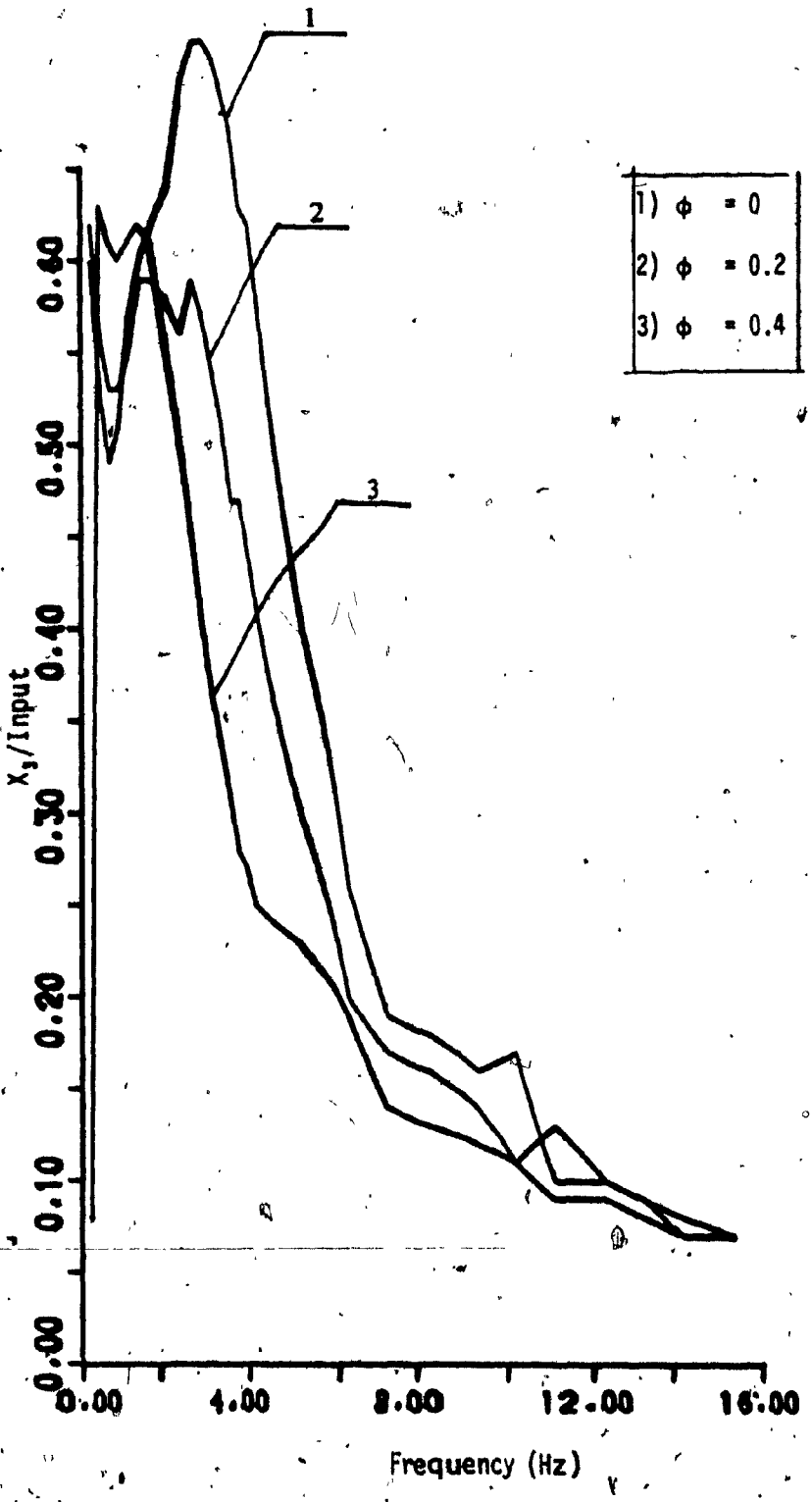

Figure 3.39: Effect of X_3 Vs f for Variation in ϕ: Input Amplitude of 1.25 cm (0.5 in).

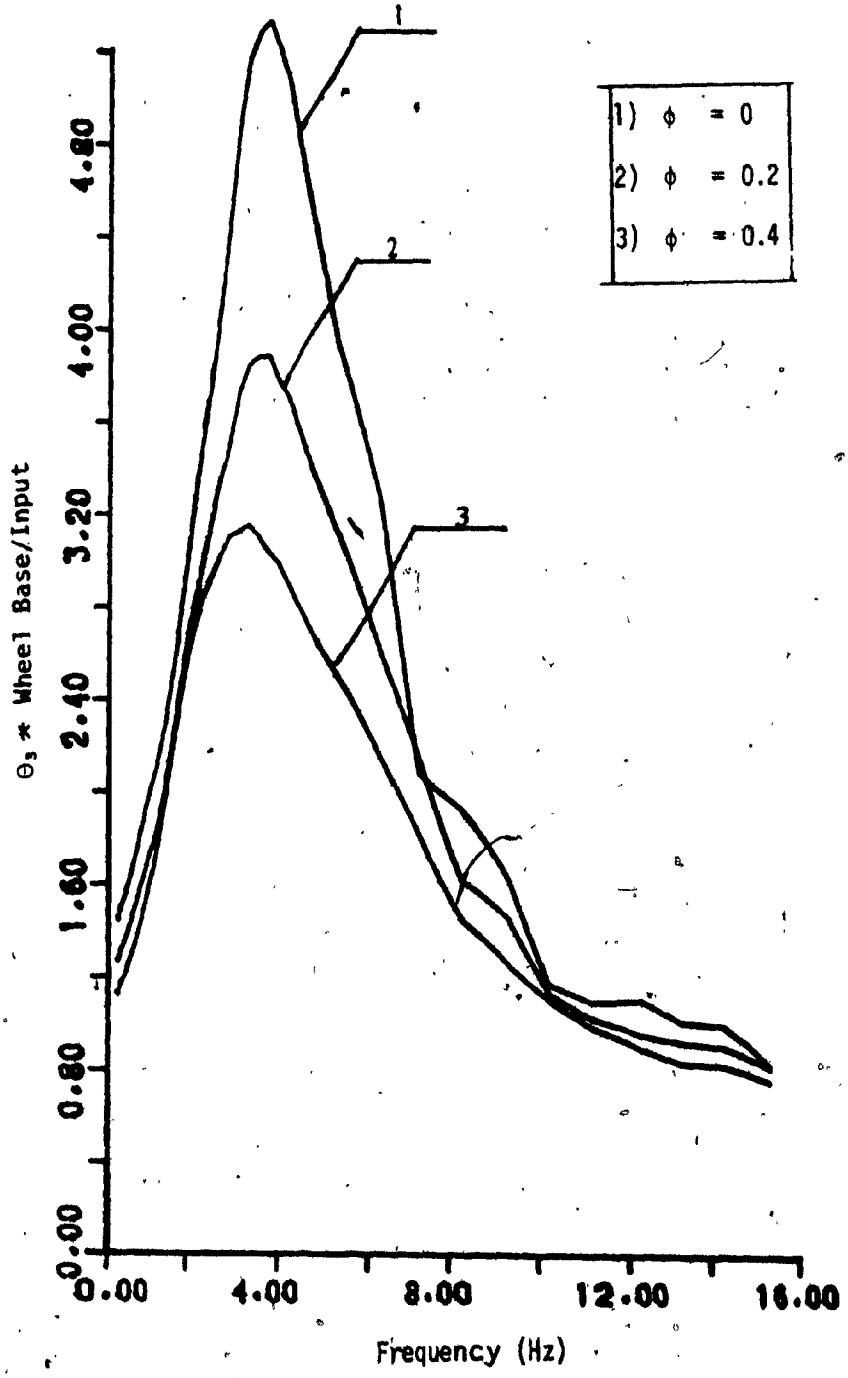

Figure 3.40: Effect of θ_3 Vs f for Variation in ϕ : Input Amplitude of 1.25 cm (0.5 in).

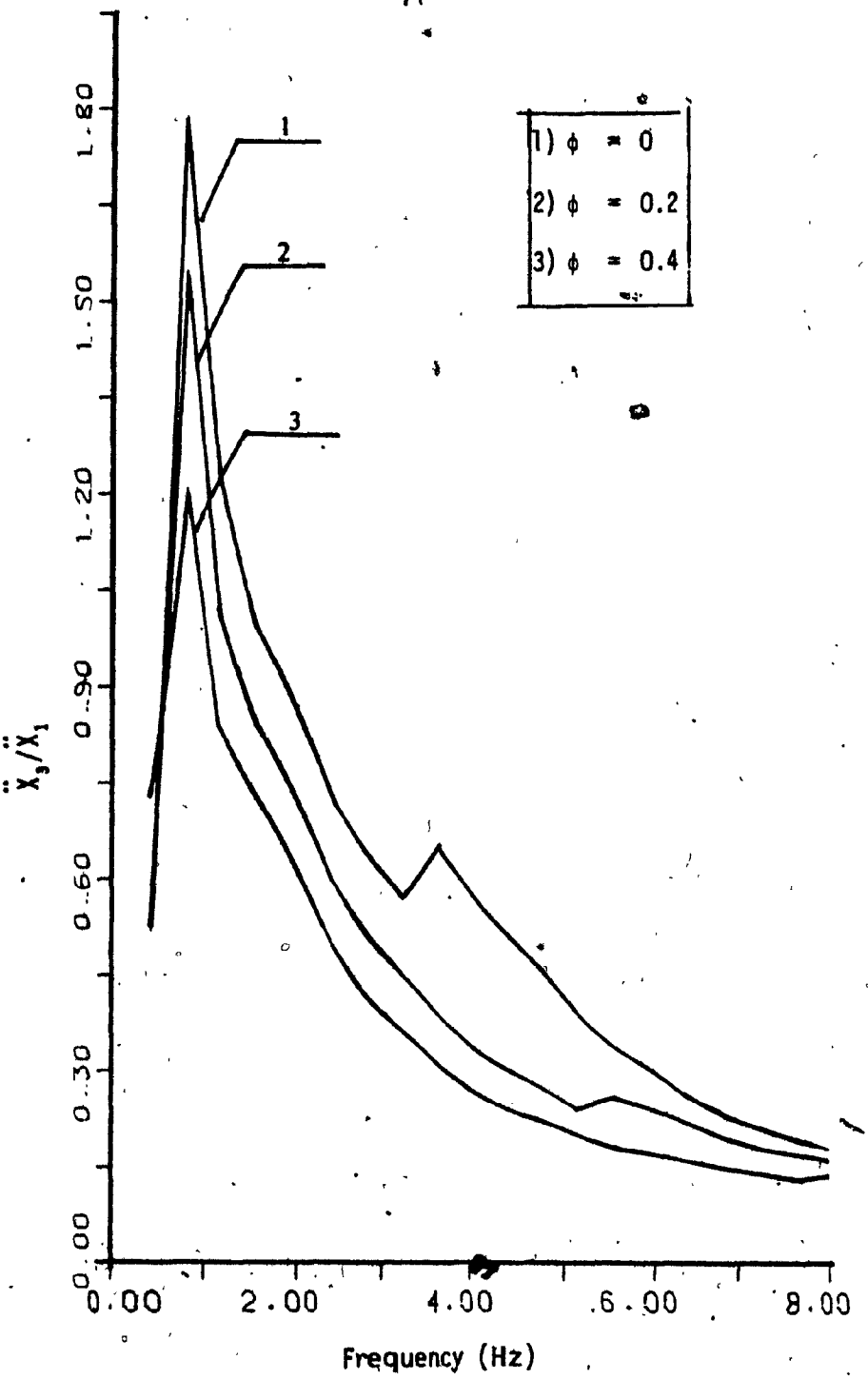

Figure 3.41: Effect of $\ddot{X}_3$ Vs f for Variation in ϕ : Input Amplitude of 1.25 cm (0.5 in).

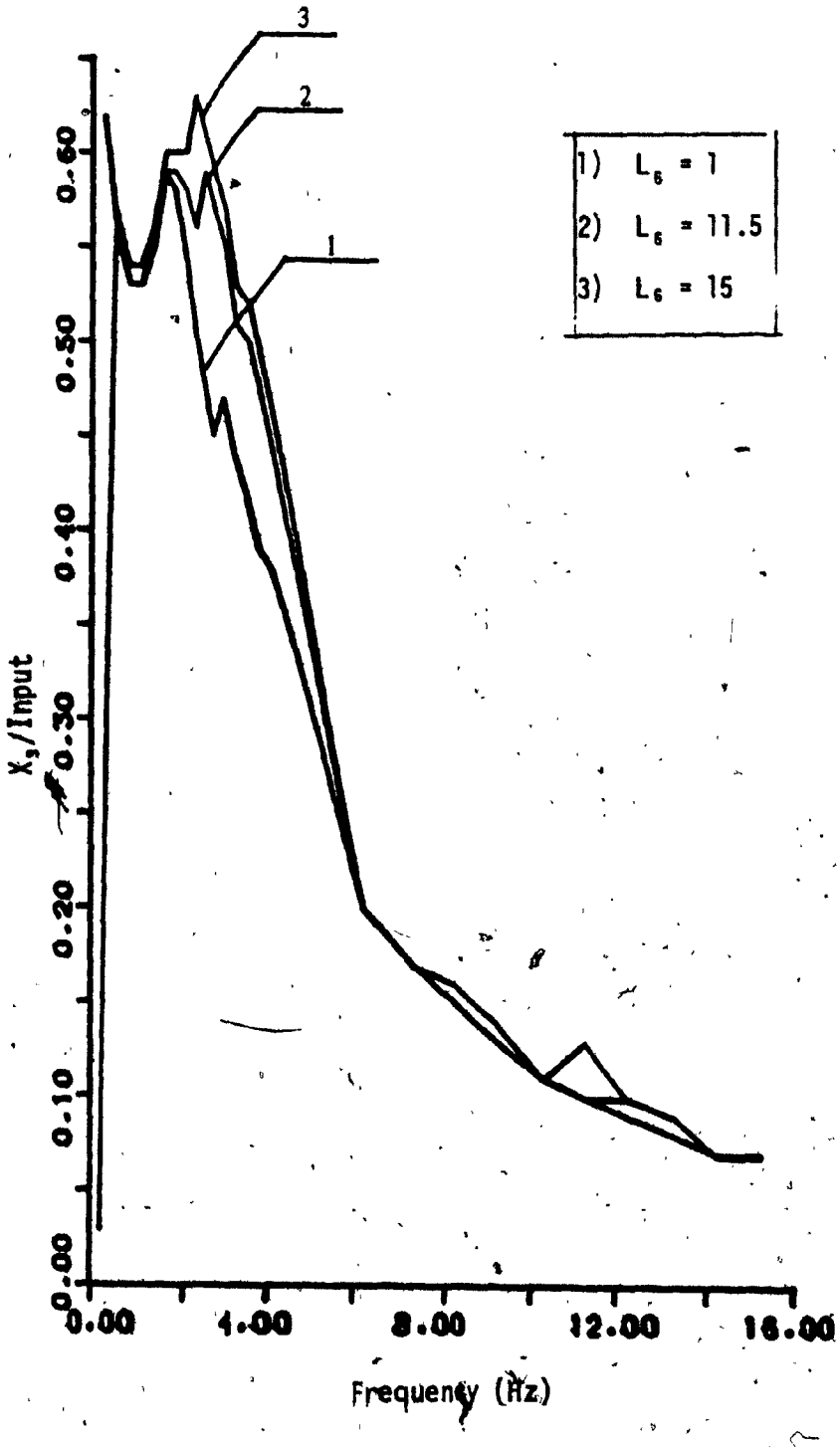

Figure 3.42: Effect of X_3 Vs f for Variation in L_6: Input Amplitude of 1.25 cm (0.5 in).

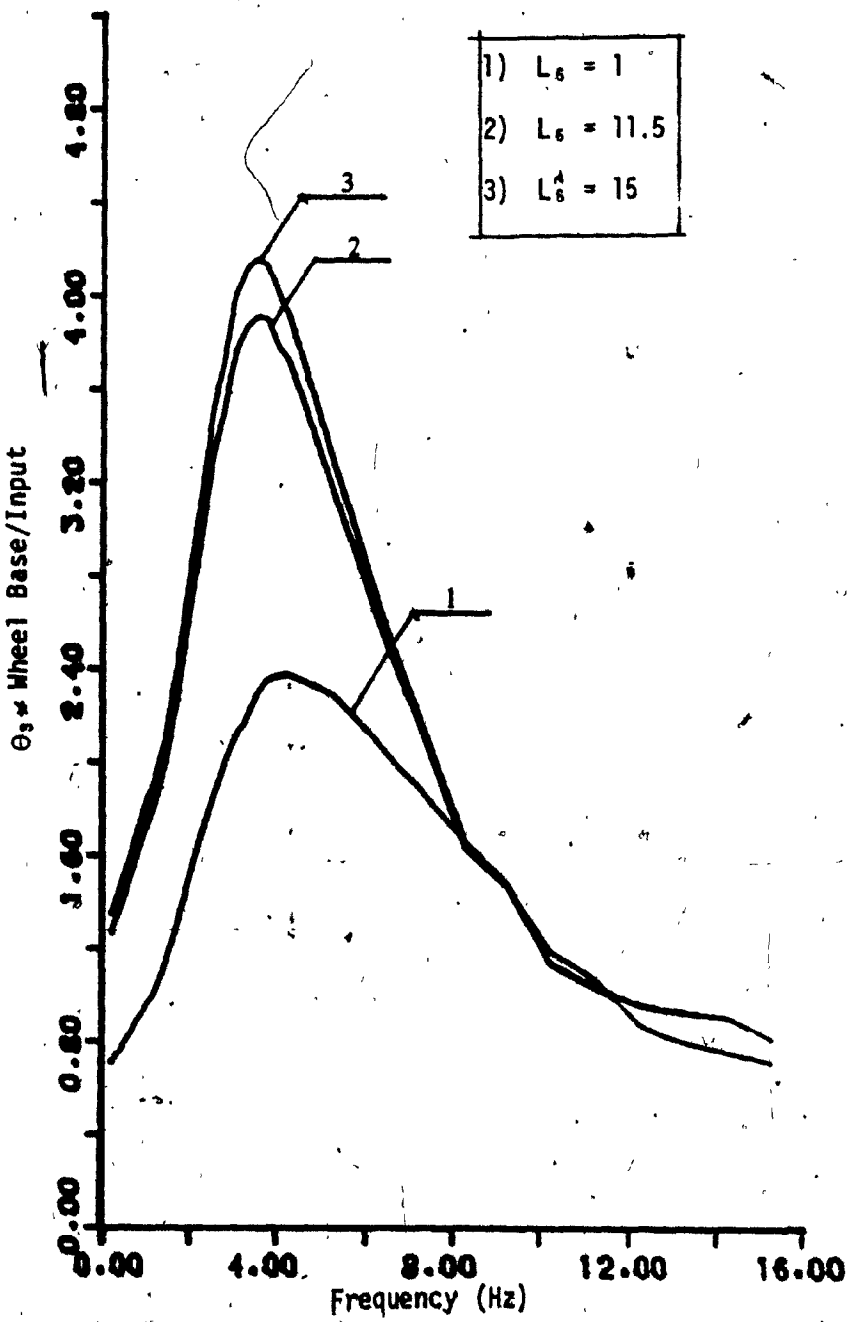

Figure 3.43 : Effect of Θ_3 Vs f for Variation in L_6: Input Amplitude of 1.25 cm (0.5 in).

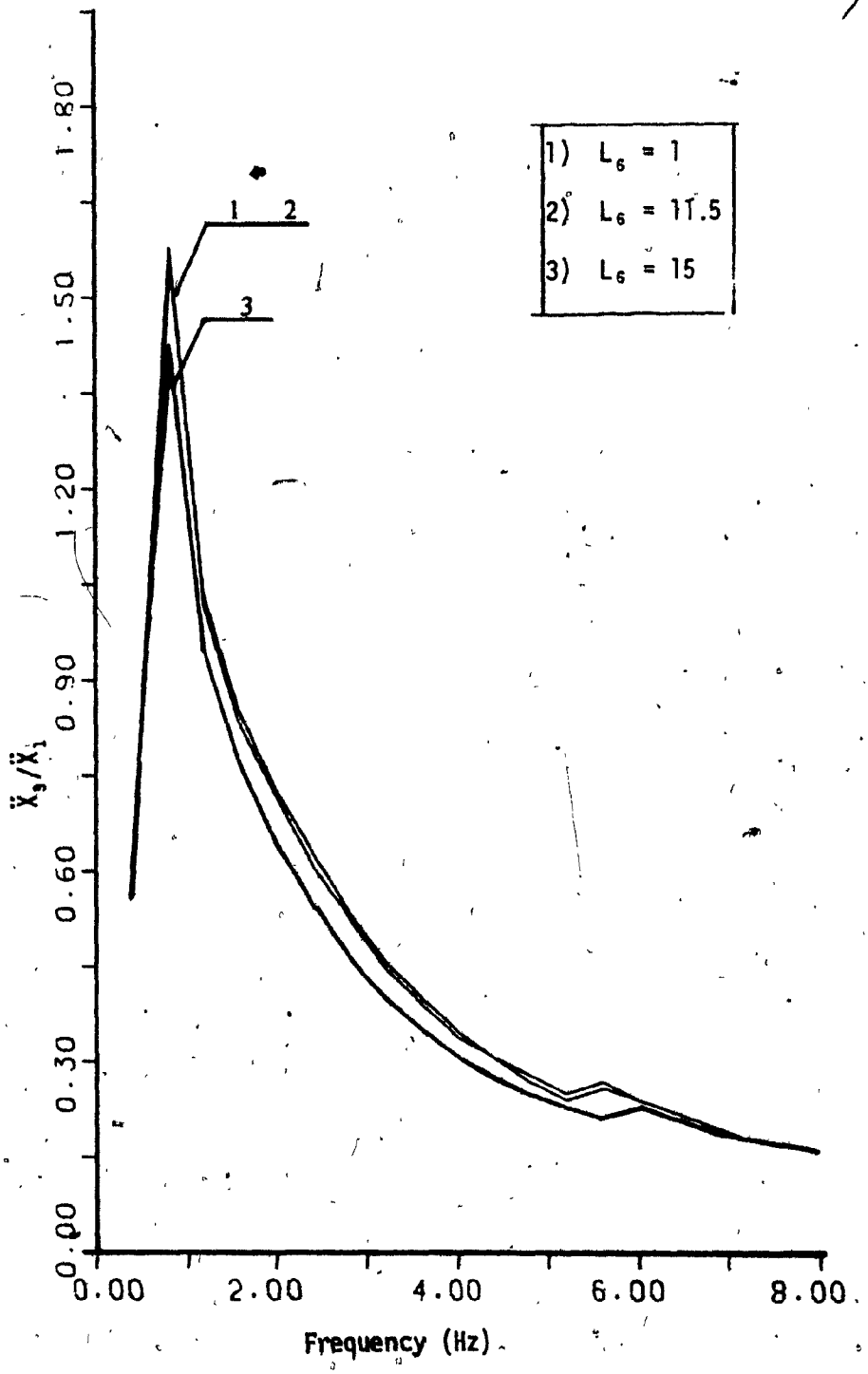

Figure 3.44: Effect of $\ddot{X}_3$ Vs f for Variation in L_6: Input Amplitude of 1.25 cm (0.5 in).

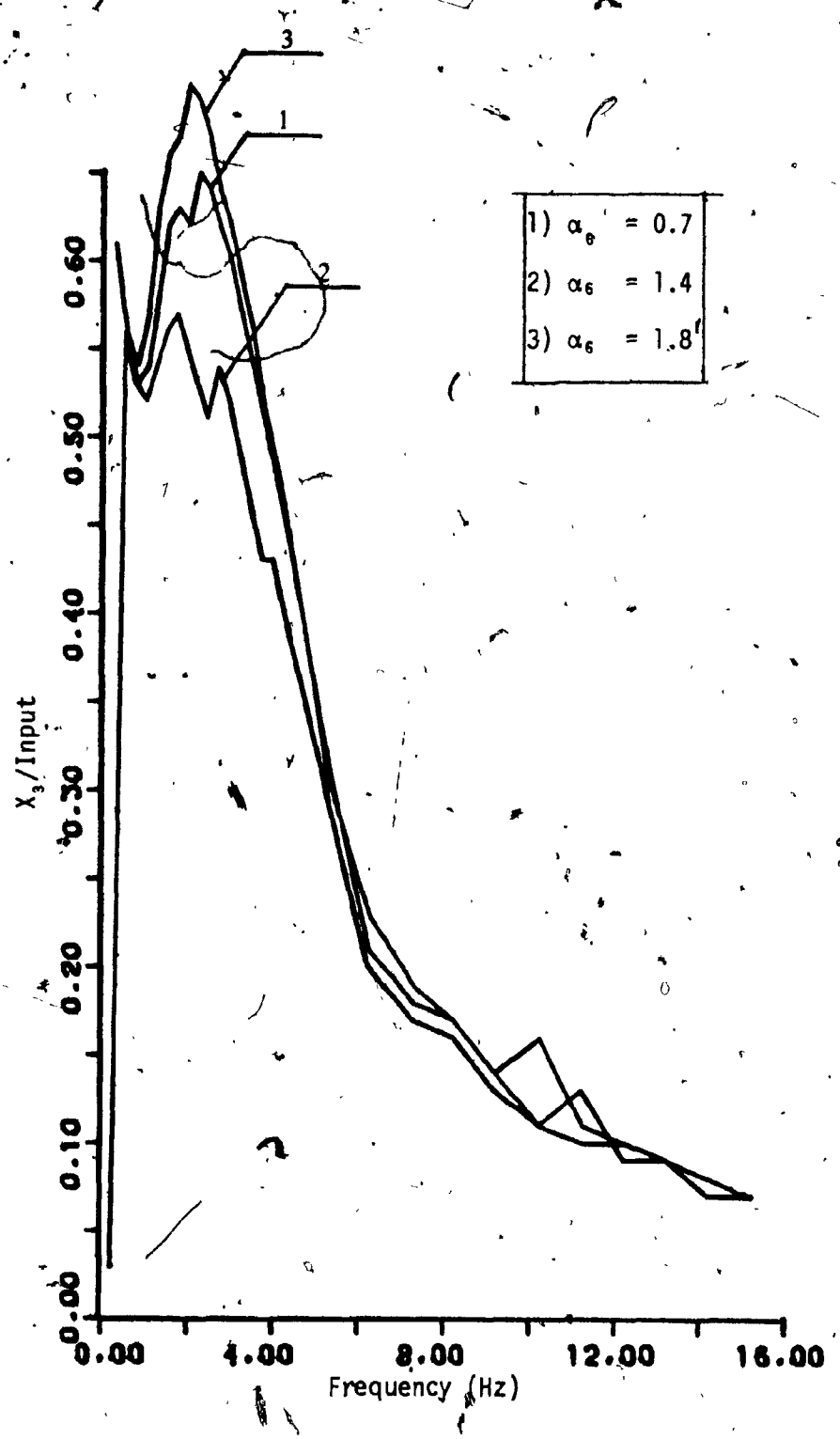

Figure 3.45: Effect of X_3 Vs f for Variation in α_6 : Input Amplitude of 1.25 cm (0.5 in).

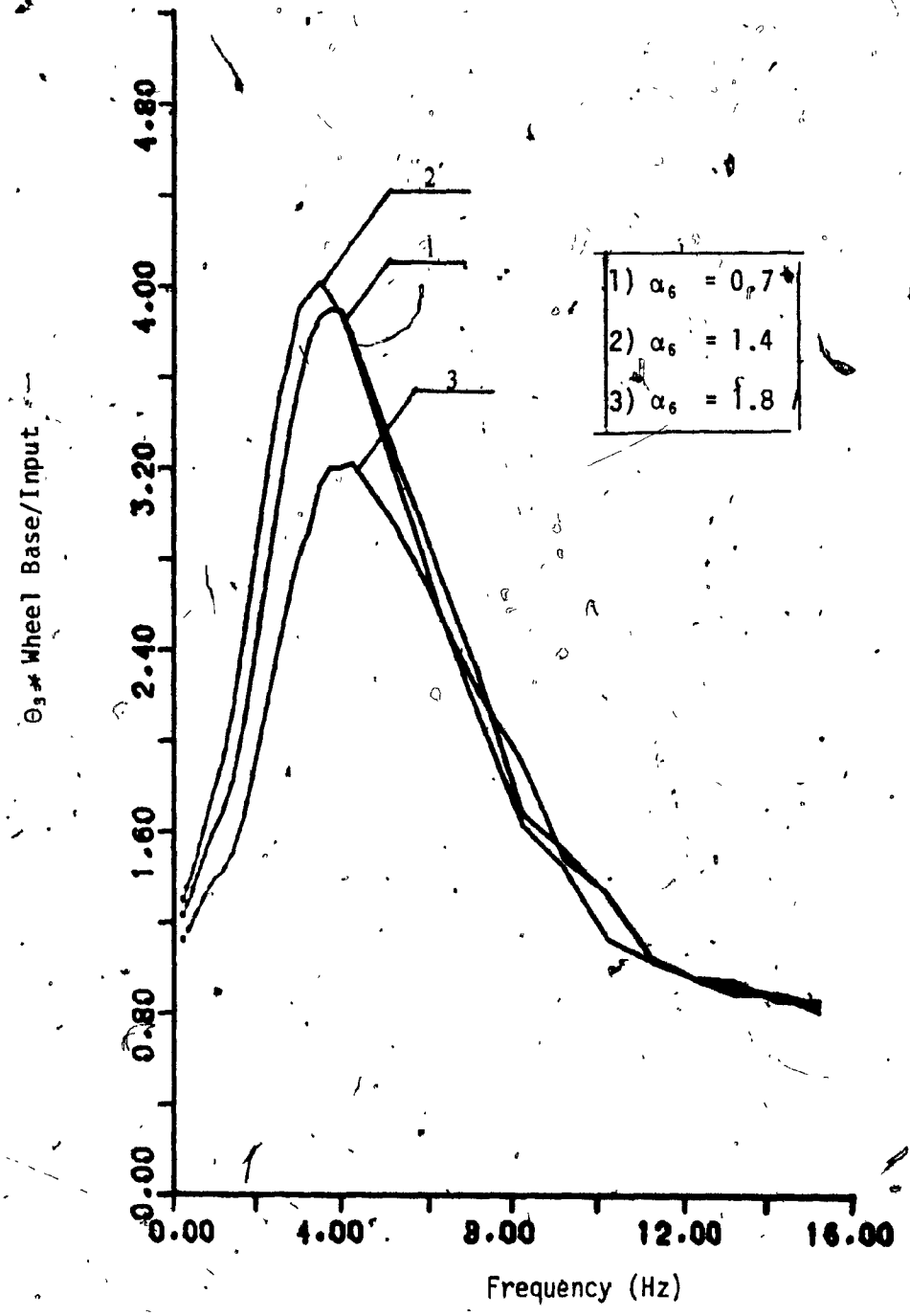

Figure 3.46: Effect of θ_3 Vs f for Variation in α_6: Input Amplitude of 1.25 cm (0.5 in).

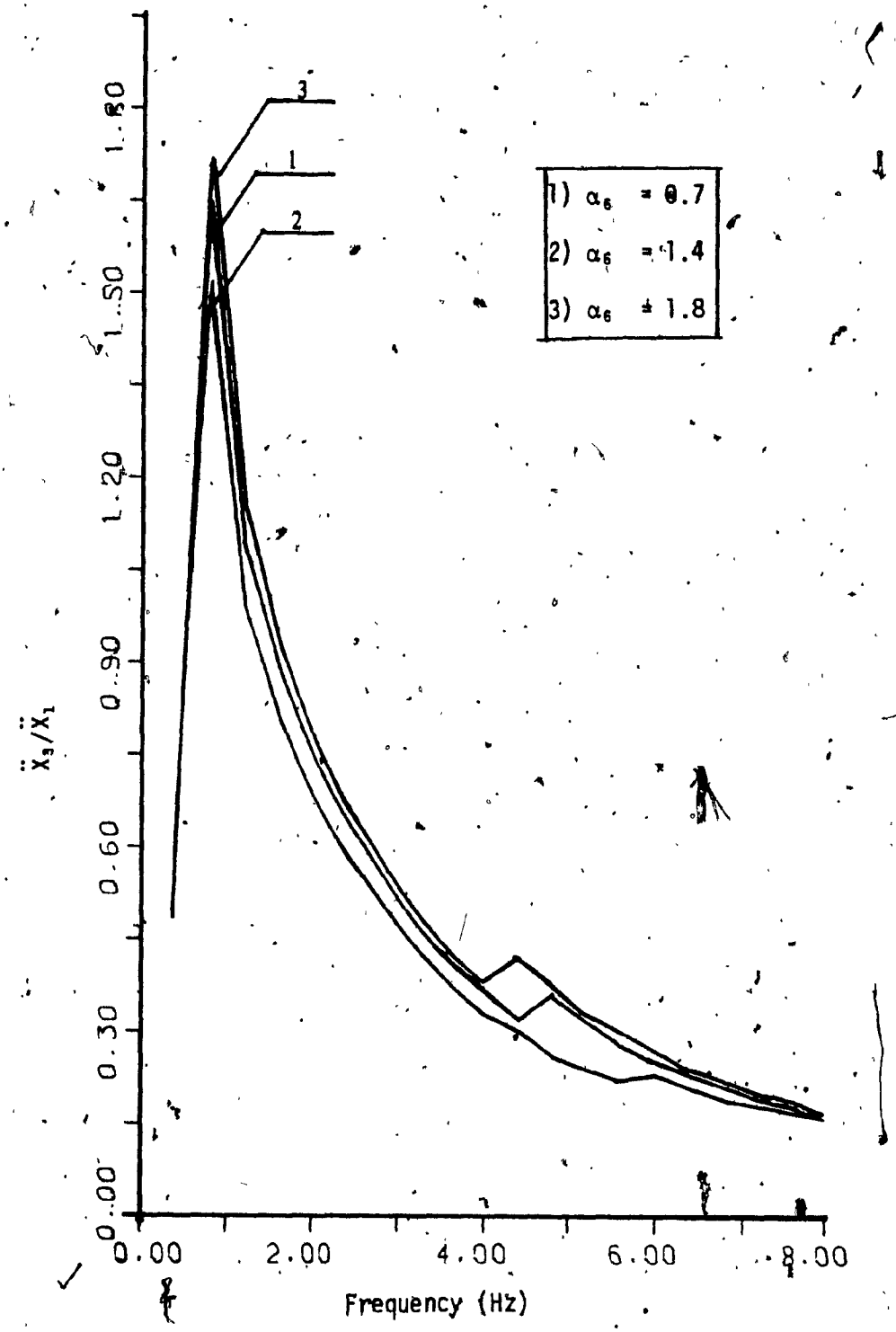

Figure 3.47: Effect of $\ddot{X}_3$ Vs f for Variation in α_6: Input Amplitude of 1.25 cm (0.5 in).

3.7 Consideration of Three Types of Damping

In section 3.3, the effect of front fork and rear shock absorber damping variations is presented. In that case, the damping is considered to be linear and having symmetrical characteristics (i.e. equal damping coefficient for both compression and extension). From practice, it is known that the damping characteristics is non-symmetric and non-linear. In order to study the effect of such a damping behavior on the motorcycle response, three types of damping for front fork and rear shock absorber are considered in this section:

1) Linear symmetrical: Compression and extension.

2) Linear non-symmetrical: Compression and extension.

3) Non-linear and non-symmetrical: Compression and extension.

Figure 3.48 a,b, and c show the general characteristics of these three types of damping. It should be pointed out that in the case #3 type damping, the characteristics are obtained from the governing equations derived and presented in Appendix A.

The transmissibility plots for all the generalized coordinates with these three types of damping behavior are presented in Figs. 3.49-3.55. The following conclusions are drawn:

1) Figure 3.49 - The non-linear and non-symmetrical damping gives considerably higher X_3-TR at resonance, however higher frequencies result in good vibration isolation. In comparison to a linear, symmetrical damping, linear, non-symmetrical damping gives higher X_3 transmissibility value at resonance.

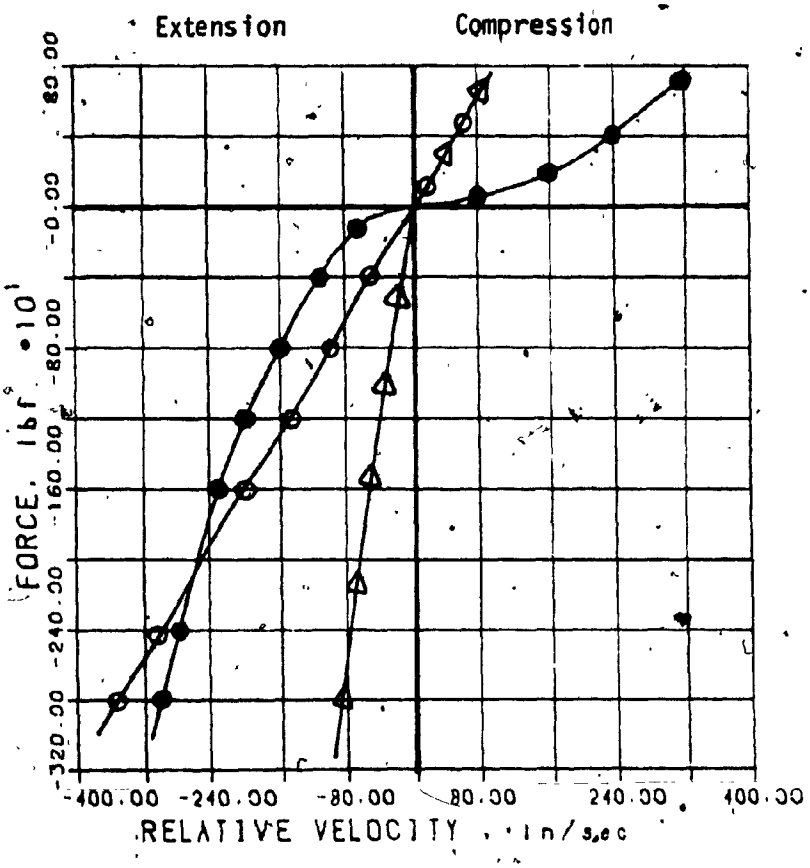

a) ○ Linear Symmetrical

b) △ Linear Non-symmetrical

c) ● Non-linear and Non-symmetrical

Note: Rear shock damping is assumed five times higher than front fork damping.

Figure 3.48: Three Types of Damping Curves (Front Fork)

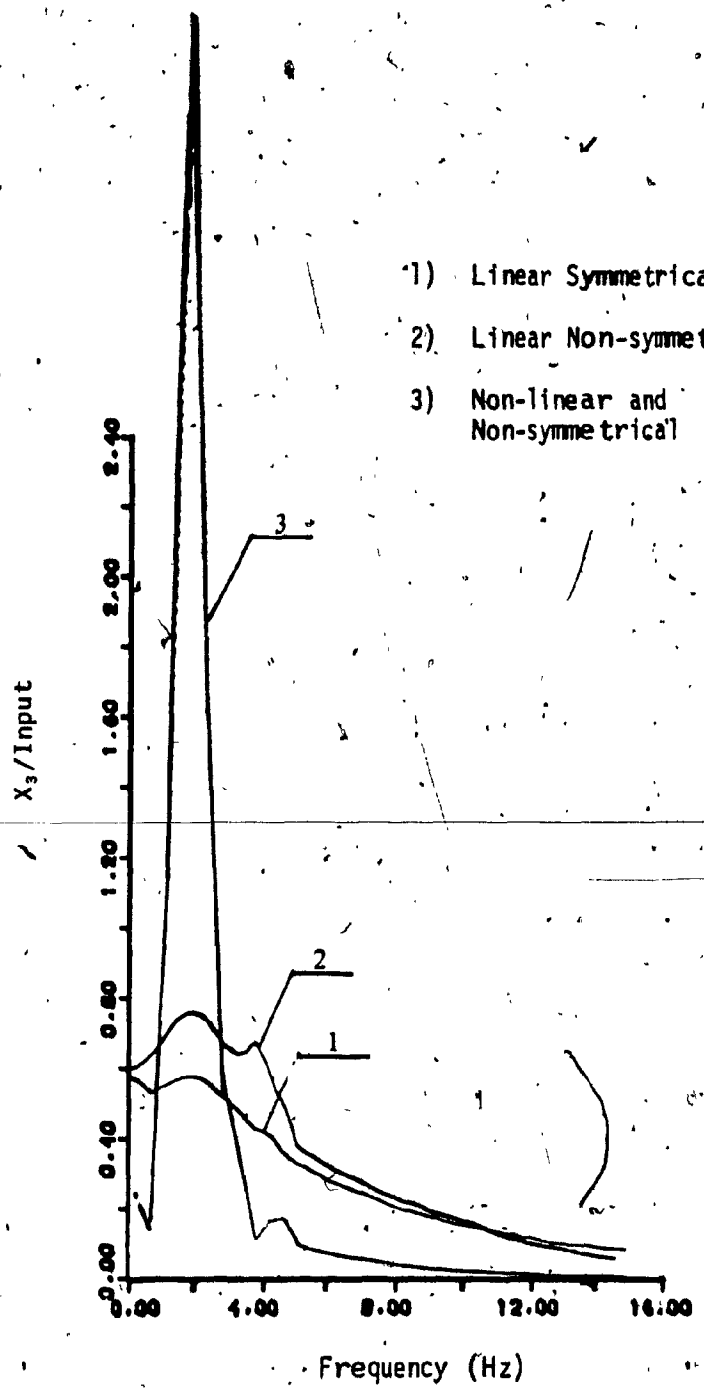

Figure 3.49: Effect of X_3 Vs f for Variation in Front and Rear Shocks Damping: Input Amplitude of 1.25 cm (0.5 in).

2) Figure 3.50 - Non-linear and non-symmetric damping gives generally the lowest θ_3 response except around 5 Hz, the response is the highest. In this case, the linear non-symmetrical damping gives lower θ_3 response compared to linear symmetrical damping.

3) Figure 3.51 - Non-linear non-symmetrical damping produces highest X_2 response.

4) Figure 3.52 - linear non-symmetric damping produces generally the lowest X_4 response.

5) Figure 3.53 - Non-linear and non-symmetric damping produces significantly higher displacement of the front fork.

6) Figure 3.54 - Non-linear and non-symmetric damping produces significantly higher relative displacement of the rear shock absorber.

7) Fig. 3.55 - Non-linear and non-symmetric damping produces significantly higher $\ddot{X}_3$ acceleration.

3.8 Conclusions

A parametric study was carried out with variations of stiffness and damping of the tires and the shock absorbers, and the mass of the rider. The peak to peak amplitude ratios of X_2/X_1, X_3/X_1, X_4/X_1 and θ_3 wheel base/X_1 were studied for different values of amplitude (road input) and frequencies.

A study on the effect of variation of the geometrical configuration of the motorcycle was carried out and it was observed that the geometric location L_3, L_6 and angles ϕ and α_6 have considerable influence on the absolute displacement X_3 and rotation θ_3.

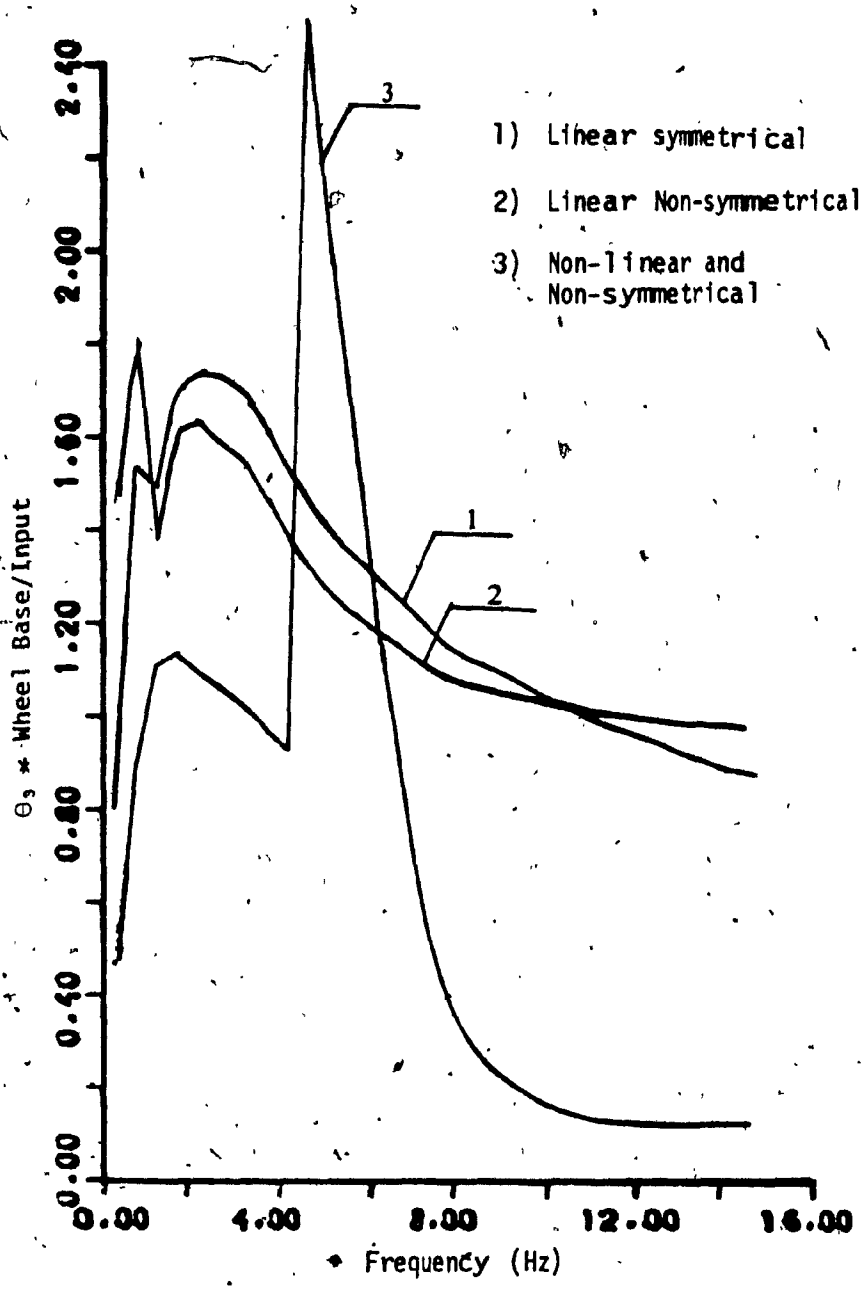

Figure 3.50 : Effect of θ_3 Vs f for Variation in Front and Rear Shocks Damping: Input Amplitude of 1.25 cm (0.5 in).

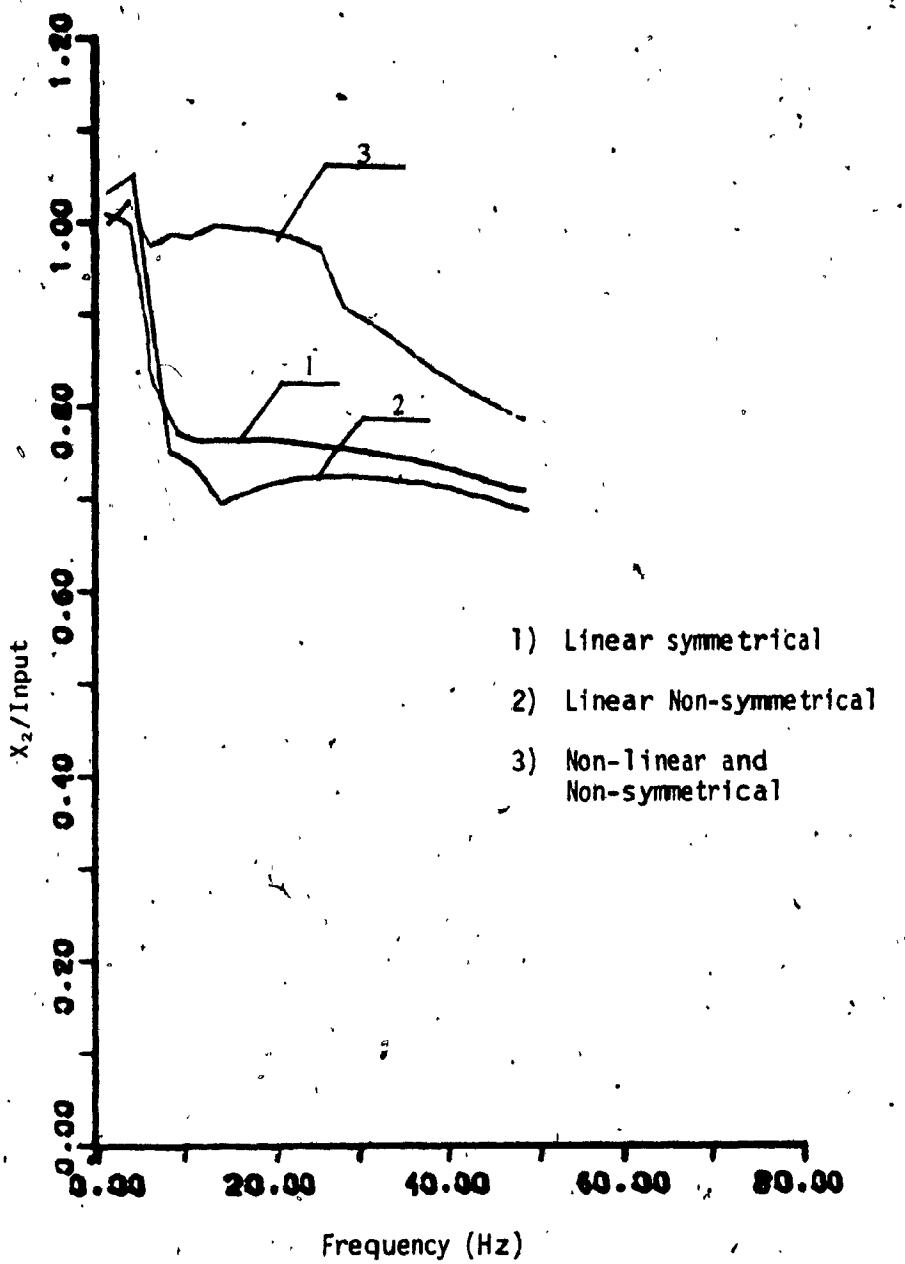

Figure 3.51: Effect of X_2 Vs f for Variation in Front and Rear Shocks Damping: Input Amplitude of 1.25 cm (0.5 in).

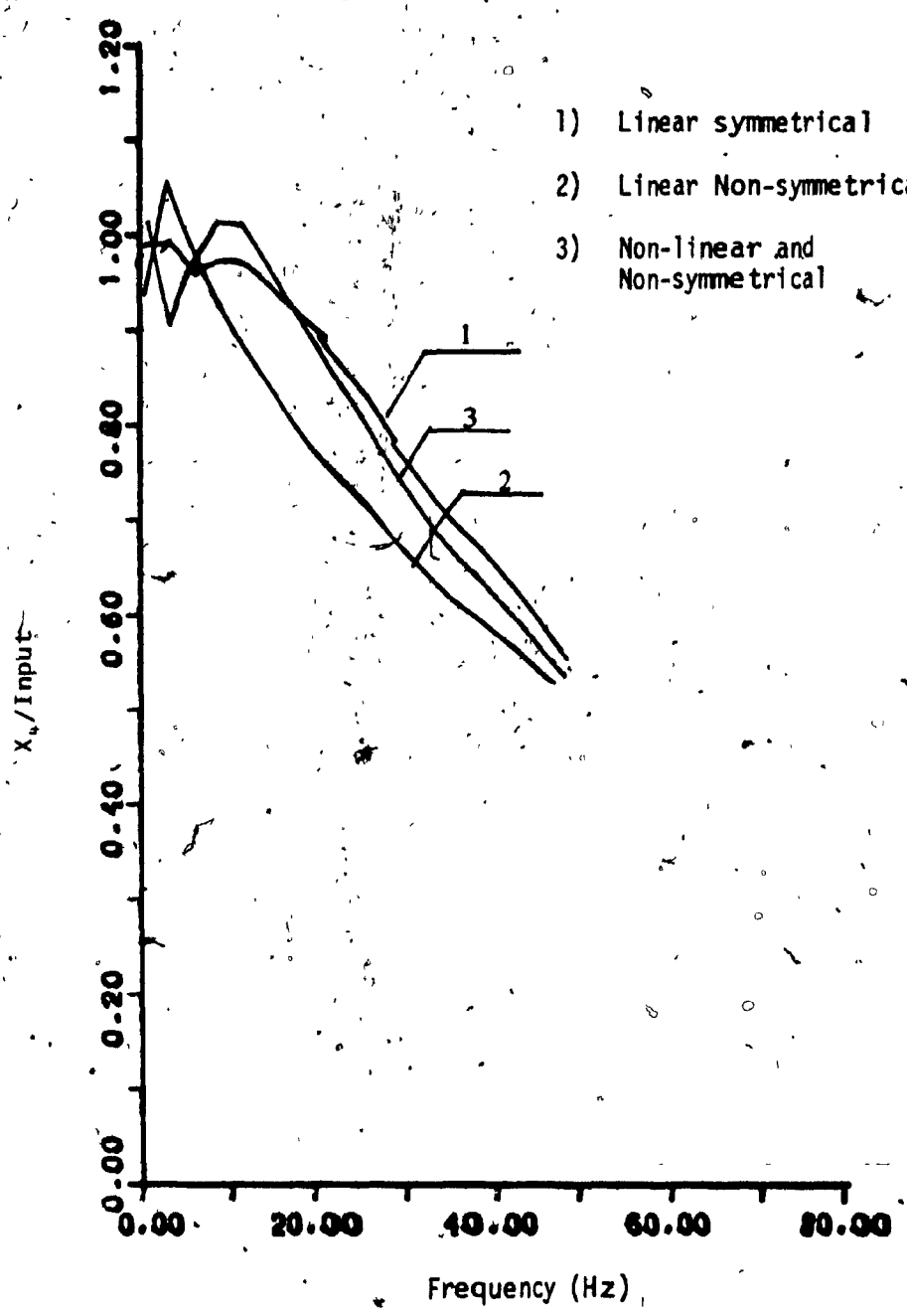

Figure 3.52: Effect of X_4 Vs f for Variation in Front and Rear Shocks Damping: Input Amplitude of 1.25 cm (0.5 in).

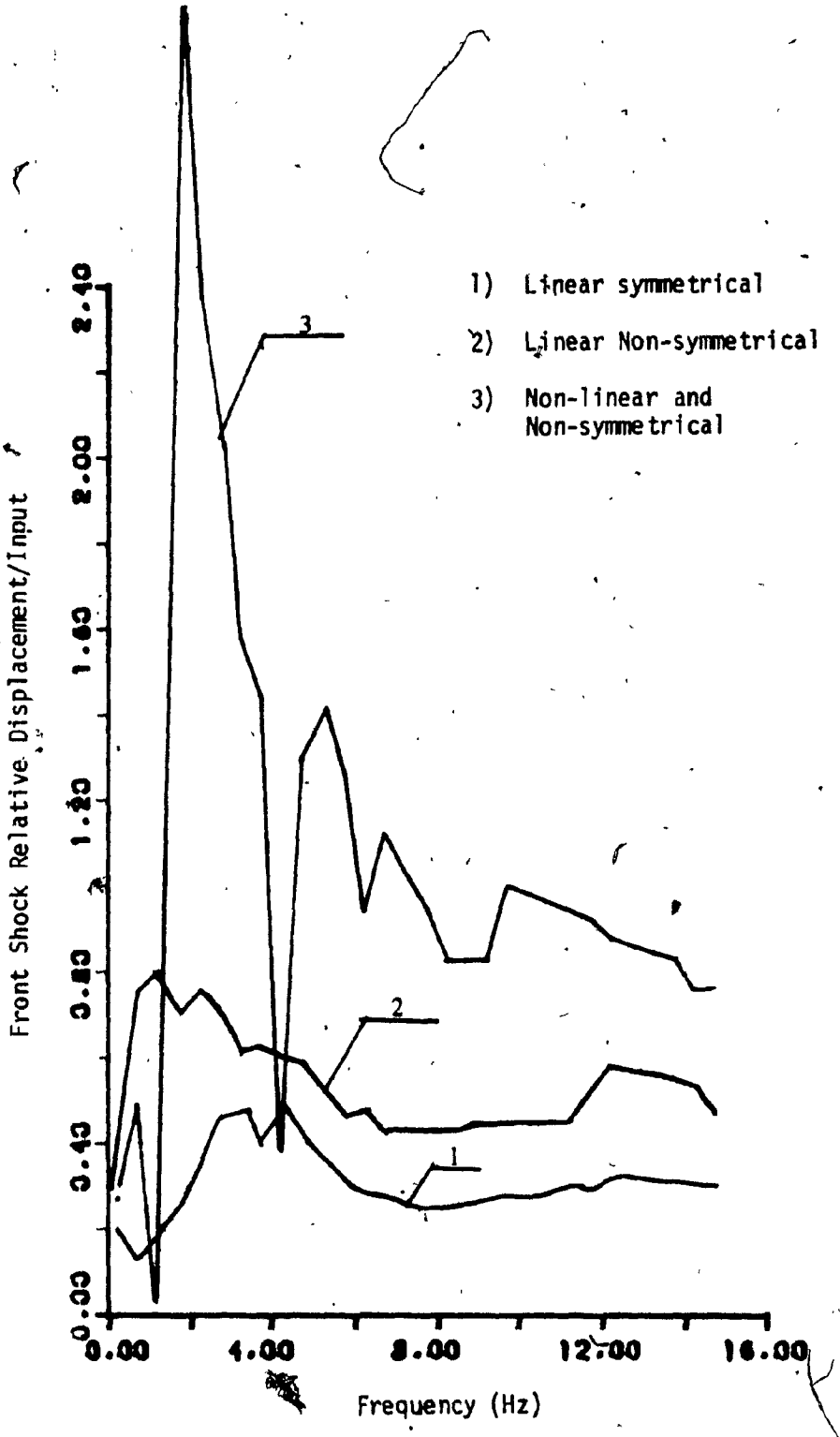

Figure 3.53: Effect of Front Shock Relative Displacement Vs f for Variation in Front and Rear Shocks Damping: Input Amplitude of 1.25 cm (0.5 in).

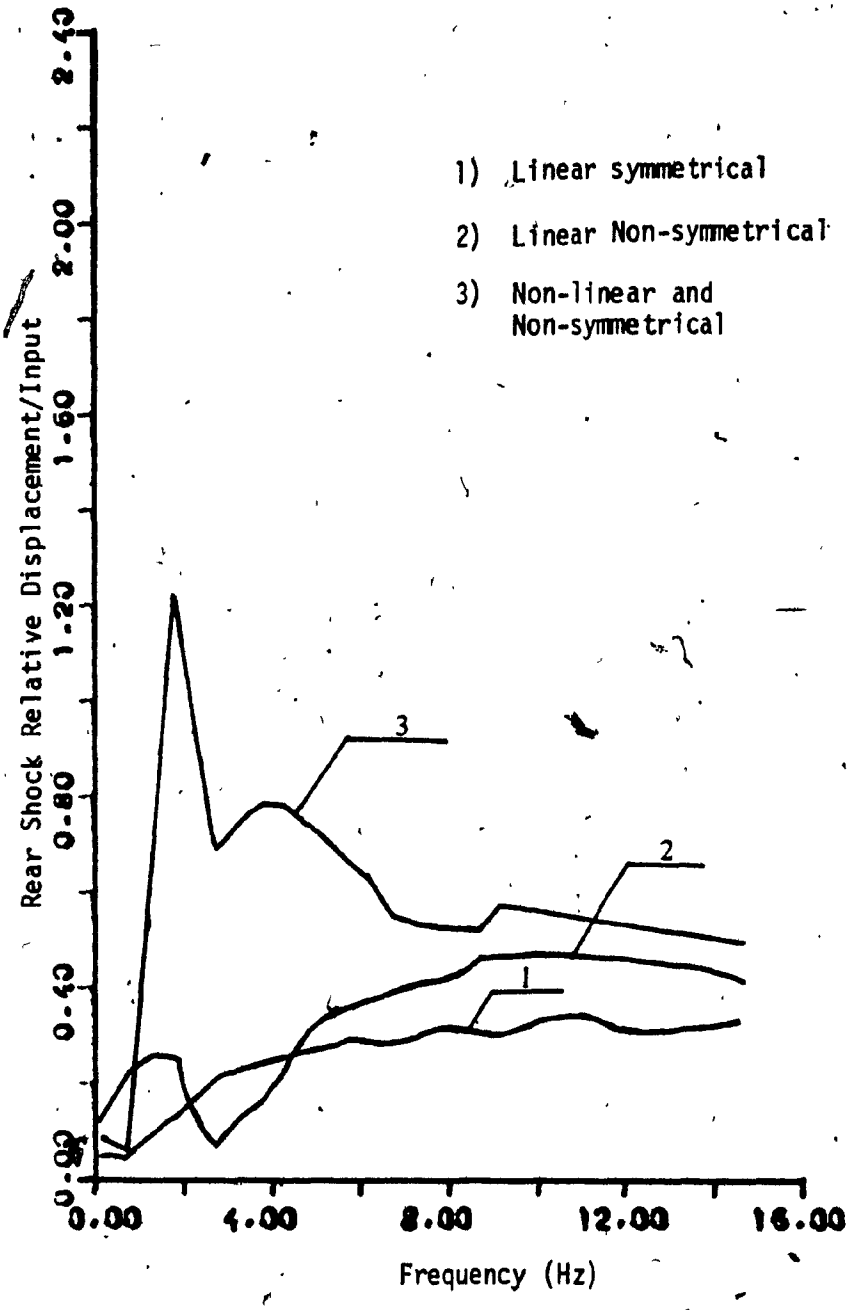

Figure 3.54: Effect of Rear Shock Relative Displacement Vs f for Variation in Front and Rear Shocks Damping: Input Amplitude of 1.25 cm (0.5 in).

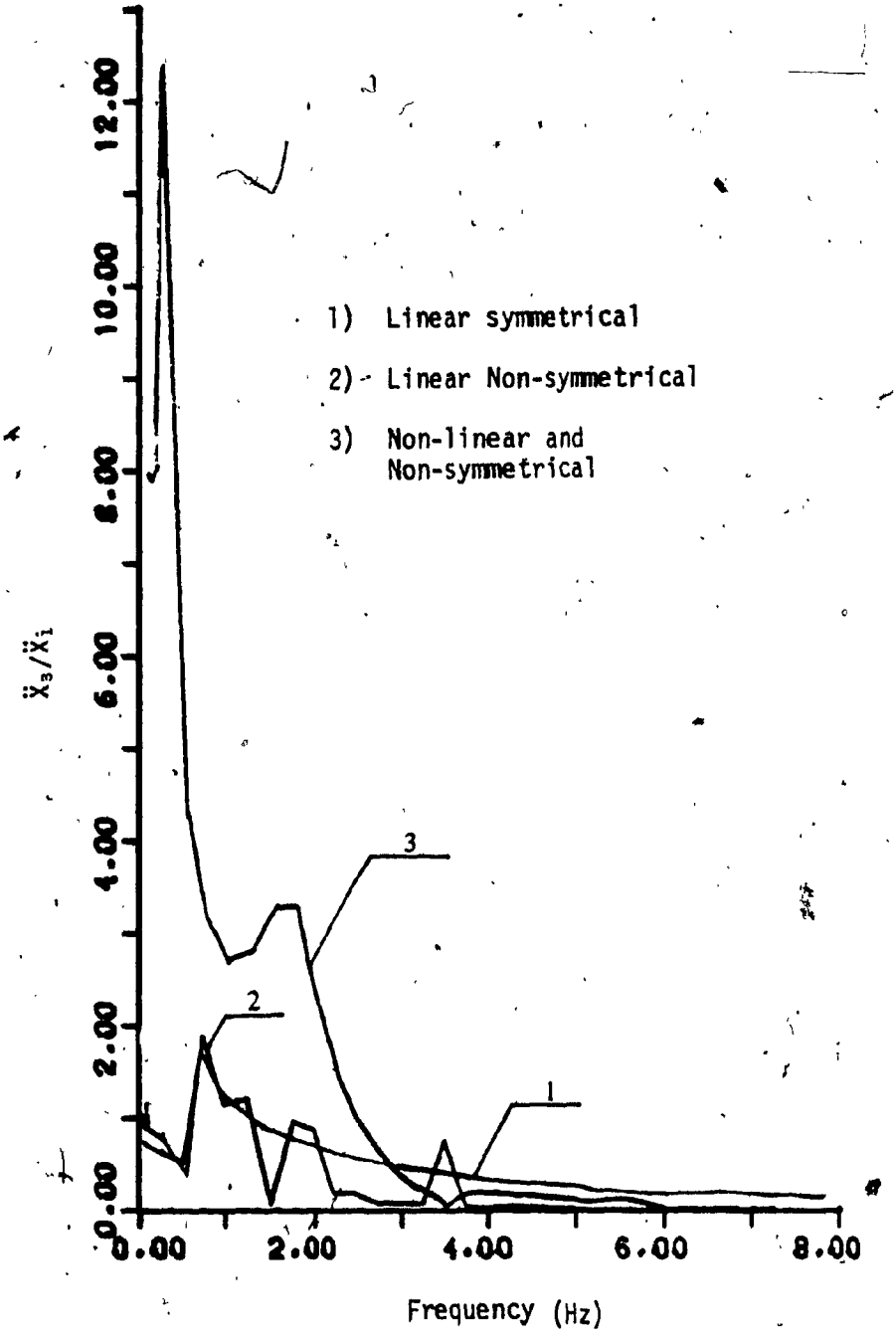

Figure 3.55: Effect of $\ddot{X}_3$ Vs f for Variation in Front and Rear Shocks Damping: Input Amplitude of 1.25 cm (0.5 in).

In the study of damping characteristics of the shocks, the non-linear and non-symmetric damping produces significantly higher responses of generalized coordinates and relative shock displacements and $\ddot{X}_3$ acceleration. In addition the linear non-symmetric shock damping produces slightly higher response of X_3, relative front and rear shocks displacements compared with symmetrical damping case.

Also the linear symmetrical shock damping produces slightly higher response of $\ddot{X}_3$, X_4, X_2 and θ_3.

CHAPTER 4

INTERACTIVE AND DYNAMIC GRAPHICS IN THE DYNAMIC ANALYSIS

4.1 Introduction

In this chapter, the development and the use of interactive and dynamic graphics in the analysis and design of an off-road motorcycle suspension are illustrated. The computer/graphics hardware facility and the details of the data management required for the interactive and dynamic graphics are described.

The methodology of developing the dynamic graphics is introduced through explanation of simpler systems and finally generation of dynamic graphics of the total motorcycle suspension. The detail responses at generalized coordinates are illustrated through the use of a menu in the interactive graphics.

4.2 Computer/Graphics System

4.2.1 Configuration of the Computer

The computer facility used for this work is a VAX 11/780 computer in the Computer Research and Interactive Graphics laboratory (CRIGL) of the Concordia University. The configuration of the computer is illustrated in Fig. 4.1. Device names are preceded by the underscore-character.

4.2.2 Configuration of Graphics System [38]

The graphics system used in this investigation is a NORPAK VDP raster graphics device. Figure 4.2 illustrates the data flow for all the graphic programs. The programs are written in Fortran 77 and are

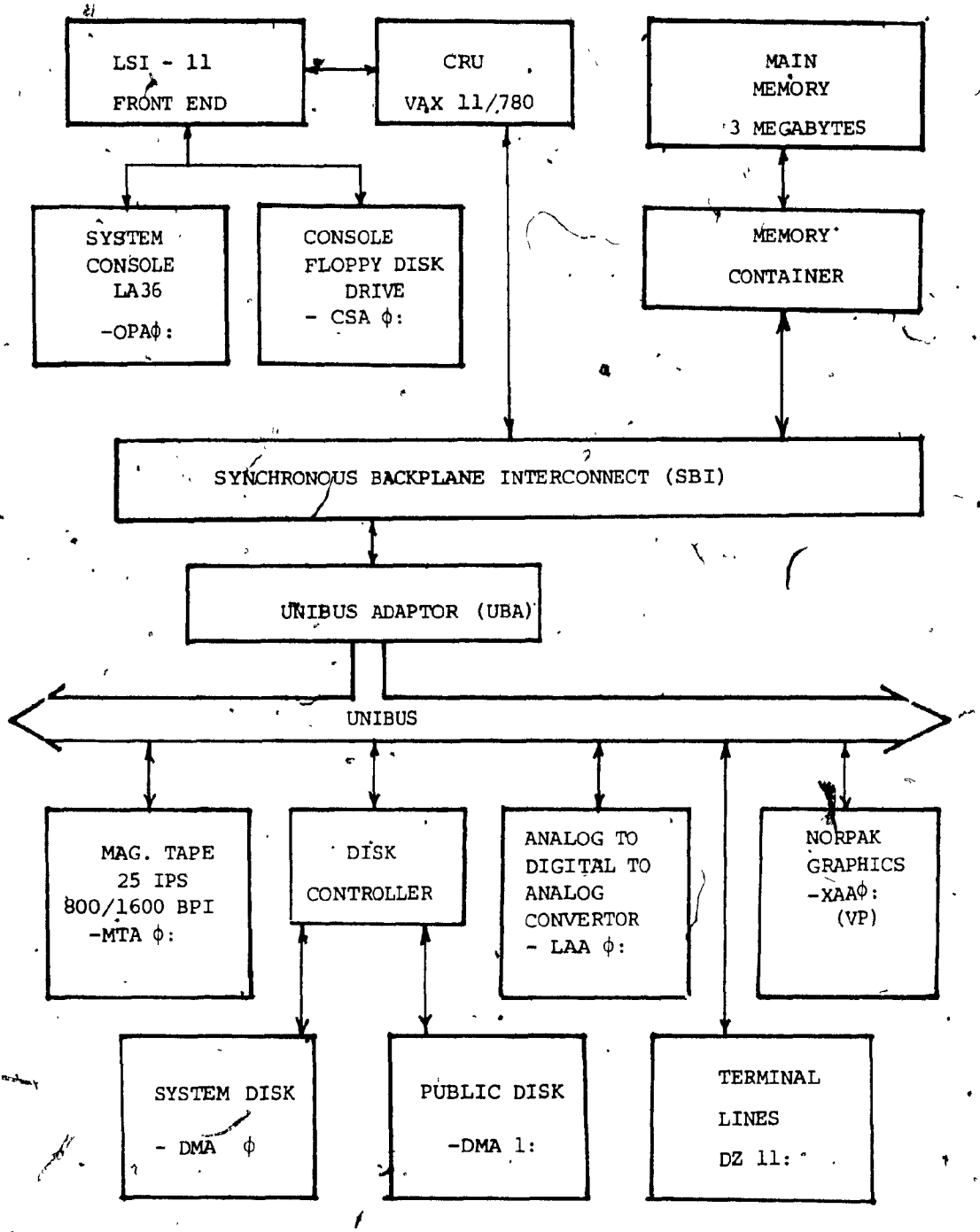

Figure 4.1: The Computer Research and Interactive Graphics Laboratory

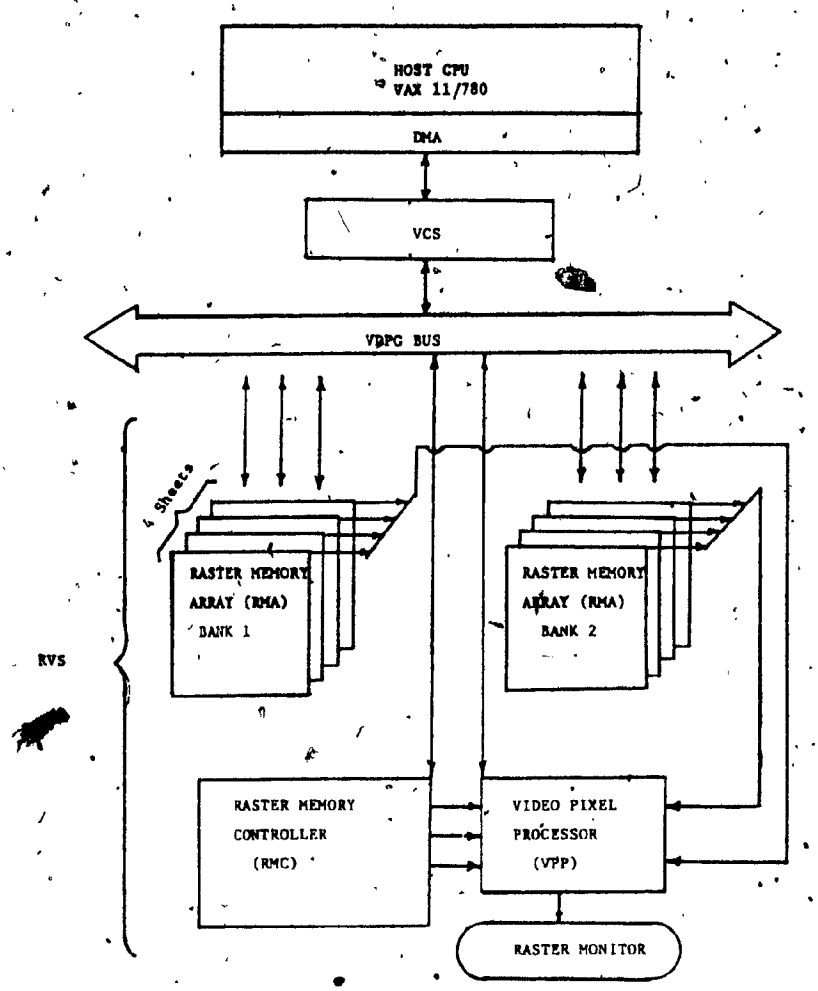

Figure 4.2: VDP System Data Flow Diagram

sent to the VDP Controller Subsystem (VCS). The VCS accepts high level graphic and usage-oriented instructions from the host communications interface post; performs their interpretation by reading and writing both data and control to the Raster Video subsystem (RVS). A typical RVS is composed of the following sub-modules:

- a raster memory controller (RMC)
- a raster memory array (RMA)
- a video pixel processor (VPP)

A simplified block diagram of the RVS is shown in Fig. 4.2. There can be several RMA's called 'banks' in an RVS. The output of the RMA's is connected to a pixel processor, VPP, which routes the data obtained from the various banks through look-up tables. The output of the tables control the values applied to D/A converters attached to the red, green and blue guns of a raster monitor.

4.3 Generation of Elements for Dynamic Graphics

To be able to display even the simplest elements dynamically, one must develop a library of basic elements. The objective is to develop the dynamic graphics to show the dynamic motion and kinematics of the motorcycle suspension. However, to be introduced to the methodology in dynamic graphics, the discussion will be limited at first to the details of generating dynamic graphics of simple systems shown in Fig. 4.3.

For these simple systems illustrated in Fig. 4.3, the basic elements needed for graphical representation are:

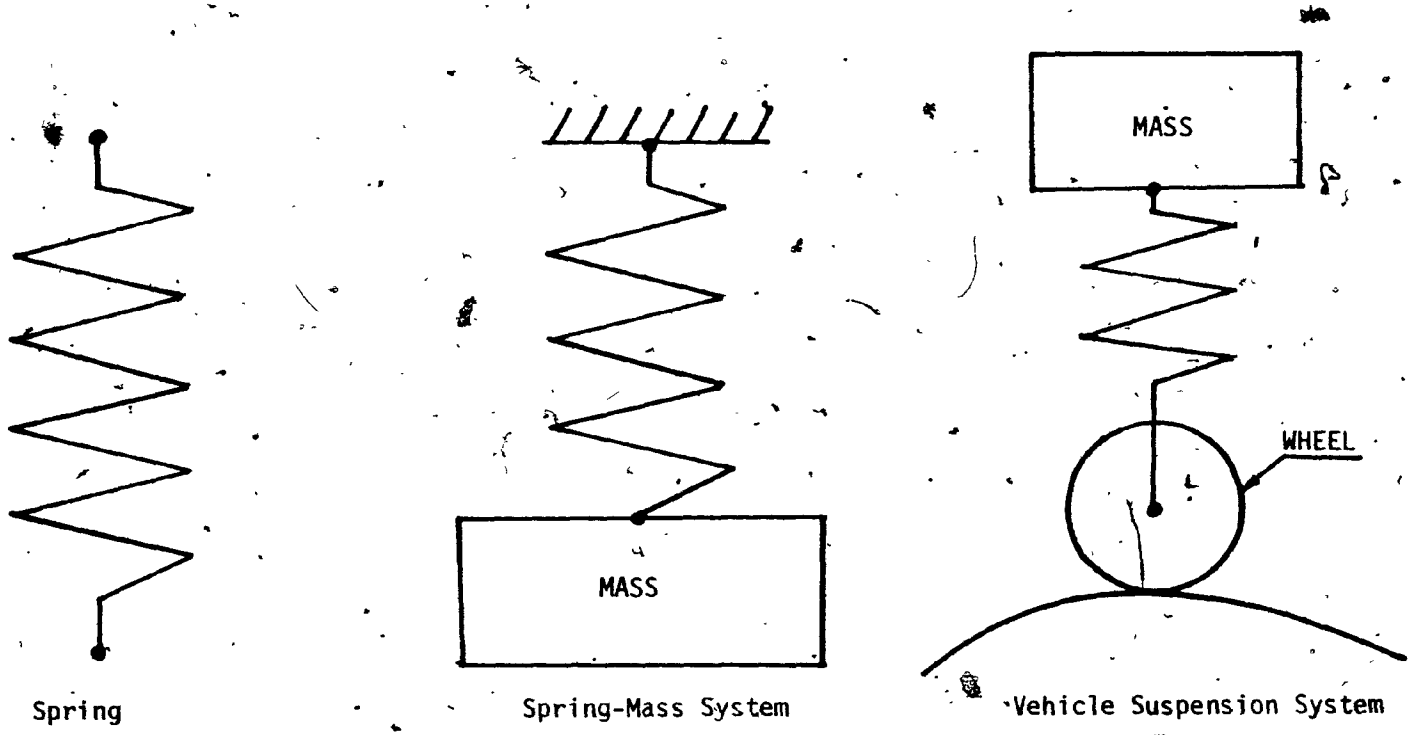

Spring Spring-Mass System Vehicle Suspension System

Figure 4.3: Simple Systems for Dynamic Graphics

1. Spring
2. Rectangle
3. Circle

4.3.1 Generation of Spring Elements

The simplest spring element generation will be explained here, in order to demonstrate the technique for generating the total system later.

Three subroutines are required to generate the spring, mainly:

1) CALL SPIX (IPIXBA, IPIXC)

. This subroutine assigns the color of the spring.

. The subroutine parameters are defined as follows:

IPIXBA - pixel value for B data path in upper 8 bits, and pixel value for A data path in lower 8 bits.

IPIXC - pixel value for C data path in lower 8 bits.

2) CALL SET (IX, IY)

. This subroutine sets the current beam position for the specified value.

. The subroutine parameters are defined as follows:

IX - X coordinate of the beam position

XY - Y coordinate of the beam position

3) CALL VEC (IDX, IDY)

. This subroutine draws a vector as specified from the current beam position.

. The subroutine parameters are defined as follows:

IDX - dx from current beam position.

IDY - dy from current beam position

NOTE: dx and dy can be either positive or negative values

Using these three subroutines the spring can be generated in the following fashion: To visualize the spring generation, it is divided into elements as shown in Fig. 4.4. From this consideration the spring drawing subroutine was developed.

SUBROUTINE SPRING (X,Y, $\Delta X1$, $\Delta Y1$, $\Delta Y2$, n).

The parameters of this subroutine are defined in Fig. 4.4.

4.3.2 Circle Generation

First, the subroutine for generating the cicrle coordinates is developed and then the drawing subroutine.

The circle coordinates are generated by using the following equations:

The X-coordinates are generated by

$X(I) = R \cos \Theta$ where $0° \leq \Theta \leq 360°$ and R = radius

and Y-coordinates are generated by

$Y(I) = R \sin \Theta$ where $0° \leq \Theta \leq 360°$ and R = radius

Following the coordinate generation, a subroutine for drawing the circle was developed using subroutine CIRC which utilizes CALL SET and CALL VEC subroutines:

SUBROUTINE CIRC (X,Y,N,XC,YC)

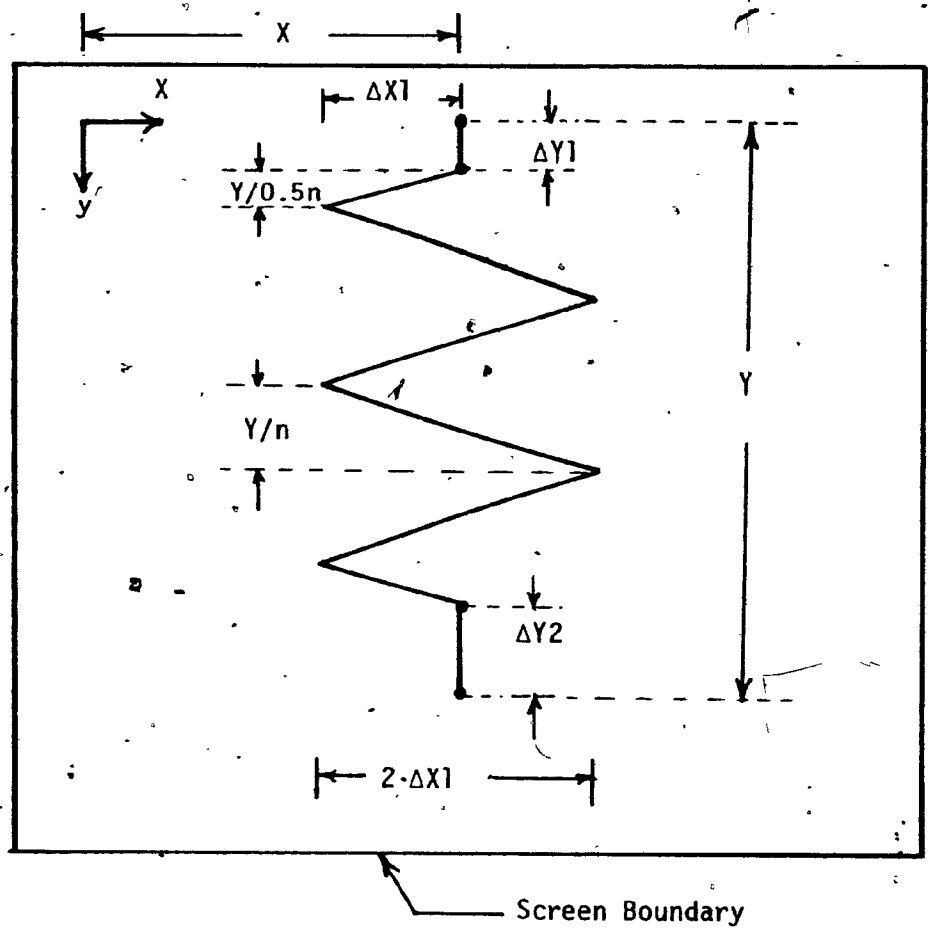


```
CALL  SPIX (80,0)
CALL  SET  (X,0)
CALL  VEC  (0,ΔY1)
CALL  VEC  (-ΔX1,ΔY/0.5n)
CALL  VEC  (2.ΔX1, Y/n)
CALL  VEC  (-2.ΔX1, Y/n)
CALL  VEC  (2.ΔX1, Y/n)
CALL  VEC  (-2.ΔX1, Y/n)
CALL  VEC  (ΔX1,ΔY1/0.5n)
CALL  VEC  (0,ΔY2)
```

Where:

n = number of nodes - 4

In our case

n = 9 - 4 = 5

Figure 4.4 : Spring Generation

where

X = X(I)

Y = Y(I)

N = number of points.

XC,YC = coordinates of circle center.

4.3.3 Rectangle Generation

The rectangle is generated by the following subroutine which in turn utilizes CALL SET and CALL VEC subroutines.

CALL RECT (IDX, IDY)

This subroutine draws a rectangle as specified from the current beam position.

The subroutine parameters are defined as follows:

IDX - size of rectangle in X-axis

IDY - size of rectangle in Y-axis

NOTE: Sizes can be either positive or negative values.

4.3.4 Road-Profile Generation

Having the road profile coordinates the road was generated using CALL SET and CALL VEC routines.

4.4 Dynamic Graphics of Simple Systems and Program Documentation

The general concept of dynamic display using VAX-11/780-Norpak system can be described as follows: After Norpak initialization, the differential equations characterizing the motion of the system are solved to compute the equations generalized coordinates at every instant of time. The system equations were programmed in FORTRAN on a VAX-11/780 digital

computer. As outlined earlier, a predictor-corrector initial value solving routine was used. For the theoretical explanation of this routine refer to Appendix D.

The data base for springs, circles, rectangles are recalled by appropriate subroutines. After displaying each position of the model, the VDP screen is cleared and the new position of the model is drawn.

To obtain the animated motion of the motorcycle suspension system, the methodology for the dynamic graphics is developed and presented in the form of a building block from the simplest system to the final form. The initial sequence of this development is as follows:

1) Dynamics graphics display of a spring-mass system (1 D.O.F model).
2) Dynamic graphics of a 1 D.O.F model of vehicle system (without damping).

The general control of dynamic display was illustrated in Section 4.2.2. Data flow diagrams are illustrated in Fig. 4.5 to 4.7.

In accordance with the flow diagrams the corresponding software, for spring mass and single degree of freedom vehicle model systems, were developed. There are two dynamic graphic packages developed for the simple vehicle suspension. In the first package the vehicle is moving across the display console and the road is stationary. In the second package a very interesting visual effect was achieved by moving the road with the velocity equivalent to the velocity of the vehicle and displaying the motion of the vehicle. The input parameters used

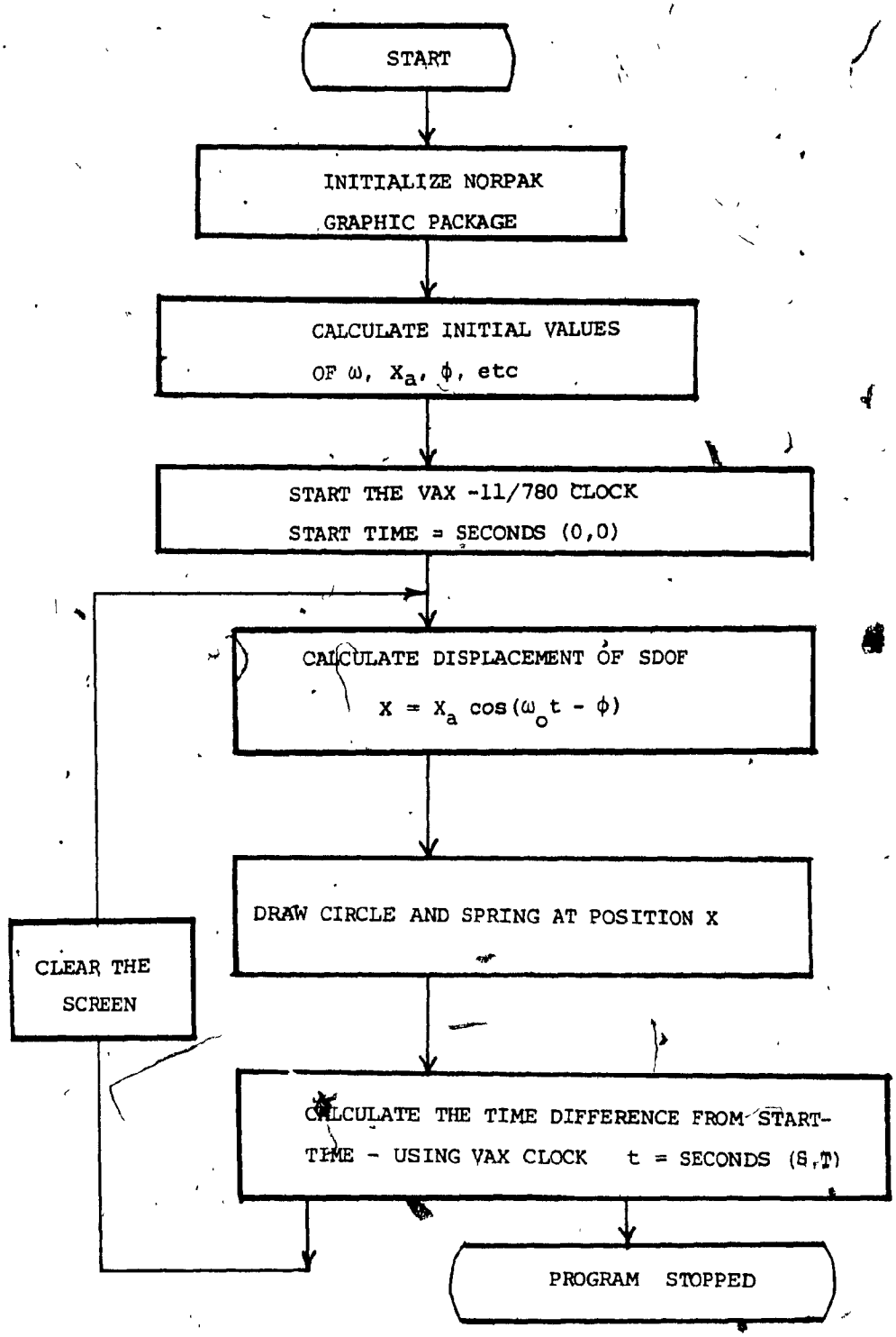

Figure 4.5: Flow Chart of SDoF System

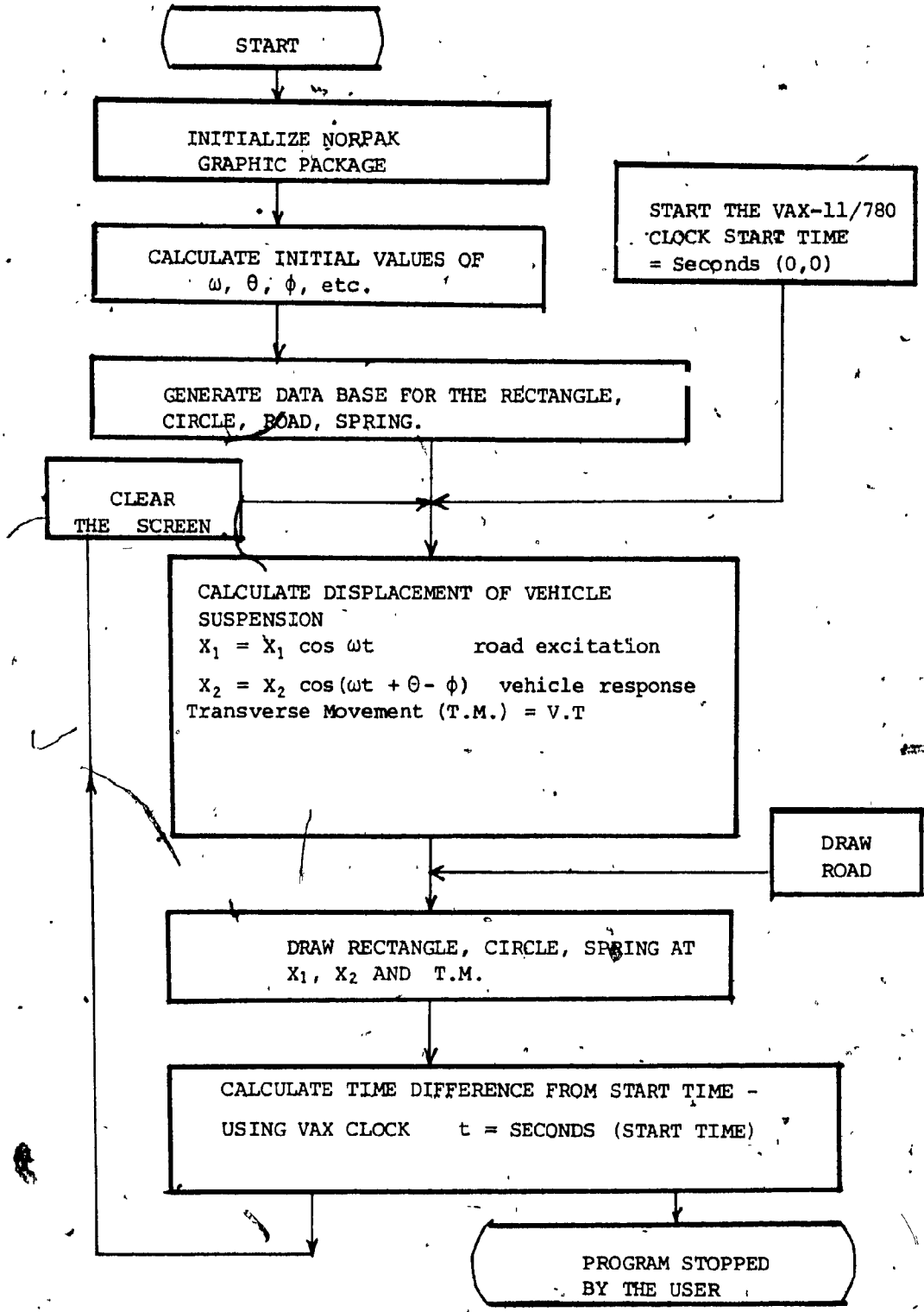

Figure 4.6: Flow Chart of Vehicle Suspensibn (Road Stationary Vehicle Moving Across the Screen)

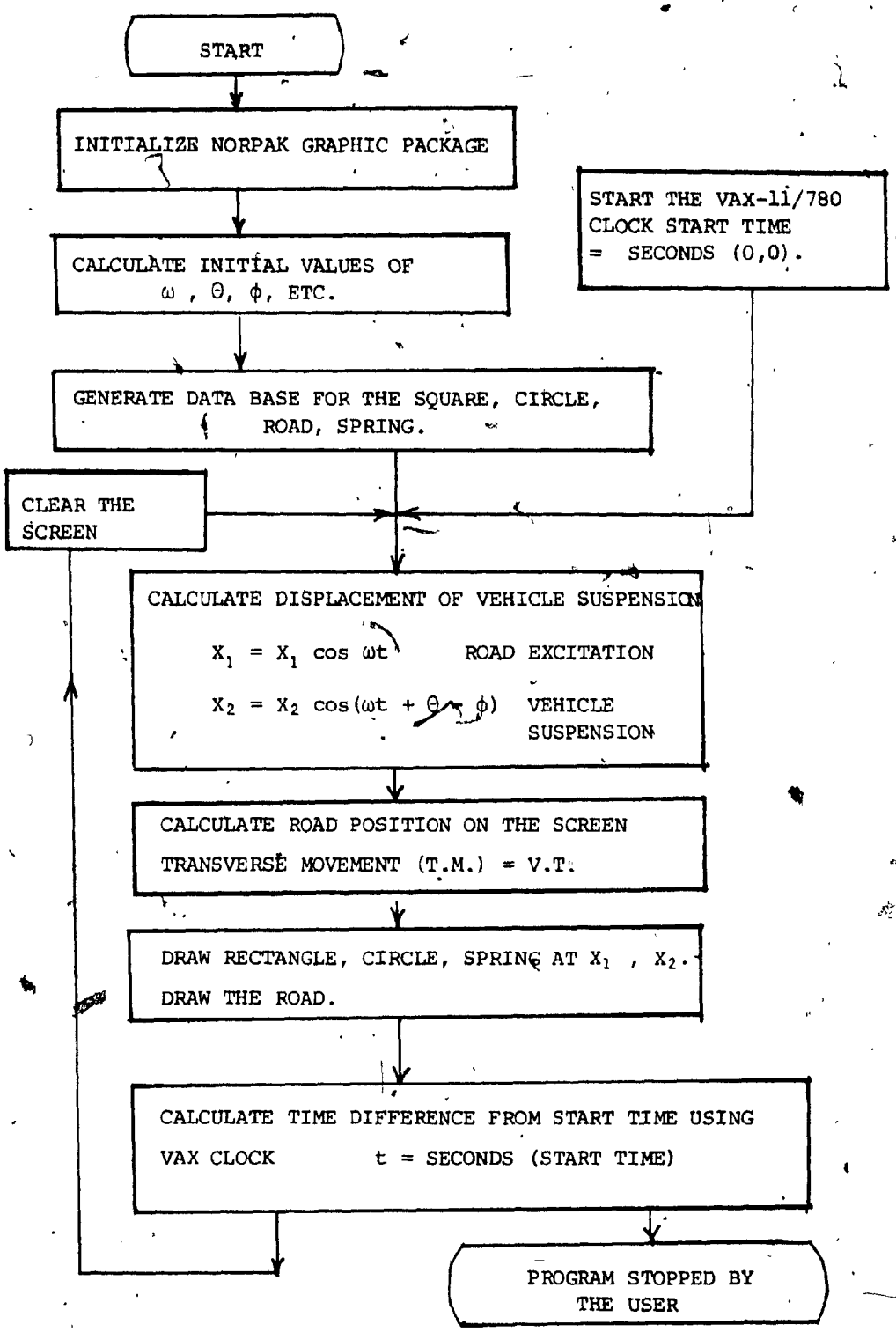

Figure 4.7 : Flow Chart of Vehicle Suspension (Road-Moving With Velocity V Across the Screen Vehicle-Vertical Motion On the Screen).

for these cases are shown in Table 4.1.

At first the user runs the requested program and then inputs the appropriate parameters interactively. The dynamic response is then seen directly on the VDP screen. Typical outputs at three arbitrary instants in time are illustrated in Figs. 4.8 to 4.10. Using dynamic graphics, one can see the dynamic response of the system for any variations in the input parameters, and this provides additional dimension in the design and calculation of responses.

4.5 Dynamic Display of the Motorcycle Suspension

In order to generate a two-dimensional dynamic display of the motorcycle suspension, it is necessary to develop spring element which can be translated and rotated. In addition, it is necessary to develop wheel and frame elements which again must have the capability of translation and rotation. Thus these three elements can be put together to form the dynamic package consisting of the solution of differential equations and drawing subroutines. In the following sections the details of generating these three elements will be described.

4.5.1 Advanced Spring Element

To display the spring of constant length on the VDP screen between any two points, it is necessary to generate the spring coordinates and then using CALL SET and CALL VEC subroutines to draw the spring. It should be noted that the translation and rotation of the spring element is taken care of in this subroutine.

The subroutine for spring generation and drawing is in the following form:

```
SUBROUTINE SPRDRWI (NPNT, LENGTH, XTOP, XBOT, YBOT, ISPX, ISPY)
```

TABLE 4.1 - Sample Cases

A. SDOF System	
User	R Spring
Vax	M,K,Xa,V
User	1,1,1,1

B. Vehicle Suspension	
User	R SZOK7 or R SZOK8
Vax	M, k, V, C, kL
User	1000, 300, 2, 120, 1

NOTE:

M = mass Kg (lb sec^2/in)

K = stiffness N/m (lb/in)

V = initial velocity m/s (in/sec)

C = damping N sec/m (lb sec/in)

KL = scaling factor

X_a = initial amplitude m (in).

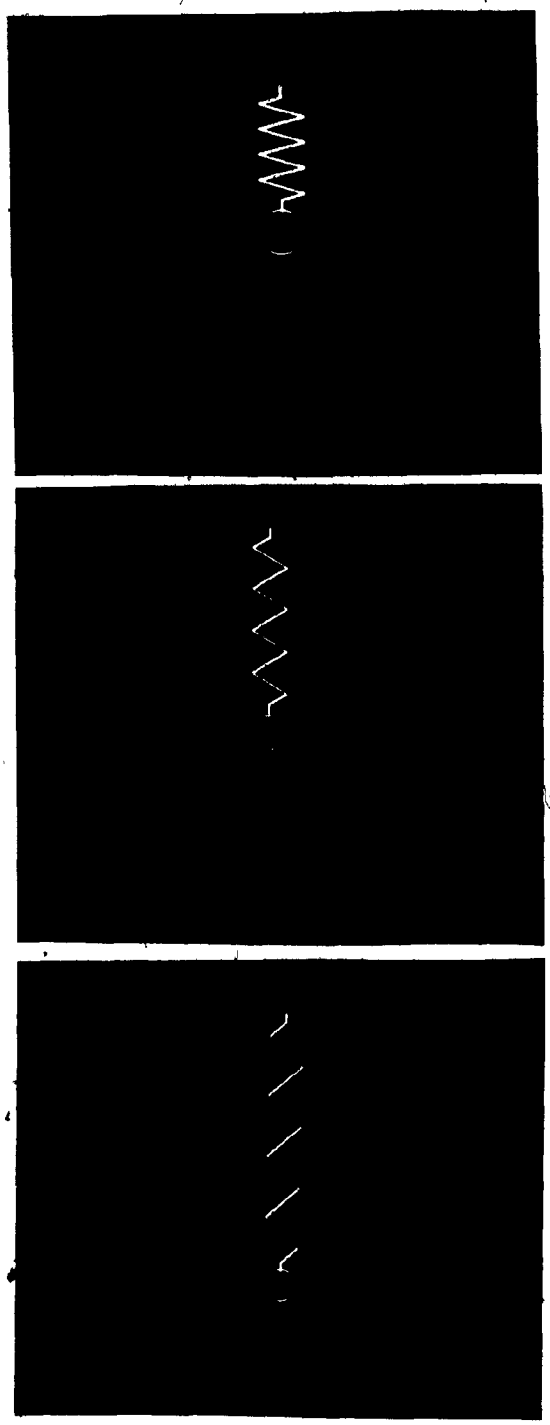

Figure 4.8: Dynamic Display of Spring-Mass System

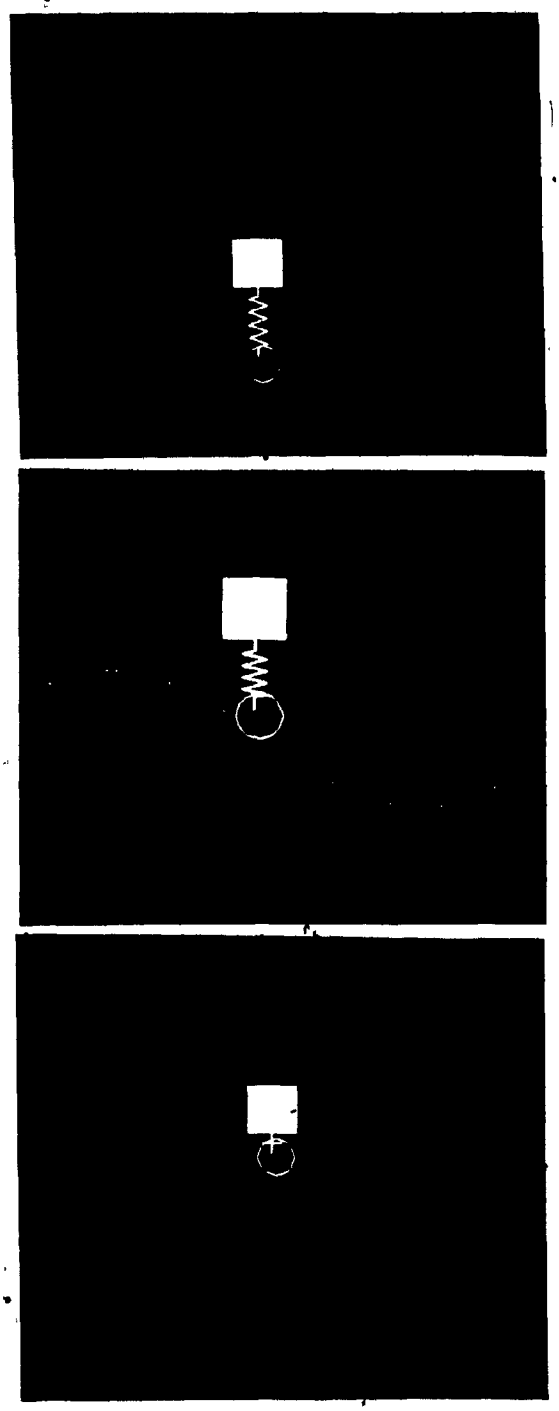

Figure 4.9 : Dynamic Display of Vehicle Suspension-Moving Road

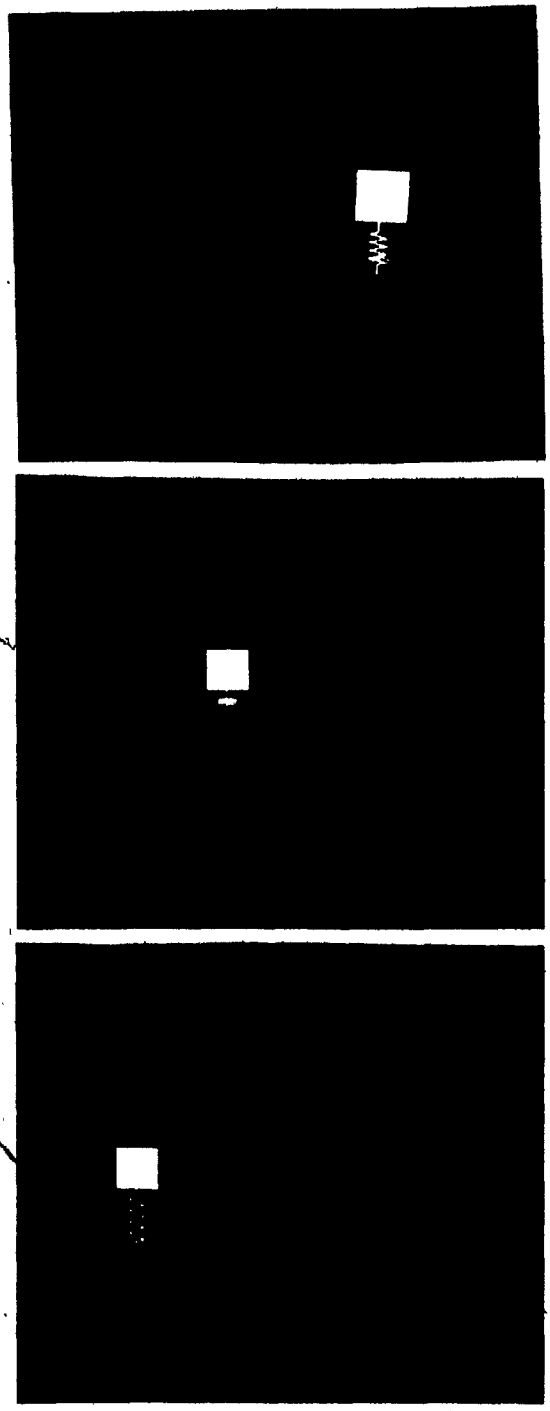

Figure 4.10: Dynamic Display of Vehicle Suspension-Road Stationary.

where

NPNT - Number of points on one side of the spring.

LENGTH - Constant length of the spring.

XTOP,YTOP - Are the coordinates of the higher point on the screen.

XBOT,YBOT - Are the coordinates of the lower point on the screen.

ISPX,ISPY - Are two arrays used to store and manipulate the spring data base.

4.5.2 Wheel Element

The wheel element is generated by drawing two circles, as explained in section 4.3.2, with different radii.

4.5.3 Rigid Frame Element

The first step in rigid frame generation is to sketch the graphical model of the frame as illustrated in Fig. 4.11. The graphical model is descretized into nodes and elements. The physical dimensions are transformed into pixel coordinates and are stored in the following subroutine:

SUBROUTINE MOTGEN (N,IX,IY,SCALE)

where

N = Number of nodes

IX,IY = Pixel coordinates of the nodes

SCALE = Scale factor

Then using CALL SET and CALL VEC subroutines the motorcycle frame is drawn.

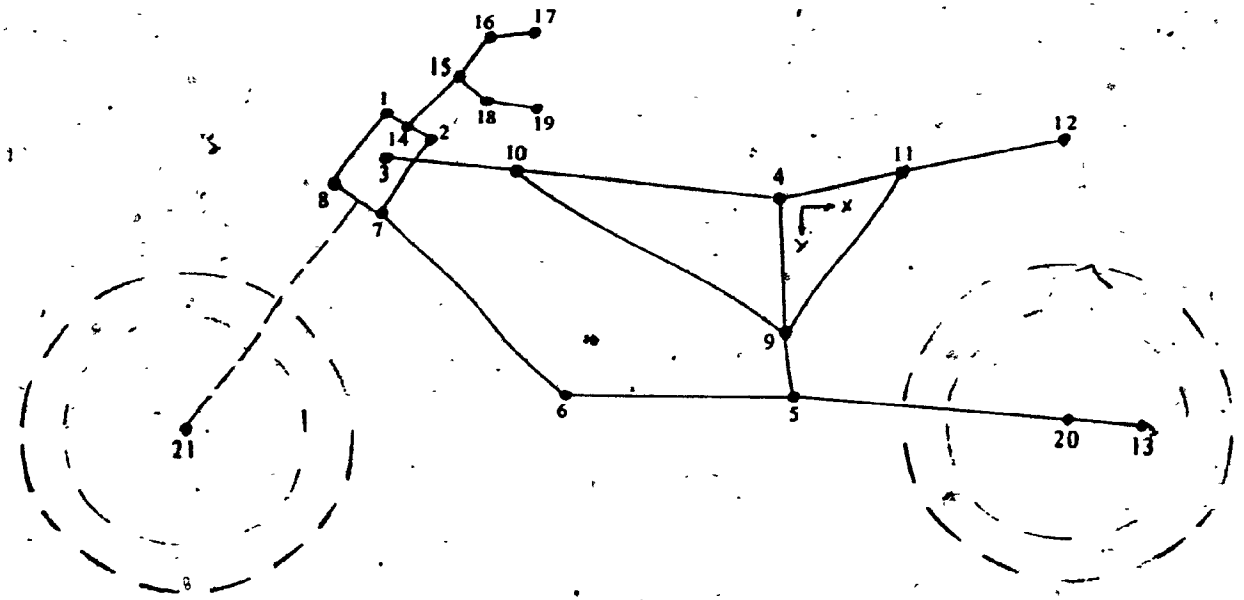

Figure 4.11: Graphical Model of Rigid Frame

4.5.4 Dynamic Graphics: Program Documentation and Display

Using the set of elements described above, the total picture of the motorcycle was drawn on the screen. It should be noted that the translation and rotation of each of the elements described are taken care of in their respective subroutines. The dynamic display was then obtained by displaying each position of the model on the VDP screen, clearing the screen and drawing the model at a new position. For this purpose, the equations derived for the lumped mass model were programmed on the VAX-11/780 digital computer and the response for a given road profile was computed. The response which provides the final coordinates of the model is then supplied to the VDP screen after the NORPAK initialization.

The details of the dynamic graphics generation of the motorcycle are illustrated in Fig. 4.12. Because the continuous dynamic output is difficult to represent graphically, the sample output of the animated displacements at three arbitrary positions are shown in Fig. 4.13.

4.6 Interactive Graphics in the Design and Analysis of the Motorcycle Suspension

The concept of interactive graphics is used in the design and analysis of the motorcycle suspension. The user is allowed to input various parameters and perform different analysis through the selectible menu. First the user inputs the physical parameters of the motorcycle: damping, stiffness, mass, inertia and geometrical length. The details of this menu are illustrated below.

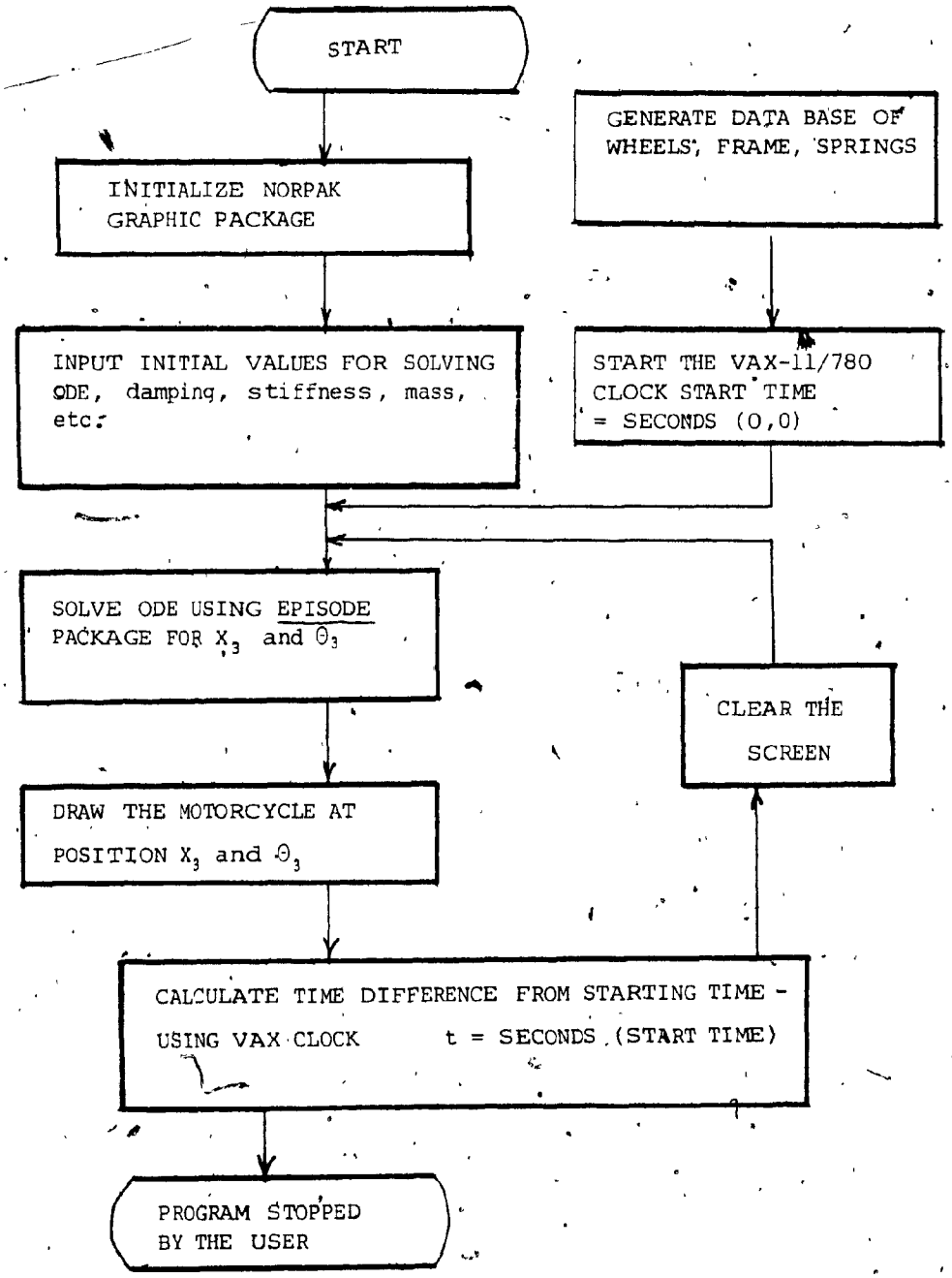

Figure 4.12: Flow Chart of the Dynamic Response of Motorcycle

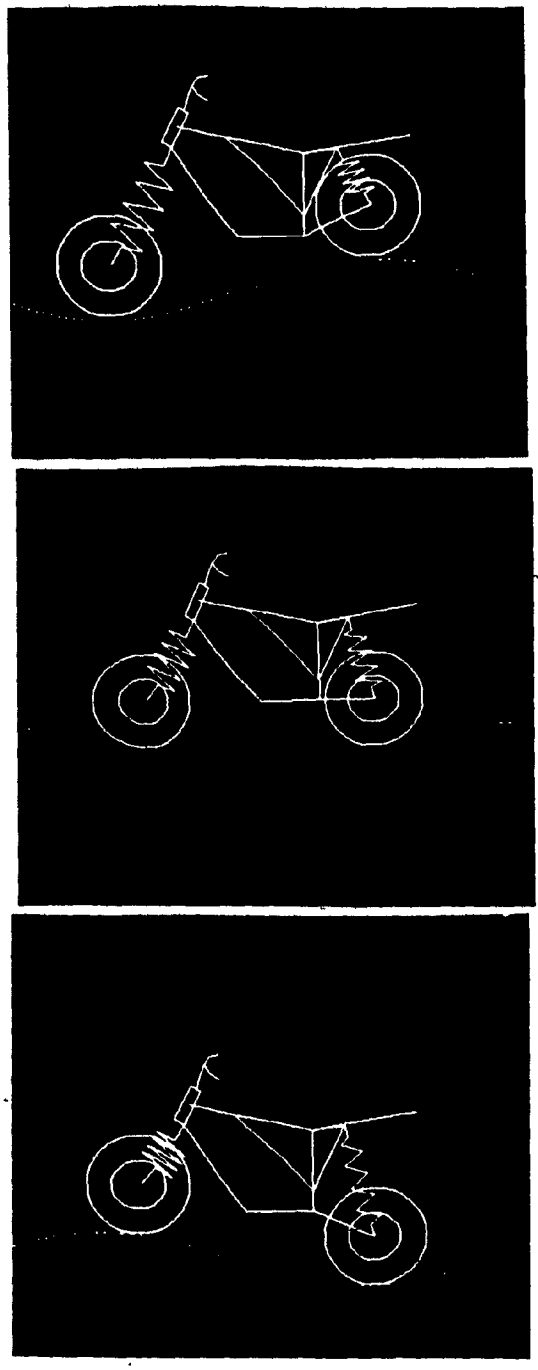

Figure 4.13: Three Positions of the Motorcycle on Sinusoidal Track

ENTER SPRING CONSTANTS	$[K_1, K_2, K_3, K_4]$	N/m	(lb/in)
ENTER DAMPING CONSTANTS	$[C_1, C_2, C_3, C_4]$	N.sec/m	(lb.sec/in)
ENTER WHEELS MASSES	$[M_1, M_2]$	kg	($lb.sec^2/in$)
ENTER MOTORCYCLE MASS	$[M_3]$	kg	($lb.sec^2/in$)
ENTER MOTORCYCLE INERTIA	$[J_3]$	$kg.m^2$	($in\text{-}lb.sec^2$)
ENTER LENGTH	$[L_2, L_3, L_4, L_5, L_6]$	cm	(in)
ENTER HEIGHT	$[H_1]$	cm	(in)
ENTER α_6, ϕ	$[\alpha_6, \phi]$	rad	(rad)
ENTER ROAD PARAMETERS	[XL, XO]	cm	(cm)
ENTER MOTORCYCLE VELOCITY	[V]	cm/sec	(cm/sec)

After the input of motorcycle parameters, the designer has three options:

1) Dynamic display of the motorcycle
2) Variation of parameters
3) Three types of damping:
   a) Linear symmetrical
   b) Linear non-symmetrical
   c) Non-linear and Non-symmetrical

The menu for items 2 and 3 is organized as follows:

ORDINATE	TYPE 1	For X_2, X_4
	TYPE 2	For X_3, θ_3, DF, DR, $\ddot{X}_3$
DAMPING	TYPE 1	For linear symmetrical
	TYPE 2	For linear non-symmetrical
	TYPE 3	For non-linear non-symmetrical

PARAMETER VARIATION CASE	TYPE 1	For Variation in C_1, C_4
	TYPE 2	For Variation in K_1, K_4
	TYPE 3	For Variation in C_2
	TYPE 4	For Variation in K_2
	TYPE 5	For Variation in C_3
	TYPE 6	For Variation in K_3
	TYPE 7	For Variation in M_2
	TYPE 8	For Variation in M_4
	TYPE 9	For Variation in M_3
	TYPE 10	For Variation in J_3
	TYPE 11	For Variation in X_0
	TYPE 12	For Variation in L_3
	TYPE 13	For Variation in ϕ
	TYPE 14	For Variation in L_6
	TYPE 15	For Variation in α_6
SELECTION OF OUTPUT	TYPE 1	For Transmissibility X_3
	TYPE 2	For Transmissibility θ_3
	TYPE 3	For Trnasmissiblity X_2
	TYPE 4	For Transmissiblity X_4
	TYPE 5	For Transmissibility $\ddot{X}_3$
	TYPE 6	For Transmissibility DF
	TYPE 7	For Transmissibility DR

First the user selects the appropriate ordinate. This is required because X_2 and X_4 coordinates have higher frequency content in the transmissibility plots. After ordinate consideration, three types of

damping can be selected. There are 15 options for varying the parameters and 7 options for selecting the output.

In option number 1 - the dynamic display of the motorcycle, the designer can select detailed generalized coordinate information about displacement, velocity and acceleration. The menu for option 1 is organized in the following fashion.

SELECTED TIME HISTORIES		
	TYPE 1	For X_3, θ_3
	TYPE 2	For X_2, X_4
	TYPE 3	For X_1, X_5
	TYPE 4	For $\dot{X}_2$, $\dot{X}_4$
	TYPE 5	For $\dot{X}_3$, $\dot{\theta}_3$
	TYPE 6	For $\ddot{X}_2$, $\ddot{X}_4$
	TYPE 7	For $\ddot{X}_3$, $\ddot{\theta}_3$
	TYPE 8	For SF1 Spectrum
	TYPE 9	For S1 Spectrum
	TYPE 10	For RF1 Spectrum
	TYPE 11	For R1 Spectrum

By typing either 1 or 2 or 3 will give the designer detailed displacement time histories. By typing either 4 or 5 will give the designer detailed velocity time histories.

By typing either 6 or 7 will give the designer detailed acceleration time histories.

In addition there is an option for generating the response spectra from time histories (8,9,10,11). These spectra are then used as a loading input to finite element model of the motorcycle frame.

4.7 Conclusions

In this chapter the VAX-11/780 system configuration is explained followed by the description of the NORPAK hardware for dynamic graphics. The methodology of developing dynamic graphics is explained on simple mechanical systems. The same methodology is then applied to the dynamic display of the motorcycle suspension. The use of interactive graphics is illustrated and the menu is explained in detail.

CHAPTER 5

FINITE ELEMENT ANALYSIS OF MOTORCYCLE FRAME

5.1 General

In this section a Finite Element Analysis (FEA) of the motorcycle frame using a general purpose software package is carried out. The software package is "ANSYS", a large scale, general purpose computer program with several analysis capabilities [37]. Analysis capabilities available include static and dynamic; elastic; plastic; creep and swelling; buckling; small and large deflections; steady state and transient. The main features of the program are as follows:

a) The matrix displacement method is employed.

b) Large number of library elements, more than forty for static and dynamic analysis.

c) Variety of elements, capable of analyzing two-and three-dimensional frame structure, piping systems, two-dimensional plane and axisymmetrical solids, three-dimensional shells.

d) Capability of non-linear analysis.

e) Uses the wave front solution method, resulting in a minimum computer time.

f) Loading on the structure may be forces, displacement, pressures, temperatures or response spectra.

g) Has excellent pre- and post-processing capabilities.

To properly model the structure for F.E. analysis and to obtain correct results and to interpret them correctly, the following steps were found helpful in modeling of any structure:

1) Obtain complete geometry definition from:

a) engineering drawings;

b) fabrication drawings;

c) sketches;

d) technical specifications.

2) Obtain full loading data.

3) Obtain all material properties

4) Determine boundary conditions

5) If the problem is large - start with a simplified model.

5.2 Finite Element Formulation

The displacement method is more desireable since its formulation is simpler for the majority of structural analysis problems.

The steps required to apply the finite element method to a problem are as follows:

1) Discretize the structural system. This requires the selection of the element type and size.

2) Generate the stiffness and mass matrices for the elements.

3) Generate the stiffness and mass matrices of the total structure.

4) Determine the unknown nodal displacements using equilibrium conditions.

5) Compute stresses and strains, natural frequencies and mode shapes.

A motorcycle manufactured by Bombardier Inc., Model 80-MX-6 is used in this analysis. The frame was discretized using three-

dimensional beam element with 6 degrees-of-freedom per each node. Figure 5.1 shows the discretization scheme with the corresponding node and beam numbering. For using the "ANSYS" finite element program, the following lists the input sequence:

1. Model preparation
2. Title card
3. Analysis type
4. Element type
5. Nodes-coordinates
6. Lumped masses
7. Elements
8. Real constants
9. Modes considered
10. Young's modulus
11. Poisson ratio
12. Density
13. Restraints
14. Iteration
15. Termination of input
16. Post processing
17. Mode shape plots.

In the first step, the model preparation, a user identifies details of the physical parameters of the frame and the type of analysis required. For the problem on hand, they are:

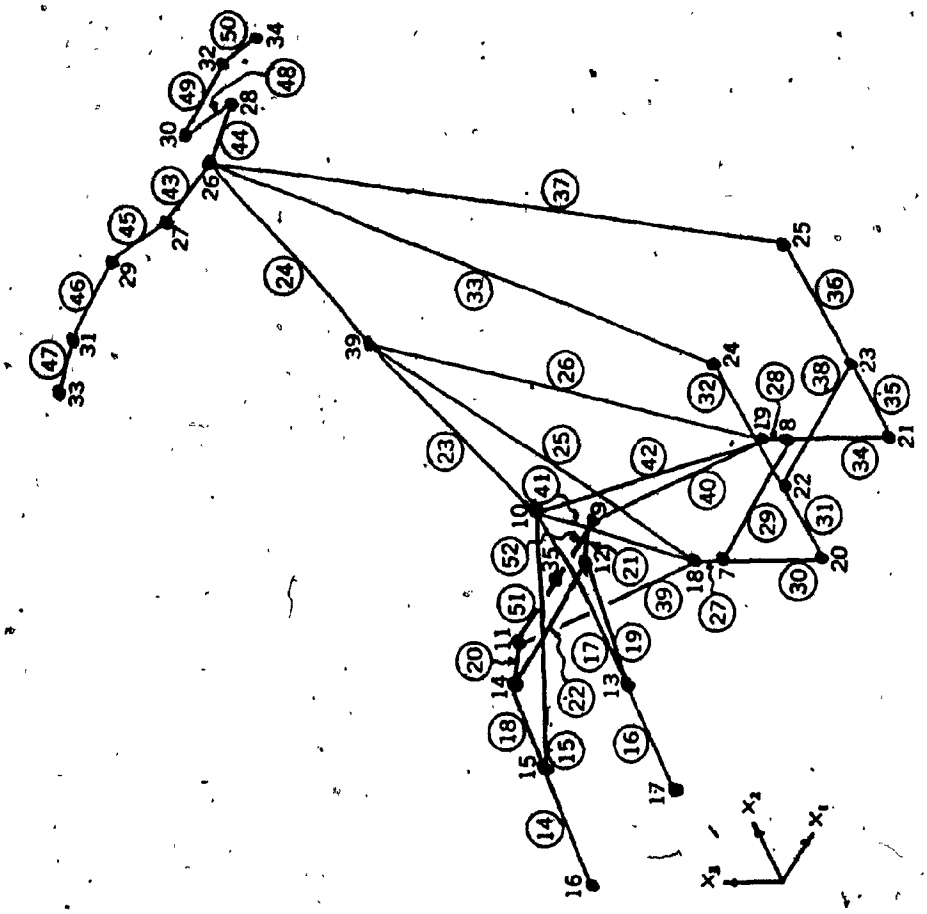

Figure 5.1: Node and Beam Numbering of Motorcycle Frame

Computer Input Data

1. Nodal coordinates
2. Nodal restrained degrees of freedom (D.O.F.)
3. Input nodal weights
4. Beam section properties

A sample of the input data is shown in Table 5.1.

Analysis Type

1. KAN-0 Static analysis
2. KAN-2 Eigenvalue/vector solution
3. KAN-2 Response spectrum analysis

To provide explanation on the data input and its sequence, a sample data file used to create the analytical model is listed in Table 5.2. Referring to this table, the numbers 1 to 17 on the left-hand side correspond to the input-sequence listed earlier.

5.3 Finite Beam Element Equation Formulation

Since the beam elements are used in the FE analysis, in this section a brief theory related to the formulation of the equation is presented. The FEM is based on the concept that if equations can be written representing each element by itself subjected to forces at its nodes then these element equations can be assembled to form a system of equations representing the equilibrium of the overall structure. The beam under consideration is shown in Fig. 5.2.

The standard element stiffness analysis is carried out as follows:

TABLE 5.1: A Sample of the Input Data for FEA

DETAILS	NODE #	X_1	X_2	X_3
Nodal Coordinates cm (in)	16	0. (0.)	0 (0.)	47. (18.5)
	17	20.3 (8.)	0. (0.)	47. (18.5)
	18	0. (0.)	50.8 (20.)	3.8 (1.5)

		X_1	X_2	X_3	X_4	X_5	X_6
*Nodal Restraints	26	1	1	1	0	1	1
	35	1	1	1	1	1	1
	7 to 34 and 39	1	0	0	0	1	1

		X_1	X_2	X_3
Nodal Masses kg;(lb.sec/in)	10	19.4 (0.111)	19.4 (0.111)	19.4 (0.111)
	11	19.4 (0.111)	19.4 (0.111)	19.4 (0.111)
	12	12.1 (0.069)	12.1 (0.069)	12.1 (0.069)

	Pipe Property #.	Outside Diameter	Pipe Thickness
Beam Section Properties cm; (in)	1	2. (0.8)	0.25 (0.1)
	2	8.6 (3.4)	0.25 (0.1)

*1 - indicates fixed DOF

0 - indicates free DOF

TABLE 5.2: ANSYS Sample Input for Motorcycle Frame

```
1  /PREP7
2  /TITLE,MODAL ANALYSIS OF THE MOTORCYCLE FRAME
3  KAN,2 $KAY,2,5
4  ET,1,9
   ET,2,21,,,2
   N,7,0,20,0
   N,8,8,20,0
   N,9,8,14.5,14.8
   N,10,4,19.3,13.5
   N,11,0,14.5,14.8
   N,12,8,11.6,16.5
   N,13,8,5.8,17
   N,14,0,11.6,16.5
   N,15,0,5.8,17
   N,16,0,0,18.5
   N,17,8,0,18.5
   N,18,0,20,1.5
   N,19,8,20,1.5
   N,20,0,20,-6
   N,21,8,20,-6
5  N,22,0,25,-6
   N,23,8,25,-6
   N,24,0,33,-6
   N,25,8,33,-6
   N,26,4,42.5,21
   N,39,4,30.5,17.6
   N,27,0,42.5,21.7
   N,28,8,42.5,21.7
   N,29,0,10,26
   N,30,8,40,26
   N,31,-5,40,26
   N,32,13,40,26
   N,33,-7.8,39,26
   N,34,15.8,39,26,
   N,35,4.,14.5,14.8
   $TYPE,2 $REAL,3
   E,9,                    $TYPE,2 $REAL,3
   E,10                    $TYPE,2 $REAL,3
   E,11                    $TYPE,2 $REAL,3
   E,12                    $TYPE,2 $REAL,4
   E,13                    $TYPE,2 $REAL,4
   E,14                    $TYPE,2 $REAL,4
6  E,15                    $TYPE,2 $REAL,4
   E,39                    $TYPE,2 $REAL,4
   E,26                    $TYPE,2 $RFAL,3
   E,22                    $TYPE,2 $REAL,6
   E,23                    $TYPE,2 $RFAL,6
   E,24                    $TYPE,2 $REAL,6
   E,25                    $TYPE,2 $RFAL,6
   $MAT,1 $TYPE,1 $RFAL,1
   E,16,15,          $MAT,1 $TYPE,1 $REAL,1
   E,15,10,          $MAT,1 $TYPE,1 $REAL,1
   E,17,13,          $MAT,1 $TYPE,1 $REAL,1
   E,13,10,          $MAT,1 $TYPE,1 $REAL,1
   E,15,14,          $MAT,1 $TYPE,1 $REAL,1
   E,13,12,          $MAT,1 $TYPE,1 $REAL,1
   E,14,11        $MAT,1 $TYPE,1 $REAL,1
7  E,12,9         $MAT,1 $TYPE,1 $REAL,1
   E,14,12        $MAT,1 $TYPE,1 $REAL,1
   E,10,39        $MAT,1 $TYPE,1 $REAL,2
   E,39,26        $MAT,1 $TYPE,1 $REAL,2
   E,18,39        $MAT,1 $TYPE,1 $REAL,1
   E,19,39        $MAT,1 $TYPE,1 $REAL,1
   E,7,18         $MAT,1 $TYPE,1 $REAL,1
   E,8,19         $MAT,1 $TYPE,1 $REAL,1
   E,7,8          $MAT,1 $TYPE,1 $REAL,1
   E,7,20         $MAT,1 $TYPE,1 $REAL,1
   E,20,22        $MAT,1 $TYPE,1 $REAL,1
   E,22,24        $MAT,1 $TYPE,1 $RFAL,1
   E,24,26        $MAT,1 $TYPE,1 $REAL,1
   E,8,21         $MAT,1 $TYPE,1 $RFAL,1
   E,21,23        $MAT,1 $TYPE,1 $REAL,1
   E,23,25        $MAT,1 $TYPE,1 $REAL,1
   E,25,26        $MAT,1 $TYPE,1 $REAL,1
   E,22,23        $MAT,1 $TYPE,1 $REAL,1
7  E,11,18        $MAT,1 $TYPE,1 $REAL,1
   E,9,19         $MAT,1 $TYPE,1 $RFAL,1
   E,18,10        $MAT,1 $TYPE,1 $REAL,1
   E,10,19        $MAT,1 $TYPE,1 $REAL,1
   E,27,26        $MAT,1 $TYPE,1 $REAL,1
   E,26,28        $MAT,1 $TYPE,1 $REAL,1
   E,27,29        $MAT,1 $TYPE,1 $REAL,1
   E,29,31        $MAT,1 $TYPE,1 $RFAL,1
   E,31,33        $MAT,1 $TYPE,1 $REAL,1
   E,28,30        $MAT,1 $TYPE,1 $RFAL,1
   E,30,32        $MAT,1 $TYPE,1 $REAL,1
   E,32,34        $MAT,1 $TYPE,1 $REAL,1
   E,11,35        $MAT,1 $TYPE,1 $REAL,1
   E,35,9         $MAT,1 $TYPE,1 $RFAL,1
   R,1,0.8,0.1
   R,2,3.4,0.1
8  R,3,.111
   R,4,.069
   R,5,0.026
   R,6,0.039
9  TOTAL,5
10 EX,1,30.E6,
11 MUXY,1,.3
12 MENS,1,.00073
   D,7,UX,,,34,1
   D,7,ROTY,,,34,1
   D,7,ROTZ,,,34,1
   D,39,UX
   D,39,ROTY
13 D,39,ROTZ
   D,35,ALL
   D,26,UX
   D,26,UY
   D,26,UZ
   D,26,ROTY
   D,26,ROTZ
14 ITER,1,1
15 AFURIT
   FINISH
16 /INPUT,27
   FINISH
   /POST22
   VIEW,1,-1,1 $ANGLE,-60 $SIZE,20,20 $CUBIC,1
   SET,1,1  $PLDISP
17 SET,1,2  $PLDISP
   SET,1,3  $PLDISP
   SET,1,4  $PLDISP
   FINISH
```

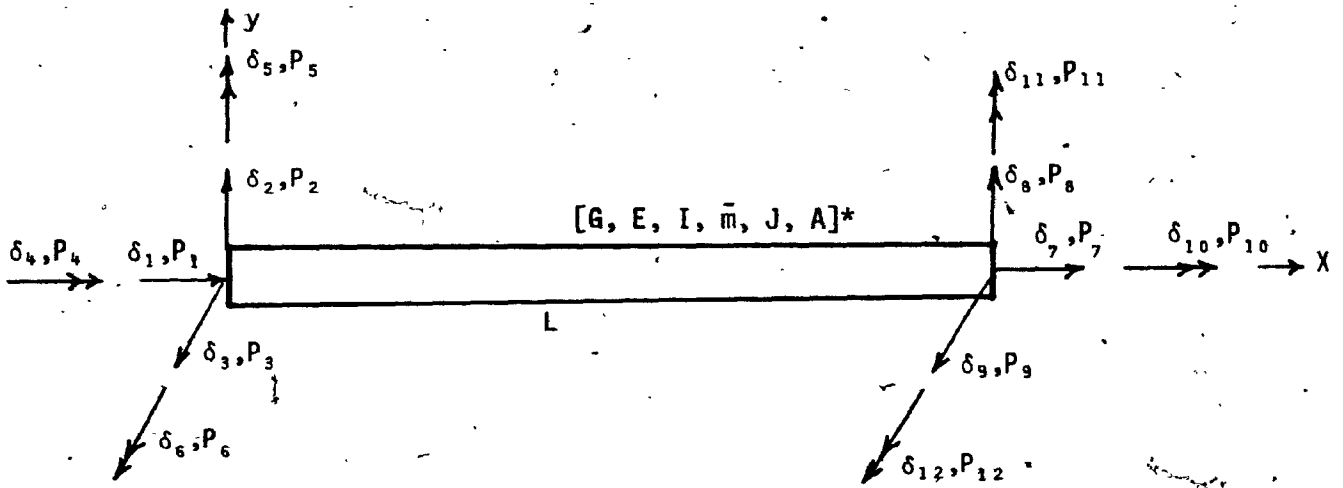

NOTE: ⟶ Represents Translation d.o.f

⟶⟶ Represents Rotation d.o.f

*G = Shear Modulus of Elasticity

E = Young's Modulus

I = Moment of Inertia

$\bar{m}$ = Distributed Mass per Unit length

J = Torsional Moment of Inertia

A = Cross-sectional Area

Figure 5.2: Order of Degrees of Freedom

1. The displacement of the nodes are the unknowns of the displacement finite element method:

$$\{\delta\} = \begin{Bmatrix} \delta_i \\ \delta_j \end{Bmatrix} = \begin{Bmatrix} \delta_1 \\ \vdots \\ \delta_6 \\ \vdots \\ \delta_{12} \end{Bmatrix}$$

The nodal displacement vector has twelve elements since there are two nodes and each has six degree of freedom.

2. Let displacements of an arbitrary point with in an element be given by

$$\{\psi\} = [N]\{\delta\}$$

where matrix [N] defines the matrix of the assumed displacement field.

3. The relationship between the strains and the modal deflections is dependent on matrix [B].

$$\{\varepsilon\} = [B]\{\delta\}$$

4. The general stress expression is related to the strain relations of the element by the elasticity matrix [D], i.e.:

$$\{\sigma\} = [D]\{\varepsilon\}$$

5. Now, the differential equations of motion can be obtained by Lagrange's method

$$\frac{d}{dt}\left\{\frac{\partial L}{\partial \dot{\delta}}\right\} - \left\{\frac{\partial L}{\partial \delta}\right\} + \left\{\frac{\partial F_D}{\partial \dot{\delta}}\right\} = 0$$

where

$$L = T - \pi$$

where

T is the kinetic energy of the structure

π is the potential energy of the structure

F_D is the dissipation energy of the structure

T_e is the kinetic energy of an element and is given by

$$T_e = \int_V \frac{\rho}{2} \{\dot{\psi}\}^T \{\dot{\psi}\} \, dV$$

π_e is the total potential energy of the element and is given by

$$\pi_e = U + V_F + V_R + V_S$$

where

U is the internal strain energy

V_F is the potential energy due to body forces (F)

V_R is the potential energy due to nodal forces (R)

V_S is the potential energy due to surface tractions (S)

$$\pi_e = \frac{1}{2} \int_V \{\varepsilon\}^T [D] \{\varepsilon\} \, dV - \int_V \rho \{\psi\}^T \{F\} \, dV - \{\rho\}^T \{R\} - \int_A \{\psi\}^T \{S\} dV$$

F_D is the dissipation energy given by

$$F_D = \frac{1}{2} \{\dot{\delta}\}^T [C] \{\dot{\delta}\}$$

Now, if the structural system has n elements, the potential energy must be summed up over n elements. In addition, using expressions for $\{\psi\}$ and $\{\varepsilon\}$ derived earlier we obtain

$$\pi = \sum_{1}^{n} \frac{1}{2} \{\delta\}^T \int_V [B]^T [D] [B] \, dV \, \{\delta\} - \{\delta\}^T \{Q\}$$

where Q is the total loading

$$\{Q\} = \sum_{1}^{n} \left[\int_V \frac{\rho}{2A} [N]^T \{F\} \, dV + \{R\} + \int_A \frac{1}{2A} [N]^T \{S\} \, dA \right]$$

and

$$T = \sum_{1} \frac{1}{2} \{\dot{\delta}\}^T \int_V \rho [N]^T [N] \, dV \, \{\dot{\delta}\}$$

The integrals

$$[k] = \int_V [B]^T D [B] \, dV$$

$$[m] = \int_V \rho [N]^T [N] \, dV$$

Substituting

$$\pi = \frac{1}{2} \{\delta\}^T [K] \{\delta\} - \{\delta\}^T \{Q\}$$

where

$$[K] = \sum_{1}^{n} [k]$$

$$T = \frac{1}{2} \{\dot{\delta}\}^T [M] \{\dot{\delta}\}$$

where

$$[M] = \sum_{1}^{n} [m]$$

$$F_D = \frac{1}{2} \{\dot{\delta}\}^T [C] \{\dot{\delta}\}$$

where

$$[C] = \sum_{1}^{n} [c]$$

Substituting into Lagrange's equation, we obtain

$$[M] \{\ddot{\delta}\} + [C] \{\dot{\delta}\} + [K] \{\delta\} = \{Q\}$$

The static equilibrium equation is

$$[K]\{\delta\} = Q$$

The resulting set of simultaneous equations is solved by the Wave Front technique.

Natural frequencies and mode shapes are obtained from the following equations:

$$[K] - \omega_i^2 [M] \{\phi\}_i = 0$$

where

ω_i = the circular natural frequency of mode;

$\{\phi\}_i$ = the reduced mode shape vector of mode i.

In ANSYS package the eigenvalues can be calculated using Jacobi or subspace iteration procedure.

5.4 Static and Modal Analysis

A load of 1 g was applied to the motorcycle frame. Using KAN = 0 in the ANSYS program, a static analysis was carried out. The resultant static deflections are shown in Fig. 5.3 and they can be used for the later use in the dynamic analysis for stress calculations.

Using KAN-2 of ANSYS, the modal analysis was performed. Table 5.3 lists the first five natural frequencies of the frame and Fig. 5.4 depicts its three fundamental mode shapes.

TABLE 5.3

Frequencies of the Motorcycle Frame

Frequency #	Frequency (Hz)
1	20.6
2	34.8
3	39.0
4	89.0
5	96.5

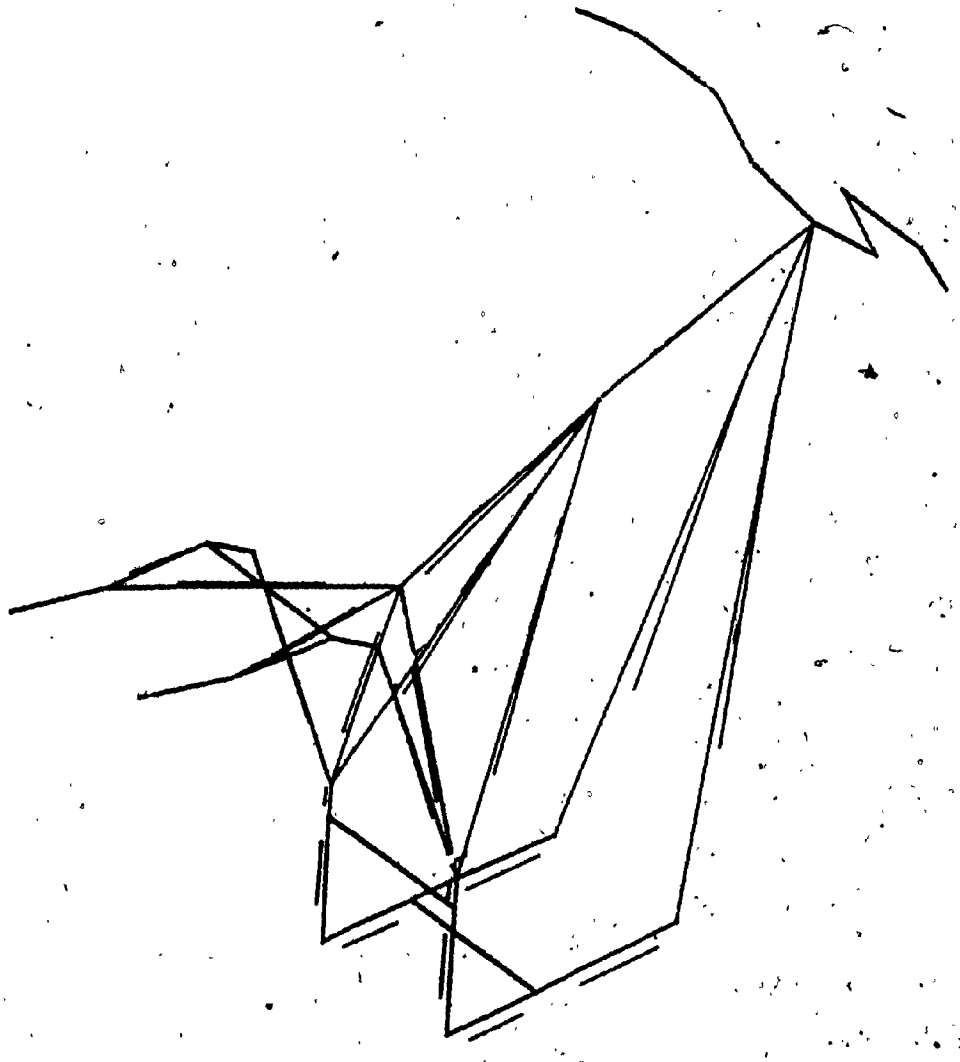

Figure 5.3: Static Deflection Plot

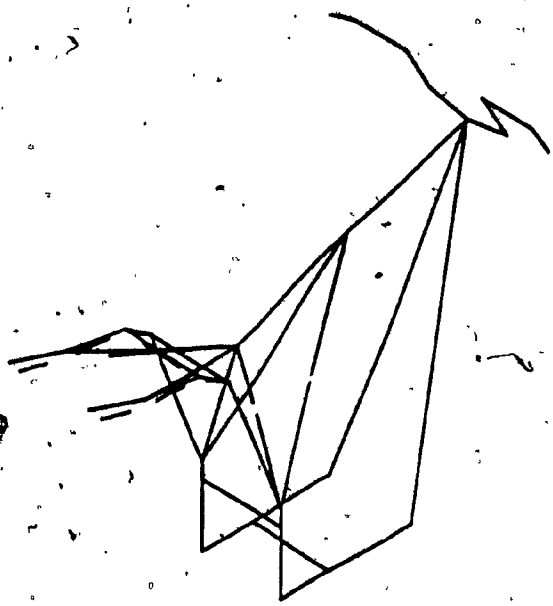

MODE 1

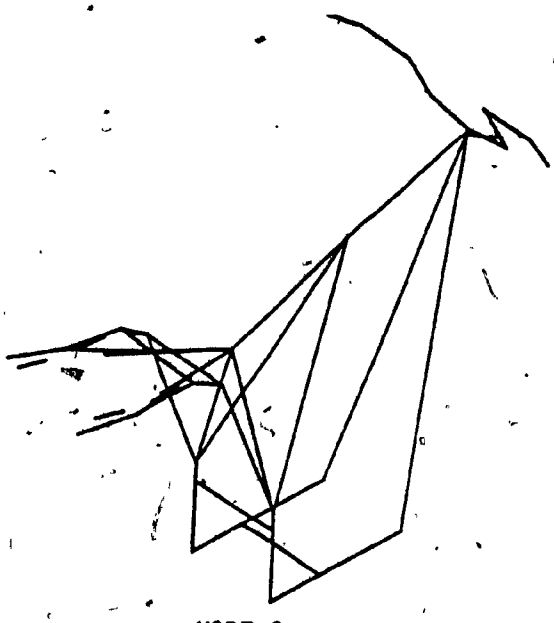

MODE 2

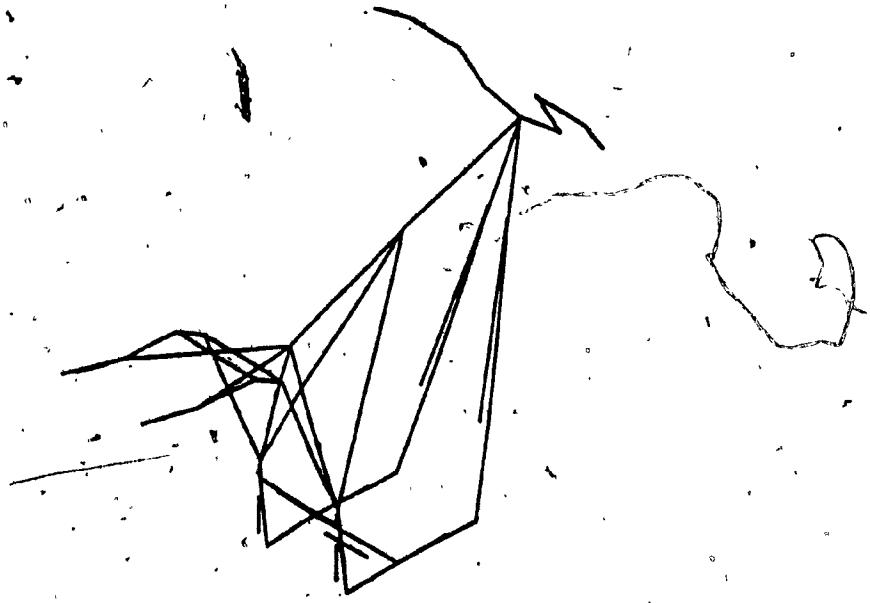

MODE 3

Figure 5.4: Mode Shape Plots

5.5 Animated Mode Shape Generation

5.5.1 Introduction

There is a great significance in evaluating the structural analysis of a model using animated mode shapes. Not only the designer can see the numerical output graphically, but also through animation he can investigate the interaction of various members. Furthermore, the animated mode shapes may indicate, for example, large structural deformations at frequencies too near the operating frequency of the product. So the configuration of the model can be changed through addition, deletion, alteration or re-arrangement of the structural members until the unwanted vibration is damped sufficiently. Since the actual modal displacements are comparatively small, distortion is highly exaggerated in the animated mode shapes.

Following is the detail description of the methodology for mode animation or response animation as applied to the motorcycle frame. This animation was developed with a digital computer VAX-11/780 and NORPAK-raster graphic display processor. The data flow diagram of the animated mode shapes is illustrated in Fig. 5.5.

5.5.2 Details of Animated Mode Shapes Generation

Figure 5.6 illustrates the model to be animated. The frame is descretized very similarly as in finite elements. To conserve the generality of the model, front and rear shocks were also included in the generation of this model.

However, if one is interested in the frame response alone, then it is very simple to suppress the nodes not required. This is achieved

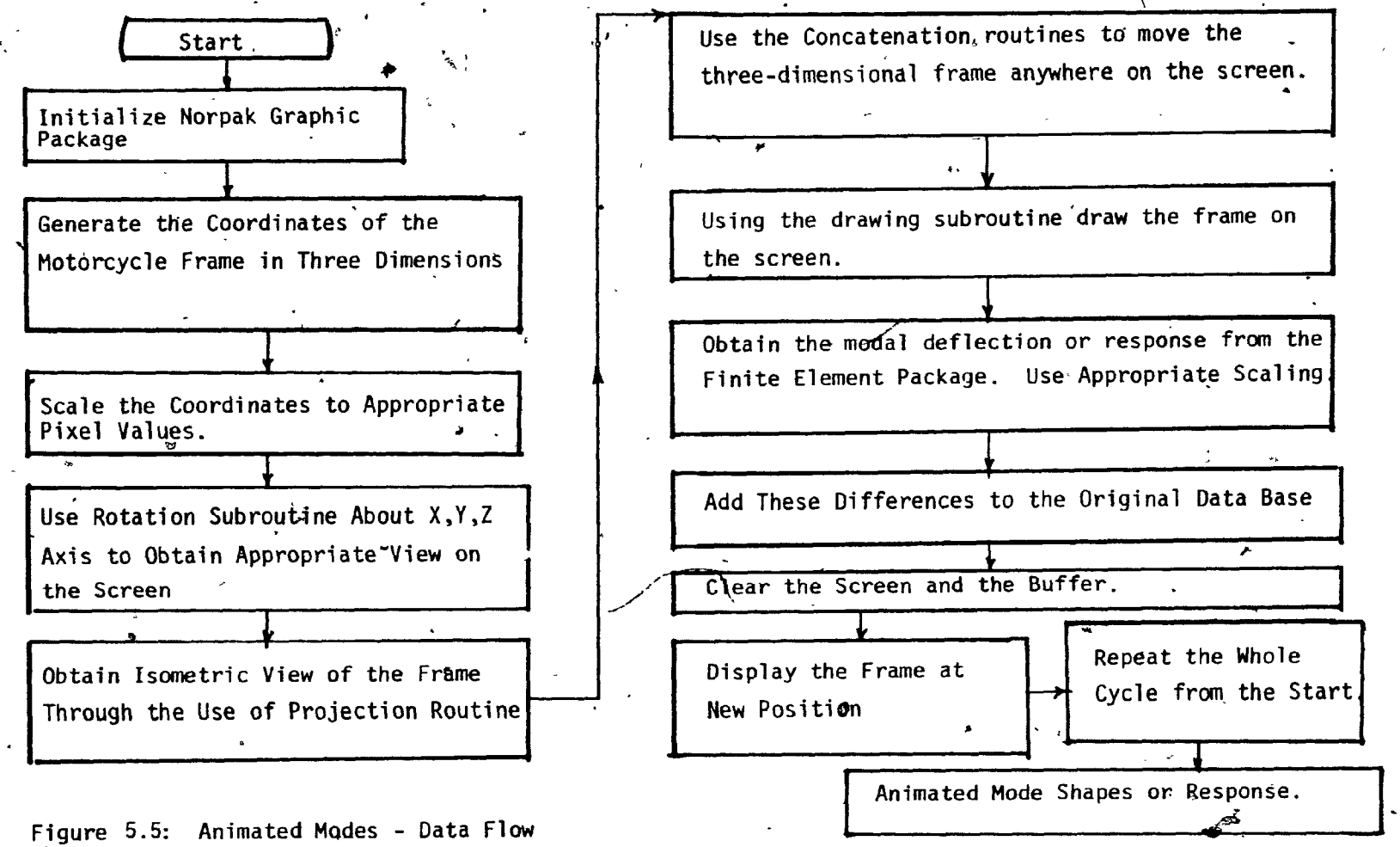

Figure 5.5: Animated Modes - Data Flow

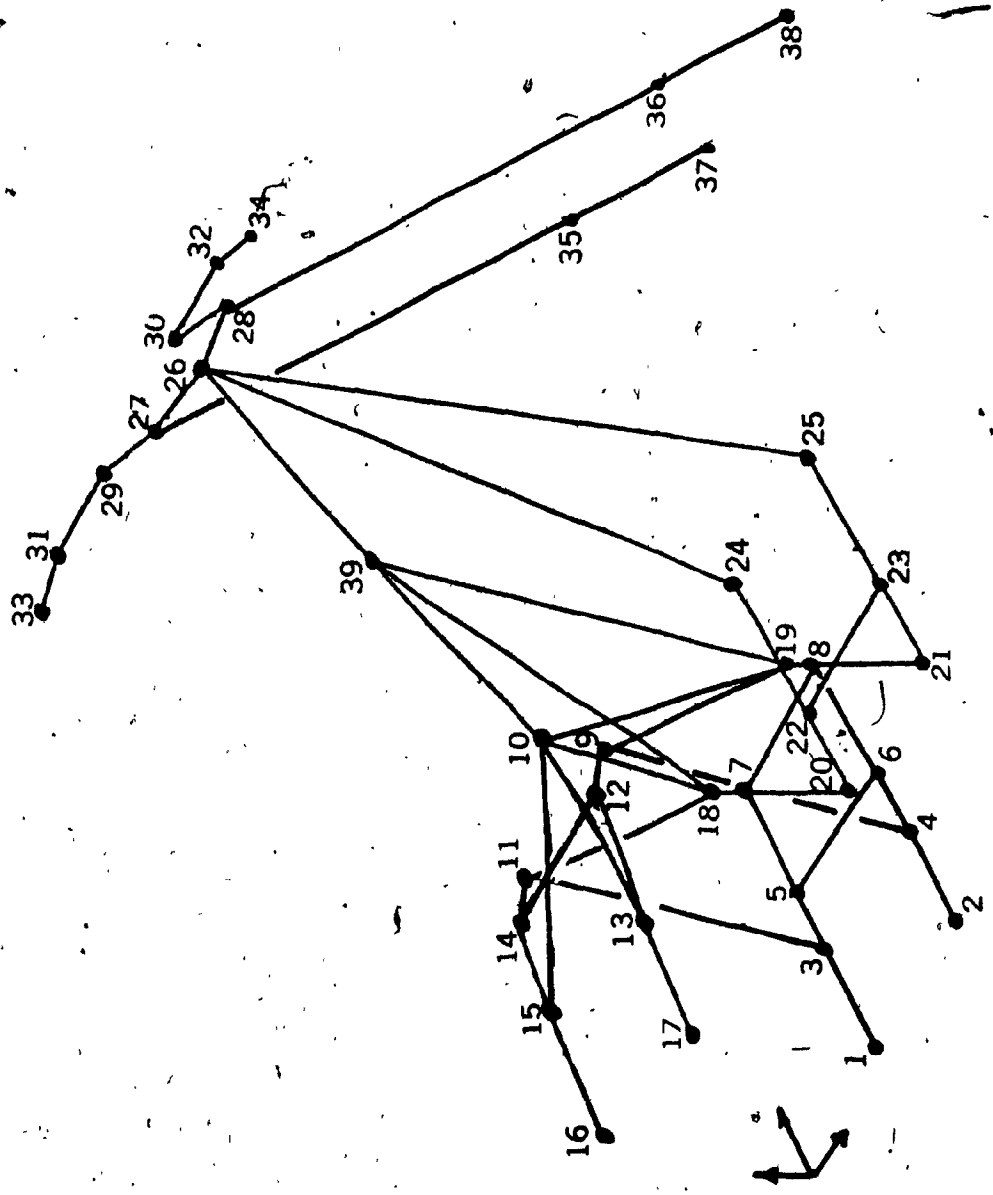

Figure 5.6: Motorcycle Frame/Suspension Configuration

basically during drawing of the members, by drawing those members to be suppressed with the color equivalent to that of the screen's color.

The typical data generation of the frame is tabulated in Table 5.4 in pixel values.

The pixel coordinates are generated and stored in the SUBROUTINE MTGN3D (NMOTPNT, IX, IY, IZ, SCALE) where:

NMOTPNT = number of points for the motorcycle frame

IX,IY,IZ = pixel coordinates of the motorcycle frame

SCALE = Scale factor for IX, IY, IZ coordinates.

After the data generation, the data base of the motorcycle frame is rotated through appropriate subroutines. These subroutines are explained below. In rotation of three-dimensional object about x-axis, the x-dimensions do not change. Thus the transformation matrix will have zeros in the first row and first column, except for unity on the main diagonal.

This leads to the transformation matrix for a rotation of angle Θ about the x-axis given by

$$[X' \; Y' \; Z' \; 1] = [X \; Y \; Z \; 1] \begin{bmatrix} 1 & 0 & 0 & 0 \\ 0 & \cos\Theta & \sin\Theta & 0 \\ 0 & -\sin\Theta & \cos\Theta & 0 \\ 0 & 0 & 0 & 1 \end{bmatrix}$$

Note: Θ is positive when standing on the X-axis and looking towards the Y-Z plane and having the rotation anticlockwise.

Based on this transformation, the subroutine was developed and is given in the following form:

TABLE 5.4

Pixel Coordinates of the Motorcycle Frame

IX(1) = 0	IY(1) = 0	IZ(1) = 0
IX(2) = 0	IY(2) = 0	IZ(2) = 8
IX(3) = 0	IY(3) = 6	IZ(3) = 0
IX(4) = 0	IY(4) = 6	IZ(4) = 8
IX(5) = 0	IY(5) = 12	IZ(5) = 0
IX(6) = 0	IY(6) = 12	IZ(6) = 8
IX(7) = 0	IY(7) = 20	IZ(7) = 0
IX(8) = 0	IY(8) = 20	IZ(8) = 8
IX(9) = 15	IY(9) = 15	IZ(9) = 8
IX(10) = 14	IY(10) = 19	IZ(10) = 4
IX(11) = 15	IY(11) = 15	IZ(11) = 0
IX(12) = 17	IY(13) = 6	IZ(12) = 8
IX(13) = 17	IY(13) = 6	IZ(13) = 8
IX(14) = 18	IY(14) = 12	IZ(14) = 0
IX(15) = 17	IY(15) = 6	IZ(15) = 0
IX(16) = 18	IY(16) = 0	IY(16) = 0
IX(17) = 18	IY(17) = 0	IZ(17) = 8
IX(18) = 20	IY(18) = 20	IZ(18) = 0
IX(19) = 20	IY(19) = 20	IZ(19) = 8
IX(20) = 6	IY(20) = 20	IZ(20) = 0
IX(21) = -6	IY(21) = 20	IZ(21) = 8
IX(22) = -6	IY(22) = 25	IZ(22) = 0
IX(23) = -6	IY(23) = 25	IZ(23) = 8
IX(24) = -6	IY(24) = 33	IZ(24) = 0
IX(25) = -6	IY(25) = 33	IZ(25) = 8
IX(26) = 22	IU(26) = 43	IZ(26) = 4
IX(27) = 22	IY(27) = 43	IZ(27) = 0
IX(28) = 22	IY(28) = 43	IZ(28) = 8
IX(29) = 26	IY(29) = 40	IZ(29) = 0
IX(30) = 26	IY(30) = 40	IZ(30) = 8
IX(31) = 26	IY(31) = 40	IZ(31) = 5
IX(32) = 26	IY(32) = 40	IZ(32) = 13
IX(33) = 26	IY(33) = 39	IZ(33) = -8
IX(34) = 26	IY(34) = 39	IZ(34) = 16
IX(35) = 10	IY(35) = 50	IZ(35) = 0
IX(36) = 10	IY(36) = 50	IZ(36) = 8
IX(37) = -2	IY(37) = 56	IZ(37) = 0
IX(38) = -2	IY(38) = 56	IZ(38) = 8
IX(39) = 17	IY(39) = 31	IZ(39) = 4

SUBROUTINE ROT3DX (NPNT, IX, IY, IZ, THETA)

INPUT

NPNT - Data base number of points to be rotated about the X-axis.

IX,IY,IZ - Data base values to be modified. Arrays of dimension NPNT.

THETA - The angle of rotation in radians.

OUTPUT

IX,Y,IZ - Modified data base

Similarly the subroutines were developed for the rotation of the frame about Y and Z axis. For completeness, these are given below. The meaning of parameters are the same as defined previously.

Rotation about Y-Axis

SUBROUTINE ROT3DY (NPNT, IX, IY, IZ, THETA)

Rotation About Z-Axis

SUBROUTINE ROT3DZ (NPNT, IX, IY, IZ, THETA)

In order to be able to move the motorcycle frame anywhere on the screen, the translation and rotation subroutine was developed with respect to the center of origin of the data base. The subroutine is based on the simple transformations of translation and rotation with respect to the screen X-Y system.

Translation: $[X'Y'1] = [XY1]\begin{bmatrix} 1 & 0 & 0 \\ 0 & 1 & 0 \\ IXG & IYG & 1 \end{bmatrix}$

Rotation: $[X'Y'1] = [X\ Y\ 1] \begin{bmatrix} \cos\Theta & -\sin\Theta & 0 \\ \sin\Theta & \cos\Theta & 0 \\ 0 & 0 & 1 \end{bmatrix}$

The corresponding subroutine is given by:

TRANSROT (IXG, IYG, THETA, NPNT, IX, IY)

where:

INPUT

NPNT - Data base number of points to be translated and rotated.

IX,IY - Data base arrays.

THETA - The angle of rotation

IXG,IYG- The coordinates of the data base center with respect to the screen X-Y system.

Having the transformed set of coordinates, we can draw the motorcycle frame on the VDP screen using drawing subroutine

SUBROUTINE MTDR3D (NPNT, IX, IY)

INPUT

NPNT - Number of nodes

IX,IY - Final transformed coordinates

This subroutine uses two NORPAK subroutines, mainly:

CALL SET (IX, IY)

This subroutine sets the current beam position to the specified value.

The subroutine parameters are defined as follows:

IX - X coordinate of the beam position

IY - Y coordinate of the beam position

The second subroutine is defined by

CALL VEC (IDX, IDY)

This subroutine draws a vector as specified from the current beam position.. The subroutine parameters are defined as follows:

IDX - dx from current beam position

IDY - dy from current beam position

NOTE: dx, dy can be either positive or negative values.

5.5.3 Sample Program for Animated Mode Shapes

Having explained the details of each subroutine necessary to generate the graphical display of the motorcycle frame, the program was written for the animated mode shapes in accordance with the block diagram shown in Fig. 5.7.

5.5.4 Graphical Output

There are two alternative approaches of displaying the animated mode shapes. In the first approach the modes can be displayed continously without clearing the VDP screen. The result of this animation is shown in Fig. 5.8.

In the second approach, VDP screen is cleared before displaying the next mode shape. In this approach a dynamic display is created. This kind of display can be viewed as static at some instance of time. Because the drawing and clearing of the screen is about 1/30 sec.,

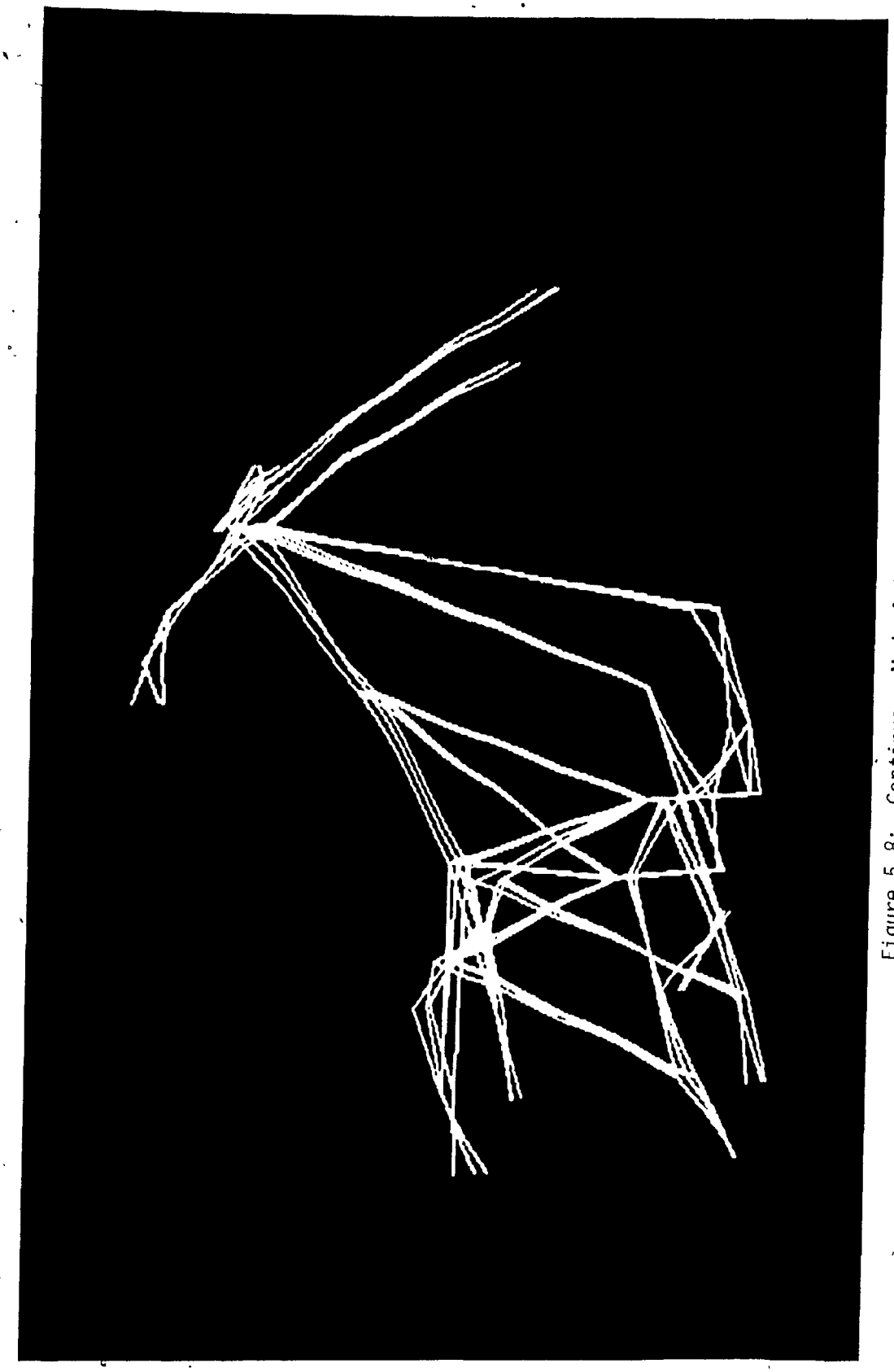

Figure 5.8: Continuous Mode Animation

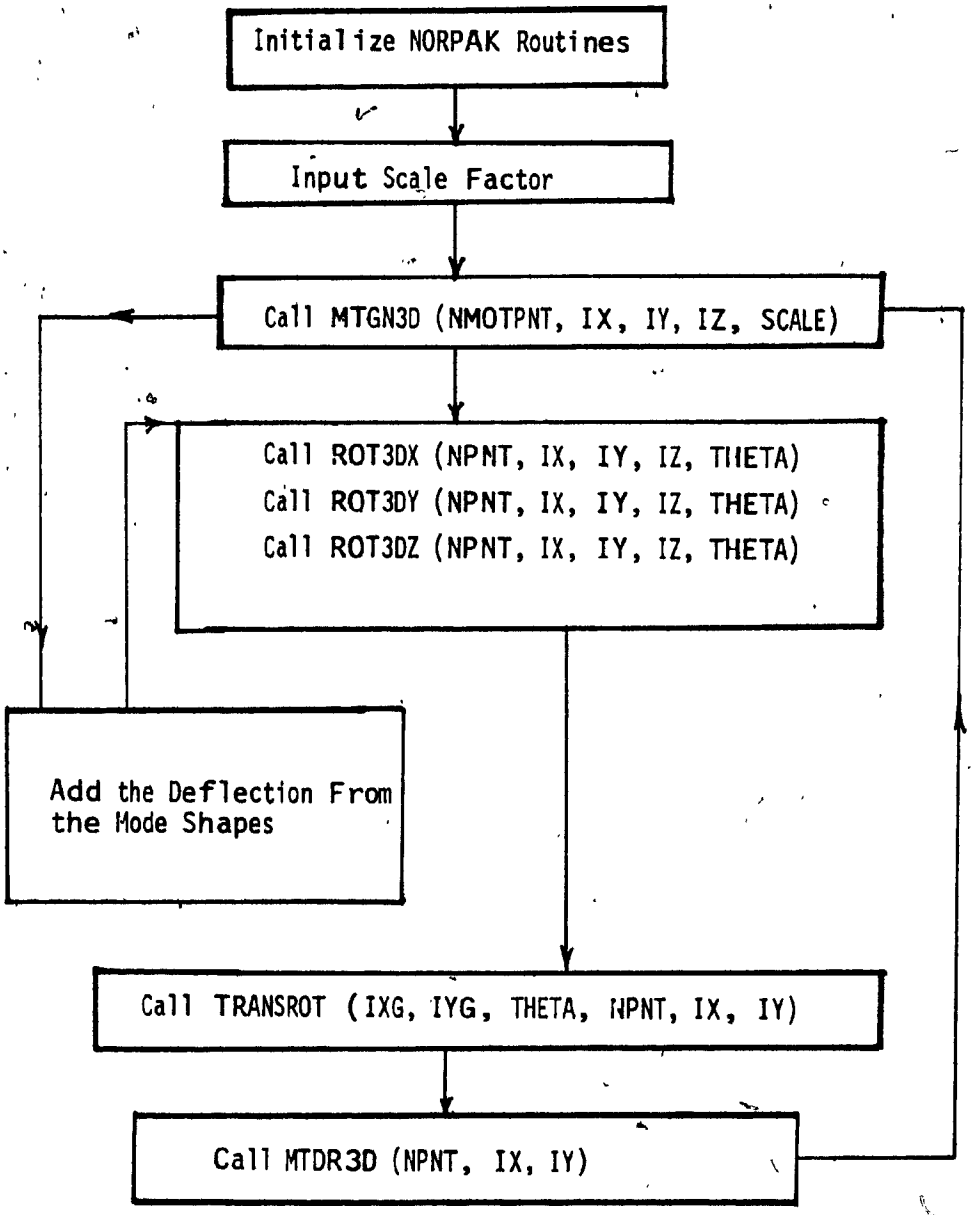

Figure 5.7: Block Diagram of Animated Mode Shapes

therefore, the eye sees the object being continuously displayed.

5.6 Conclusion

In this chapter, the analysis of the motorcycle frame was performed using finite element method. Theoretical aspects and various steps required in FEA were discussed with an example of typical input data sequence for the motorcycle frame. Graphical representation of the static deflections and mode shapes calculated from the ANSYS-FEA package were illustrated. Procedure for developing graphics for mode animation was explained in detail.

CHAPTER 6

CONCLUSIONS

6.1 CAE Concept

Computer aided engineering approach for the design and analysis of an off-road motorcycle has been proposed. Due to the severity of shock and vibration to the rider, a very broad and extensive analysis of the entire suspension and frame was performed using the CAE concept.

The general concept of CAE as it was applied to the motorcycle is illustrated in Fig. 6.1.

The steps involved in CAE are:

1. Physical model of the motorcycle
2. Computer simulation and testing of shock absorbers.
3. Time domain - dynamic analysis of lumped mass model.
4. Parametric variation of the lumped mass model for optimal suspension characteristics.
5. Finite element analysis of the frame.
6. Development of interactive and dynamic graphics of the lumped mass model and animated mode shapes of the frame.

6.2 Major Highlights

1. This thesis illustrates the concept of computer-aided engineering in the design and analysis of an off-road motorcycle suspension and frame.

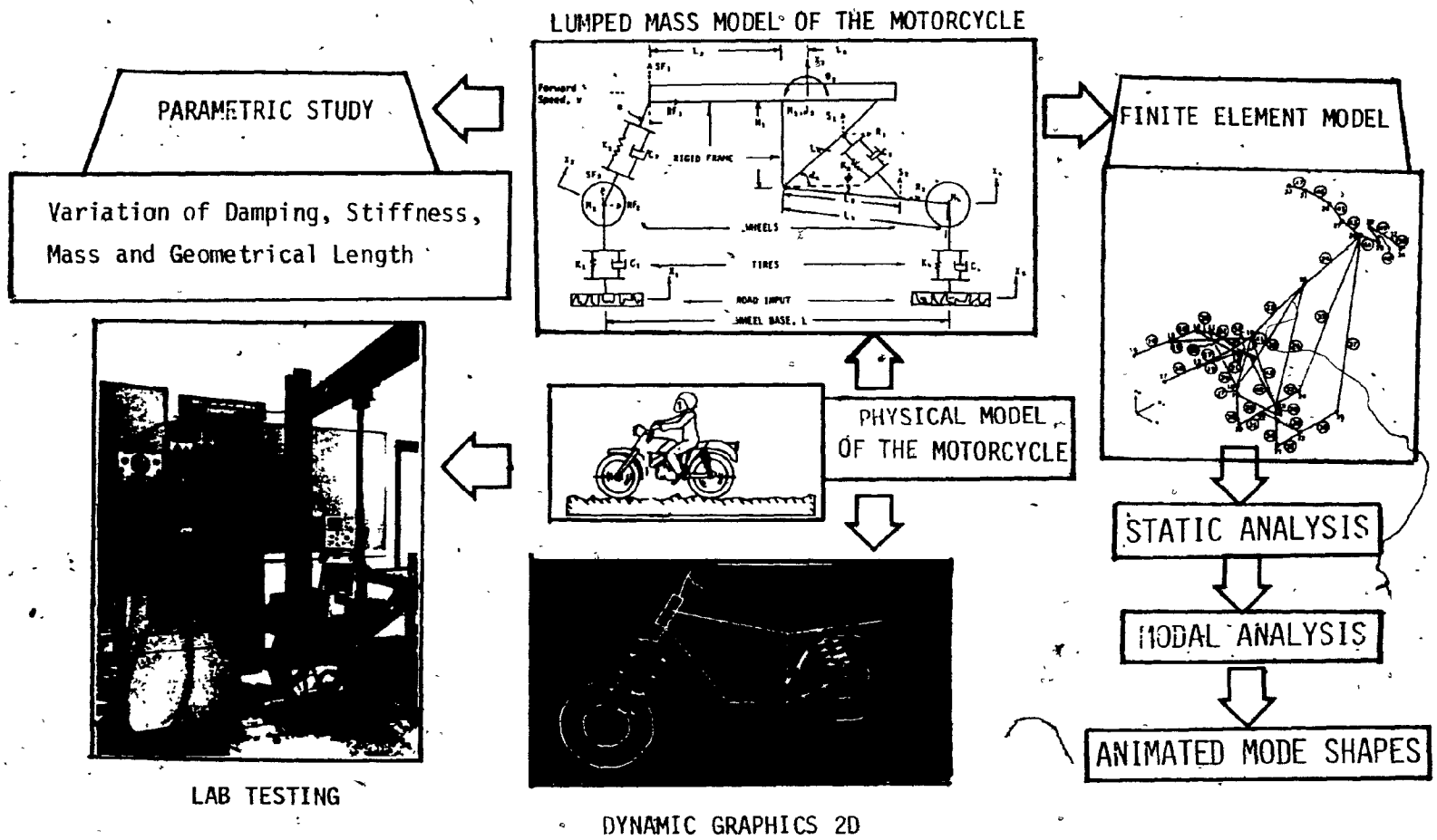

Figure 6.1: Overall CAE Concept of the Off-Road Motorcycle

2. The general concept of CAE as applied to the motorcycle was divided into four main stages:

a) computer simulation and experimental investigation of motorcycle shock absorber

b) lumped mass analysis of the entire motorcycle suspension

c) dynamic graphics

d) finite element analysis of the motorcycle structure and animated mode shapes.

3. A comprehensive mathematical model of the suspension system was developed. The model takes into account the front fork assembly, the rear shock absorber mounted on the swing arm, the frame, the front and rear wheels and the mass of the rider.

4. A parametric study was carried out with variations of stiffness and damping of the tires and the shock absorbers and the mass of the rider. The transmissibility versus frequency curves of generalized coordinates were obtained. A study on the effect of variation of the geometrical configuration of the motorcycle was carried out and it was observed that the geometric location L_3, L_6 and angles ϕ and α_6 have considerable influence on the absolute displacement X_3 and rotation θ_3. Increase in L_3 from 2.54 cm (1 in.) to 27.2 cm (11.5 in.) decreased the X_3 transmissibility twice at the resonance. However, for large values of L_3 (i.e. L_3 = 50.8 cm, (L_3 = 20 in.)) the X_3 response started to increase. Increase in L_6 from 2.54 cm (1 in.) to 38.1 cm (15. in.) increased the θ_3 response twice. Increase of ϕ from 0 to 0.4 radians decreased the θ_3 response about twice. Increase in α_6 from 0.7 to 1.4 radians decreased the X_3 response by about 20% at resonance.

5. Three types of damping for front fork and rear shock absorber were considered:

a. linear symmetrical: compression and extension

b. linear non-symmetrical: compression and extension

c. non-linear and non-symmetrical: compression and extension.

In the study of damping characteristics of the shock, the non-linear and non-symmetrical damping produced four times higher X_3 response at resonance, compared with linear type damping. At higher frequencies X_3 response for non-linear damping was four times lower than the response for linear damping. The riders acceleration $\ddot{X}_3$ was found to be six times higher at resonance compared with linear damping.

6. The VAX-11/780 system configuration and NORPAK hardware for dynamic graphics were explained. The methodology of developing dynamic graphics software was explained for both simple systems and motorcycle suspension. The use of interactive graphics was illustrated and the menu was explained in detail.

7. The finite element analysis of the motorcycle frame was performed. Natural frequencies and mode shapes of the motorcycle frame were obtained. Procedure for developing graphics for mode animation was illustrated.

6.3 Benefits of the Thesis

From the above study it can be concluded that the outlined method of computer aided engineering of the motorcycle can be applicable to other vehicles. Application of the computer aided engineering can subtantially reduce the cost of the vehicle. The expense of building and testing prototype exceeds that of analytical design. The need for prototypes can be reduced significantly through the CAE methodology. This thesis shows de-

tailed stages of developing a good analytical model. Using the procedure outlined, the design engineer can design and analyze the suspension and frame in a few hours as opposed to weeks or months. The designer will not only have the most efficient and safe vehicle on the market but also through the use of a menu the designer can input the parameters interactively and can see their effect through dynamic display. The use of animated modal display in finite element analysis can be used to improve interpretation of complex model behaviour by revealing the interaction of various parts of the structure. All this speeds up the evaluation of design and analysis. Having such a package the manufacturers can produce the optimum vehicle with respect to its reliability performance and cost.

The advantages of using the CAE approach as outlined in the thesis are tremendous. The methodology developed can be easily followed in the design and analysis of other vehicles or mechanical structures and mechanisms. And it can even be applied to today's emerging field of 'Robotics'.

6.4 Recommendation for Future Work

Due to the complexity of motorcycle problems, only some aspects of the computer aided engineering concept have been investigated. The direction of future work is outlined below.

1. Include, in the CAE concept, optimization of the lumped mass analysis to minimize the rider's response. The optimization parameters should be chosen on the basis of the extensive parametric study presented in the thesis.

2. Optimization of the finite element model of the frame can be carried out to minimize the weight.

3. Include, in the CAE concept, the generation of manufacturing drawings for the motorcycle frame. In this investigation the three-dimensional data base for the frame was generated and therefore only requires three projection views, dimensioning and bill of materials.

4. Verify the motorcycle suspension mathematical model by test using hydraulic shaker facility.

5. In this thesis, the differential equations developed assume small deflections. Because of the off-road environment, large deflections occur and the simulation should be repeated for this condition and compared with the present results. The governing equations for large deflections are derived and presented in Appendix C.

6. To speed up the motorcycle graphical animation, it may be preferable to store the deflections and then use them for display.

7. Shock and random road inputs should be investigated.

8. The lumped mass model has the capability of investigating the wheel lift-off and the effect of braking. This again could be looked at in detail.

9. In this thesis only a particular linkage configuration for the rear shock absorber mounting was considered. Other linkages could be investigated and compared for the responses.

10. Following the modal analysis as outlined in the thesis, the dynamic response could be evaluated through the use of response spectrum technique.

11. Fatigue analysis of the frame should also be considered due to the severity of the off-road input.

REFERENCES

1. Structural Dynamics Research Coorporation, Modern Engineering Methods - A Seminar Describing the Benefits of Computer Aided Engineering, 1980, Milford, Ohio.

2. J.R. Lemon, S.K. Tolani, A.L. Klosterman, Integration and Implementation of Computer-Aided Engineering and Related Manufacturing Capabilities into Mechanical Product Development Process, Saarbrucken, Federal Republic of Germany, October 1, 1980.

3. A.L. Klosterman, R.H. Ard, J.W. Klahs, A Geometric Modelling Program for the System Designer. Conference on CAD/CAM Technology in Mechanical Engineering, March 24-26, 1982, Massachusetts Institute of Technology.

4. A. Baer, C. Eastman, M. Henion, Geometric Modeling: A Survey Computer Aided Design, Vol. 11, Sept. 5, 1979.

5. J.K. Krouse, Geometric Models for CAD/CAM, Machine Design, July 24, 1980.

6. J.K. Krouse, Automated Drafting: The First Step to CAD/CAM, Machine Design, May 21, 1981.

7. J.K. Krouse, Computer-Aided Design for Every Pocketbook, Machine Design, November 20, 1980.

8. T.J. Cokonis, Minicomputers Tackle CAD/CAM, Machine Design, January 8, 1981.

9. K.E. Fulton, Overview of Integrated Programs for Aerospace - Vehicle Design, NASA, September 1980.

10. T. Winkler, Modular Construction of CAD Drawings, Computer Aided Design, Vol. 15, January 1, 1983.

11. R.A. Shryock, J.W. Klahs, D.A. Diterich, System Modelling Techniques to Improve the Ride and Vibration Isolation Characteristics of Heavy Equipment, SAE - 770594.

12. R.S. Sharp, The Stability and Control of Motorcycles, Journal of Mechanical Engineering Science, Vol. 13, No. 5, 1971.

13. R.S. Sharp, Research Note: The Influence of Frame Flexibility on the Lateral Stability of Motorcycles, Journal of Mechanical Engineering Science, Vol. 16, No. 2, 1974.

14. G.E. Roe, W.M. Pickering, A.ZINOBER, The Oscillations and the Effect of Front Fork Stability of Motorcycles, SAE-780.

15. D.H. Weir, J.W. Zellner, Lateral-Directional Motorcycle Dynamics and Rider Control, SAE-780304, 1978.

16. S.H. Black, D.L. Taylor, Simulation of Off-Road Motorcycle Ride Dynamics, SAE 790261.

17. J.A. Stricklin, W.E. Haisler, Journal of Solution Procedures for Nonlinear Stochastic Dynamic Analyses, SEA-740317, 1971.

18. D.C. Krinke, R.T. Huston, An Analysis of Algorithm for Solving Differential Equations, Computers and Structures, Vol. 11, pp. 69-74, 1980.

19. M. van Vliet, S. Sankar, Computer Aided Analysis and Experimental Verification of a Motorcycle Suspension, ASME, November 30, 1981.

20. J.K. Horvath, Structural and System Models, SAE - 750135.

21. M. Kamal, J.A. Wolf, Finite Element Models for Automotive Vehicle Vibration, ASME, 1977.

22. M.M. Kamal, J.A. Wolf, Modern Automotive Structural Analysis, van Nostrand Reinhold Company, 1982.

23. K.H. Wadleigh, Application of Finite Element Methods to Complete Automobile Structural Design Evaluation, SAE-740322.

24. Y.W. Luk, L.D. Mitchell, A Microprocessor-Based Interactive Beam Analysis Program with Graphics, Dynamic and Static, ASME-81-DE-12.

25. J.E. Fowler, K.F. Newman, The Use of Computer Simulation for the Design of Super Vehicles, I Mech E, 1980.

26. A. Hathaway, General Electric, CADMAT Mechanical News, December 1979.

27. M. van Vliet, S. Sankar, C.N. Bapat, "Frequency and Time Domain Analysis of Off-Road Motorcycle Suspension", to appear in 53rd Shock and Vibration Bulletin, Washington, D.C., 1983.

28. M. van Vliet, S. Sankar, Optimal Design of an Off Road Motorcycle Suspension, to appear in the ASME Transactions, Journal of Mechanical Design.

29. R. Burden, J. Faires, A. Reynolds, Numerical Analysis, Prindle, Weber & Schmidt, Boston Massachusetts, 1981.

30. CALMA - Interactive Graphics Systems, Information Pamphlets.

31. APPLICON - Information Pamphlets.

32. COMPUTER VISION - Information Pamphlets

33. LOCKHEEH-CADAM - Information Pamphlets

34. PERKIN-ELMER - Information Pamphlets

35. AUTO-TROI - Information Pamphlets

36. NES - Information Pamphlets

37. Swanson Analysis System, Inc., ANSYS, Engineering Analysis System, User's Manual, Vol. I & II, Revision 4, 1982.

38. NORPAK/VDP-2, Fortran Library.

APPENDIX A

APPENDIX A

Mathematical Modeling of Motorcycle Front Fork and Rear Shock Absorber [19, 27, 28]

For a realistic lumped mass analysis of the motorcycle suspension, it is highly desirable to include the nonlinear damping characteristics of the front fork and rear shock absorber. This requires a detailed mathematical modeling of front fork and rear shock absorber.

Ref. [17, 27, 28] illustrate the application of computer-aided analysis and experimental verification of a motorcycle front fork and shock absorber. The motorcycle suspension normally consists of a pair of front fork and rear shock absorbers. Various configurations of front fork and rear shock absorber are used, however all have the same basic design.

The front fork consists of an oil filled telescopic fork in which the frame mounted stanchion tubes and wheel mounted sliders effect the springing and damping by various means of spring and valving mechanisms as shown in Fig. A1.

The rear shock absorber consists of a piston moving in a oil filled chamber with an externally mounted spring. The spring is sometimes replaced by an air column.

The front fork and rear shock were modelled mathematically for laminar and turbulent flows. Referring to Fig. A2, the damping force is given by:

Laminar Flow:

$$F = Lv$$

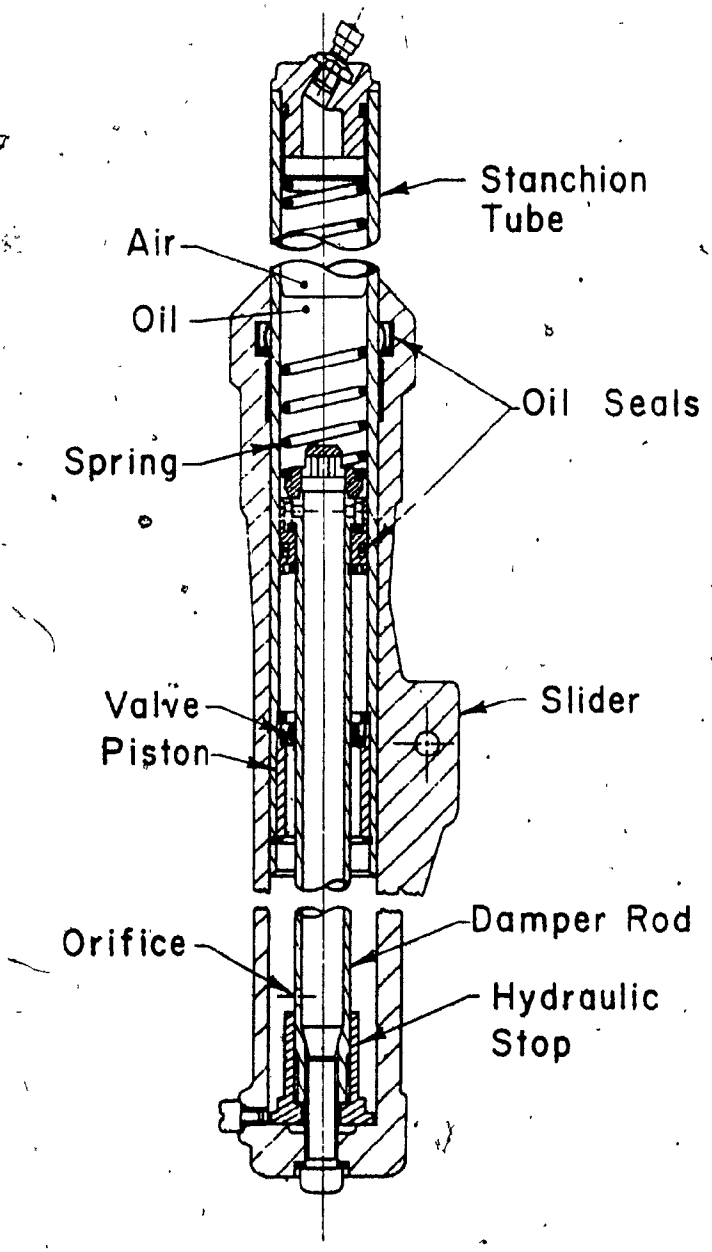

Figure A1: Cross Sectional View of a 38mm Marzocchi Fork

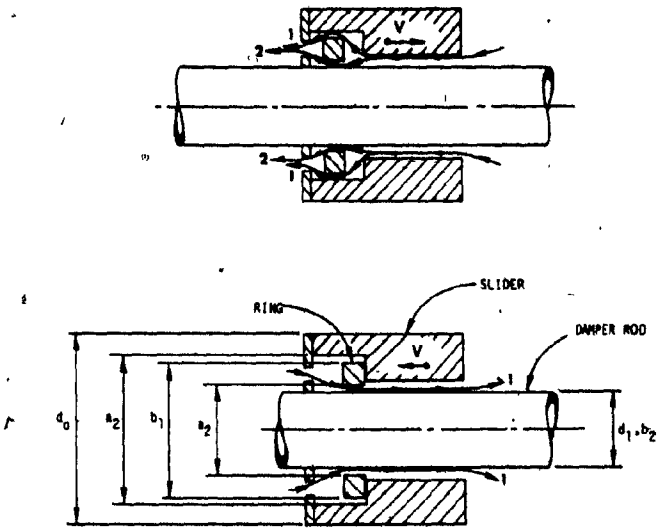

Figure A2: Laminar Flow Path (Front Fork)

where:

$\bar{v}$ is piston velocity

L_m is Laminar flow coefficient given by

For compression

$$L_c = 8 \mu l A^2/\pi \sum_{i=1}^{2} [(a_i^4 - b_i^4) - (a_i^2 - b_i^2)^2 / \ln (a_i/b_i)$$

For extension

$$L_e = \mu l A^2/\pi [(a_2^4 - b_2^4) - (a_2^2 - b_2^2)/ \ln (a_2/b_2)]$$

where:

a and b are outer and inner annular diameters respectively,

μ is the dynamic viscosity of the fluid

l is the piston length

A is the piston area

Turbulent Flow:

$$F = T v^2$$

T is the turbulent flow coefficient and is given by

$$T = \frac{A^3 \rho}{2 C_d^2 A^{*2}}, \text{ for compression}$$

and

$$T = \frac{A^3 \rho}{2 C_d^2 A_r^{*2}}, \text{ for extension}$$

where:

ρ is the mean density

C_d is the orifice discharge coefficient, dimensionless

A^* is the flow area at piston

A_r^* is the orifice flow area at ring

The force exerted by the entrapped column of air can be expressed as

$$F_s = \frac{m\ Rt\ A}{V_0 - A_c x}$$

where:

$m\ Rt$ is the gas constant

V_0 is the volume before displacement

A_c is the area of air column

x is the displacement

In summary, the governing equations of a front fork take the form:

$$F = \frac{m\ Rt\ A}{V_0 - A_c x} + L_m v \text{ for laminar flow}$$

$$F = \frac{m\ Rt\ A}{V_0 - A_c x} + T\ v^2 \text{ for turbulent flow}$$

Similarily the derivation was carried out for the rear shock absorber.

Following the detailed derivation, the mathematical models were simulated for sinusoidal, transient and random displacement inputs. Further, the simulation results were verified using laboratory testing of commercially available front forks and shock absorbers. The test set-up consisted of an electro-hydraulic shaker driving the end of either a front fork or a shock absorber. The other end was fixed to an inertial frame through a load cell or attached to an equivalent inertial load simulating the weight of the motorcycle and the rider. The comparison between theoretical and experimental results show a good correlation, and thus justify the mathematical model.

APPENDIX B

APPENDIX B

Detailed Derivation of Equations of Motion of the Motorcycle Suspension System (Small Displacement)

The objective of this appendix is to develop the differential equations of motion for the motorcycle illustrated in Fig. 2.2. Referring to this figure, the displacements X_2, X_3, θ_3 and X_4 are considered to be the generalized coordinates and hence the generalized vector is given by

$$\{q\} = \{X_2, X_3, \theta_3, X_4\}^T$$

The various assumptions in modeling of the motorcycle are same as discussed in Chapter 2. The final set of differential equations are nonlinear and are valid for small deflections only.

B.1 Deflection of Rear Shock Absorber

Consider the rigid frame as illustrated in Figs. B1 and B2. Then

$$S_1 = X_3 - L_3 \sin(\alpha_4 - \theta_4) + L_3 \sin\alpha_4 \qquad (B.1)$$

$$R_1 = L_3 \cos(\alpha_4 - \theta_3) - L_3 \cos\alpha_4 \qquad (B.2)$$

$$SS_1 = X_3 - L_7 \sin(\theta_3 + \alpha_5) + L_7 \sin\alpha_5 \qquad (B.3)$$

$$RR_1 = L_7 \cos\alpha_5 - L_7 \cos(\theta_3 + \alpha_5) \qquad (B.4)$$

Now taking into consideration the rear swing arm as shown in Fig. B3, gives

$$S_2 = SS_1 + L_3 \sin\alpha + L_3 \sin\phi \qquad (B.5)$$

$$R_2 = RR_1 + L_3 \cos\alpha - L_3 \cos\phi \qquad (B.6)$$

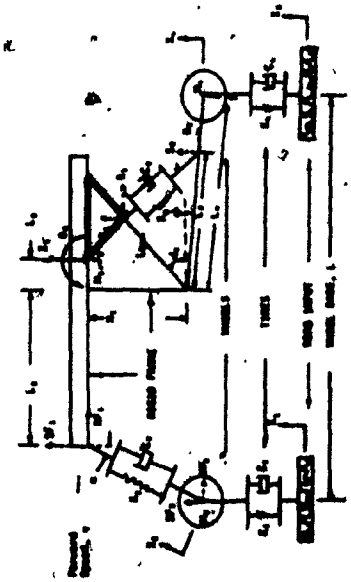

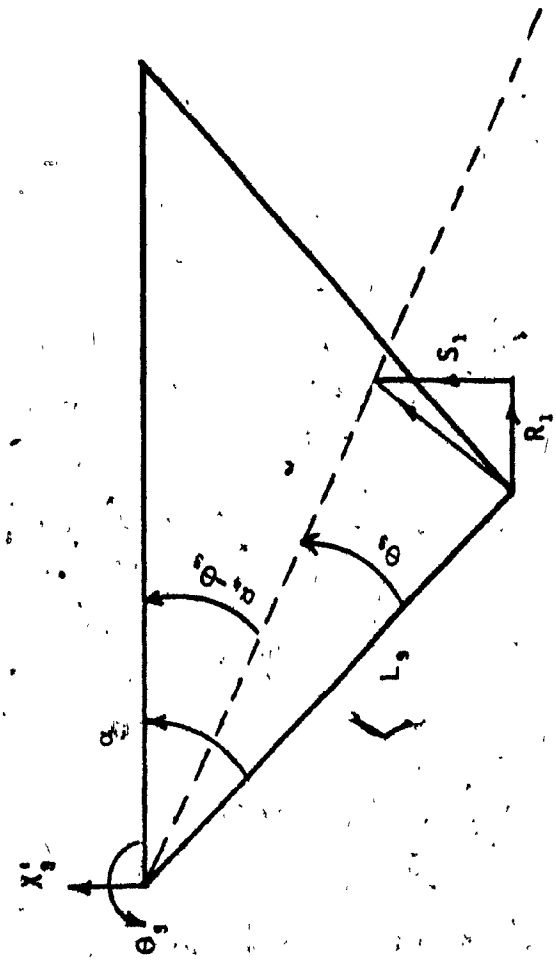

Figure B1 : Upper Part of Rigid Frame

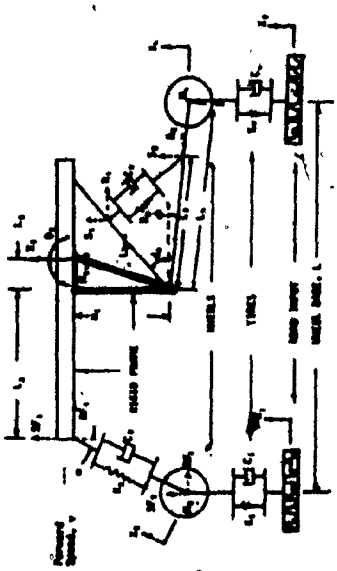

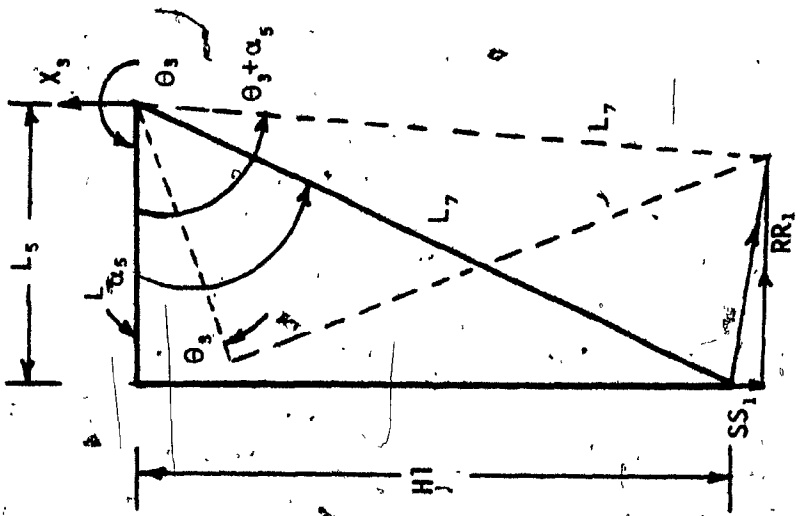

Figure B2 : . Lower Part of Rigid Frame

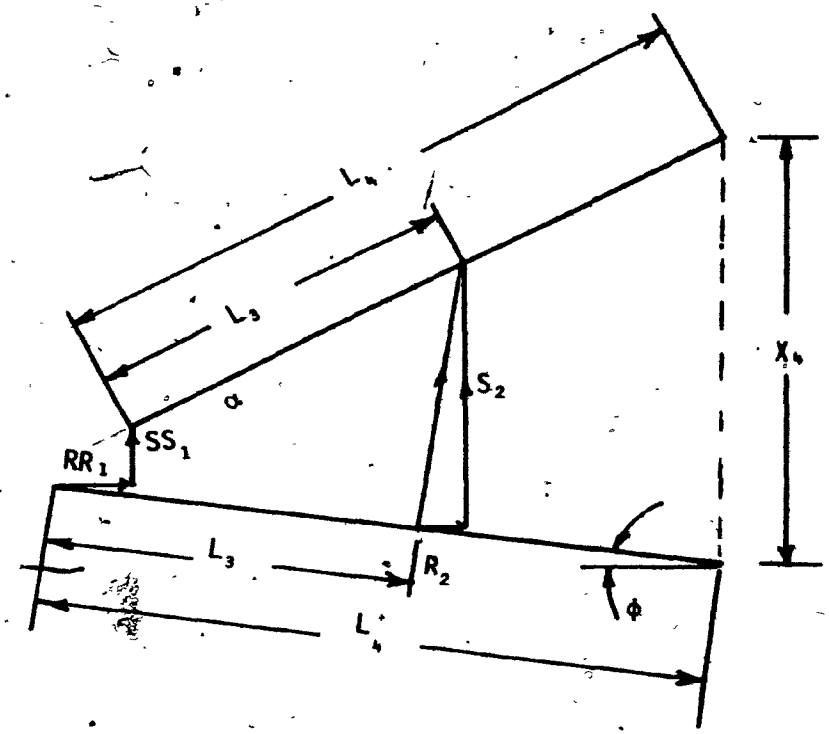

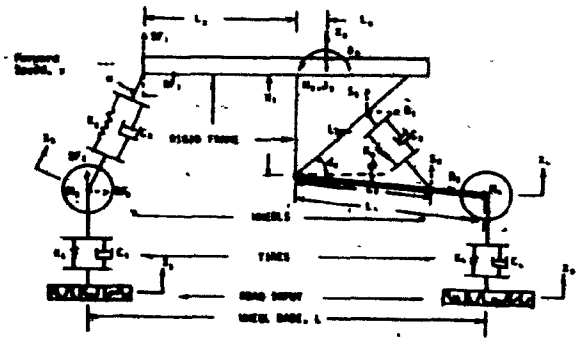

Figure B3 : Rear Swing Arm of the Motorcycle

Substituting for SS_1 and RR_1 in Eqs. (B.5) and (B.6) yields:

$$S_2 = X_3 - L_7 \sin(\theta_3 + \alpha_5) + L_7 \sin\alpha_5 + L_3 \sin\alpha + L_3 \sin\phi \quad (B.7)$$

$$R_2 = L_7 \cos\alpha_5 - L_7 \cos(\theta_3 + \alpha_5) + L_3 \cos\alpha - L_3 \cos\phi \quad (B.8)$$

where

$$\text{Sin } \alpha = \frac{X_4 - SS_1 - L_4 \sin\phi}{L_4}$$

$$\cos\alpha = \frac{\sqrt{L_4^2 - [X_4 - SS_1 - L_4 \sin\phi]^2}}{L_4}$$

Substituting for SS_1, $\sin\alpha$ and $\cos\alpha$ becomes

$$\text{Sin } \alpha = \frac{X_4 - L_4 \sin\phi - [X_3 - L_7 \sin(\theta_3 + \alpha_5) + L_7 \sin\alpha_5]}{L_4} \quad (B.9)$$

$$\cos\alpha = \frac{\sqrt{L_4^2 - [X_4 - L_4 \sin\phi - X_3 + L_7 \sin(\theta_3 + \alpha_5) - L_7 \sin\alpha_5]^2}}{L_4} \quad (B.10)$$

For small deflections of S_1, S_2, R_1 and R_2, the change of length of the rear shock absorber is given by

$$DELTAR = \{[S_1 - S_2]^2 + [R_1 - R_2]^2\}^{\frac{1}{2}} \quad (B.11)$$

where S_1, R_1, S_2 and R_2 are as defined in Eqs. (B.1), (B.2), and (B.7) and (B.8).

B.2 Deflection of Front Fork

Referring to Fig. B.4,

$$SF1 = X_3 - L_2 \sin\theta_3 \quad (B.12)$$

$$RF1 = -(L_2 - L_5)\cos\theta_3 - H_1 \sin\theta_3 + (L_2 - L_5) + L_4 \cos\phi - L_4 \cos\alpha \quad (B.13)$$

From Fig. B.5

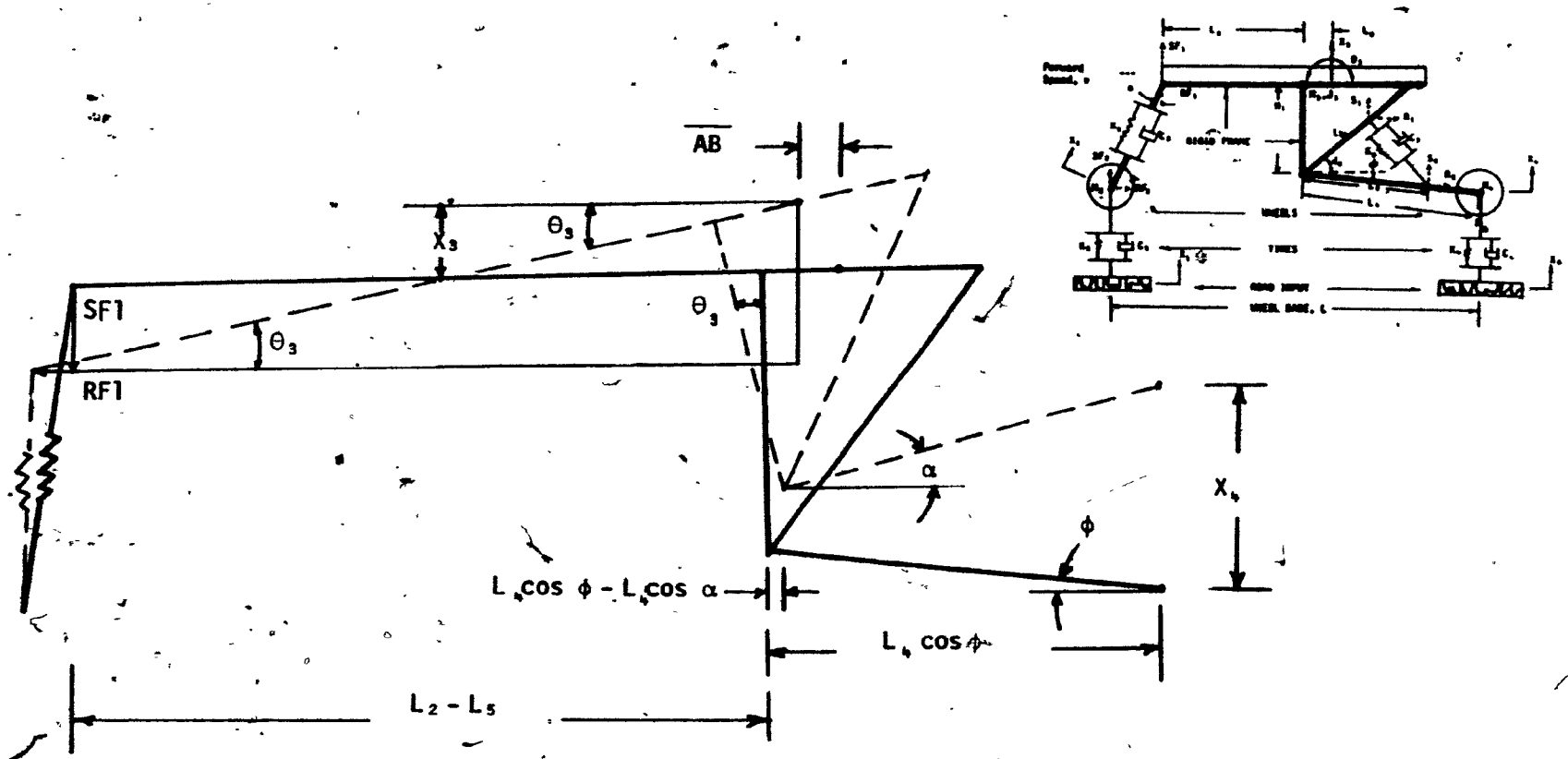

Figure B4 : Deflection of Front Fork

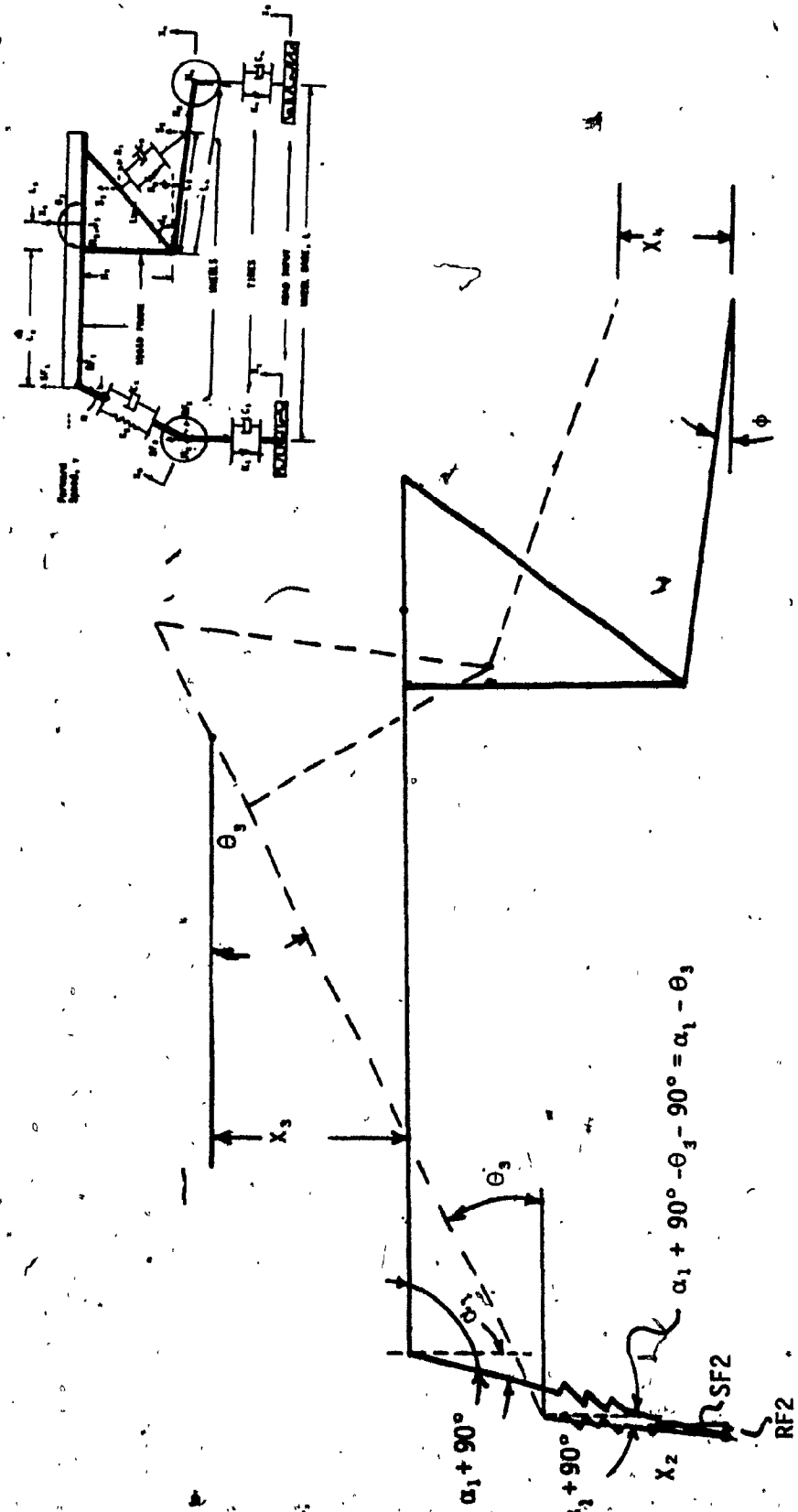

Figure B5 : Deflection of Front Wheel

$$SF2 = X_2 \cos(\alpha_1 - \theta_3) \tag{B.14}$$

$$RF2 = X_2 \sin(\alpha_1 - \theta_3) \tag{B.15}$$

For small deflections of SF1, SF2, RF1 and RF2, the change of length of the front fork is given by

$$DELTAF = \{[SF1 - SF2]^2 + [RF1 - RF2]^2\}^{\frac{1}{2}} \tag{B.16}$$

B.3 Lagrange's Equation

The Lagrange's equation can be written as:

$$\frac{d}{dt}\frac{\partial(T)}{\partial \dot{q}_i} - \frac{\partial(T)}{\partial q_i} + \frac{\partial(V)}{\partial q_i} + \frac{\partial(D)}{\partial \dot{q}_i} = Q_i \tag{B.17}$$

where

T = kinetic energy of the system

V = potential energy of the system

D = dissipation energy of the system

Q_i = generalized external force acting on the system

$\{q\} = \{X_2, X_3, \theta_3, X_4\}^T$

Kinetic Energy

$$T = \frac{1}{2} m_2 \dot{X}_2^2 + \frac{1}{2} m_3 \dot{X}_3^2 + \frac{1}{2} J_3 \dot{\theta}_3^2 + \frac{1}{2} m_4 \dot{X}_4^2 \tag{B.18}$$

Potential Energy

$$V = \frac{1}{2} K_1 [X_2 \cos(\alpha_1 - \theta_3) - X_1]^2 + \frac{1}{2} K_2 \Delta F^2 + \frac{1}{2} K_3 \Delta R^2 + \frac{1}{2} K_4 (X_4 - X_5)^2 \tag{B.19}$$

Dissipation Energy

$$D = \frac{1}{2} C_1 [\dot{X}_2 \cos(\alpha_1 - \theta_3) - \dot{X}_1]^2 + \frac{1}{2} C_2 \dot{\Delta F}^2 + \frac{1}{2} C_3 \dot{\Delta R}^2 + \frac{1}{2} C_4 (\dot{X}_4 - \dot{X}_5)^2 \tag{B.20}$$

where

$$\Delta F = \{[X_3 - L_2 \sin\theta_3 - X_2 \cos(\alpha_1 - \theta_3)]^2 + [-(L_2 - L_5)\cos\theta_3 - H_1 \sin\theta_3 + (L_2 - L_5) + L_4 \cos\phi - L_4 \cos\alpha - X_2 \sin(\alpha_1 - \theta_3)]^2\}^{\frac{1}{2}}$$

$$\Delta R = \{[X_3 - L_9 \sin(\alpha_4 - \theta_3) + L_9 \sin\alpha_4 - X_3 + L_7 \sin(\theta_3 + \alpha_5) - L_7 \sin\alpha_5 - L_3 \sin\alpha - L_3 \sin\phi]^2 + [L_9 \cos(\alpha_4 - \theta_3) - L_9 \cos\alpha_4 - L_7 \cos\alpha_5 + L_7 \cos(\theta_3 + \alpha_5) - L_3 \cos\alpha + L_3 \cos\phi]^2\}^{\frac{1}{2}}$$

Before calculating $\Delta\dot{R}$ and $\Delta\dot{F}$, we have to calculate $d\alpha/dt$.

Let

$$W = X_4 - L_4 \sin\phi - X_3 + L_7 \sin(\theta_3 + \alpha_5) - L_7 \sin\alpha_5$$

$$V = \sqrt{L_4^2 - [X_4 - L_4 \sin\phi - X_3 + L_7 \sin(\theta_3 + \alpha_5) - L_7 \sin\alpha_5]^2}$$

$$U = \frac{W}{V}$$

Calculation of α

$$\alpha = \tan^{-1}(U) = \tan^{-1}\left(\frac{W}{V}\right)$$

$$\frac{d\alpha}{dt} = \frac{d}{dt}\tan^{-1}(U) = \frac{1}{1+U^2}\frac{du}{dt}$$

$$\frac{du}{dt} = \frac{d}{dt}\left(\frac{W}{V}\right) = \frac{V\left(\frac{dW}{dt}\right) - W\left(\frac{dV}{dt}\right)}{V^2}$$

$$\frac{dW}{dt} = \frac{dW}{dX_3}\frac{dX_3}{dt} + \frac{dW}{dX_4}\frac{dX_4}{dt} + \frac{dW}{d\theta_3}\frac{d\theta_3}{dt}$$

$$\frac{dV}{dt} = \frac{dV}{dX_3}\frac{dX_3}{dt} + \frac{dV}{dX_4}\frac{dX_4}{dt} + \frac{dV}{d\theta_3}\frac{d\theta_3}{dt}$$

$$\frac{dU}{dt} = \frac{V[\dot{X}_4 - \dot{X}_3 + L_7\cos(\theta_3+\alpha_5)\dot{\theta}_3]}{V^2} -$$

$$-W\left\{\frac{(-2)[X_4 - L_4\sin\phi - X_3 + L_7\sin(\theta_3+\alpha_5) - L_7\sin\alpha_5]}{2V}\right\}$$

$$\frac{}{V^2}$$

$$\cdot\,[\dot{X}_4 - \dot{X}_3 + L_7\cos(\theta_3+\alpha_5)\dot{\theta}_3]$$

$$= \frac{[\dot{X}_4 - \dot{X}_3 + L_7\cos(\theta_3+\alpha_5)\dot{\theta}_3]}{L_4\cos\alpha} + \frac{\sin^2\alpha\, L_4^2}{\cos^3\alpha\, L_4^3}\cdot$$

$$\cdot[\dot{X}_4 - \dot{X}_3 + L_7\cos(\theta_3+\alpha_5)\dot{\theta}_3]$$

Calculation of $\dot{\alpha}$

$$\dot{\alpha} = \frac{1}{1+\frac{\sin^2\alpha}{\cos^2\alpha}}\frac{dU}{dt}$$

$$= \frac{1}{1+\frac{\sin^2\alpha}{\cos^2\alpha}}\cdot\left\{\frac{[\dot{X}_4 - \dot{X}_3 + L_7\cos(\theta_3+\alpha_5)\dot{\theta}_3]}{L_4\cos\alpha} + \frac{\sin^2\alpha}{\cos^3\alpha\, L_4}\cdot\right.$$

$$\left.\cdot\,[\dot{X}_4 - \dot{X}_3 + L_7\cos(\theta_3+\alpha_5)\dot{\theta}_3]\right\}$$

Now we need to derive

$$\frac{d\alpha}{dX_3},\ \frac{d\alpha}{d\theta_3},\ \frac{d\alpha}{dX_4},\ \frac{d\dot{\alpha}}{dX_3},\ \frac{d\dot{\alpha}}{d\theta_3},\ \frac{d\dot{\alpha}}{dX_4}$$

$$\dot{\alpha} = [\dot{X}_4 - \dot{X}_3 + L_7\cos(\theta_3+\alpha_5)\ \dot{\theta}_3]\sec^2\alpha\,\frac{\cos\alpha}{L_4}$$

$$\therefore\quad \frac{d\dot{\alpha}}{dX_3} = \frac{1}{L_4}[\dot{X}_4 - \dot{X}_3 + L_7\cos(\theta_3+\alpha_5)\,\dot{\theta}_3]\,\frac{d}{dX_3}(\sec^2\alpha\cos\alpha)$$

where

$$\frac{d}{dX_3}(\sec^2\alpha\cos\alpha) = 2\sec\alpha\sec\alpha\tan\alpha\frac{d\alpha}{dX_3}\cos\alpha - \sec^2\alpha\sin\alpha\frac{d\alpha}{dX_3}$$

$$\frac{d\dot{\alpha}}{d\theta_3} = [-L_7\sin(\theta_3+\alpha_5)\dot{\theta}_3]\sec^2\alpha\cos\alpha/L_4 + \frac{1}{L_4}[\dot{X}_4 - \dot{X}_3 + L_7\cos(\theta_3+\alpha_5)\dot{\theta}_3]\frac{d}{d\theta_3}(\sec^2\alpha\cos\alpha)$$

where

$$\frac{d}{d\theta_3}(\sec^2\alpha\cos\alpha) = 2\sec\alpha\sec\alpha\tan\alpha\frac{d\alpha}{d\theta_3}\cos\alpha - \sec^2\sin\alpha\frac{d\alpha}{dX_3}$$

$$\therefore \quad \frac{d\dot{\alpha}}{dX_4} = \frac{1}{L_4}[\dot{X}_4 - \dot{X}_3 + L_7\cos(\theta_3+\alpha_5)\dot{\theta}_3]\frac{d}{dX_4}(\sec^2\alpha\cos\alpha)$$

where

$$\frac{d}{dX_4}(\sec^2\alpha\cos\alpha) = 2\sec\alpha\sec\alpha\tan\alpha\frac{d\alpha}{dX_4}\cos\alpha - \sec^2\sin\alpha\frac{d\alpha}{dX_4}$$

$$\alpha = \mathrm{TAN}^{-1}(U) = \mathrm{TAN}^{-1}\left(\frac{W}{V}\right)$$

$$\therefore \quad \frac{d\alpha}{dX_3} = \frac{d}{dX_3}\mathrm{TAN}^{-1}(U) = \frac{1}{1+U^2}\frac{dU}{dX_3}$$

where

$$\frac{dU}{dX_3} = -\frac{1}{V} - \frac{W^2}{V^3}\ ;\ \text{Since}\ W = L_4\sin\alpha\ ,\ V = L_4\cos\alpha\ ,$$

$$\frac{d\alpha}{dX_3} = -\frac{1}{L_4\cos\alpha}\ ;\quad \frac{d\alpha}{d\theta_3} = \frac{1}{1+U^2}\frac{dU}{d\theta_3}$$

where

$$\frac{dU}{d\theta_3} = L_7\cos(\theta_3+\alpha_5)\left[\frac{1}{V}+\frac{1}{V}\cdot\frac{W^2}{V^2}\right]$$

$$\frac{d\alpha}{d\theta_3} = \frac{L_7\cos(\theta_3+\alpha_5)}{L_4\cos\alpha}\ ;\quad \frac{d\alpha}{dX_4} = \frac{1}{L_4\cos\alpha}$$

$$\Delta\hat{F} = [\hat{SF1} - \hat{SF2}]^2 + [\hat{RF1} - \hat{RF2}]^2)^{\frac{1}{2}} \qquad (B.21)$$

$$\dot{SF1} = \dot{X}_3 - L_2 \cos\theta_3 \dot{\theta}_3$$

$$\dot{SF2} = \dot{X}_2 \cos(\alpha_1 - \theta_3) + X_2 \sin(\alpha_1 - \theta_3)\dot{\theta}_3$$

$$\dot{RF1} = (L_2 - L_5)\sin\theta_3\dot{\theta}_3 - H_1\cos\theta_3\dot{\theta}_3 + L_4 \sin\alpha\,\dot{\alpha}$$

$$\dot{RF2} = \dot{X}_2 \sin(\alpha_1 - \theta_3) - X_2\cos(\alpha_1 - \theta_3)\dot{\theta}_3$$

$$\Delta\dot{R} = \{[\dot{S}_1 - \dot{S}_2] + [\dot{R}_1 - \dot{R}_2]^2\}^{\frac{1}{2}} \qquad \text{(B.22)}$$

$$\dot{S}_1 = \dot{X}_3 + L_9\cos(\alpha_4 - \theta_3)\dot{\theta}_3$$

$$\dot{S}_2 = \dot{X}_3 - L_7\cos(\theta_3 + \alpha_5)\dot{\theta}_3 + L_3\cos\alpha\,\dot{\alpha}$$

$$\dot{R}_1 = L_9\sin(\alpha_4 - \theta_3)\dot{\theta}_3$$

$$\dot{R}_2 = L_7\sin(\theta_3 + \alpha_5)\dot{\theta}_3 - L_3\sin\alpha\,\dot{\alpha}$$

Rearranging

$$\Delta\dot{F} = \{[\dot{X}_3 - L_2\cos\theta_3\dot{\theta}_3 - \dot{X}_2\cos(\alpha_1 - \theta_3) - X_2\sin(\alpha_1 - \theta_3)\dot{\theta}_3]^2$$
$$+ [(L_2 - L_5)\sin\theta_3\dot{\theta}_3 - H_1\cos\theta_3\dot{\theta}_3 + L_4\sin\alpha\,\dot{\alpha} -$$
$$- \dot{X}_2\sin(\alpha_1 - \theta_3) + X_2\cos(\alpha_1 - \theta_3)\dot{\theta}_3]^2\}^{\frac{1}{2}} \qquad \text{(B.23)}$$

$$\Delta\dot{R} = \{[\dot{X}_3 + L_9\cos(\alpha_4 - \theta_3)\dot{\theta}_3 - \dot{X}_3 + L_7\cos(\theta_3 + \alpha_5)\dot{\theta}_3 -$$
$$- L_3\cos\alpha\dot{\alpha}]^2 + [L_9\sin(\alpha_4 - \theta_3)\dot{\theta}_3 - L_7\sin(\theta_3 + \alpha_5)\dot{\theta}_3 +$$
$$+ L_3\sin\alpha\,\dot{\alpha}]^2\}^{\frac{1}{2}} \qquad \text{(B.24)}$$

$\dot{\alpha}$ was derived earlier in this ~~appendix~~.

From Eq. (B.18)

$$\frac{\partial T}{\partial \dot{X}_2} = m_2\dot{X}_2 \qquad \frac{d}{dt}\frac{\partial T}{\partial \dot{X}_2} = m_2\ddot{X}_2$$

$$\frac{\partial T}{\partial \dot{X}_3} = m_3\dot{X}_3 \qquad \frac{d}{dt}\frac{\partial T}{\partial \dot{X}_3} = m_3\ddot{X}_3$$

$$\frac{\partial T}{\partial \dot{\theta}_3} = J_3\dot{\theta}_3 \qquad \frac{d}{dt}\frac{\partial T}{\partial \dot{\theta}_3} = J_3\ddot{\theta}_3$$

$$\frac{\partial T}{\partial \dot{X}_4} = m_4\dot{X}_4 \qquad \frac{d}{dt}\frac{\partial T}{\partial \dot{X}_4} = m_4\ddot{X}_4$$

From Eq. (B.19),

$$\frac{\partial V}{\partial X_2} = K_1\,[X_2\cos(\alpha_1 - \theta_3) - X_1]\cos(\alpha_1 - \theta_3) +$$

$$+ \frac{1}{2}K_2\,[\,2[SF1 - SF2]\;(-\cos(\alpha_1 - \theta_3)) +$$

$$+ 2[RF1 - RF2]\;(-\sin(\alpha_1 - \theta_3))\}$$

$$\frac{\partial V}{\partial X_3} = \frac{1}{2}K_2\,[\,2[SF1 - SF2] + 2[RF1 - RF2]\,L_4\sin\alpha\frac{d\alpha}{dX_3} +$$

$$+ \frac{1}{2}K_3\{2[S1 - S2]\,(-L_3\cos\alpha)\frac{d\alpha}{dX_3} +$$

$$+ 2[R1 - R2]\;(L_3\sin\alpha)\frac{d\alpha}{dX_3}\}$$

$\frac{d\alpha}{dX_3}$ was derived earlier in this appendix.

$$\frac{d\alpha}{dX_3} = -\frac{1}{L_4\cos\alpha}$$

$$\frac{\partial V}{\partial \theta_3} = K_1[X_2\cos(\alpha_1 - \theta_3) - X_1]\,X_2\sin(\alpha_1 - \theta_3) +$$

$$+ \frac{1}{2}K_2\{2[SF1 - SF2]\,[-L_2\cos\theta_3 - X_2\sin(\alpha_1 - \theta_3)] +$$

$$+ 2[RF1 - RF2]\,[(L_2 - L_5)\sin\theta_3 - H_1\cos\theta_3 + X_2\cos(\alpha_1 - \theta_3) +$$

$$+ L_4\sin\alpha\frac{d\alpha}{d\theta_3}]\} + \frac{1}{2}K_3[2[S1 - S2]\,[+L_9\cos(\alpha_4 - \theta_3) +$$

$$+ L_7\cos(\theta_3 + \alpha_5) - L_3\cos\alpha\frac{d\alpha}{d\theta_3} + 2[R1 - R2]\,[L_9\sin(\alpha_4 - \theta_3) -$$

$$- L_7\sin(\theta_3 + \alpha_5) + L_3\sin\alpha\frac{d\alpha}{d\theta_3}]\}$$

$$\frac{\partial V}{\partial X_4} = \frac{1}{2} K_2 2[RF\dot{1} - RF2]\ (L_4 \sin\alpha)\ \frac{d\alpha}{dX_4} +$$

$$\frac{1}{2} K_3 \{2[S1 - S2]\ (-L_3 \cos\alpha)\ \frac{d\alpha}{dX_4} + 2[R1 - R2]\ L_3 \sin\alpha\ \frac{d\alpha}{dX_4}$$

$$+ K_4(X_4 - X_5)\}$$

$\frac{d\alpha}{d\Theta_3}$ and $\frac{d\alpha}{dX_4}$ were derived earlier in this appendix.

$$\frac{d\alpha}{d\Theta_3} = \frac{L_7 \cos(\Theta_3 + \alpha_5)}{L_4 \cos\alpha} \qquad \frac{d\alpha}{dX_4} = \frac{1}{L_4 \cos\alpha}$$

From Eq. (B.20)

$$\frac{\partial D}{\partial \dot{X}_2} = C_1[\dot{X}_2 \cos(\alpha_1 - \Theta_3) - \dot{X}_1] \cos(\alpha_1 - \Theta_3) + \frac{1}{2} C_2\{2[S\dot{F}1 - S\dot{F}2]$$

$$(-\cos(\alpha_1 - \Theta_3)) + 2[R\dot{F}1 - R\dot{F}2]\ (-\sin(\alpha_1 - \Theta_3))\}$$

$$\frac{\partial D}{\partial \dot{X}_3} = \frac{1}{2} C_2\{2[S\dot{F}1 - S\dot{F}2] + 2[R\dot{F}1 - R\dot{F}2]\ [L_4 \sin\alpha\ \frac{d\dot{\alpha}}{d\dot{X}_3}] +$$

$$+ \frac{1}{2} C_3\{2[\dot{S}1 - \dot{S}2]\ (-L_3 \cos\alpha)\ \frac{d\dot{\alpha}}{d\dot{X}_3} + 2[\dot{R}1 - \dot{R}2] L_3 \sin\alpha\ \frac{d\dot{\alpha}}{d\dot{X}_3}\}$$

$d\dot{\alpha}/d\dot{X}_3$ was derived earlier in this appendix.

$$\frac{d\dot{\alpha}}{d\dot{X}_3} = -\frac{\sec^2\alpha \cos\alpha}{L_4}$$

$$\frac{\partial D}{\partial \dot{\Theta}_3} = \frac{1}{2} C_2\{2[S\dot{F}1 - S\dot{F}2]\ [-L_2 \cos\Theta_3 - X_2 \sin(\alpha_1 - \Theta_3)] +$$

$$+ 2[R\dot{F}1 - R\dot{F}2]\ [(L_2 - L_5) \sin\Theta_3 - H_1 \cos\Theta_3 + X_2 \cos(\alpha_1 - \Theta_3) +$$

$$+ L_4 \sin\alpha \frac{d\dot{\alpha}}{d\dot{\Theta}_3}] + \frac{1}{2} C_3\{2[\dot{S}1 - \dot{S}2]\ [L_9 \cos(\alpha_4 - \Theta_3) +$$

$$+ L_7 \cos(\Theta_3 + \alpha_5) - L_3 \cos\frac{d\dot{\alpha}}{d\dot{\Theta}_3}] + 2[\dot{R}1 - \dot{R}2]\ [L_9 \sin(\alpha_4 - \Theta_3) -$$

$$- L_7 \sin(\Theta_3 + \alpha_5) + L_3 \sin\alpha \frac{d\dot{\alpha}}{d\dot{\Theta}_3}]\}$$

$\frac{d\dot{\alpha}}{d\dot{\theta}_3}$ was derived earlier in this appendix.

$$\frac{d\dot{\alpha}}{d\dot{\theta}_3} = \frac{L_7}{L_4} \cos(\theta_3 + \alpha_5) \sec^2\alpha \cos\alpha$$

$$\frac{\partial D}{\partial \dot{X}_4} = \frac{1}{2} C_2 \{ [\dot{RF1} - \dot{RF2}] L_4 \sin\alpha \frac{d\dot{\alpha}}{d\dot{X}_4} \} + \frac{1}{2} C_3 \{ [\dot{S1} - \dot{S2}] (-L_3 \cos\alpha) \frac{d\dot{\alpha}}{d\dot{X}_4} + [\dot{R1} - \dot{R2}] L_3 \sin\alpha \frac{d\dot{\alpha}}{d\dot{X}_4} + C_4(\dot{X}_4 - \dot{X}_5) \}$$

$\frac{d\dot{\alpha}}{d\dot{X}_4}$ was derived earlier in this appendix.

$$\frac{d\dot{\alpha}}{d\dot{X}_4} = \frac{\sec^2\alpha \cos\alpha}{L_4}$$

B.4 Compression and Extension of Front Fork and Rear Shock Absorber

Since the damping is different for the extension and compression in a shock absorber, it becomes important to determine whether the shock absorber is in compression or extension.

Consider the front fork as illustrated in Fig. B6.

Original Length, QFL $= \sqrt{AF^2 + BF^2}$

New Length, QFL2 $= \sqrt{(AF + RF1 - RF2)^2 + (BF + SF1 - SF2)^2}$

The Change in Length, Δ = QFL - QFL2

if $\Delta > 0$ = compression

if $\Delta < 0$ = extension

Considering the rear shock as shown in Fig. B7

Original Length, QRL $= \sqrt{L_3^2 + L_6^2 - 2L_3L_6\cos(\alpha_6 + \phi)}$

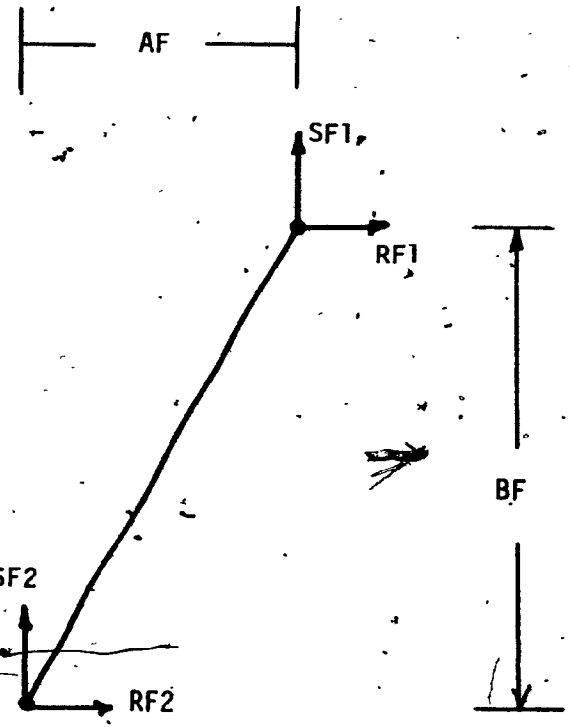

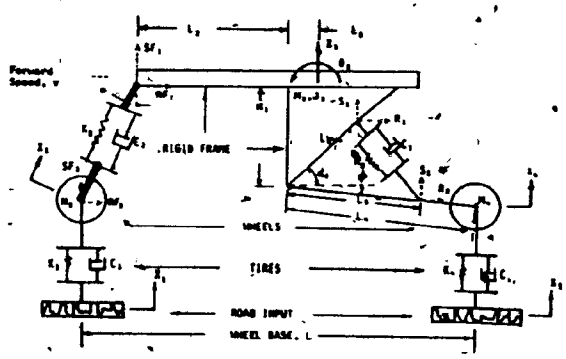

Figure B7 : Front Fork Displacement

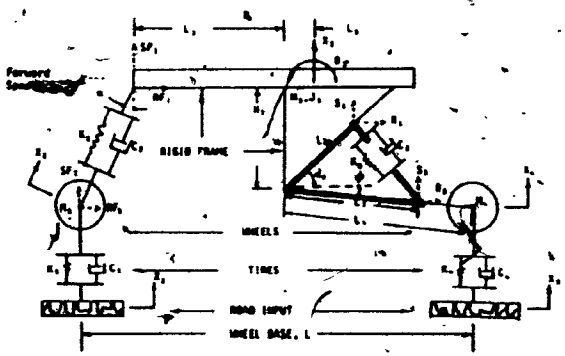

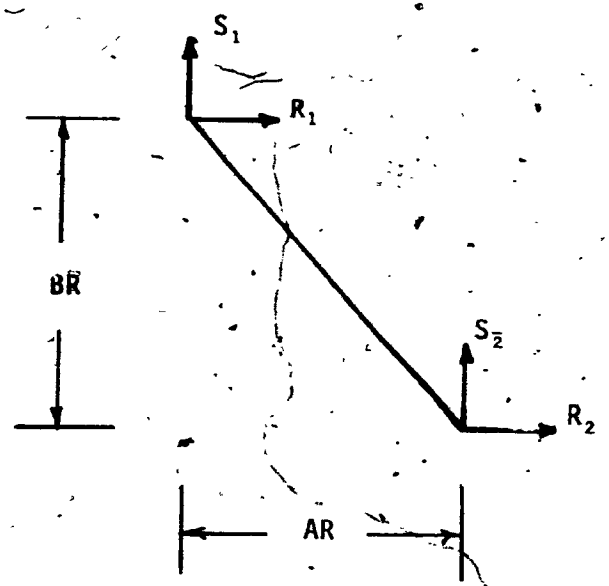

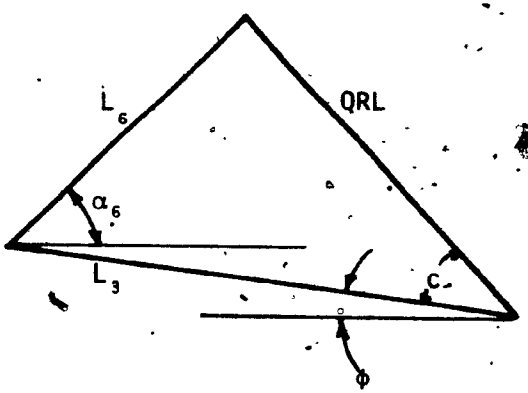

Figure B6 : Rear Shock Dispalcements

$$\cos(C) = \frac{QRL^2 + L_3^2 - L_6^2}{2\ QRL\ L_3}$$

$$AR = QRL * \cos(C + \phi)$$

$$BR = QRL * \sin(C + \phi)$$

$$\text{New Length, QRL2} = \sqrt{(AR + R1 - R2)^2 + (BR + S1 - S2)^2}$$

The change in Length, DDTR = QRL - QRL2

if DDTR > 0 ⇒ compression

if DDTR < 0 ⇒ extension

APPENDIX C

APPENDIX C

Detailed Derivation of Equations of Motion of the Motorcycle Suspension System (Large Displacements)

The differential equations of motion for the motorcycle, using Lagrange's method, are derived in this appendix for large displacements and including the motion in the horizontal direction. The lumped mass model of the motorcycle illustrated in Fig. 2.2 can also be used for this case.

The generalized coordinates chosen are:

$$\{q\} = \{X_2, X_3, \theta_3, X_4\}^T$$

C.1 Deflection of Rear Shock Absorber

Consider the rigid frame as illustrated in Figs. C.1 and C.2. Then

$$S_1 = L_9 \sin(360 - \alpha_4 + \theta_3) + X_3 \tag{C.1}$$

$$R_1 = L_9 \cos(360 - \alpha_4 + \theta_3) \tag{C.2}$$

$$SS_1 = X_3 + L_7 \sin(180 + \alpha_5 + \theta_3) \tag{C.3}$$

$$RR_1 = L_7 \cos(180 + \alpha_5 + \theta_3) \tag{C.4}$$

Now taking into consideration the rear swing arm as shown in Fig. C.3, we get

$$S_2 = SS_1 + L_3 \sin\alpha \tag{C.5}$$

$$R_2 = RR_1 + L_3 \cos\alpha \tag{C.6}$$

Substituting for RR_1 and SS_1 in Eqs. (C.5) and (C.6) yields:

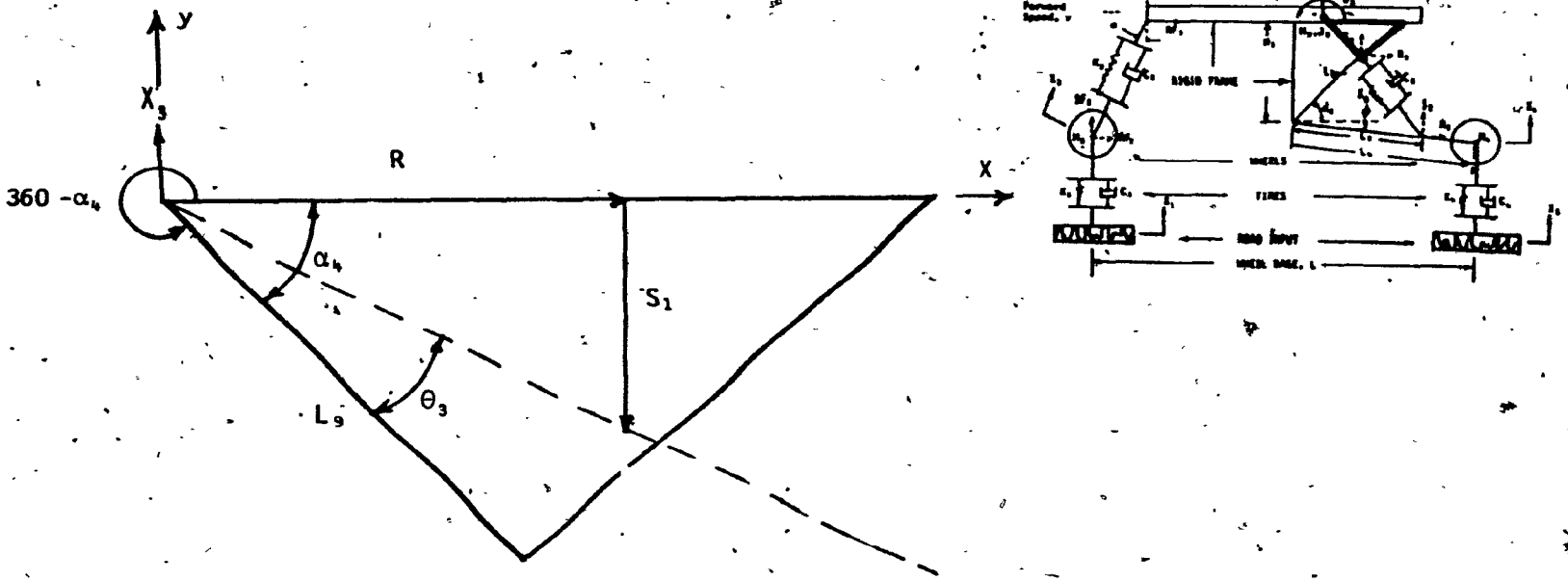

Figure C1.: Upper Part of Rigid Frame

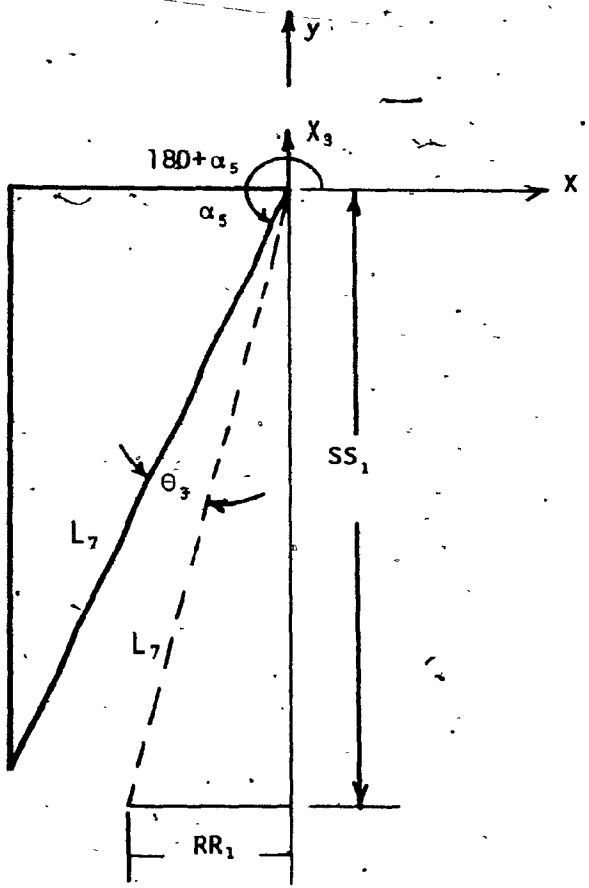

Figure C2. Lower Part of Rigid Frame

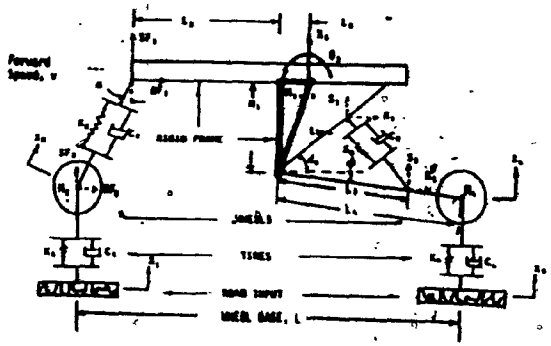

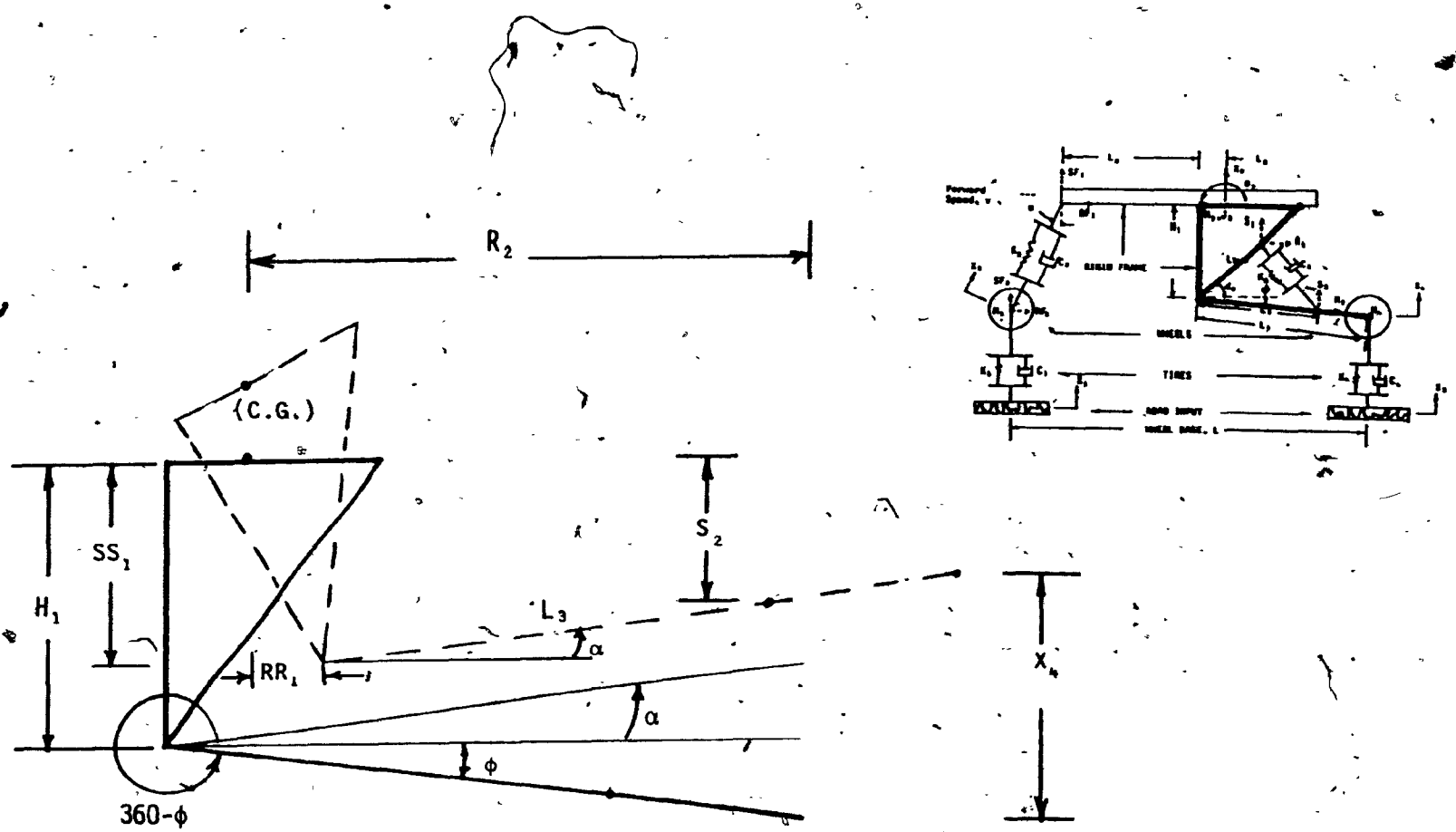

Figure C3 : Rear Swing Arm of the Motorcycle

$$S_2 = X_3 + L_7 \sin(180 + \alpha_5 + \theta_3) + L_3 \sin\alpha \quad (C.7)$$

$$R_2 = L_7 \cos(180 + \alpha_5 + \theta_3) + L_3 \cos\alpha \quad (C.8)$$

where

$$\sin\alpha = \frac{-H_1 + L_4 \sin(360 - \phi) - SS_1 + X_4}{L_4}$$

$$\cos\alpha = \frac{\sqrt{L_4^2 - [-H_1 + L_4 \sin(360 - \phi) - SS_1 + X_4]^2}}{L_4}$$

Substituting for SS_1 and RR_1, sin α and cosα becomes

$$\sin\alpha = \frac{X_4 + L_4 \sin(360 - \phi) - H_1 - X_3 - L_7 \sin(180 + \alpha_5 + \theta_3)}{L_4} \quad (C.9)$$

$$\cos\alpha = \frac{\sqrt{L_4^2 - [X_4 + L_4 \sin(360-\phi) - H_1 - X_3 - L_7 \sin(180+\alpha_5+\theta_3)]^2}}{L_4} \quad (C.10)$$

Change in length of the rear shock absorber ,

DELTAR = undeformed length - New length

Referring to Fig. C.4

Undeformed length, $OLR = \sqrt{(X_{11} - X_{10})^2 + (Y_{11} - Y_{10})^2}$

New length, NEWLENR $= \sqrt{(R_2 - R_1)^2 + (S_2 - S_1)^2}$

Therefore,

DELTAR = OLR - NEWLENR (C.11)

Referring to Fig. 2.2

$$Y_{10} = -H_1 + L_6 \sin\alpha_6$$

$$Y_{11} = -H_1 - L_3 \sin\phi$$

$$X_{10} = L_6 \cos\alpha_6 - L_5$$

$$X_{11} = L_3 \cos\phi - L_5$$

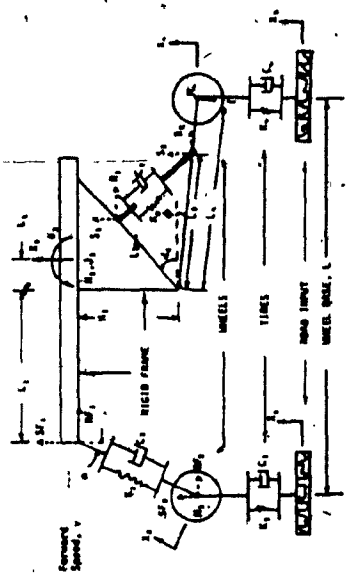

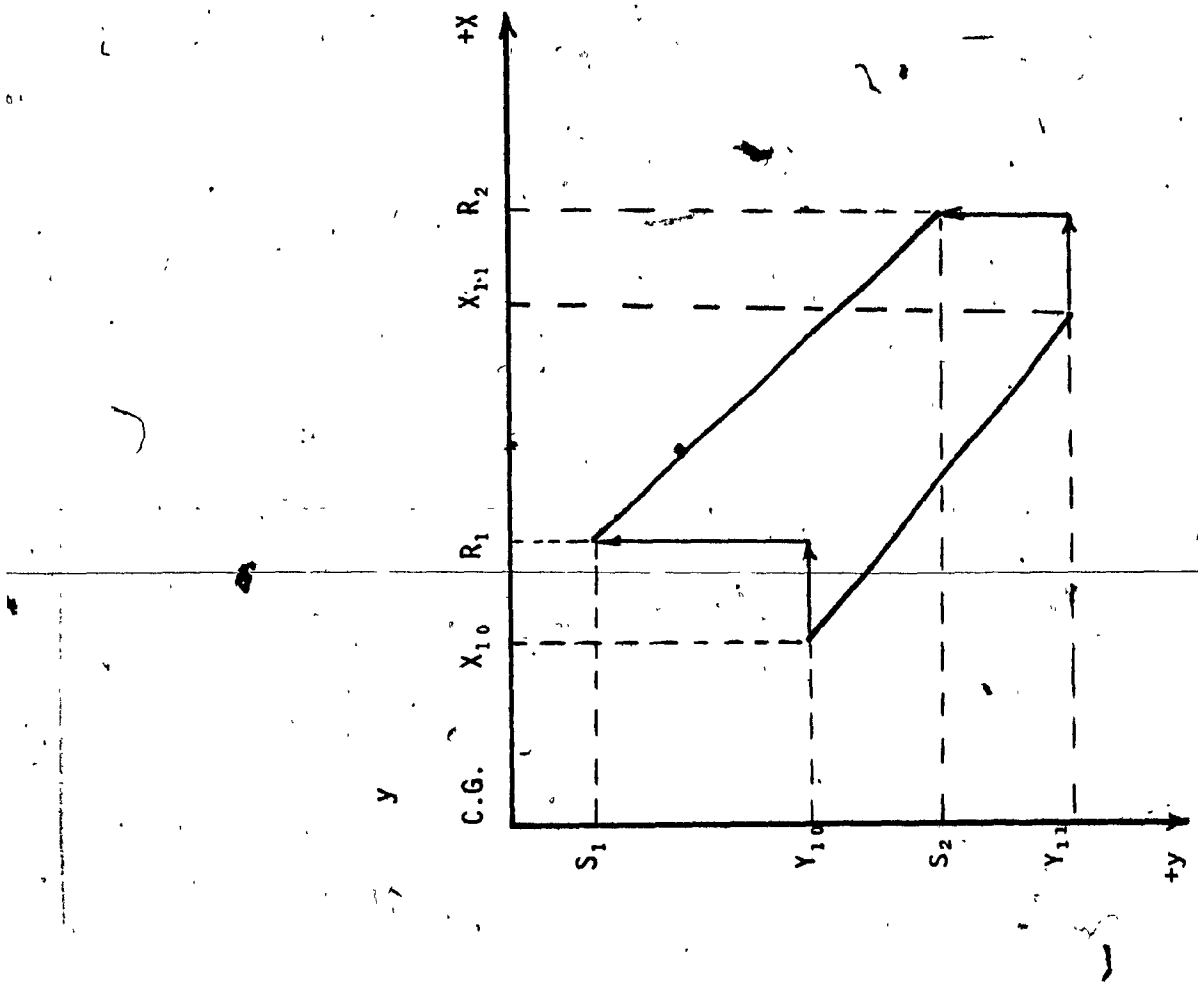

Figure C4 : Deflection of Rear Shock Absorber

and S_1, R_1, S_2, R_2 are given by Eqs. (C.1), (C.2), and (C.7) and (C.8).

C.2 Deflection of Front Fork

Referring to Fig. C.5

$$SF1 = X_3 + L_2 \sin(180 + \theta_3) \quad (C.12)$$

$$RF1 = (L_2 - L_5)\cos(180 + \theta_3) + H_1 \sin(270 + \theta_3) - L_4 \cos(360 - \phi) + L_4 \cos\alpha - L_5 \quad (C.13)$$

$$SF2 = L_{20} \sin(270 - \alpha_1) - X_2 \sin(270 - (\alpha_1 - \theta_3)) \quad (C.14)$$

$$RF2 = -L_2 + L_{20} \cos(270 - \alpha_1) + X_2 \cos(270 - (\alpha_1 - \theta_3)) \quad (C.15)$$

Change in Length, DELTAF = Undeformed Length - New Length.

Referring to Fig. C.6,

$$\text{Undeformed length, OLF} = \sqrt{(X_{13} - X_{12})^2 + (Y_{13} - Y_{12})^2}$$

$$\text{New length, NEWLENF} = \sqrt{(RF2 - RF1)^2 + (SF2 - SF1)^2}$$

Therefore,

$$DELTAF = OLF - NEWLENF \quad (C.16)$$

Referring to Fig. 2.2

$$X_{12} = -L_2$$

$$X_{13} = -L_2 - L_{20} \sin\alpha_1$$

$$Y_{12} = 0$$

$$Y_{13} = L_{20} \cos\alpha_1.$$

SF1, RF1, SF2 and RF2 are as given by Eqs. (C.12), (C.13), (C.14) and (C.15).

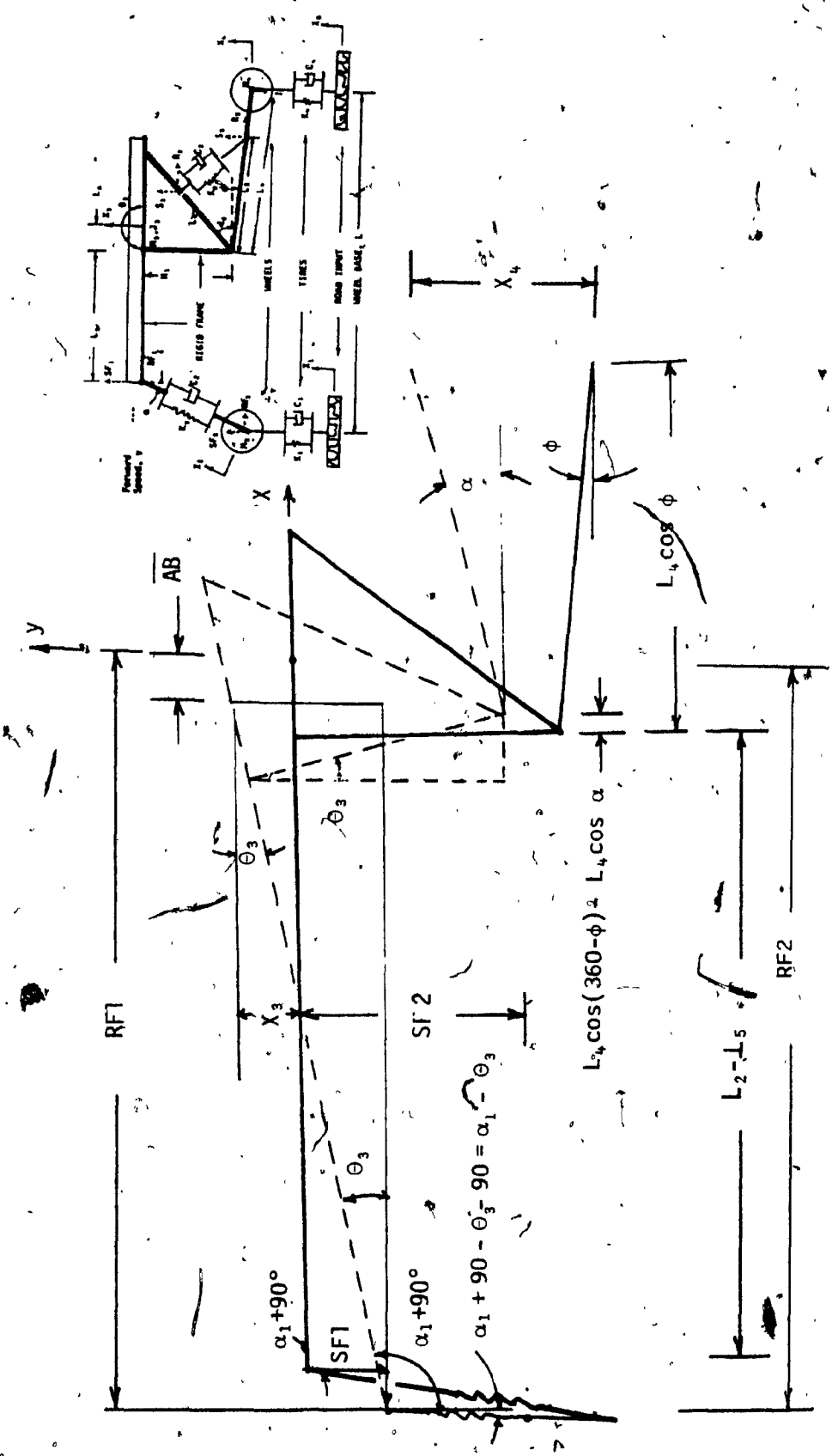

Figure C5 : Deflection of Front Fork

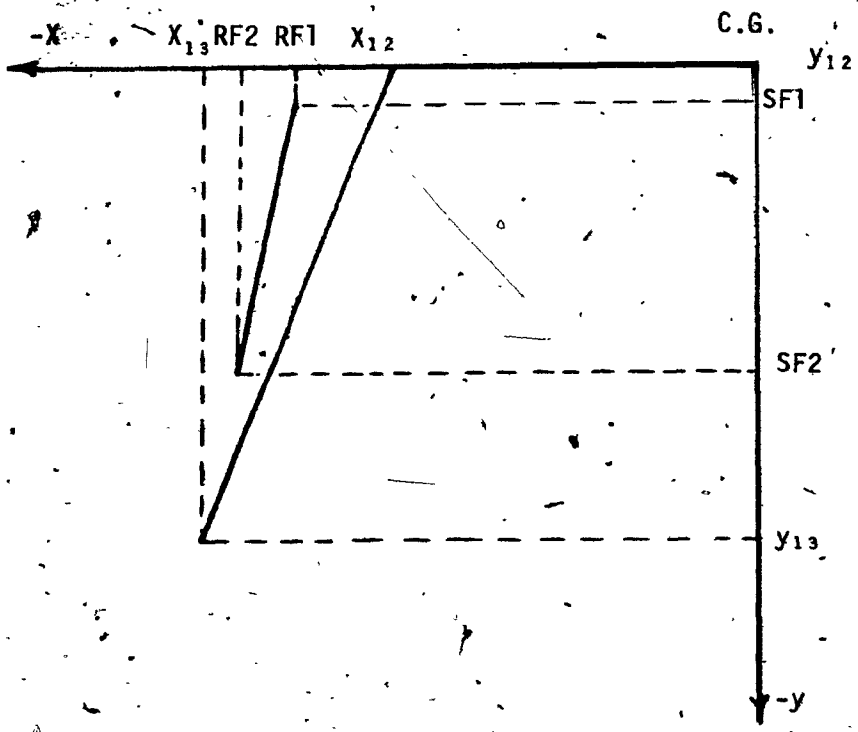

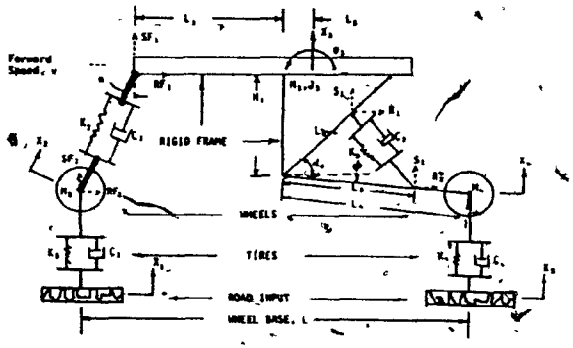

Figure C6 : Deflection of Front Shock

C.3 Calculation of Horizontal Displacement $\overline{AB}$

Referring to Fig. C5,

$$\overline{AB} = RF_1 + L_2 \cos\theta_3 = (L_2 - L_5)\cos(180+\theta_3) + H_1 \sin(270+\theta_3) - \\ - L_4 \cos(360-\phi) + L_4 \cos\alpha - L_5 + L_2 \cos\theta_3 \quad (C.17)$$

C.4 Lagrange's Equation

The Lagrange's equation can be written as

$$\frac{d}{dt}\frac{\partial(T)}{\partial\dot{q}_i} - \frac{\partial(T)}{\partial q_i} + \frac{\partial(V)}{\partial q_i} + \frac{\partial(D)}{\partial\dot{q}_i} = Q_i \quad (C.18)$$

where:

T = kinetic energy of the system

V = potential energy of the system

D = dissipation energy of the system

Q_i = generalized external force acting on the system

$\{q\} = \{X_2, X_3, \theta_3, X_4\}^T$

Kinetic Energy

$$T = \frac{1}{2} m_2 \dot{X}_2^2 + \frac{1}{2} m_3 \dot{X}_3^2 + \frac{1}{2} J_3 \dot{\theta}_3^2 + \frac{1}{2} m_4 \dot{X}_4^2 + \frac{1}{2} m_3 \dot{\overline{AB}}^2 \quad (C.19)$$

Potential Energy

$$V = \frac{1}{2} K_1 [X_2 \cos(\alpha_1 - \theta_3) - X_1]^2 + \frac{1}{2} K_2 \Delta F^2 + \frac{1}{2} K_3 \Delta R^2 + \\ + \frac{1}{2} K_4 (X_4 - X_5)^2 \quad (C.20)$$

Dissipation Energy

$$D = \frac{1}{2} C_1 [\dot{X}_2 \cos(\alpha_1 - \Theta_3) - \dot{X}_1]^2 + \frac{1}{2} C_2 \Delta\dot{F}^2 + \frac{1}{2} C_4 \Delta\dot{R}^2 + \frac{1}{2} C_4 (\dot{X}_4 - \dot{X}_5)^2 \qquad (C.21)$$

where

$$\Delta F = OLF = \{[-L_2 + L_{20}\cos(270 - \alpha_1) + X_2 \cos(270 - \alpha_1 + \Theta_3) - (L_2 - L_5)\cos(180 + \Theta_3) - H_1 \sin(270 + \Theta_3) + L_4 \cos(360 - \phi) - L_4 \cos\alpha + L_5]^2 + [-L_2 + L_{20}\cos(270 - \alpha_1) + X_2 \cos(270 - \alpha_1 + \Theta_3) - X_3 - L_2 \sin(180 + \Theta_3)]^2\}^{\frac{1}{2}}$$

$$\Delta R = OLR - \{[L_7 \cos(180 + \alpha_5 + \Theta_3) + L_3 \cos\alpha - L_9 \cos(360 - \alpha_4 + \Theta_3)]^2 + [X_3 + L_7 \sin(180 + \alpha_5 + \Theta_3) + L_3 \sin\alpha - L_9 \sin(360 - \alpha_4 + \Theta_3) - X_3]^2\}^{\frac{1}{2}}$$

Before calculating $\dot{\overline{AB}}$, $\Delta\dot{R}$, $\Delta\dot{F}$, we have to calculate $d\alpha/dt$ (detailed derivation was performed in Appendix-B).

$$\dot{\alpha} = \frac{1}{1 + \frac{\sin^2\alpha}{\cos^2\alpha}} + \left\{\frac{[\dot{X}_4 - \dot{X}_3 + L_7 \cos(\Theta_3 + \alpha_5)\dot{\Theta}_3]}{L_4 \cos\alpha} + \frac{\sin^2\alpha}{\cos^3\alpha\, L_4} [\dot{X}_4 - \dot{X}_3 + L_7 \cos(\Theta_3 + \alpha_5)\dot{\Theta}_3]\right\}$$

Calculations of $\dot{\overline{AB}}$, $\Delta\dot{R}$, $\Delta\dot{F}$

$$\dot{\overline{AB}} = -(L_2 - L_5)\sin(180 + \Theta_3)\dot{\Theta}_3 + H_1 \cos(270 + \Theta_3)\dot{\Theta}_3 - L_4 \sin\alpha\,\dot{\alpha} - L_2 \sin\Theta_3\dot{\Theta}_3$$

$$= (L_2 - L_5)\sin\Theta_3\dot{\Theta}_3 + H_1 \sin\Theta_3\dot{\Theta}_3 - L_4 \sin\alpha\,\dot{\alpha} - L_2 \sin\Theta_3\dot{\Theta}_3$$

Assuming that the initial velocities are zero

$$\dot{\Delta R} = \sqrt{(\dot{R}_2 - \dot{R}_1)^2 + (\dot{S}_2 - \dot{S}_1)^2}$$

$$\dot{S}_1 = L_9 \cos(360 - \alpha_4 + \Theta_3)\dot{\Theta}_3 + \dot{X}_3$$

$$\dot{R}_1 = -L_9 \sin(360 - \alpha_4 + \Theta_3)\dot{\Theta}_3$$

$$\dot{S}_2 = \dot{X}_3 + L_7 \cos(180 + \alpha_5 + \Theta_3)\dot{\Theta}_3 + L_3 \cos\alpha\ \dot{\alpha}$$

$$\dot{R}_2 = -L_7 \sin(180 + \alpha_5 + \Theta_3)\dot{\Theta}_3 - L_3 \sin\alpha\ \dot{\alpha}$$

$$\dot{\Delta F} = \sqrt{(\dot{RF2} - \dot{RF1})^2 + (\dot{SF2} - \dot{SF1})^2}$$

$$\dot{SF1} = \dot{X}_3 + L_2 \cos(180 + \Theta_3)\dot{\Theta}_3$$

$$\dot{RF1} = -(L_2 - L_5)\sin(180 + \Theta_3)\dot{\Theta}_3 + H_1 \cos(270 + \Theta_3)\dot{\Theta}_3 - L_4 \sin\alpha\ \dot{\alpha}$$

$$\dot{SF2} = -\dot{X}_2 \sin(270 - \alpha_1 + \Theta_3) - X_2 \cos(270 - \alpha_1 + \Theta_3)\dot{\Theta}_3$$

$$\dot{RF2} = \dot{X}_2 \cos(270 - \alpha_1 + \Theta_3) - X_2 \sin(270 - \alpha_1 + \Theta_3)\dot{\Theta}_3$$

From Eq. (C.19),

$$\frac{\partial T}{\partial \dot{X}_3} = m_2 \dot{X}_2$$

$$\frac{\partial T}{\partial \dot{X}_3} = m_9 \dot{X}_9 + m_3 \dot{\overline{AB}} \cdot \frac{d\,\dot{\overline{AB}}}{d\dot{X}_3}$$

$$\frac{\partial T}{\partial \dot{\Theta}_3} = J_3 \dot{\Theta}_3 + m_3 \dot{\overline{AB}} \cdot \frac{d\,\dot{\overline{AB}}}{d\dot{\Theta}_3}$$

$$\frac{\partial T}{\partial \dot{X}_3} = m_4 \dot{X}_4 + m_3 \dot{\overline{AB}} \cdot \frac{d\,\dot{\overline{AB}}}{d\dot{X}_4}$$

where

$$\frac{d\,\overline{AB}}{d\dot{X}_3} = -L_4 \sin\alpha \frac{d\dot{\alpha}}{d\dot{X}_3}$$

where

$$\frac{d\dot{\alpha}}{d\dot{X}_3} = -\frac{1}{1+\tan^2\alpha}\,\frac{1}{L_4\cos\alpha} - \frac{1}{1+\tan^2\alpha}\,\frac{\sin^2\alpha}{\cos^3\alpha\, L_4}$$

Upon substitution and rearranging

$$\frac{d\dot{\overline{AB}}}{d\dot{X}_3} = \tan\alpha$$

$$\frac{d\dot{\overline{AB}}}{d\dot{\Theta}_3} = (L_2 - L_5)\sin\Theta_3 + H_1\sin\Theta_3 - L_2\sin\Theta_3 - L_4\sin\alpha_5\,\frac{d\dot{\alpha}}{d\dot{\Theta}_3}$$

where

$$\frac{d\dot{\alpha}}{d\dot{\Theta}_3} = \frac{1}{1+\tan^2\alpha}\,\frac{1}{L_4\cos\alpha}\,L_7\cos(\Theta_3+\alpha_5) + \frac{1}{1+\tan^2\alpha}\,\frac{\sin^2\alpha}{\cos^3\alpha\, L_4}\,L_7\cos(\Theta_3+\alpha_5)$$

Upon substituting and rearranging

$$\frac{\partial\dot{\overline{AB}}}{\partial\dot{\Theta}_3} = (L_2 - L_5)\sin\Theta_3 + H_1\sin\Theta_3 - L_2\sin\Theta_3 - L_7\cos(\Theta_3+\alpha_5)\tan\alpha$$

$$\frac{d\dot{\overline{AB}}}{d\dot{X}_4} = -L_4\sin\alpha\,\frac{d\dot{\alpha}}{d\dot{X}_4}\,; \quad \frac{d\dot{\alpha}}{d\dot{X}_4} = \frac{1}{1+\tan^2\alpha}\left[\frac{1}{L_4\cos\alpha} + \frac{\sin^2\alpha}{\cos^2\alpha L_4}\right]$$

Upon substituting and rearranging

$$\frac{d\dot{\overline{AB}}}{d\dot{X}_4} = -\tan\alpha\,; \quad \text{Also} \quad \frac{d}{dt}\,\frac{\partial T}{\partial\dot{X}_2} = m_2\ddot{X}_2$$

$$\frac{d}{dt}\,\frac{\partial T}{\partial\dot{X}_3} = m_3\ddot{X}_3 + m_3\dot{\overline{AB}}\,\frac{d}{dt}\left(\frac{d\dot{\overline{AB}}}{d\dot{X}_3}\right) + m_3\,\frac{d\dot{\overline{AB}}}{d\dot{X}_3}\,\frac{d\dot{\overline{AB}}}{dt}$$

$$\frac{d}{dt}\,\frac{\partial T}{\partial\dot{\Theta}_3} = J_3\ddot{\Theta}_3 + m_3\dot{\overline{AB}}\,\frac{d}{dt}\left(\frac{d\dot{\overline{AB}}}{d\dot{\Theta}_3}\right) + m_3\,\frac{d\dot{\overline{AB}}}{d\dot{\Theta}_3}\,\frac{d\dot{\overline{AB}}}{dt}$$

$$\frac{d}{dt}\,\frac{\partial T}{\partial\dot{X}} = m_4\ddot{X}_4 + m_3\dot{\overline{AB}}\,\frac{d}{dt}\left(\frac{d\dot{\overline{AB}}}{d\dot{X}_4}\right) + m_3\,\frac{d\dot{\overline{AB}}}{d\dot{X}_4}\,\frac{d\dot{\overline{AB}}}{dt}$$

where

$$\frac{d}{dt}\left(\frac{d\overline{AB}}{d\dot{X}_3}\right) = \sec^2\alpha\,\dot{\alpha}$$

$$\frac{d}{dt}\left(\frac{d\overline{AB}}{d\dot{\Theta}_3}\right) = (L_2 - L_5)\cos\theta_3\dot{\theta}_3 + H_1\cos\theta_3\dot{\theta}_3 - L_2\cos\theta_3\dot{\theta}_3 + L_7\sin(\theta_3+\alpha_5)\,\dot{\theta}_3\tan\alpha - L_7\cos(\theta_7+\alpha_5)\sec^2\alpha\,\dot{\alpha}$$

$$\frac{d}{dt}\left(\frac{d\overline{AB}}{d\dot{X}_4}\right) = -\sec^2\alpha\,\dot{\alpha}$$

$$\frac{d\overline{AB}}{dt} = (L_2 - L_5)\cos\theta_3\dot{\theta}_3^2 + (L_2 - L_5)\sin\theta_3\ddot{\theta}_3 + H_1\cos\theta_3\dot{\theta}_3^2 + H_1\sin\theta_3\ddot{\theta}_3^2 - L_4\cos\alpha\dot{\alpha}^2 - L_4\sin\alpha\ddot{\alpha} + L_2\sin\theta_3\dot{\theta}_3^2 - L_2\cos\theta_3\ddot{\theta}_3$$

Calculation of $\ddot{\alpha}$

Rewriting $\dot{\alpha}$ ($\dot{\alpha}$ is taken from Appendix B)

$$\dot{\alpha} = \frac{\dot{X}_4 - \dot{X}_3 + L_7\cos(\theta_3+\alpha_5)\dot{\theta}_3}{L_4\cos\alpha + \frac{L_4\sin^2\alpha}{\cos\alpha}} + \frac{\sin^2\alpha[\dot{X}_4 - \dot{X}_3 + L_7\cos(\alpha_3+\theta_5)\dot{\theta}_3]}{L_4\cos^3\alpha + L_4\sin^2\alpha\cos\alpha}$$

$$= \frac{\tan^2\alpha[\dot{X}_4 - \dot{X}_3 + L_7\cos(\theta_3+\alpha_5)\dot{\theta}_3] + [\dot{X}_4 - \dot{X}_3 + L_7\cos(\theta_3+\alpha_5)\dot{\theta}_3]}{L_4\cos\alpha + \frac{L_4\sin^2\alpha}{\cos\alpha}}$$

$$= \frac{[\dot{X}_4 - \dot{X}_3 + L_7\cos(\theta_3+\alpha_5)\dot{\theta}_3][\tan^2\alpha + 1]}{\frac{L_4\cos^2\alpha + L_4\sin^2\alpha}{\cos\alpha}}$$

$$= [\dot{X}_4 - \dot{X}_3 + L_7\cos(\theta_3+\alpha_5)\dot{\theta}_3]\sec^2\alpha\cos\alpha / L_4$$

Therefore,

$$\ddot{\alpha} = [\ddot{X}_4 - \ddot{X}_3 + L_7 \cos(\theta_3 + \alpha_5)\ddot{\theta}_3 - L_7 \sin(\theta_3 + \alpha_5)\dot{\theta}_3^2] \frac{\sec^2\alpha \cos\alpha}{L_4}$$

$$+ [\dot{X}_4 - \dot{X}_3 + L_7 \cos(\theta_3 + \alpha_5)\dot{\theta}_3] [-\sec^2\alpha \frac{\sin\alpha}{L_4} \dot{\alpha} +$$

$$+ \frac{\cos\alpha}{L_4} 2 \sec\alpha . \sec\alpha \tan\alpha \dot{\alpha}]$$

Calculation of Terms $\frac{\partial(T)}{\partial q_1}$

$$\frac{\partial T}{\partial X_2} = m_3 \dot{\overline{AB}} \frac{d\dot{\overline{AB}}}{dX_2}$$

$$\frac{\partial T}{\partial X_3} = m_3 \dot{\overline{AB}} \frac{d\dot{\overline{AB}}}{dX_3}$$

$$\frac{\partial T}{\partial \theta_3} = m_3 \dot{\overline{AB}} \frac{d\dot{\overline{AB}}}{d\theta_3}$$

$$\frac{\partial T}{\partial X_4} = m_3 \dot{\overline{AB}} \frac{d\dot{\overline{AB}}}{dX_4}$$

where

$$\frac{d\dot{\overline{AB}}}{dX_2} = 0$$

$$\frac{d\dot{\overline{AB}}}{dX_3} = -L_4 \sin\alpha \frac{d\dot{\alpha}}{dX_3} - L_4 \cos\alpha \frac{d\alpha}{dX_3} \dot{\alpha}$$

$$\frac{d\dot{\overline{AB}}}{d\theta_3} = (L_2 - L_5) \cos\theta_3 \dot{\theta}_3 + H_1 \cos\theta_3 \dot{\theta}_3 - L_2 \cos\theta_3 \dot{\theta}_3 - L_4 \sin\alpha \frac{d\dot{\alpha}}{d\theta_3} -$$

$$- L_4 \cos\alpha \frac{d\alpha}{d\theta_3} \dot{\alpha}$$

$$\frac{d\dot{\overline{AB}}}{dX_4} = -L_4 \sin\alpha \frac{d\dot{\alpha}}{dX_4} - L_4 \cos\alpha \frac{d\dot{\alpha}}{dX_4} \dot{\alpha}$$

Derivation of

$$\frac{d\alpha}{dX_3}, \frac{d\alpha}{d\theta_3}, \frac{d\alpha}{dX_4}, \frac{d\dot{\alpha}}{dX_3}, \frac{d\dot{\alpha}}{d\theta_3}, \frac{d\dot{\alpha}}{dX_4}$$

can be found in Appendix B and the final form is repeated here for convenience.

$$\frac{d\alpha}{dX_3} = -\frac{1}{L_4 \cos\alpha}$$

$$\frac{d\alpha}{d\Theta_3} = \frac{L_7 \cos(\Theta_3 + \alpha_5)}{L_4 \cos\alpha}$$

$$\frac{d\alpha}{dX_4} = \frac{1}{L_4 \cos\alpha}$$

$$\frac{d\dot{\alpha}}{dX_4} = \frac{1}{L_4}\left[\dot{X}_4 - \dot{X}_3 + L_7 \cos(\Theta_3 + \alpha_5)\dot{\Theta}_3\right]\left[2\sec^2\alpha \tan\alpha \frac{d\alpha}{dX_3}\cos\alpha - \right.$$
$$\left. - \sec^2\alpha \sin\alpha \frac{d\alpha}{dX_3}\right]$$

$$\frac{d\dot{\alpha}}{d\Theta_3} = \left[-L_7 \sin(\Theta_3 + \alpha_5)\dot{\Theta}_3\right]\sec^2\alpha \frac{\cos\alpha}{L_4} +$$
$$\frac{1}{L_4}\left[\dot{X}_4 - \dot{X}_3 + L_7 \cos(\Theta_3 + \alpha_5)\dot{\Theta}_3\right]\left[2\sec^2\alpha \tan\alpha \frac{d\alpha}{d\Theta_3}\cos\alpha - \right.$$
$$\left. \sec^2\alpha \sin\alpha \frac{d\alpha}{dX_3}\right]$$

$$\frac{d\dot{\alpha}}{dX_4} = \frac{1}{L_4}\left[\dot{X}_4 - \dot{X}_3 + L_7 \cos(\Theta_3 + \alpha_5)\dot{\Theta}_3\right]\left[2\sec^2\alpha \tan\alpha \frac{d\alpha}{dX_4}\cos\alpha - \right.$$
$$\left. - \sec^2\alpha \sin\alpha \frac{d\alpha}{dX_4}\right]$$

Calculation of Terms $\left(\frac{\partial V}{\partial q_i}\right)$

$$\frac{\partial V}{\partial X_2} = K_1\left[X_2 \cos(\alpha_1 - \Theta_3) - X_1\right]\cos(\alpha_1 - \Theta_3) +$$
$$+ K_2 \Delta F\left(-\frac{1}{2}\right)\left[(RF2 - RF1)^2 + (SF2 - SF1)^2\right]^{-\frac{1}{2}}\left[2(RF2 - RF1)\cdot\right.$$
$$\left.\cdot \cos(270 - \alpha_1 + \Theta_3) + 2(SF2 - SF1)\cos(270 - \alpha_1 + \Theta_3)\right]$$

$$\frac{\partial V}{\partial X_3} = K_2 \Delta F \cdot \left(-\frac{1}{2}\right) [(RF2 - RF1)^2 + (SF2 - SF1)^2]^{\frac{1}{2}}$$

$$\{[2(RF2 - RF1)\ (\frac{L_4 \sin\alpha}{L_4 \cos\alpha}) + 2(SF2 - SF1)\ (-1)] +$$

$$+ K_3 \Delta R\ (-\frac{1}{2})\ [(R2 - R1)^2 + (S2 - S1)^2]^{-\frac{1}{2}} [2(R2 - R1)\ (\frac{-L_3 \sin\alpha}{L_4 \cos\alpha}) +$$

$$2(S2 - S1)\ \frac{L_3 \cos\alpha}{L_4 \cos\alpha}]\}$$

$$\frac{\partial V}{\partial \Theta_3} = K_1 [X_2 \cos(\alpha_1 - \Theta_3) - X_1]\ X_2 \sin(\alpha_1 - \Theta_3) +$$

$$K_2 \Delta F\ (-\frac{1}{2})\ [RF2 - RF1)^2 + (SF2 - SF1)^2]^{-\frac{1}{2}} \{[2(RF2 - RF1)$$

$$(-X_2 \sin(270 - \alpha_1 + \Theta_3) + (L_2 - L_5) \sin(180 + \Theta_3) -$$

$$-H_1 \cos(270 + \Theta_3) + L_4 \sin\alpha\ \frac{L_7 \cos(\Theta_3 + \alpha_5)}{L_4 \cos\alpha}] +$$

$$+ [2(SF2 - SF1)\ (-X_2 \sin(270 - \alpha_1 + \Theta_3) - L_2 \cos(180 + \Theta_3)] +$$

$$K_3 \Delta R\ (-\frac{1}{2})\ [(R1 - R2)^2 + (S2 - S1)^2]^{\frac{1}{2}} \{[2(R2 - R1)\ .$$

$$(-L_7 \sin(180 + \alpha_5 + \Theta_3) - L_3 \sin\alpha\ \frac{L_7 \cos(\Theta_3 + \alpha_5)}{L_4 \cos\alpha} +$$

$$+ L_9 \sin(360 - \alpha_4 + \Theta_3))] + [2(S2 - S1)\ L_7 \cos(180 + \alpha_5 + \Theta_3) +$$

$$+ L_3 \cos\alpha\ \frac{L_7 \cos(\Theta_3 + \alpha_5)}{L_4 \cos\alpha} - L_9 \cos(360 - \alpha_4 + \Theta_3)]\}$$

$$\frac{\partial V}{\partial X_4} = K_4\ (X_4 - X_5) + K_2\ \Delta F\ (-\frac{1}{2})\ [RF2 - RF1)^2 + (SF2 - SF1)^2]^{-\frac{1}{2}}$$

$$2(RF2 - RF1)\ L_4 \sin\alpha\ \frac{1}{L_4 \cos\alpha} + K_3\ \Delta R\ (-\frac{1}{2})\ [(R2 - R1)^2 +$$

$$+ (S2 - S1)^2]^{-\frac{1}{2}} \{2(R2 - R1)\ (-L_3 \sin\alpha)\ \frac{1}{L_4 \cos\alpha} +$$

$$+ 2(S2 - S1)\ L_4 \cos\alpha \frac{1}{L_4 \cos\alpha}\}$$

Calculation of Terms $\left(\frac{\partial D}{\partial \dot{q}_i}\right)$

First we derive

$$\frac{d\dot{\alpha}}{d\dot{X}_3}, \quad \frac{d\dot{\alpha}}{d\dot{\Theta}_3}, \quad \frac{d\dot{\alpha}}{d\dot{X}_4}$$

$$\frac{d\dot{\alpha}}{d\dot{X}_3} = -\frac{\sec^2\alpha \cos\alpha}{L_4}$$

$$\frac{d\dot{\alpha}}{d\dot{\Theta}_3} = \frac{L_7}{L_4}\cos(\Theta_3 + \alpha_5)\ \sec^2\alpha \cos\alpha$$

$$\frac{d\dot{\alpha}}{d\dot{X}_4} = \frac{\sec^2 \cos\alpha}{L_4}$$

$$\frac{\partial D}{\partial \dot{X}_2} = C_1[\dot{X}_2 \cos(\alpha_1 - \Theta_3) - \dot{X}_1]\cos(\alpha_1 - \Theta_3) +$$

$$+ \frac{1}{2} C_2\{2(R\dot{F}2 - R\dot{F}1)\cos(270 - \alpha_1 + \Theta_3) +$$

$$+ 2(S\dot{F}2 - S\dot{F}1)(-\sin(270 - \alpha_1 + \Theta_3))\}$$

$$\frac{\partial D}{\partial \dot{X}_3} = \frac{1}{2} C_2\{2(R\dot{F}2 - R\dot{F}1)\ L_4 \cos\left(\frac{-\sec^2\alpha \cos\alpha}{L_4}\right) +$$

$$+ 2(S\dot{F}2 - S\dot{F}1)(-1)\} + \frac{1}{2} C_3\{2(\dot{R}2 - \dot{R}1)(-L_3 \sin\alpha) \cdot$$

$$\left(\frac{-\sec^2\alpha \cos\alpha}{L_4}\right) + 2(\dot{S}2 - \dot{S}1)\ L_3 \cos\alpha \left(\frac{-\sec^2\alpha \cos\alpha}{L_4}\right)\}$$

$$\frac{\partial D}{\partial \dot{\Theta}_3} = \frac{1}{2} C_2\{2(R\dot{F}2 - R\dot{F}1)[-X_2 \sin(270 - \alpha_1 + \Theta_3) +$$

$$+ (L_2 - L_5)\sin(180 + \Theta_3) - H_1 \cos(270 + \Theta_3) +$$

$$+ L_4 \sin\frac{L_7}{L_4}\cos(\Theta_3 + \alpha_5)\ \sec^2\alpha \cos\alpha] +$$

$$+ 2(S\dot{F}2 - S\dot{F}1)[-X_2 \cos(270 - \alpha_1 + \Theta_3) - L_2 \cos(180 + \Theta_3)]\} +$$

$$+ \frac{1}{2} C_3 \{2[\dot{R}2 - \dot{R}1] [-L_7 \sin (180 + \alpha_5 + \Theta_3) - L_3 \sin \alpha \cdot \frac{L_7}{L_4} \cos(\Theta_3 + \alpha_4) \sec^2\alpha \cos \alpha + L_3 \sin (360 - \alpha_4 + \Theta_3)] +$$

$$+ 2[\dot{S}2 - \dot{S}1] [L_7 \cos (180 + \alpha_5 + \Theta_3) + L_3 \cos \alpha \cdot \frac{L_7}{L_4} \cos (\Theta_3 + \alpha_4) \sec^2\alpha \cos \alpha - L_3 \cos (360 - \alpha_4 + \Theta_3)]\}$$

$$\frac{\partial D}{\partial \dot{X}_4} = C_4 (\dot{X}_4 - \dot{X}_5) + \frac{1}{2} C_2 \{ 2[\dot{RF}2 - \dot{RF}1] [L_4 \sin \alpha \frac{\sec^2 \cos \alpha}{L_4}] +$$

$$\frac{1}{2} C_3 \{2[\dot{R}2 - \dot{R}1] [-L_3 \sin \alpha \frac{\sec^2\alpha \cos \alpha}{L_4}] +$$

$$+ 2[\dot{S}2 - \dot{S}1] [L_3 \cos \alpha \frac{\sec^2 \cos\alpha}{L_4}]\}$$

APPENDIX D

APPENDIX D

Adams Predictor-Corrector Method

This appendix gives the outline of the numerical solution of the initial value problem for first order systems of ordinary differential equations.

$$y' = f(t,y), \qquad a \leq t \leq b, \qquad y(t) = \alpha$$

The method used in this thesis is the variable-step, variable-order Adams predictor-corrector method [17, 18, 29].

This is a multi-step method whose difference equation for finding the approximation W_{i+1} of the mesh point t_{i+1} can be represented by

$$W_{i+1} = a_{m-1} W_i + a_{m-2} W_{i-1} + \ldots a_0 W_{i+1-m} + h[b_m f(t_{i+1}, W_{i+1}) + b_{m-1} f(t_i, W_i) + \ldots b_0 f(t_{i+1-m}, W_{i+1-m})]$$

where

m = integer greater than 1

$i = m-1, m, \ldots N-1$

Starting values: $W_0 = \alpha_0$, $W_1 = \alpha_1$, $W_2 = \alpha_2$, $\ldots W_{m-1} = \alpha_{m-1}$

$h = (b-a)/N$

If $b_m = 0$, then the method is explicit;

if $b_m \neq 0$, then the method is implicit.

In using predictor-corrector methods with variable step size, it is necessary to

a) have a method for obtaining the necessary starting value initially,

b) have a method for obtaining the necessary values of y at half steps when the interval is halved, and

c) have a method for obtaining the necessary values of y when the interval is doubled.

Special formulae can be worked out for each of these three situations. However, a fairly ideal combination is to use the fourth-order Runge-Kutta method together with a fourth-order predictor-corrector pair.

Predictor:

$$W_0 = \alpha_0, \quad W_1 = \alpha_1, \quad W_2 = \alpha_2, \quad W_3 = \alpha_3$$

$$W_{i+1} = W_i + \frac{h}{2y}\left(55 f_i - 59 f_{i-1} + 37 f_{i-2} - 9 f_{i-3}\right)$$

Corrector:

$$W_0 = \alpha_0; \quad W_1 = \alpha_1, \quad W_2 = \alpha_2$$

$$W_{i+1} = W_i + \frac{h}{2y}\left(9 f_{i+1} + 19 f_{i-1} + f_{i-2}\right)$$

The Runge-Kutta method can then be used for starting the solution initially for halving, and for doubling, while predictor-corrector pair can be used for normal continuation when the step size is kept fixed.